SOLID-BOOSTED NOVA VEHICLE SYSTEM STUDY

Document D2-22431

VOLUME III

CURRENT TECHNOLOGY VEHICLE

- Structures and Weights
- Environment and Control
- Design Configuration
- Payload Growth

April 1963

GEORGE C. MARSHALL SPACE FLIGHT CENTER
National Aeronautics and Space Administration

FINAL REPORT

Prepared Under Contract Number NAS8-2438
Phase II, Task 3
Control No. TP-64015
Requisition No. TP-3-74003 S2(1F)

By

THE BOEING COMPANY
Aero-Space Division
Seattle, Washington

CONTENTS

3.2.8 Structures

3.2.8.1 Introduction

The structural analysis of the T65 vehicle was performed to establish the structural configuration and to provide detailed analysis of the structure for systems evaluation purposes.

The first-stage structural configuration was selected on the basis of information developed during a preceding portion of Contract NAS8-2438 which evaluated various clustering concepts for a four-motor cluster. Second-stage trade studies were performed for various bulkhead shapes and three tankage concepts: clustered, multicell, and single tank. Stress analysis of major structural components was performed on the second stage, interstage, cluster structure, and support structure and is presented in detail with margins of safety indicated.

Insulation requirements for base heating protection and cryogenic tankage were established. Allowable stresses for unpressurized motor case handling and launch pad buckling loads were determined. Vehicle loads were predicted for wind shear plus gust, nozzles full gimbal, 20-degree angle of attack with null nozzles, unsymmetrical tailoff, and symmetrical maximum thrust. Aerodynamic heating temperature predictions were made for the interstage regions.

3.2.8.2 Summary

The single-tank concept was selected as the second-stage configuration, a decision based primarily on manufacturing and cost superiority. Bulkhead trade studies indicated that nested bulkheads produced shorter configurations of approximately equal weight. Thrust structure mounting of the LO_2 tank would provide a possible second-stage weight saving if dual-plane separation were used. However, the slightly longer separate tank concept was chosen utilizing single-plane separation and featuring relatively greater ease of fabrication. The resulting second-stage mass fraction was 0.9025.

The clustering structure (Figure 3.2.8-1) for the six 260-inch motors consisted of motorcase skirt extensions tied together by shear intercostals and redistribution rings. Cross-beams were used to stabilize the cross section and to redistribute axial loads. The aft end of the motor cases were tied together by links that permit differential growth.

The vehicle was supported on the launch pad by motor case base skirts, with three support points for each skirt and six redistribution longerons to distribute the concentrated loads. The resulting first-stage mass fraction was 0.8892.

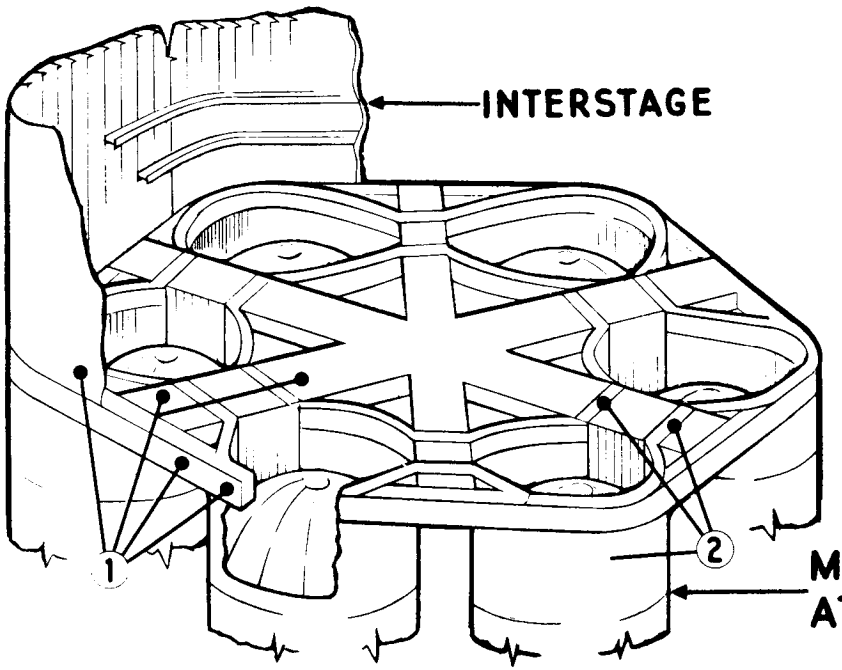

LOCATION	DESIGN LOAD	COMPONENT	WEIGHT
①	SYMMETRICAL MAX g'S	BOX RINGS	42,180
②	UNSYMMETRICAL TAIL-OFF	BOX BEAM	16,300
		SKIRT EXTENSION	118,500
		INTERCOSTALS	4,100
			181,080

Figure 3.2.8-1 CLUSTER STRUCTURE ASSEMBLY

3.2.8.3 Second-Stage Tankage Trade Study

The study was conducted to select a tank configuration concept for second-stage detail design. The concepts evaluated (Figure 3.2.8-2) are the single tank, the multicell tank, and the clustered tank. All configurations have five M-1 engines and a total propellant capacity of 8,218,000 pounds. Relative merits of the three concepts were evaluated from the standpoint of structural requirements, weight, ease of manufacture and assembly, and cost effectiveness.

3.2.8.3.1 Summary

The results of the study indicate that all three concepts are structurally feasible for second stage boosters. Table 3.2.8-1 compares the structural characteristics of the three concepts. The weight analysis indicates the multicell tank configuration is 8.5 percent and 38 percent lighter than the single tank and clustered tank, respectively. The large weight penalty for the clustered tank concept is due to cluster requirements and increased tank sidewall weight resulting from eccentric axial loads in the clustered tanks. A more efficient second-stage clustering concept might be designed if the number of second-stage tank engine modules equaled the number of first-stage motors. The manufacturing and cost analyses indicate that the single-tank concept has lowest manhour requirements and lowest total development and operating cost.

SECOND-STAGE TANKAGE CONCEPTS COMPARISON

	1 Single Tank	2 Multicell Tank	3 Clustered Tank
Weight (pounds) (Second Stage Structure)	449,100	410,720	659,790
Length (feet) (Second Stage)	155.4	139	186
Stiffness	---	---	Reduced
Slosh Provisions	Additional Requirements	Webs Provide Baffling	Additional Requirements
Interstage Transition	---	Complex	Complex
Development Testing	---	Increased Testing Required	Increased Testing Required
Secondary Stresses	---	Inherent in Design	---
Undetected Flaws	Thicker Welds	Weld Complexity (Hand Welds, More Lineal Inches)	More Lineal Inches
Cluster Structure	Not Applicable	Not Applicable	Complex

Table 3.2.8-1

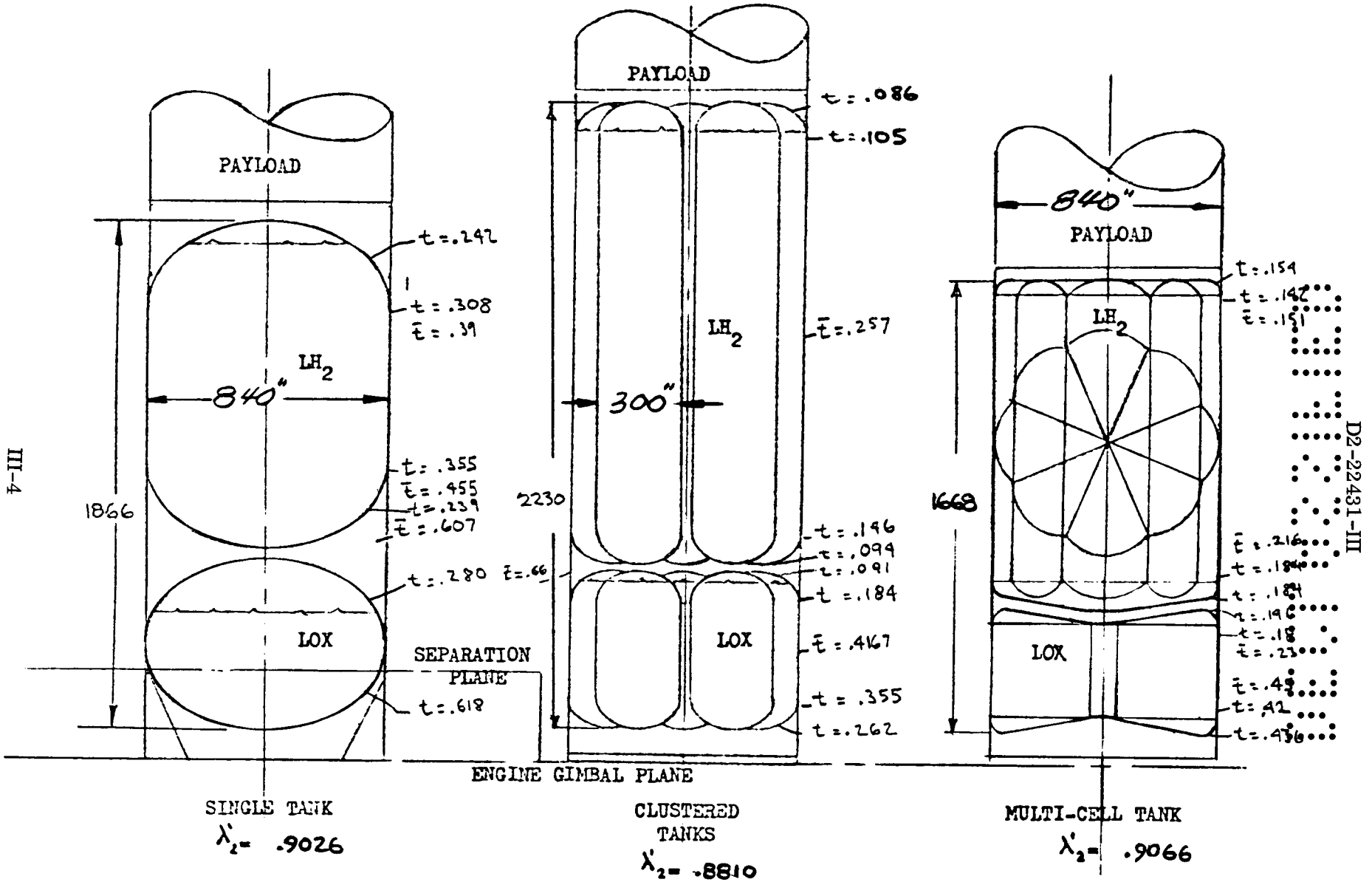

Figure 3.2.8-2 SECOND-STAGE TANK CONFIGURATIONS

3.2.8.3.2 Criteria and Loads

The loads criteria are given in 3.2.8.6.2 for the single-tank concept. Bending loads for the other concepts were scaled from the single-tank loads.

All three tank concepts were sized for equal ullage pressures plus thrust-acceleration gradients. All tankage concepts required stiffening of the sidewalls to resist the bending moments occurring during maximum-q load conditions.

With as-welded allowables in the weld zones, 2219-T87 material properties were used for all base metal shell structure (see 3.2.8.6.3.3). Unwelded material used was 7075-T6. To simplify the analysis, proof test design requirements were not considered for this trade study.

3.2.8.3.3 Single Tank

The single tank concept, Figure 3.2.8-2, utilized tapered waffle pattern stiffening in the LH_2 tank sidewalls. The heads were of constant thickness. The LO_2 tank was an off-loaded configuration, using 70.7- and 80-percent elliptical heads. The thrust structure consisted of crossbeams attached to a skin-stringer cone frustum.

The skin thickness requirements for this configuration are indicated in Figure 3.2.8-2. The maximum base metal thickness is 0.618 inch, which would require a weld thickness of 1.236 inches. The large Y ring will require considerable development to establish fabrication methods.

3.2.8.3.4 Clustered Tanks

The clustered tank concept, Figure 3.2.8-2, utilized tapered milled stringer stiffening in the sidewalls. The percent sidewall stiffening required for this configuration was greater than for the other concepts because of the greater shell loading per inch. This high loading was a direct result of the smaller effective cross section resisting bending and the eccentric axial load distribution caused by the interstage attachment to the outer edge. A trade was not performed on the additional cluster structure required to remove the eccentric load versus the tank penalty required to react the load.

Additional structural complexity is introduced in this concept because of the clustering requirements. A cluster structure is required at both ends of the second stage to provide shear continuity in the stage.

The maximum thickness of base metal in this design is 0.355 inch, which would require a weld thickness of 0.710 inch. The Y-ring requirements would be considerably less than for the single-tank concept.

3.2.8.3.5 Multicell Tanks

The multicell tank concept, Figure 3.2.8-2, used tapered waffle stiffening in the sidewalls. The heads were of tapered thickness. Separate tanks were used for the hydrogen and oxygen. The intercell webs in the upper tank were sized for the mass of the hydrogen in addition to the internal pressure. They were designed as stiffened shear-resistant webs of 7075-T6 material.

The webs in the oxygen tank were sized for a combination of the thrust load, oxygen mass, and internal pressure. They were designed as stiffened shear-resistant webs of 7075-T6 material. The thrust structure consisted of shear-resistant beams spanning the tank diameter and supported at the mid-point of the oxygen tank. The intersection of the skin panels and web used a Y-section extrusion. The maximum base-metal thickness for this design was 0.436 inch, which would result in a weld thickness of 0.872 inch.

3.2.8.3.6 Manufacturing Evaluation of Second-Stage Tankage

Configurations of liquid-second-stage tankage evaluated by the Manufacturing Department are shown in Figure 3.2.8-2.

The purpose of the evaluation was to compare the configurations in terms of:

- Manufacturing lead time and development
- Tooling requirements
- Fabrication and assembly processes
- Manpower, space, and equipment requirements.

The following program ground rules were used for the trade study:

- Program time period: R&D program 1965 through 1970, followed by a 10-year operational program.
- Maximum production rate: 12 stages per year.
- A new factory setup for the 70-foot-diameter tank will be required.
- Factory location will allow water transport of vehicles.

The results of the manufacturing evaluation are presented in 3.2.8.3.6.9 and 3.2.8.3.6.10.

3.2.8.3.6.1 Manufacturing Lead Time

The manufacturing lead-time differences were estimated from the general manufacturing plan and the production flow illustrations (Figures 3.2.8-3, 3.2.8-4, and 3.2.8-5).

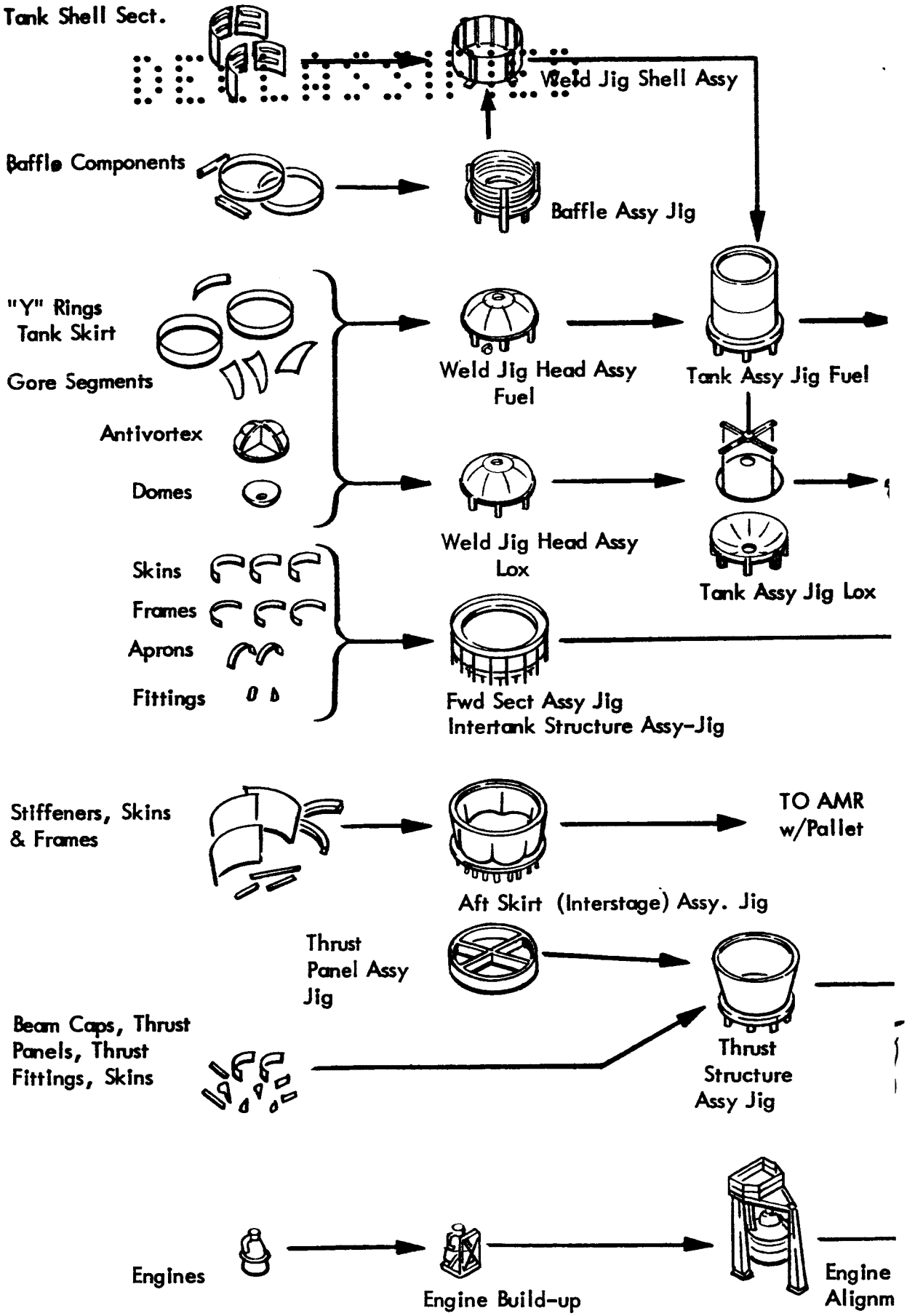

Figure 3.2.8-3 BODY P

Clean, Weigh & Balance
Detail Parts & Assemblies

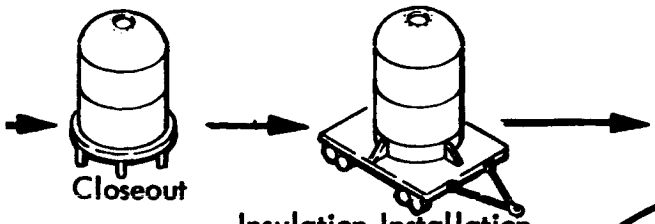

TANK TEST AND CLEANING FACILITY

1. Hydrostatic proof test
2. Determine volume by weights
3. Clean and seal

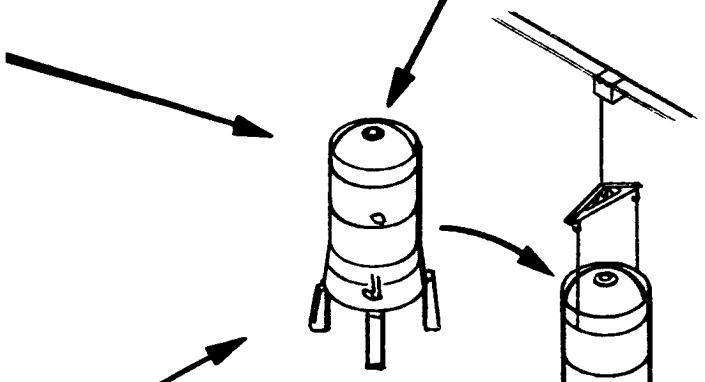

INSTALLATION OPERATIONS

1. Install mechanical, electrical and electronic subsystems
2. Weigh and balance

Transfer to standard handling pallet (This pallet is used on all operations until transfer to 1st stage at launch pad.)

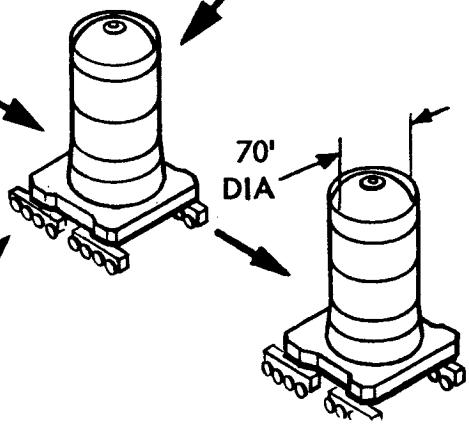

To Mfg. Tests

FLOW — SINGLE TANK

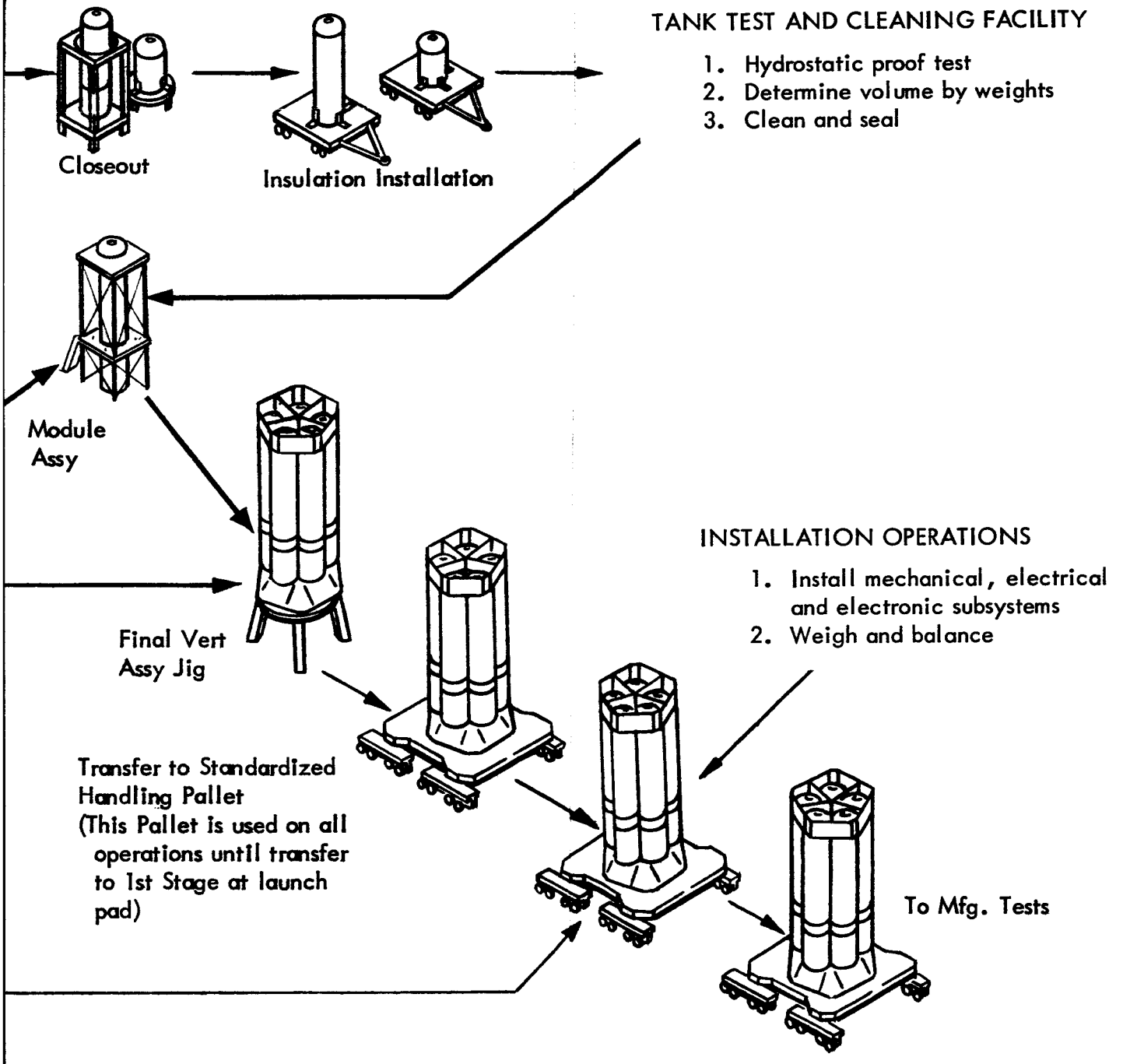

N FLOW — CLUSTER OF FIVE

2

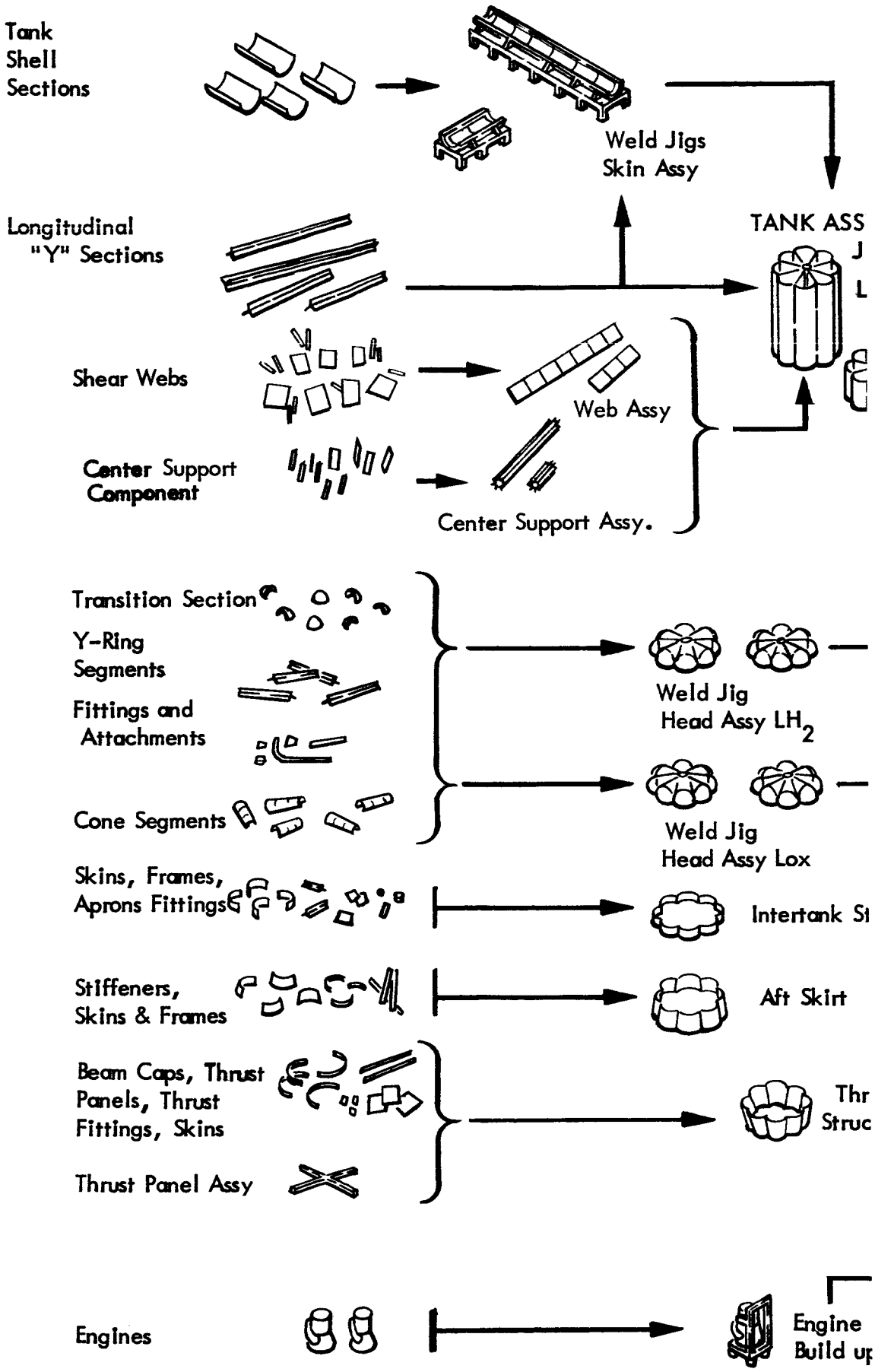

Figure 3.2.8-5

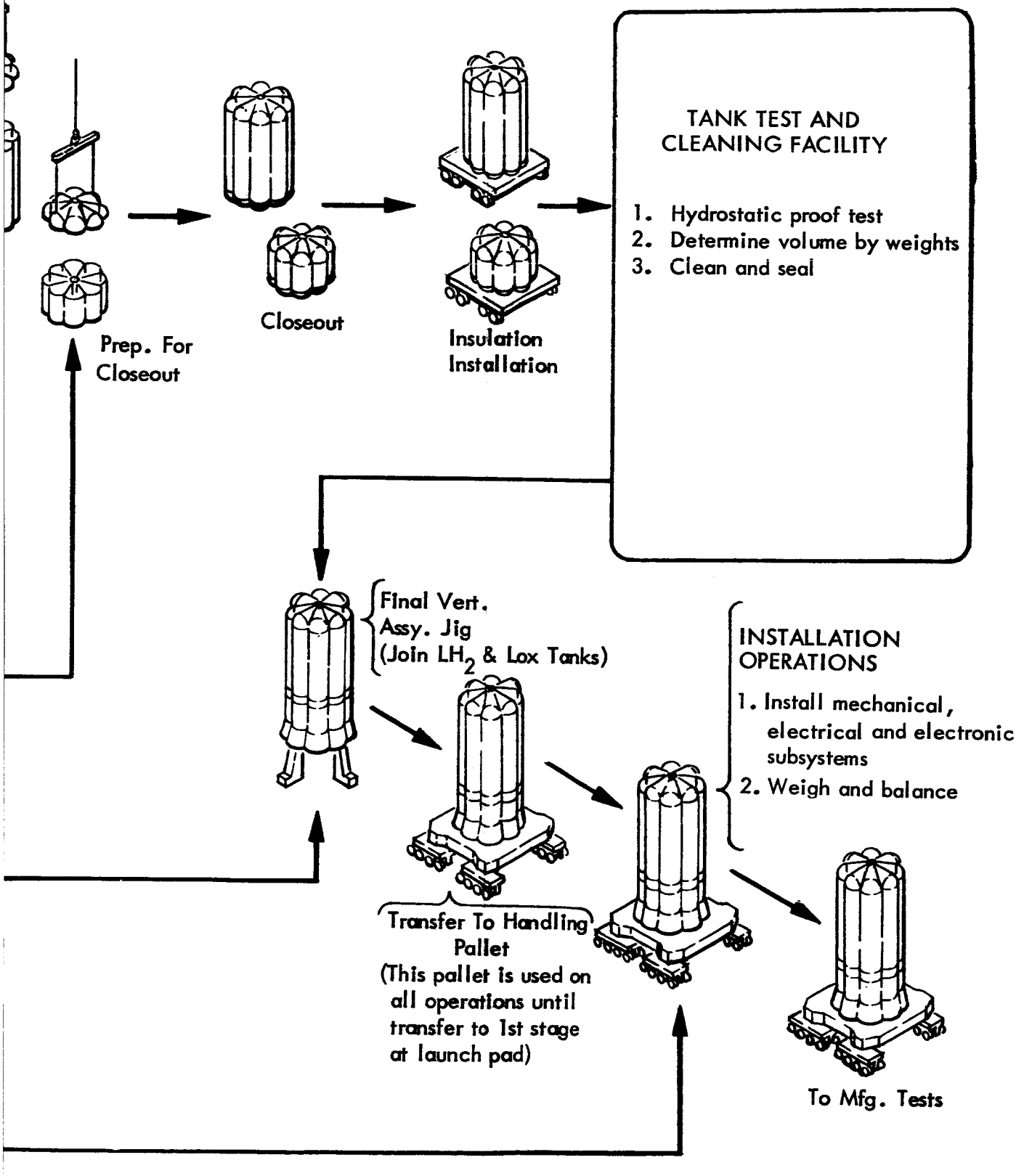

I FLOW — SEGMENTED TANK

The lead-time differences were not considered significant for the multicell and single tanks. The clustered tank could be produced, except for stage assembly, in existing facilities. Manufacture could thus begin earlier on the clustered tank, and the time till first-unit production could be reduced accordingly.

3.2.8.3.6.2 Tooling Requirements

The tooling required for the large single tank must be capable of handling larger and heavier parts than for the other configurations. Multicell tank assembly involves joining more parts and requires more tools of greater sophistication. The cluster structure will require the greatest number of major jigs due to the multiplicity of sub- and major assemblies involved in manufacture.

The major tooling for all configurations is programmed as hard tooling, capable of achieving the quality requirements and of enduring for the scheduled rates of the 10-year program.

3.2.8.3.6.3 Fabrication Processes

Large Single Tank — The fabrication processes for the large single tank were divided into the following areas: Y rings, tank-wall skins, heads, and fittings. Each area will be discussed briefly. A detailed manufacturing plan may be found in Section 3.4.1.

The manufacture of the Y rings for the large tank will be a major problem area. A detailed discussion is presented in 3.4.1.

Fabrication of tank-wall skins will be a major problem area because of component size. To reduce the amount of welding, the largest available sheet sizes should be used. The major problem will be forming the skins containing integral stiffening.

The tank heads must be fabricated from many segments because of sheet size limitations. The parts can be standardized so that only seven major contoured shapes will be required. The proposed subassembly weld sequence will allow payoff trim after welding so that part fit-up and coordination will be reduced to a minimum. This will also provide good weld-inspection position.

The large tank will have several fittings for filling, draining, venting, and cleaning. The machining of these fittings, which are later welded into the tank, will be a problem area. Of the three configurations, the large tank will contain the least number of these problems.

Clustered Tank — The fabrication requirements for the clustered tank will be similar to those of the single tank. No specific problems are visualized that will not be solved on the Saturn S-IC and S-II contracts. The main disadvantage is high manufacturing cost compared with the single tank or multicell tank. The

main advantages are saving of some facilities and tooling costs and salvage of other capital expenditures on the Saturn program. The greater learning-curve improvement possible with this configuration (5 tanks of the same size per vehicle) did not alter the total manufacturing cost disadvantage because of the low total vehicle quantity requirements and high cost of thrust and cluster structure.

Multicell Tank — The fabrication processes for the multicell tank were divided into the following areas: Y rings, tank-wall skins, head segments, and fittings. The major process steps for these items are illustrated in Figure 3.2.8-6.

The multicell tank has different Y-ring problems than the large single or clustered tanks. Each cell segment will be joined to the other by a Y longitudinal, and Y-ring segments will also be required to join the heads, skirts, and walls. The number of Y-ring segments will, therefore, be greater for multicell tanks. The number of shapes required complicates the fit problem, and the joining of Y-ring segments is a major problem. Special forged fittings can be used at intersection points to reduce the fit and weld intersect problems.

The Y-ring segments will be machined as flat spar mill parts from bar stock. This method will allow milling cross-sectional buildups for weld joints and to obtain minimum part weight. Forming and trim-for-fit will follow the machining operations. Stringent detail part tolerances will be required because of fit requirements for welding.

The tank walls will be a major problem area because of size and shape. The major problem will be forming of the skins containing waffle-pattern stiffening (and integral Y ring, if this option is adopted). Some of these problems will be solved on the Saturn program.

The tank heads are made from several segments because of sheet size limitations. By standardizing the part size, a minimum of forming and trimming tools will be required. A major welding problem exists at the intersection of the center close-out ring and the head segment subassemblies. Fit-up problems with the close-out ring, Y-ring segments, and skins are greatest with this configuration.

The multicell tank has several fittings for fill, drain, and vent openings; manholes; and the center close-out ring. The fit problems with the mating parts will be a major problem for weld quality. The multicell tank will have more fittings than the other two configurations; therefore, more fit-up problems are expected.

3.2.8.3.6.4 Assembly Methods

Single Tank — The assembly methods for the single tank were divided into subassembly, tank final assembly and test, and vehicle joining.

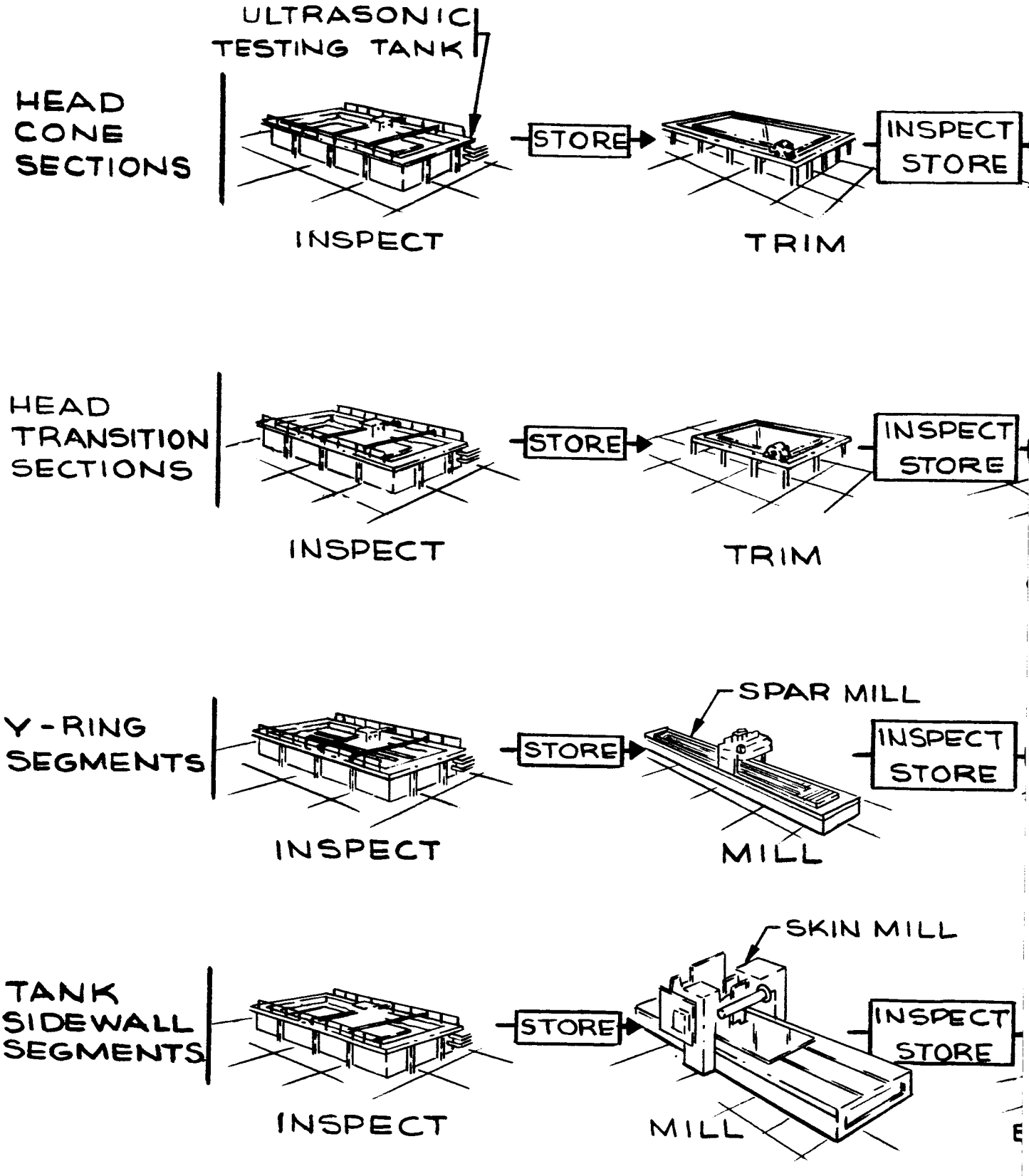

Figure 3.2.8-6 MULTICELL

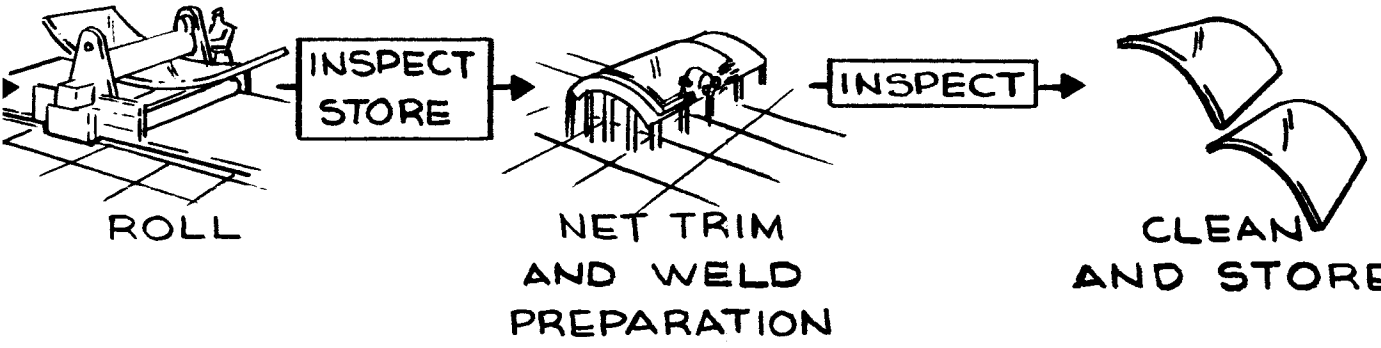

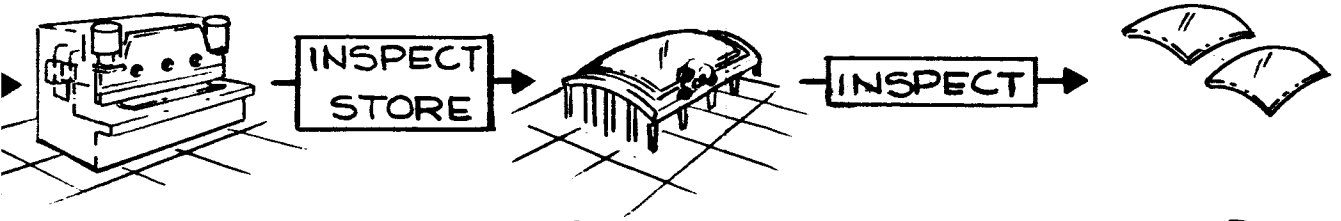

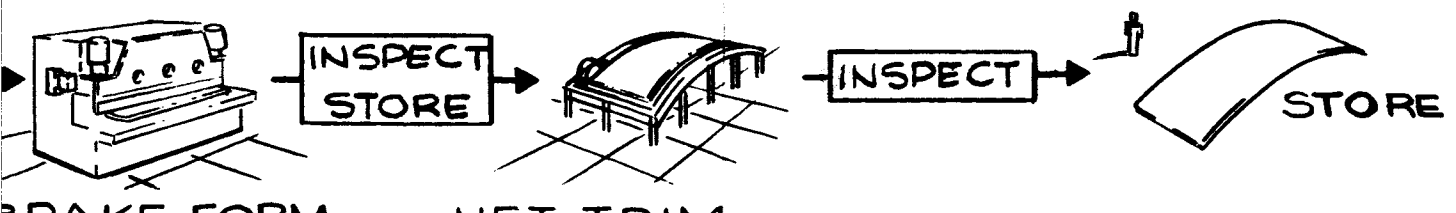

DETAIL FABRICATED PARTS

Vehicle subassembly has been sequenced into subassemblies of heads, sidewall hoops, internal baffles, and external structure. The head subassembly production break was selected so that the final assembly joining weld would be a lower-stress circumferential weld. This break will also allow trim of head assembly and sidewall hoop assemblies after subassembly welding. Mismatch of detail parts will not be as critical, which will allow less stringent detail part forming and trimming tolerances. The only critical coordination will be circumference (pi tape check) and flat plane (level check).

The sidewalls will be made by welding formed segments into hoops. Control of circumference can be obtained by special trim prior to making the last weld. Quality control check of the higher-stress longitudinal weld joint can be easily accomplished by X-ray methods, and weld repair can be accomplished readily in this subassembly position. Clamping, weld-joint backup, and starting tabs are easily provided.

The internal baffle subassembly will be accomplished in separate tooling, which will allow most efficient assembly. The baffle subassembly will then be installed in the completed head or tank-wall hoop assembly prior to final subassembly joining. Tank-final-assembly work activity will thus be reduced to a minimum.

The skirt and thrust structure will be nearly the same for all three tank configurations. This structure will present no major problems other than size. The intertank structure of the large tank will be longer than that of the multicell tank, but will replace some of the tank sidewall.

The final assembly of the tank will consist of joining the selected subassemblies by welding. This operation will be accomplished similar to the Saturn S-IC method of tank assembly. This method eliminates gravity side effects and gives uniform weld position so that constant equipment settings can be used. One problem area will be the X-ray inspection of the close-out welds for joining. This may be solved by special work platforms. After welding is completed, the tank assemblies will be cleaned, proof tested, and joined with the other major structure subassemblies.

The final vehicle joining operation will be in the vertical position for the same reasons given for vertical tank assembly. One problem at vehicle joining will be the clamping and fitting of subassemblies prior to joining. A second will be the requirement to coordinate circumferences of the subassemblies. The single large tank is the best of the three configurations when considering this problem because interfaces will be circular shapes in a single plane.

The vehicle assembly will be moved in the vertical position directly to a reusable GSE handling pallet. This pallet system will be used as a line dolly in the remaining factory operations.

The single tank has much plumbing between engines, pumps, and tanks. Of the three configurations, the piping problem is minimum for the large tank.

The insulation of the hydrogen tank will be a major problem. However, the simple cylinder body and elliptic head shape of the large tank make this the easiest to insulate of the three configurations.

Other installation problems common to all configurations were not investigated during this phase of the study.

Clustered Tank — The assembly methods for the clustered-tank vehicle will be similar to the single large tank vehicle except for tank size, quantity, and clustering requirements.

The 25-foot tank diameter will make all tank fabrication problems easier, but the quantity of five tank assemblies per vehicle will approximately double the work required when compared to the single-tank vehicle. To this will be added the clustering operations, so that, from a manufacturing cost standpoint, the clustered tank is the least desirable of the three configurations. Complete evaluation of this configuration was not made.

Multicell Tank — The assembly methods for the multicell tank were divided into subassembly, tank final assembly and test, and final vehicle joining.

The multicell tank can be assembled by several sequences. One method considered would make subassemblies of the cells as units that are assembled to the center column. The selected method will use head and body shell subassemblies that will be joined in the vertical position similarly to that proposed for the large single tank. A special detail trade study was made to make this selection and is tabulated in data following. The major reasons for the selection were increased reliability and decreased work load in the final assembly joining position. A discussion of the selected method follows.

The multicell tank was broken into head and body shell subassemblies and further subassemblies. The head subassembly is shown in Figure 3.2.8-7.

This breakdown will allow X-ray inspection and repair and proof test of the higher-stressed longitudinal weld joints in the subassembly work position. Clamping and weld backup will be more easily provided. The close-out final assembly joining welds will be in flat planes along the lower-stressed circumferential joints. Also, the length of weld accomplished in final assembly joining will be minimum.

The body shell subassembly will consist of all structure between the head circumferential joints. Sub-subassemblies of outer skin details, longitudinal Y joints, and interior tension webs and center columns will be joined in the position shown in Figures 3.2.8-8 and 3.2.8-9.

This breakdown subassembly method will allow welding of one-half of the high-stress longitudinal welds in the flat position. It will provide excellent clamping, weld backup, weld preheat, weld postheat, and trim arrangements.

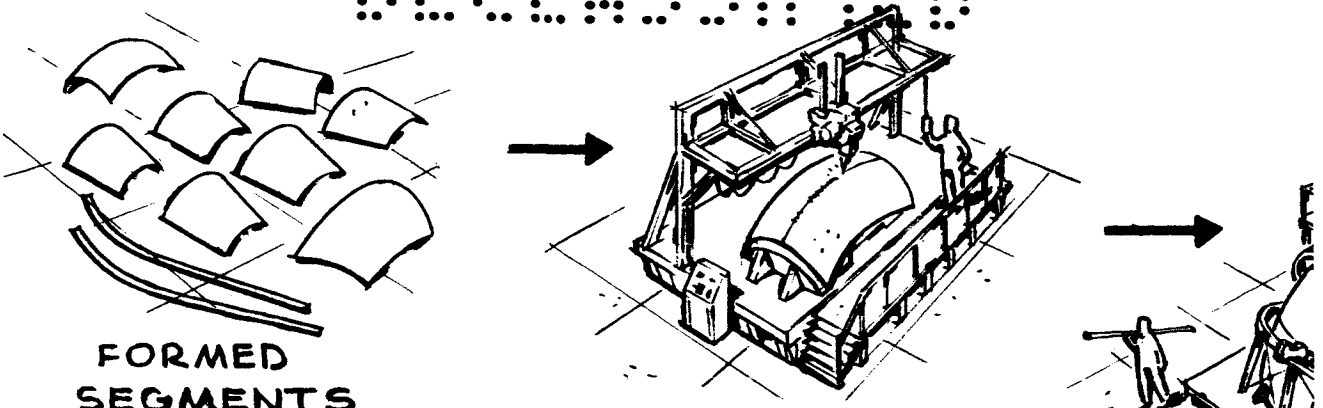

FORMED SEGMENTS AND "Y" SEGMENTS

JOIN SPHERICAL FORMED SEGMENTS

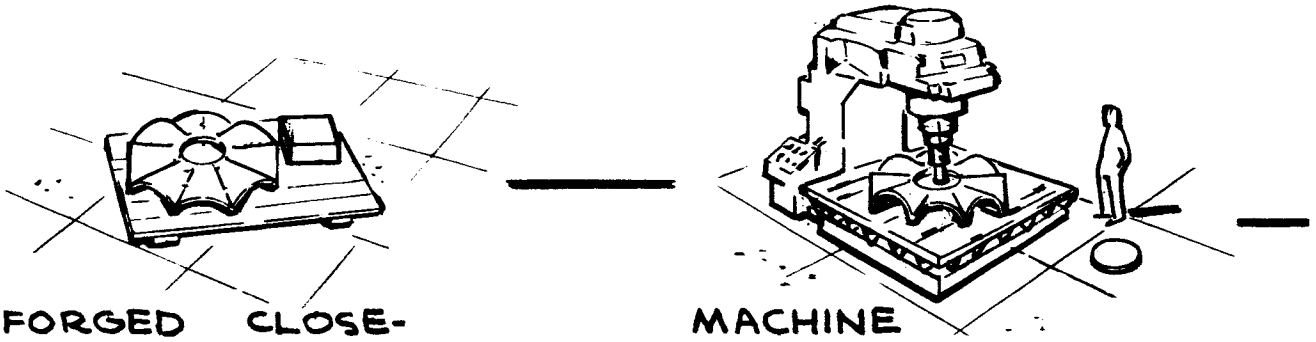

FORGED CLOSE-OUT RING & MANHOLE COVER FROM PLATE STOCK

MACHINE FORGED RING & MANHOLE COVER

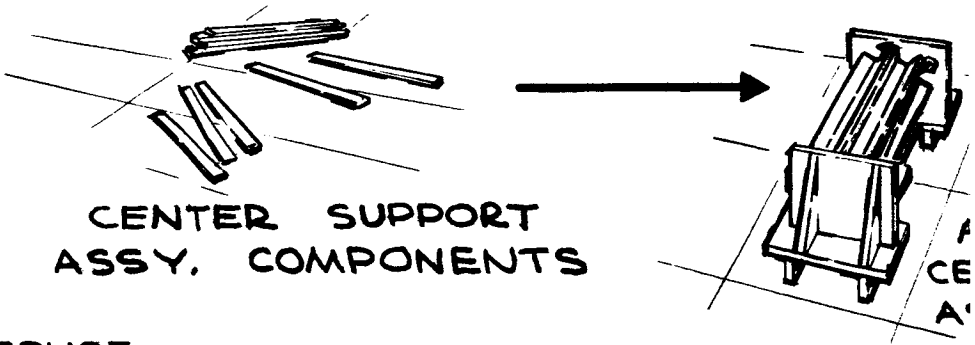

CENTER SUPPORT ASSY. COMPONENTS

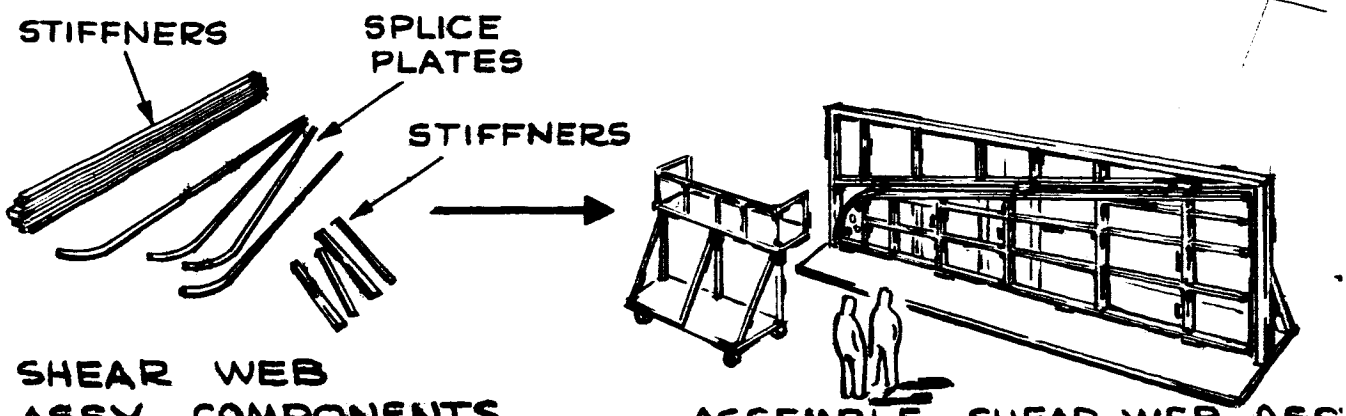

SHEAR WEB ASSY COMPONENTS

ASSEMBLE SHEAR WEB ASS

Figure 3.2.8

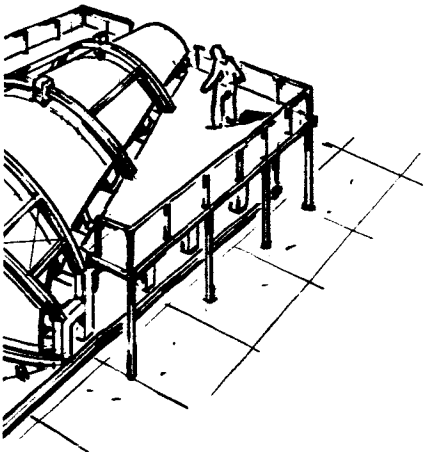

ASSEMBLE
HEAD SECTIONS,
ATTACH "Y" SEGMENTS

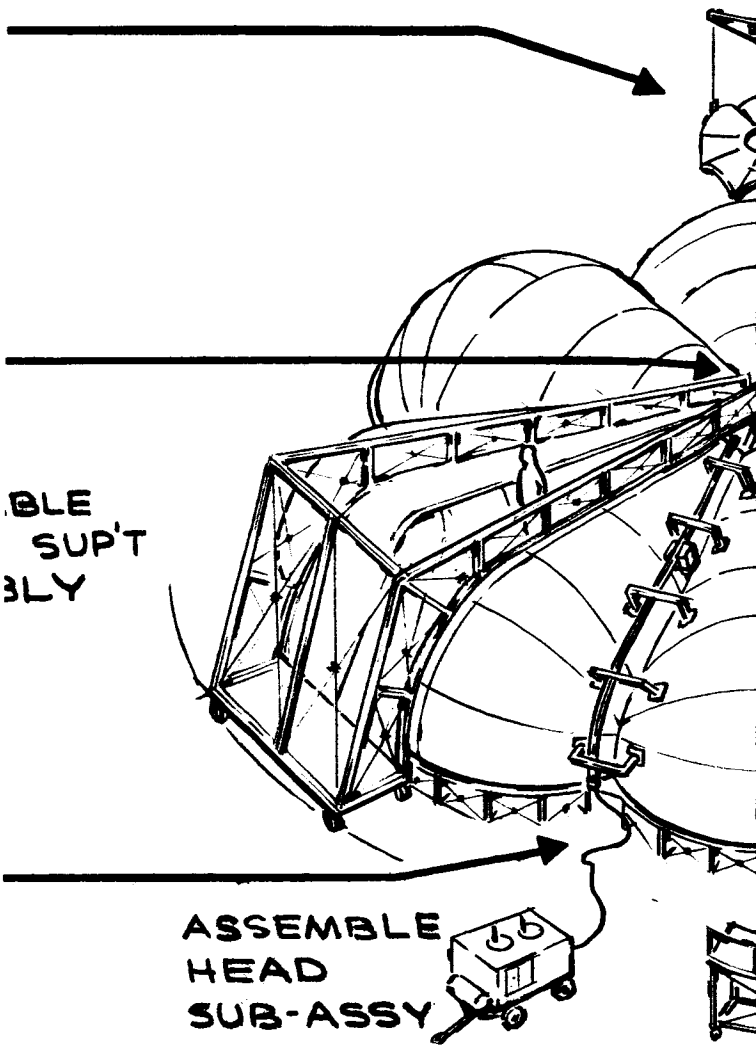

.BLE
SUP'T
3LY

ASSEMBLE
HEAD
SUB-ASSY

.TICELL HEAD ASSEMBLY

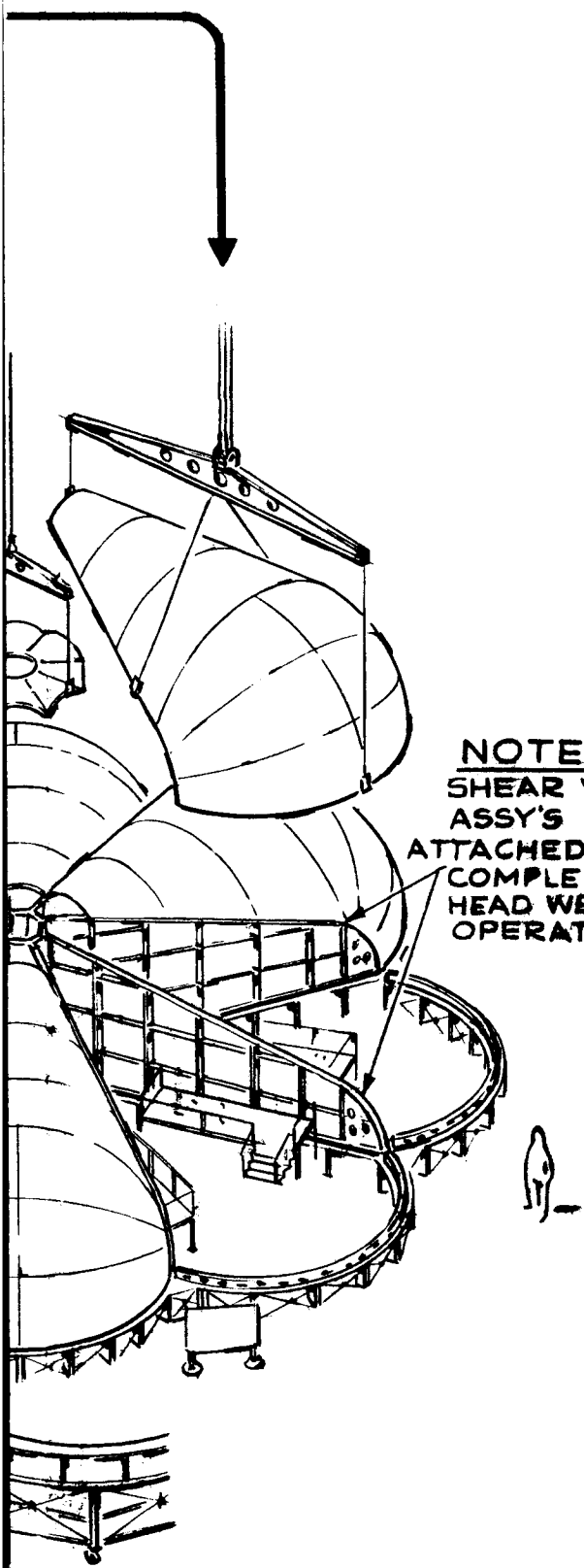
NOTE:
SHEAR WEB ASSY'S ATTACHED AFTER COMPLETION OF HEAD WELDING OPERATION.

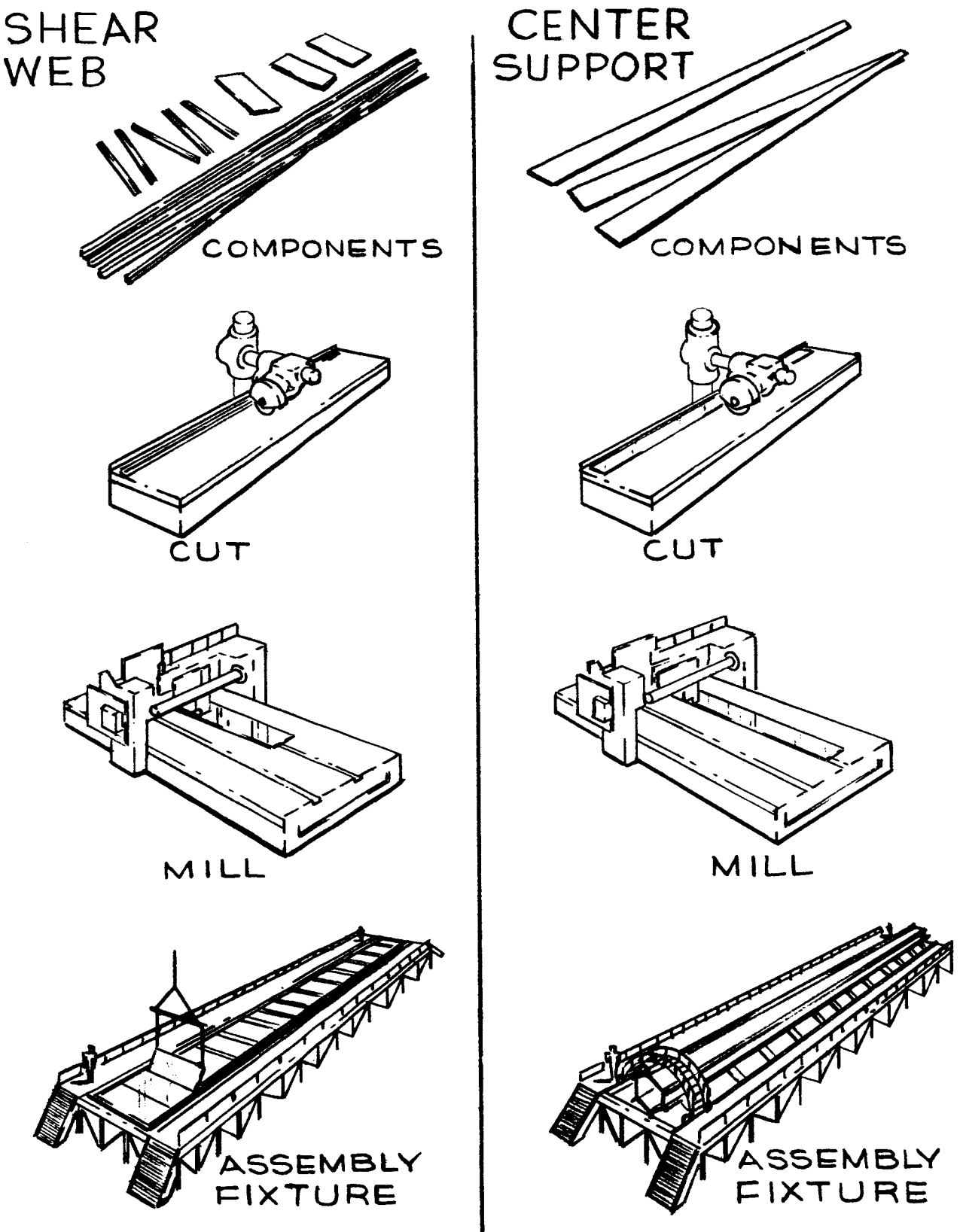

Figure 3.2.8-8 MULTICELL TANK TYPICAL MINOR ASSEMBLY

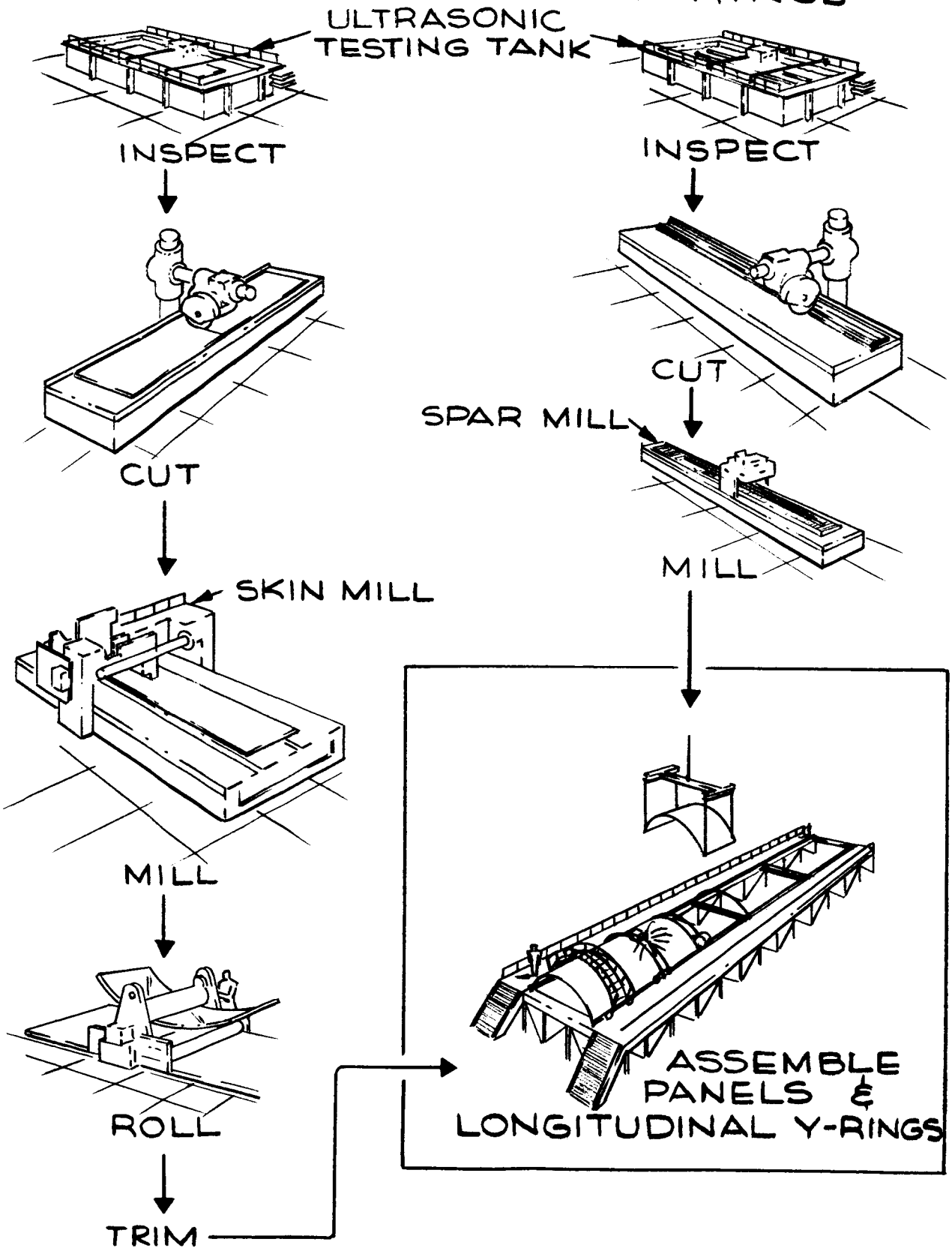

Figure 3.2.8-9 MULTICELL TANK SIDEWALL ASSEMBLY

The sub-subassemblies will be loaded into a vertical assembly jig where the remaining eight longitudinal welds will be completed. This position will eliminate gravity side effects and give single-plane weld position so that track and constant equipment settings can be used. This is shown as Operation No. 1 on Figure 3.2.8-10. This arrangement will allow weld backup and clamping, and X-ray inspection of all higher-stressed longitudinal welds prior to close-out welding. This assembly sequence will provide higher tank quality. The work position and sequence of the head-joining close-out welds are shown in Operations 2 and 3 on Figure 3.2.8-10.

After completion of welding operations, the final attachment of the shear web assemblies to the Y flange will be made. This will allow clamping adjustment and fitting of parts for the weld operations.

The completed tank will be cleaned, tested, and then joined with the other major assemblies. The final joining of the major assemblies will be accomplished in the vertical position similar to the single-tank joining method. The major differences are the increased difficulties resulting from the multicell shape. The skirts, intertank, and thrust structure will have this shape and the forward skirt will have a transition from the multicell shape to the circular payload section shape.

The multicontour of the multicell tank will make installation of insulation more difficult; the increased number of manholes, drain fittings, and plumbing, and the coordination of circumferential multicell joints will be more difficult.

Multicell Tank Subassembly Method Trade Study — A trade study was made to determine an optimum multicell tank subassembly sequence. Two methods were compared: (1) subassembly of fuel cell and center-post assembly, and (2) subassembly of heads with shear webs and center post and subassembly of sidewalls with shear web and center post.

Advantages of full cell method (Method 1) are as follows:

- Shear web can be assembled in one piece.
- Joint of web to center post in one length.
- Best assembly method for small quantity R&D program by elimination of some subassembly positions.

Disadvantages of full cell method:

- More difficult to provide backup clamping and X-ray inspection of close-out welds.
- Sequence of weld starting tabs is cumbersome.
- Must coordinate eight interfaces that are compound curved surfaces in eight planes, for a total length of 1200 feet (both tanks).

BLANK

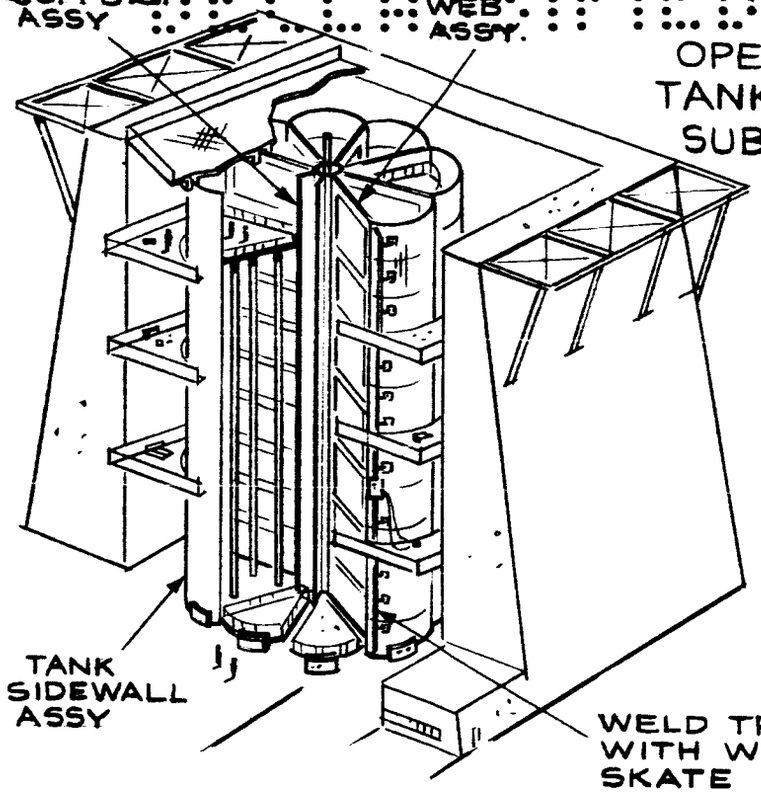

OPERATION #1 TANK BODY SHELL SUB-ASSEMBLY

1. INSTALL CENTER SUPPORT SECTION
2. INSTALL SHEAR WEB ASSY'S AND TANK SIDEWALL ASSY'S
3. FIT PARTS & CLAMP (VACUUM CHUCK). INSTALL WELD BACK-UP BARS.
4. WELD LONGITUDINAL "Y" JOINTS (8) PLACES.
5. X-RAY INSPECT
6. COMPLETE MECHANICAL FASTENING OF SHEAR WEBS.

TOP JIG HEA
& WORK PL
FORM IN RE
TRACKED
POSITION

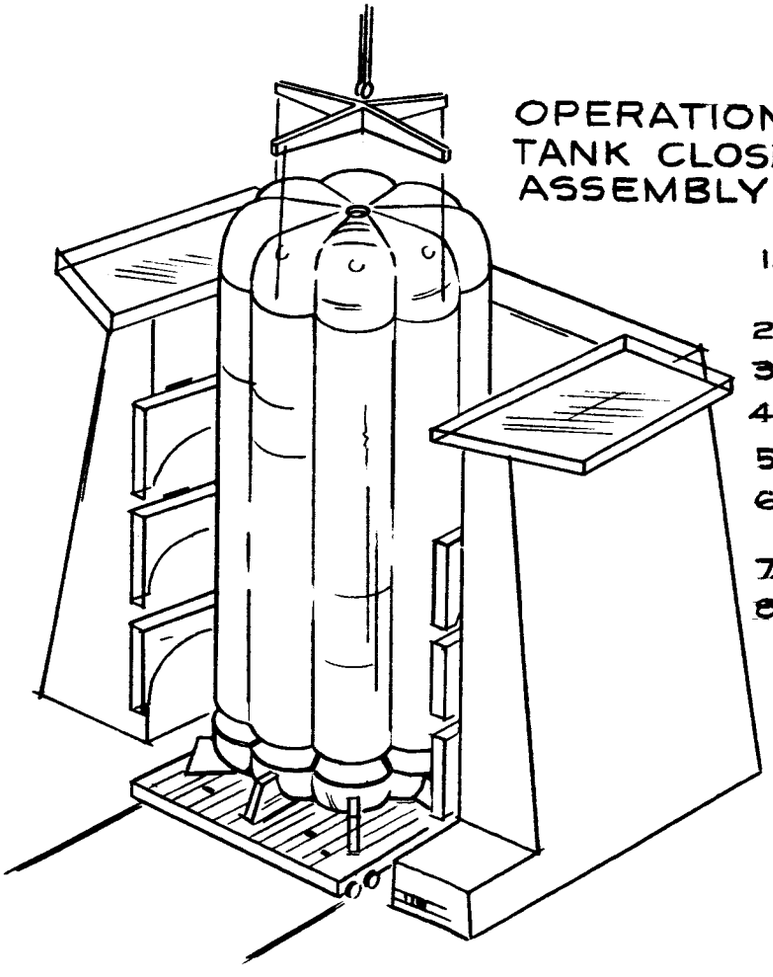

OPERATION #3 TANK CLOSE OUT ASSEMBLY (BOTTOM)

1. TRANSFER LOAD FROM LWR. SU
   TO OVERHEAD CRANE SUPPORT
2. REMOVE INTERNAL VACUUM CLA
3. LOWER INTERNAL PLATFORM ASS
4. INSTALL SCAFFOLDING IN LWR.
5. POSITION BOTTOM HEAD FOR W
6. FIT PARTS & CLAMP (VACUUM
   & INSTALL WELD BACK UP BA
7. WELD CIRCUMFERENTIAL JOI
8. X-RAY INSPECT

Figure 3.2.8-10 MULTI

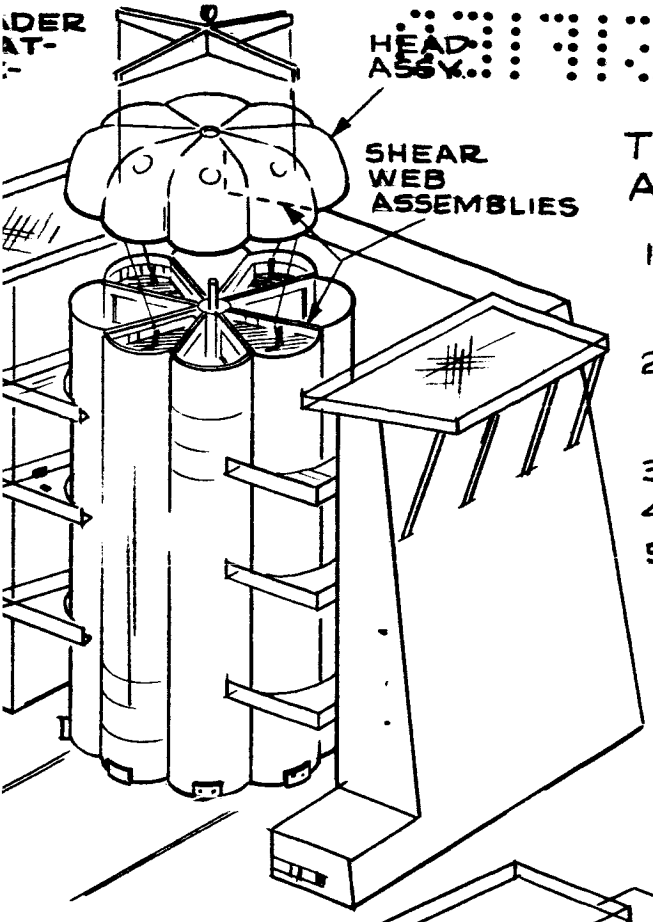

OPERATION # 2
TANK CLOSE OUT ASSEMBLY (TOP)

1. REMOVE TOP JIG HEADER AND REPLACE WITH COMPLETED HEAD ASSY.
2. FIT PARTS & CLAMPS (VACUUM CHUCK) & INSTALL WELD BACK UP BAR.
3. WELD CIRCUMFERENTIAL JOINT.
4. X-RAY INSPECT
5. COMPLETE SPLICING OF INTERNAL SHEAR WEBS.

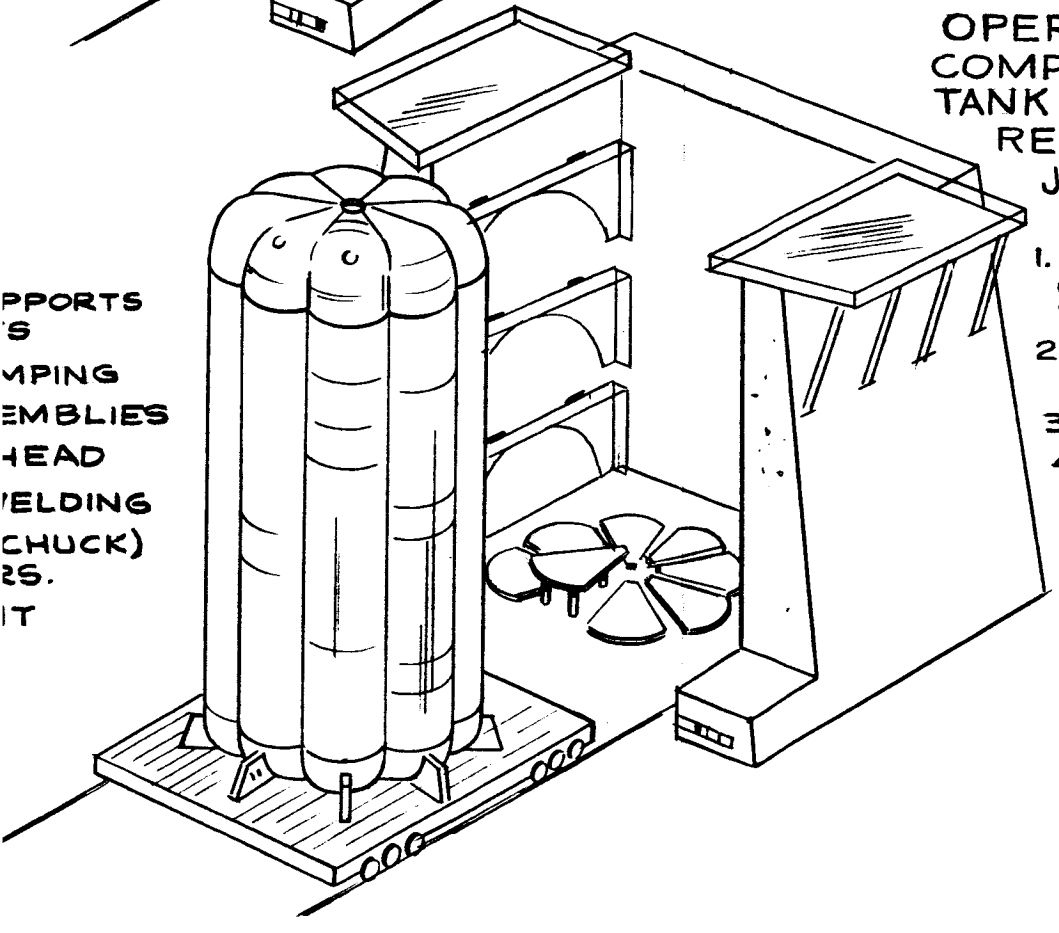

OPERATION # 4
COMPLETE ASSEMBLY TANK INSPECTION & REMOVAL FROM JIG

1. COMPLETE SPLICING OF INTERNAL SHEAR WEBS.
2. REMOVE INTERNAL SCAFFOLDING
3. CLEAN
4. FINAL INSPECTION
5. REMOVE FROM JIG

▼

TO CHEM CLEANING & HYDRO STATIC TEST

CELL TANK ASSEMBLY

- Nine major pieces must be subassembled.
- Size of major subassembly piece is approximately 27.5 x 35 x 110 feet.
- Close-out weld joint is highest-stress longitudinal weld.
- Work position is vertical over full length of tank.
- Weld is vertical and overhead (or must turn tank over to eliminate overhead welding).
- Assembly area must be larger to provide clearance on eight sides.
- Must weld inner fitting on head in the final assembly position.

Advantages of head-sidewall subassembly method (Method 2):

- Close-out weld is circumferential and in only two horizontal planes for a total length of 440 feet.
- Weld joint is lower-stress circumferential type at close-out.
- Starting tabs only needed two places for close-out.
- Only three major subassemblies.
- Size of pieces is 70-foot diameter with height of 20 feet for heads and 70 feet for body shells.
- Work position is horizontal at top and bottom, inside and outside.
- Assembly does not have to be rotated to eliminate overhead welding.
- Vertical jig has one-side loading only, thus saving floor space.
- Best high-production breakdown.
- Center close-out ring fitting is welded as a subassembly operation.
- Subassemblies are lightest.
- Backup for welding and internal scaffolding easier to provide.
- Easier to preheat and postheat weld areas.

Disadvantages of head-sidewall subassembly method:

- Must join shear web internally requiring scaffolding and cleanup.
- Must coordinate interface between three subassemblies.
- Shear web has splices at head-to-shell break point.

3.2.8.3.6.5 Equipment Requirements

The equipment requirements were compared for noncommon items only. The heavier gages in the single tank will require equipment capable of handling heavier material. The large elliptical heads will also have many more sections

to be bulge-formed than the multicell tank heads. The large single tank will need a much larger machine for preparation of the Y rings than will the clustered vehicle. Machining requirements for the tank skins will be greatest for the clustered and multicell tank and least for the large cylindrical configuration.

The single tank will require the fewest pieces of equipment for processing heavier material and the clustered concept will require more individual pieces of equipment. The difference in equipment requirements for the three configurations did not significantly affect the trade study results.

3.2.8.3.6.6 Space Requirements

The manufacturing flow would be similar for each configuration. This would indicate that the space requirements would be nearly equal for either vehicle.

The size of the multicell and the single tank configurations is such that consideration of the manufacture of either structure in an existing facility is prohibited. Component parts for all configurations, however, could be fabricated in existing plants.

The clustered tank is small enough to be manufactured in facilities that are being prepared for the Saturn program. Final stage integration would then require new facilities either adjacent to this existing plant or at the test facility.

3.2.8.3.6.7 Manufacturing Process Development

The manufacturing development work required for all three configurations is a major problem. The clustered tank is more related to the Saturn S-IC program in size and shape and, therefore, will require the least development work.

The single tank will require more thick-gage welding development work. The forming problems are more stringent for the multicell tank. The single tank and multicell tank are about even in the amount of development work required.

3.2.8.3.6.8 Manufacturing Manpower Requirements

Manufacturing manpower estimates made for the three configurations were based on the preceding manufacturing plan, the engineering definition, and preliminary engineering weight statements. The order of preference is: (1) single tank, (2) multicell tank, and (3) the clustered tanks.

The primary factors affecting the manpower requirements were identified as total number of parts, forming and machining requirements, and assembly complexity. Although the single-tank configuration will use heavier individual parts with consequent increases in handling, machining, and forming problems, the number of parts will be fewer and, hence, the assembly operations will be simpler and require less manpower. Also, tooling requirements will be less than for the other configurations.

The multicell configuration was penalized by the large number of parts required for the tankage and the increased assembly complexity. The clustered tank concept is the most expensive to produce, caused primarily by the need for relatively large numbers of detail parts, subassemblies, and major assemblies.

3.2.8.3.6.9 Summary

The preceding analysis has allowed the comparison of the three tank concepts from producibility and cost considerations. Several manufacturing comparisons are indicated in Table 3.2.8-2.

The advantages and disadvantages anticipated in the manufacture of the various concepts are summarized as follows.

Advantages of single tank:

- Least linear feet of weld joint.
- Least sidewall area to machine, form, and trim.
- Simpler shapes for heads and detail parts.
- Subassembly interfaces are simple circles joining on one plane.
- Coordination of subassemblies can be checked with simple pi tape measurements.
- Forming tolerances of detail parts are less stringent.
- Interior baffles are easier to install and create less trouble during final assembly than multicell shear webs.
- Weld X-ray procedures and techniques are developed and accessibility problems for inspection are fewer and less complex.
- Easier to clean because of less internal structure.
- Final assembly work can be accomplished at fewer work-level positions.

Disadvantages of single tank:

- More head area to chem mill or machine.
- Heaviest detail parts and subassemblies.
- Thicker plates will require heavier tooling.
- Gage thicknesses generally require multiple-pass welds.
- Gage thicknesses require more X-ray inspect times per weld and longer exposure time per inspect.
- More weld starts and stops than multicell tank.

MANUFACTURING FACTORS FOR CONFIGURATION COMPARISON (1)

CONSIDERATION	CONFIGURATION: Multicell Percent Total Task (Weighted)		CONFIGURATION: Single Percent Total Task		CONFIGURATION: Clustered Percent Total Task (Weighted)	
Welding	45		30		54	
Total Length of Welded Joint		151		100		189
Total Dist. Weld Head Travel		49		100		64
Total Starts and Stops (2)		96		100		177
Total Number of Joints (3)		156		100		183
Handling (4)	5		5		3	
Details — Heads		32		100		42
Subassembly — Heads		46		100		30
Head Sections		36		100		32
Details — Tanks		54		100		69
Subassembly — Tanks		23		100		13
Tank Section		220		100		85
Welded Parts Fabrication	33		20		58	
Total Number of Parts		115		100		144
Pocket-Machined Parts (Area)		237		100		610
Taper-Machined Parts (Area)		70		100		70
Y Rings (Length)		100		100		179
Nonwelded Parts Fab & Assy	17		25		33	
Total Weight		68		100		121
Joining and Miscellaneous	25		20		37	
TOTAL MANUFACTURING TASK	125		100		185	

(1) This table compares the multicell and the clustered configurations with the single-tank configuration on a relative basis for each consideration. The single-tank configuration was given a rating of 100 for each consideration. The processes were then rated to determine the percent of the total task that they represent for each configuration. The total manufacturing task comparison is indicated in each column.

(2) Includes starts and stops required for X-ray inspection as well as initial start and final stop.

(3) Total number of interfaces that will require separate weld setup.

(4) Considers both weight and quantity.

Table 3.2.8-2

- Y-ring fabrication requires considerable development.
- Several circular interfaces to coordinate during subassembly.

Clustered Tanks:

The clustered tank was analyzed sufficiently to determine that the machining, welding, and forming tasks were greater than for the other configurations, but that detail parts and subassemblies were smaller, lighter, and easier to handle. The biggest advantage of using the clustered tank is that the work could be accomplished, to a great extent, in existing facilities using tools, equipment, and procedures that have been or are being developed. The increased quantity of tanks would allow greater improvement-curve efficiency. Preliminary cost estimates established that this concept was most costly, and further study was not made.

Advantages of multicell tank:

- Most detail parts and subassemblies are lighter and smaller.
- Skin thicknesses and part sizes ease detail-part forming problems.
- Some subassemblies can be accomplished in existing facilities.
- Single-pass welding satisfactory for most skin thicknesses.
- Less exposure time required for X-ray weld inspection.
- Fewer starts and stops during welding.
- Less head area to machine or chem mill.

Disadvantages of multicell tank:

- Complex curvature and join pattern of parts creates requirement for close detail-part forming tolerances.
- Geometry and internal structure complicates fit-up.
- Fixtures for fit-up and weld backup are complicated and expensive.
- Weld X-ray inspection difficult and expensive due to scaffolding requirements and accessibility problems.
- More joint length to fit-up and weld than on single tank.
- More welded detail parts to fabricate, handle, and fit-up.
- More integral-stiffened sidewall machining required.
- Hand welding required in several places.
- Tack welds, which must be chipped out and rewelded, may be required at several places during assembly.
- Cleanliness problems increased due to need for more internal structure and internal mechanical joints.

- Must weld Y longitudinals.
- More configurations required in detail parts and subassemblies.

3.2.8.3.6.10 Conclusions

The three concepts are all considered to be producible designs. The preceding analysis has indicated a somewhat different approach for the three designs in fabrication and assembly, but represents a practical method of completing the task for each configuration. The most important differences are in the areas of manufacturing technical risk and total manufacturing manpower requirements.

The single tank was selected as the most desirable candidate from the manufacturing standpoint. This concept has lowest manpower requirements and lowest technical risk.

The multicell structure, which is higher in both areas, is the next preference for manufacture. The clustered tank, which is closer to an existing design than either of the other concepts, has the lowest order of technical difficulty but would require the most manhours. The clustered tank configuration was thus considered least desirable for manufacture.

3.2.8.3.7 Cost Effectiveness Analysis

Guide Lines — Cost effectiveness for a system composed of the T65A system but with three different designs of second-stage tankage is shown in a comparison using the study data listed below:

- T65A development and operating cost with cost changes due to second-stage tankage structure changes (single, clustered, or multicell tanks) as shown in Tables 3.2.8-3 and 3.2.8-4. Costs are for a total of 140 launches in a 10-year period.
- Vehicle cumulative average reliabilities shown are the same as used for the T65A vehicle, Section 3.1.10.8.
- Vehicle payloads of 1,114,550 pounds for the vehicle with single second-stage tankage, 896,090 pounds with clustered tankage, and 1,152,680 pounds with multicell tankage. Payloads are to a 225-kilometer orbit.

Development of Costs — The cost in dollars per pound of payload in orbit is the total system cost divided by the total payload placed in orbit. The total payload placed in orbit is the product of the launch vehicle reliability, the number of launches attempted, and the payload weight per launch.

Cost Tables — A comparison of the cost effectiveness of the three tankage designs with data used is shown in Tables 3.2.8-5 and 3.2.8-6.

LAUNCH VEHICLE COST EFFECTIVENESS COMPARISON WITH SECOND-STAGE TANKAGE VARIATIONS (Total Development and Operating Cost)						
T65A Vehicle System	Payload Lbs x 10^6	Launches	Reliability	Total Payloads Lbs x 10^6	Systems Cost Dollars x 10^6	$/Lb. In Orbit
Single Tank Stage II	1.115	140	0.878	137.09	14,647.684	107
Clustered Tank Stage II	0.896	140	0.878	110.22	18,128.512	164
Multicell Tank Stage II	1.153	140	0.878	141.78	15,735.101	111

Table 3.2.8-3

LAUNCH VEHICLE COST EFFECTIVENESS COMPARISON WITH SECOND-STAGE TANKAGE VARIATIONS (Operating Cost Only)						
T65A Vehicle System	Payload Lbs x 10^6	Launches	Reliability	Total Payloads Lbs x 10^6	System Cost Dollars x 10^6	$/Lb. In Orbit
Single Tank Stage II	1.115	140	0.878	137.09	10,896.432	79
Clustered Tank Stage II	0.896	140	0.878	110.22	13,232.774	120
Multicell Tank Stage II	1.153	140	0.878	141.78	11,598.739	82

Table 3.2.8-4

NOVA VEHICLE TOTAL DEVELOPMENT COST
(In Thousands)

T65A Vehicle System With Second-Stage Tankage Variations
Trade Study — Boeing Estimated Motor Costs

Item	Single Tank*	Clustered Tank	Multicell Tank
Engine Development, Stage Engineering, Design & Development Testing, Vehicle Systems, Program Management, Integration:			
Stage I	$ 509,327	$ 509,327	$ 509,327
Stage II	614,838	614,838	614,838
Airframe and Propulsion Unit	1,219,181	2,192,575**	1,511,784**
Tooling for Stages	518,166	689,258**	610,673**
AGE	550,000	550,000	550,000
Facilities Maintenance and GSE Spares	167,000	167,000	167,000
Operations (Stage Transportation Launch Operations Propellants and High Pressure Gases Miscellaneous)	172,740	172,740	172,740
Total	$3,751,252	$4,895,738**	$4,136,362**
Number of Flight Test Vehicles	13	13	13

* Same as in 3.1.14.1
** Changes for Tankage Variations

Table 3.2.8-5

NOVA VEHICLE TOTAL OPERATIONAL COST
(In Thousands)

T65A Vehicle System With Second-Stage Tankage Variations
Trade Study — Boeing Estimated Motor Costs

Item	Single Tank*	Clustered Tank	Multicell Tank
Vehicle Costs			
Stage I Including Solid Propellant	$4,960,097	$4,960,097	$4,960,097
Stage II	2,926,280	5,262,622**	3,628,587**
AGE	1,000,000	1,000,000	1,000,000
Facilities Maintenance and GSE Spares	930,000	930,000	930,000
Propellant — Liquid Only — Stage II	216,080	216,080	216,080
Transportation	60,620	60,620	60,620
Launch Operations	354,450	354,450	354,450
Spares			
Stage I	205,497	205,497	205,497
Stage II	190,208	190,208	190,208
Range Cost and General Overhead	53,200	53,200	53,200
Total	$10,896,432	$13,232,774**	$11,598,739**

* Same as in 3.1.14.1
** Changes for Tank Variations

Table 3.2.8-6

BLANK

3.2.8.4 Second-Stage Tankage Bulkhead Trades

3.2.8.4.1 Introduction

Six bulkhead configuration combinations were evaluated for the 70-foot-diameter second-stage single-tank concept. Three nested intermediate bulkhead concepts and three opposed intermediate bulkhead concepts were considered (Figure 3.2.8-11). Minimum volume and off-loaded LO_2 tanks were included.

The configurations were evaluated on the basis of weight, length, and manufacturability. Honeycomb compression bulkheads and conical thrust structures of skin stiffener construction were used. Common bulkheads were not considered at the request of the contracting agency. Eighty-percent elliptical bulkheads were used for lower closures to reduce hoop buckling stresses due to fluid head pressure effects.

Tank sidewalls and intertank regions were designed by maximum-q load conditions. Tank sidewalls and intertank structure were of waffle construction for this trade study and were sized by stability criteria with tank skin thickness defined by internal pressure.

The interstage was designed by symmetrical maximum thrust loads and sized using skin-stringer construction.

The internal pressures in the LH_2 and LO_2 tanks were 40 psia and 45 psia, respectively.

Single-plane separation was used for all comparisons, but the effect of dual-plane separation is also indicated when it would affect the evaluation.

Residual-gas weight penalties were found to have insignificant variations between concepts and were not included.

The configuration comparisons were made on the basis of comparing the candidate concepts with Configuration Number 1 of Figure 3.2.8-11. The structural components that varied from this configuration were analyzed, and the change in weight was predicted. The evaluation results are, therefore, in the form of a weight change item rather than a complete weight statement for each configuration.

3.2.8.4.2 Summary

The bulkhead comparison study is summarized in Table 3.2.8-7. Nested Bulkhead Configuration Number 3 was the minimum structural weight system utilizing single-plane separation. With dual-plane separation, Minimum Volume LO_2 Tank Configuration Number 6 was the minimum second-stage structural weight system. However, increased retrorocket requirements of the first stage would negate most of this saving. The opposed bulkhead systems were the simplest to

manufacture. Nested Bulkhead Configuration Number 4 with surfaces concave upward was the minimum-length and maximum-weight design. The large weight penalty was due primarily to the LO_2 head pressure increasing the design load on the compression bulkhead.

The opposed bulkhead concept, Configuration Number 1, was selected as the final design concept. Single-plane separation was chosen from a reliability standpoint. The compression bulkhead designs did not offer sufficient length or weight savings to justify the additional manufacturing complexity of a 70-foot-diameter reinforced bulkhead. The choice between Configurations 1 and 5 was made on the basis of the improved fixturing requirements and manufacturing simplicity of Configuration 1. Configuration 5 requires three different head shapes rather than two and a large internal ring to react the kick loads from the constant-radius heads.

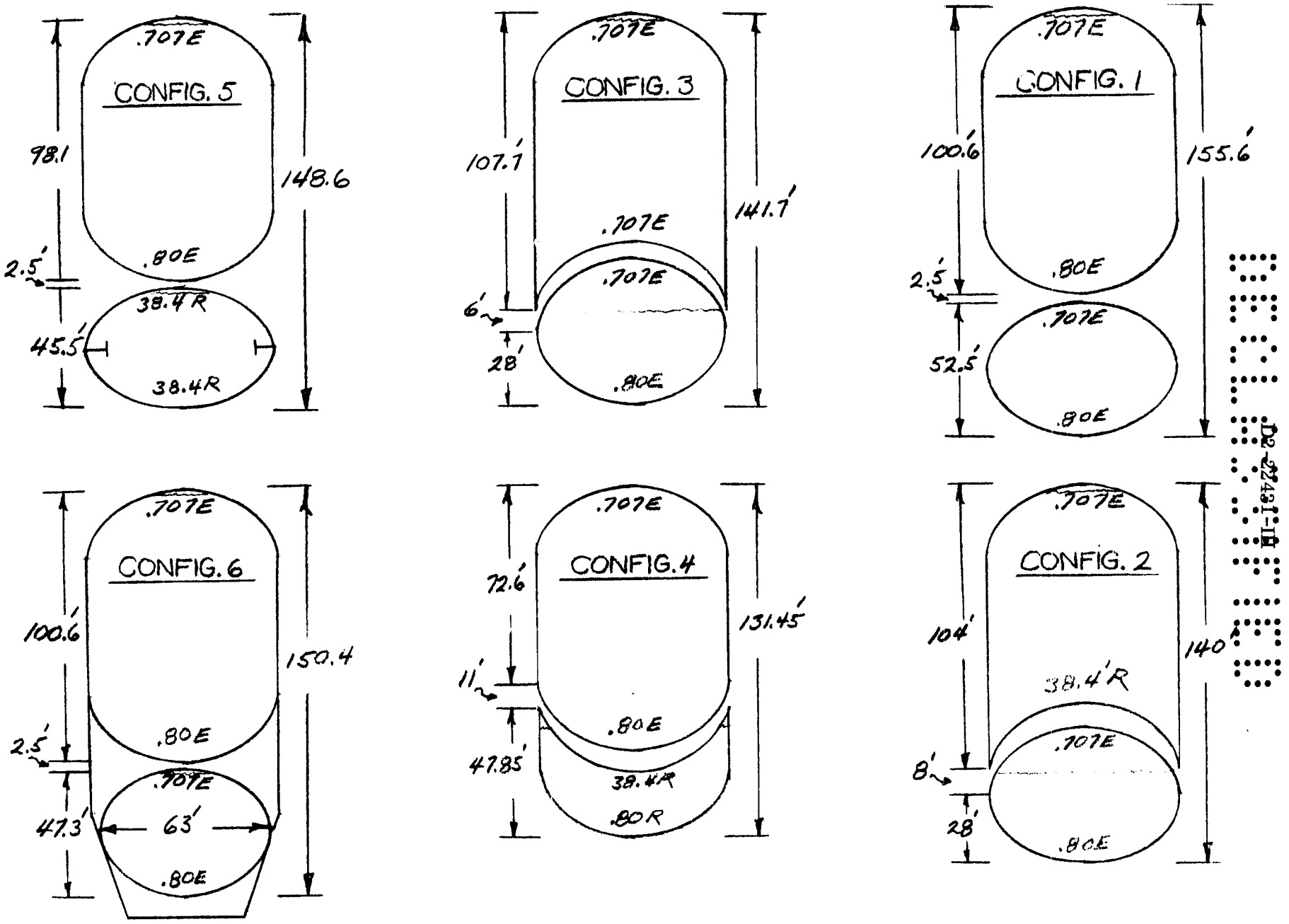

Figure 3.2.8-11 SECOND-STAGE TANKAGE BULKHEAD TRADES

SECOND STAGE BULKHEAD TRADE SUMMARY

CONFIGURATION NO.		(1)	(2)	(3)	(4)	(5)	(6)
		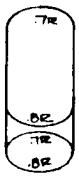	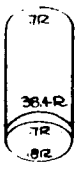	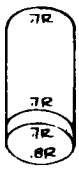	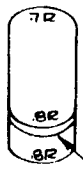	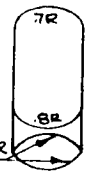	
LOX TANK SIDEWALL	LENGTH				19.85'		
	WEIGHT	0	0	0	38,900	0	0
Δ LH_2 SIDEWALL	LENGTH	0	31.4'	35.1'	0	0	0
	WEIGHT	0	44,300	49,500	0	0	0
AFT LH_2 TANK HEAD	WEIGHT	29,850	60,300	65,200	29,850	29,850	29,850
LH_2 TANK KICK LOAD RING	WEIGHT	0	10,100	0	0	0	0
Δ INTER-TANK	LENGTH	0	-47'	-49'	-44'	-1.7	-10.8
	WEIGHT	0	90,000	-93,950	-84,250	-3,260	-20,600
LOX TANK FWD HEAD	WEIGHT	25,200	25,200	25,200	90,950	30,800	18,400
LOX TANK AFT HEAD	WEIGHT	63,500	63,500	63,500	79,200	49,600	51,700
LOX TANK RING	WEIGHT	0	0	0	18,700	34,150	0
Δ INTERSTAGE	LENGTH					-5.3'	5.6'
	WEIGHT	0	0	0	0	-17,900	18,900
Δ THRUST STRUCTURE	WEIGHT	0	0	0	0	0	27,670
Δ STRUCTURAL WEIGHT TOTAL		(1) 0	-5,150	-9,000	+54,800	+4,690	-53,630 (2) / +7,370 (3)
Δ LENGTH (FT.)		0	-15.6	-13.9	-24.15	-7.0	-5.2

(1) TOTAL STRUCT. WT. 2ND STAGE 449,650 LB
(2) DUAL PLANE SEPARATION-RETRO PENALTY NOT INCLUDED
(3) SINGLE PLANE SEPARATION

Table 3.2.8-7

3.2.8.5 Second-Stage Thrust Structure Trades

3.2.8.5.1 Introduction

Three types of second-stage thrust structure were investigated (see Figure 3.2.8-12).

All types of thrust structure utilized a pattern of four M-1 engines arranged symmetrically about a center engine supported on beams spanning between outboard engine mounts. The beams were attached to the engine mounts to react the kick loads, which would otherwise be taken by the engine mount support ring. The alternative of attaching the beams to the support ring at midpoints between motors would distribute the axial loads more evenly at the expense of increased ring loads. The net effect would be a weight increase and a stiffness reduction. The transition structure between the motor mounts and the second-stage skirt consisted of truss members, monocoque skin, or stringer frame design in the shape of a cone frustum.

A dynamic load factor of 1.4 was used to define limit load. The center engine support beams were designed by the conservative assumption that all outboard engines were gimbaled 7.5-degrees outward, imposing axial loads in addition to the bending moments. The structure used throughout was 7075-T6 aluminum.

The purpose of this investigation was to obtain representative weight comparisons. Therefore, the structural analysis used approximate methods to estimate panel redistribution loads and made certain other assumptions which would necessarily require refinement in the detail-design process. Similar assumptions were made for all concepts; therefore, the relative comparisons should be valid.

3.2.8.5.2 Summary

The stringer-frame conical shell design was the most efficient of the concepts investigated. The truss-beam concept was slightly heavier, while the ring-stiffened shell was markedly heavier.

The truss beam concept was less efficient because of the concentrated loads that must be redistributed into the sidewall. The conical-shell concept achieves redistribution before the sidewall is reached.

The stringer-frame concept indicates a considerable weight saving over the ring-stiffened shell concept (which utilizes unstiffened panel stability between rings and is basically less efficient for this application).

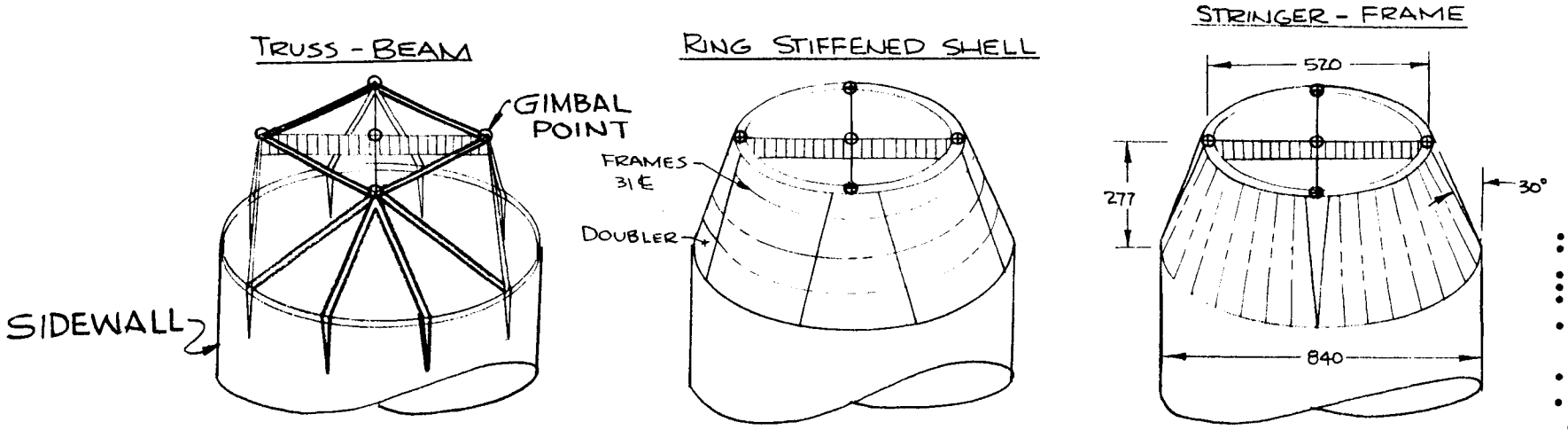

COMPONENT	WEIGHT
STRUTS	13500
END CONNECTIONS	800
RING, SIDEWALL	22000
BRACES, GIMBAL PL.	3400
BEAMS	22600
REDISTRIBUTION	28200
	90,750 LBS

COMPONENT	WEIGHT
SHELL	65800
FRAMES	13 80
DOUBLERS	17 540
BEAMS	22 600
RING, SIDEWALL	12 180
RING, GIMBAL PL.	10 800
	130,300 LBS

COMPONENT	WEIGHT
SHELL + STRINGERS	29100
FRAMES	9480
BEAMS	22600
RING, SIDEWALL	12180
RING, GIMBALL PL.	10800
	84,160 LBS

Figure 3.2.8-12 SECOND-STAGE THRUST STRUCTURE TRADES

3.2.8.5.3 Truss-Beam Thrust Structure

The truss-beam thrust structure (Figure 3.2.8-12) used compression-tube members extending in pairs from the four outboard motor-mount locations to a ring located at the sidewall intersection point. The geometry of the tubes was chosen to provide an ultimate strength of 48,000 psi at a diameter of 33 inches.

The redistribution panel at the tube-ring-sidewall intersection provided for the redistribution of the eight concentrated tube loads. The panel was designed on the assumption that the shear lag redistribution angle was 20 degrees and the redistribution structure was operating at 40,000 psi ultimate stress.

The engine support beams were designed as beam columns. Overlapping assumptions were used to design the lateral bracing members connecting the motor mounts. Lateral loads were reacted by the engine support beams and the lateral bracing members. For simplicity, both structures were designed to carry the loads independently.

The resulting structural weights are shown in Figure 3.2.8-12.

3.2.8.5.4 Ring-Stiffened Shell Thrust Structure

This structure used a simple monocoque shell of cone-frustum shape with internal ring-stiffeners spaced 31 inches apart at the motor mount end and increasing linearly to 52 inches at the opposite end. At the load concentration points, doublers were used to redistribute the concentrated loads. The doublers were 24 inches wide at the motor mounts and increased to 272 inches wide at the sidewall intersection. The doublers, plus backing skin, were sized for panel stability under full engine thrust. Overlapping assumptions were used in the sizing of the basic cone shell, which was conservatively sized for a uniform load distribution.

The engine support beams were identical to those used for the truss-beam concept. The ring in the engine-mount plane was sized as a curved beam of constant radius supported at the ends of a 90-degree arc. Ring instability was the sizing criteria and a unform load distribution was assumed. The ring located at the sidewall was sized for a nonuniform circumferential load distribution.

The resulting structural weights are shown in Figure 3.2.8-12.

3.2.8.5.5 Stringer-Frame Thrust Structure

The stringer-frame thrust structure used a semimonocoque shell of cone-frustum shape. Tapered redistribution panels were used at the engine mounts. Redistribution panel weight was estimated by sizing a stringer-skin panel, which was bounded by 20-degree shear lag lines, for the full engine load. The remainder of the structure was conservatively sized for a uniform load distribution.

The engine support beams were identical to those used for the truss-beam concept. The upper and lower rings are identical to those used for the ring-stiffened shell concept.

The resulting structural weights are shown in Figure 3.2.8-12.

3.2.8.6 Detail Design Analysis of T65 Vehicle

3.2.8.6.1 Structural Requirements, Design Conditions, and Margin-of-Safety Summary

The detail design analysis of the T65 vehicle was performed to delineate particular structural problem areas that often become apparent under more intensive evaluation and to provide more accurate weight predictions. The analysis is presented in the form of margin-of-safety indications. The analysis was not intended to be a rigorous evaluation as required in a formal stress analysis; therefore, approximate design methods and data are occasionally used to predict component strengths. However, detailed investigations of the major structural components of both first and second stage have been completed and the structural concepts are judged to be representative, in terms of weight, of a final vehicle design.

Detailed structural trades, such as the choice between zee-section or corrugated interstages, have not been exercised. The structural concepts used represent a reasonable solution to a given problem rather than an optimized one. More general structural trades were performed on the second-stage tankage and thrust structure and are discussed in 3.2.8.3, 3.2.8.4, and 3.2.8.5.

The structural configuration of the first stage was selected on the basis of information developed during a preceding portion of Contract NAS8-8428, which evaluated various clustering concepts for a cluster of four motors.

The vehicle was designed for the structural conditions tabulated in Table 3.2.8-8.

Margin-of-Safety Summary

Tables 3.2.8-9, -10, -11, and -12 indicate the margins of safety of the vehicle structural components. The appropriate sections of the document containing the detail analyses are referenced.

STRUCTURAL DESIGN CONDITIONS

LOAD CONDITIONS				SOURCE
• Vehicle trimmed at maximum dynamic pressure. NASA 99-percent wind-shear, 40 fps, 1-cosine gust.				3.2.8.6.2.1, Figure 3.2.8-13
• Symmetrical maximum thrust.				3.2.8.6.2.1, Figure 3.2.8-22
• Unsymmetrical thrust termination.				3.2.8.6.2.1, Figure 3.2.8-20
• Failure condition — nozzles hard-over at maximum dynamic pressure.*				3.2.8.6.2.1, Figure 3.2.8-16
• Failure condition — 20-degree angle of attack, nozzles null.*				3.2.8.6.2.1, Figure 3.2.8-17
• NASA 99.9-percent ground wind.				3.2.8.6.2.2, Figure 3.2.8-23
PRESSURES**				
• Motor MEOP — 800 psia limit				
• LH_2 Tank-Limit	50.6 psia — cryogenic temp. 39.2 psia — room temp.			3.2.8.6.3.2, Figure 3.2.8-25
• LO_2 Tank-Limit	Room Temp.	Cryogenic Temp.		
Upper head -	78.5 psia	92.5 psia		3.2.8.6.3.2, Figure 3.2.8-25
Lower head -	101.2 psia	119.2 psia		
HEAT RATES (First Stage)				
• Heat shield — center	500 Btu/ft^2-sec.			3.2.10.2.3
• Heat shield — edge	250 Btu/ft^2-sec.			
TEMPERATURES				
• Upper skirt — second stage (t_s = .109)	195°F Burnout, 83°F Max. q			3.2.10.4, Figure 3.2.10-10
• Intertank skirt (t_s = .183)	154°F Burnout, 88°F Max. q			
• Interstage (t_s = .29)	126°F Burnout, 85°F Max. q			

The following factors of safety were applied:

- General Structure

  Yield factor of safety = 1.10.
  Ultimate factor of safety = 1.40.

* A factor of safety of 1.0 was used on failure conditions.

** External overpressure and differential negative internal tank pressures were not used for design.

Table 3.2.8-8

STRUCTURAL DESIGN CONDITIONS

- Propellant Tanks

  Proof Pressure = 1.05
  Yield Pressure = 1.10
  Burst Pressure = 1.40

- Solid-Propellant Motor Cases

  Proof Pressure = 1.05
  Yield Pressure = 1.20
  Ultimate Pressure = 1.40
  where limit pressure is equal to maximum expected operating pressure (MEOP)

- A weld efficiency factor of 90 percent was assumed.

---

* An ultimate factor of safety of 1.4 was used in addition to a yield factor of 1.2 in the motor-case design because: There is no need to make an unconservative modification of established policies when no significant gains in vehicle performance result. The gain in payload, if the ultimate factors were not included, would be 1.7 percent, assuming no reduction in allowables strength for fracture-toughness considerations. In vehicles of this size, unconservatism should be minimized due to the immense cost of a failure.

Table 3.2.8-8 (Cont.)

SECOND STAGE

MINIMUM MARGINS OF SAFETY

STRUCTURAL COMPONENT	CRITICAL LOAD CONDITION	MINIMUM M.S.	TYPE OF FAILURE	REFERENCE
FORWARD HYDROGEN HEAD	- PROOF TEST	0	-TENSION	3.2.8.6.3.4
SIDEWALL HYDROGEN TANK	- MAX q, 20° ANGLE OF ATTACK - PROOF TEST	.07 .06	- SHELL BUCKLING - TENSION	3.2.8.6.3.4
AFT HEAD HYDROGEN TANK	- PROOF TEST	0	-TENSION	3.2.8.6.3.4
INTER TANK SHELL	- MAX q, 20° ANGLE OF ATTACK	0	- SHELL BUCKLING	3.2.8.6.3.5
FORWARD HEAD LO_2 TANK	- PROOF TEST	0	-TENSION	3.2.8.6.3.6
AFT HEAD LO_2 TANK	- PROOF TEST - FIRST STAGE BURN OUT	0 0	-TENSION -SHELL BUCKLING	
THRUST STRUCTURE CROSS BEAM WEB	- SECOND STAGE START-UP	.02	-WEB CRIPPLING	3.2.8.6.3.7
THRUST STRUCTURE ENGINE MOUNT RING	- SECOND STAGE START-UP	.10	-RING BUCKLING	
THRUST STRUCTURE FORWARD RING	- SECOND STAGE START-UP	.01	-TENSION	
THRUST STRUCTURE LONGERON	- SECOND STAGE START-UP	.12	-COLUMN BUCKLING	
SHEAR WEBS	- SECOND STAGE START-UP	.07	-WEB CRIPPLING	
STRINGERS	- SECOND STAGE START-UP	.02	-COLUMN BUCKLING	
FORWARD INTERSTAGE	- MAX q, 20° ANGLE OF ATTACK	0	- SHELL BUCKLING	3.2.8.6.3.8
THRUST STRUCTURE INTERMEDIATE CONE SECTION	- SECOND STAGE START BURN	.58	- SKIN BUCKLING	3.2.8.6.3.7

Table 3.2.8-9

FIRST STAGE

CLUSTERING STRUCTURE

MINIMUM MARGINS OF SAFETY

STRUCTURAL COMPONENT	CRITICAL LOAD CONDITION	MINIMUM MS	TYPE OF FAILURE	REFERENCE
OUTER-TIE	SYMMETRICAL BURNOUT	.01	WEB STABILITY	3.2.8.6.4.4
RINGS	SYMMETRICAL BURNOUT	.02	WEB STABILITY	
MAIN CROSSBEAM (OUTER SEGMENT)	SYMMETRICAL BURNOUT	.02	STIFFENED PANEL STRENGTH	
MAIN CROSSBEAM (INTERCOSTAL AREA)	SYMMETRICAL BURNOUT	.02	STIFFENED PANEL STRENGTH	
INTERCOSTAL	UNSYMMETRICAL THRUST TERMINATION	.05	WEB STABILITY	
FORWARD SKIRT EXT.	UNSYMMETRICAL THRUST TERMINATION			
STRINGER		.10	FLANGE STRESS	
SKIN		.10	BUCKLING	
FRAME		.13	FLANGE STRESS	3.2.8.6.4.4
INTERSTAGE	SYMMETRICAL BURNOUT	.06	COMPRESSION BUCKLING OF SKIN	3.2.8.6.4.5

Table 3.2.8-10

FIRST STAGE BASE SKIRT
MINIMUM MARGIN OF SAFETY

STRUCTURAL COMPONENT	CRITICAL LOAD CONDITION	MIN. M.S.	TYPE OF FAILURE	REFERENCE
SUPPORT COLUMN	PRELAUNCH GROUND WIND	.02	BEAM COLUMN	3.2.8.6.4.6
TENSION STRUTS	PRELAUNCH GROUND WIND	.17	TENSION	
AFT RING	PRELAUNCH GROUND WIND	.16	TENSION	
CLUSTERING LINKS	UNSYMMETRICAL BURNOUT	.22	SHORT COLUMN	
FORWARD RING	PRELAUNCH GROUND WIND	0	LATERAL BUCKLING	
LONGERON	↕	.05	SHORT COLUMN	
SHEAR WEBS	↕	.22	SHEAR BUCKLING	
STRINGERS	PRELAUNCH GROUND WIND	.09	SHORT COLUMN	
FRAMES	STABILITY CRITERIA	.33	—	
BASE SKIRT FAIRING	MAX. q	.03	CYLINDER BUCKLING	
BASE HEAT SHIELD	MAX. q	.12	FACE MATERIAL	3.2.8.6.4.7
HEAT SHIELD SUPPORT BEAMS	MAX. q	.04	FLANGE CRIPPLING	3.2.8.6.4.7

Table 3.2.8-11

MOTOR CASE (FIRST STAGE)
MINIMUM MARGINS OF SAFTY

STRUCTURAL COMPONENT	CRITICAL LOAD CONDITION	MINIMUM M.S.	TYPE OF FAILURE	REFERENCE
SOLID MOTOR CASES	GROUND WIND	0	BUCKLING	3.2.8.6.4.8
	MAX OPERATING PRESSURE	0	TENSION	

Table 3.2.8-12

BLANK

3.2.8.6.2 Loads

3.2.8.6.2.1 Flight Loads

Flight loads for the T65 vehicle were obtained for the following conditions of expected maximum loading:

- Vehicle trimmed to a NASA 99-percent wind-shear profile at maximum q (Figure 3.2.8-13).
- A failure condition of the nozzles at full gimbal counteracting the angle of attack due to the NASA 99-percent wind-shear profile at maximum q.
- A failure condition with the vehicle at an angle of attack of 20 degrees at maximum q with nozzles in the null position.
- Unsymmetrical first-stage burnout resulting in one motor at one-half thrust and five motors at full thrust.
- Maximum symmetrical first-stage thrust.

Flight Bending Loads — The angle of attack and nozzle gimbal due to the wind-shear profile at maximum q was determined from a 6-degree-of-freedom analysis. This method includes pitch, yaw, and translation. The limit bending loads were found to be most severe in the yaw plane and are shown in Figure 3.2.8-14 for the trim condition. The yaw angle of attack was increased by 14 percent to account for gust and increased by 10 percent to account for flexible body effects.

The limit bending loads for this condition are shown in Figure 3.2.8-15, along with the ultimate loads.

The nozzle full gimbal is a NASA malfunction condition previously defined during Contract NAS8-2438 and the associated bending loads are shown in Figure 3.2.8-16.*

The bending loads for the 20-degree-angle-of-attack failure conditions with the nozzles in the null position are shown in Figure 3.2.8-17.

The bending loads for the nozzle full gimbal and the 20-degree-angle-of-attack failure conditions were calculated for the T65A baseline vehicle and were scaled for subsequent iterations. Figure 3.2.8-18 shows the ultimate bending loads due to wind shear, the nozzle full gimbal bending loads, and the bending loads for the 20-degree-angle-of-attack failure condition. The failure moments were larger than the trim condition for all portions of the vehicle.

For the unsymmetrical thrust burnout conditions, one motor was assumed to be at half thrust and the other five motors at full thrust. The pressure variations in Figure 3.2.8-19 show this to be a conservative assumption. The figure also

* A factor of safety of 1.0 was used on failure conditions.

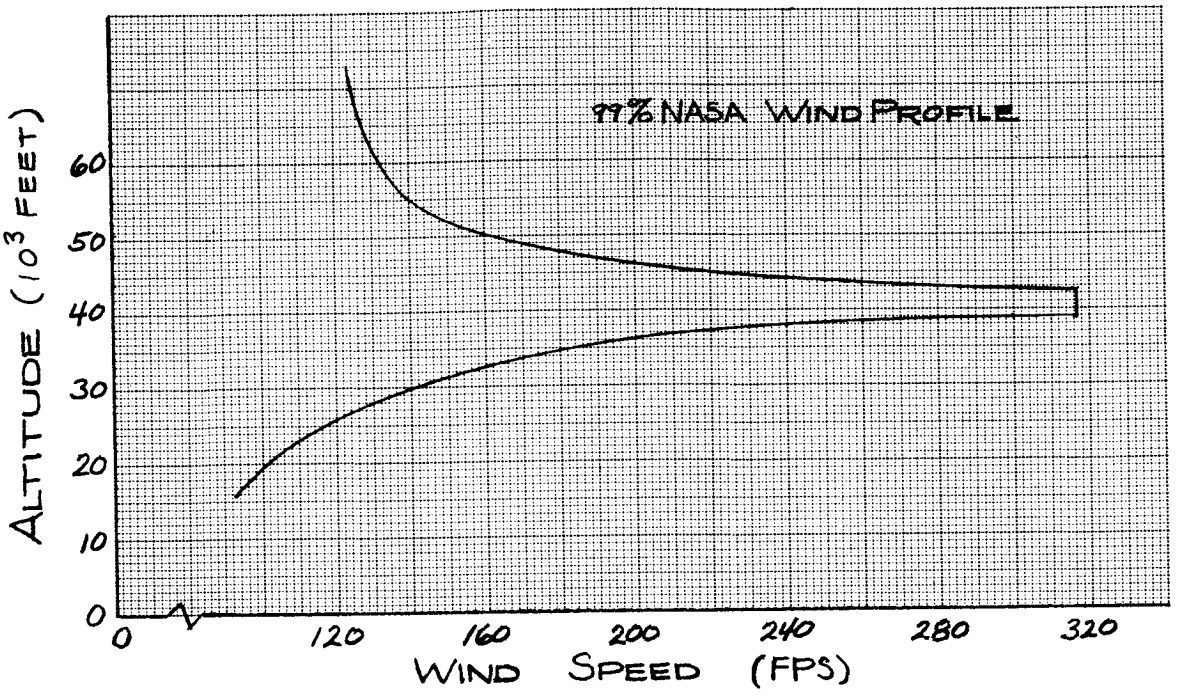

Figure 3.2.8-13 WIND SPEED PROFILE
Cape Canaveral, Florida

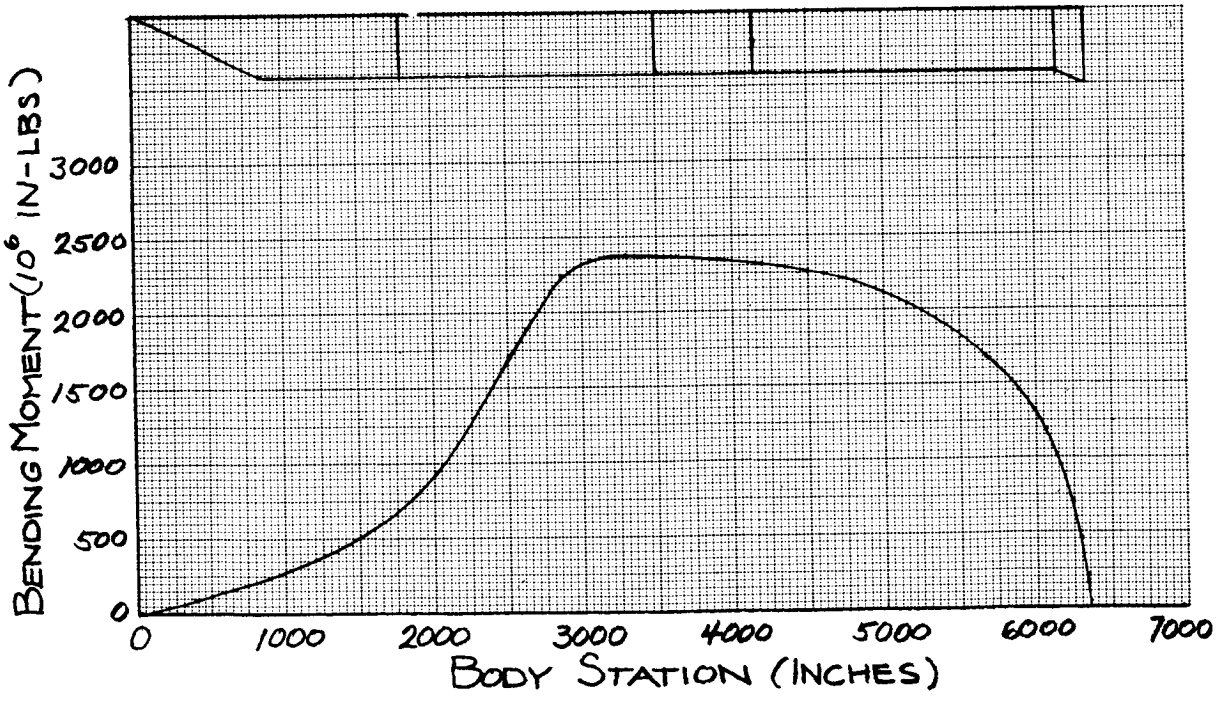

Figure 3.2.8-14 LIMIT BENDING MOMENT DUE TO WIND SHEAR

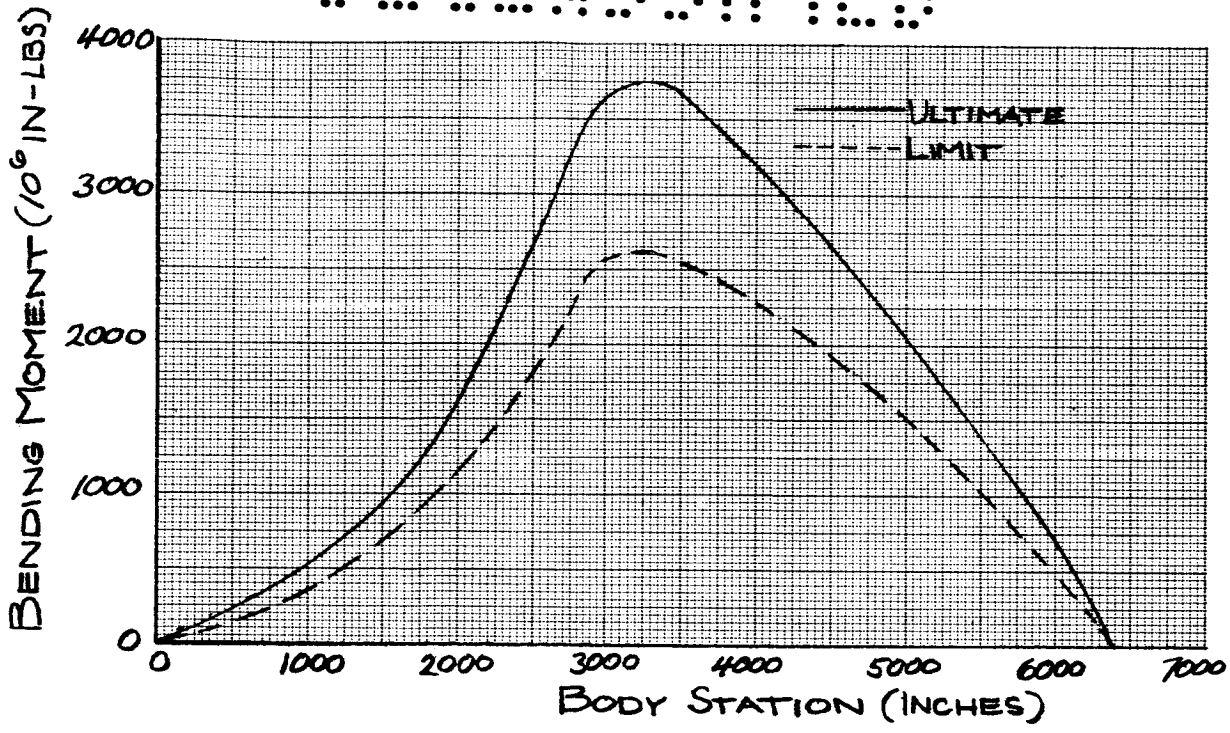

Figure 3.2.8-15 BENDING MOMENT DUE TO WIND SHEAR
Gust and Dynamic Magnification

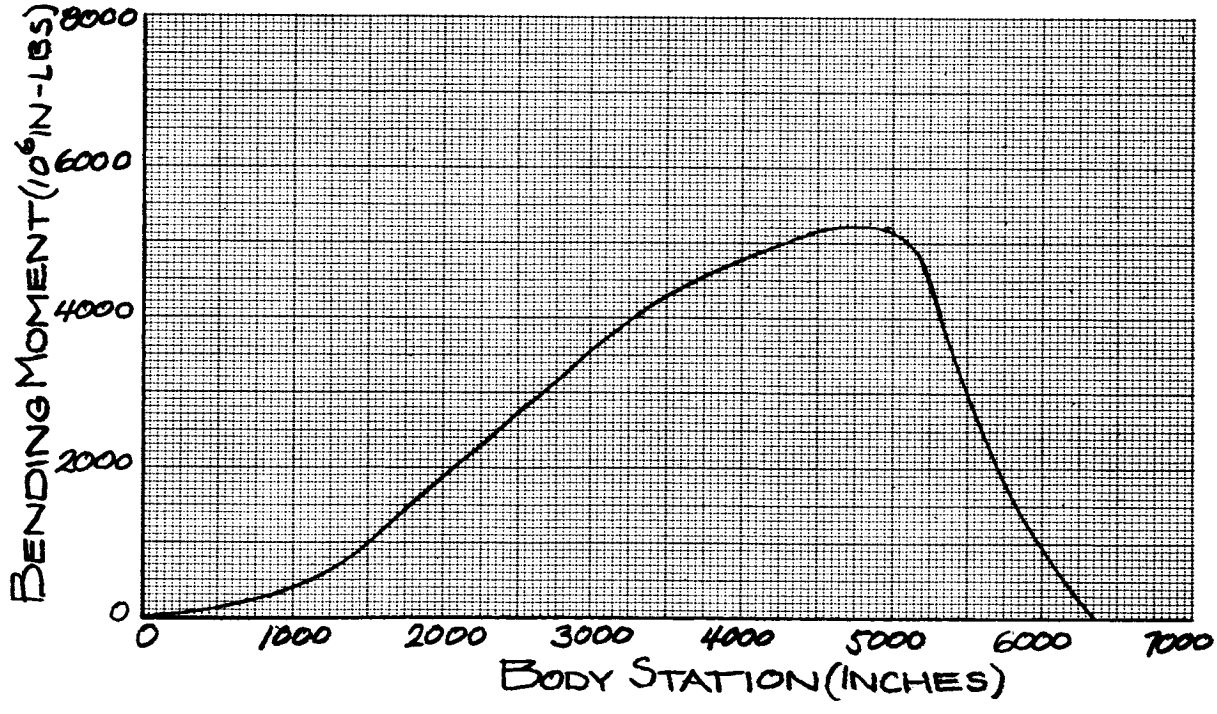

Figure 3.2.8-16 ULTIMATE BENDING MOMENT DUE TO FULL
GIMBAL CONDITION

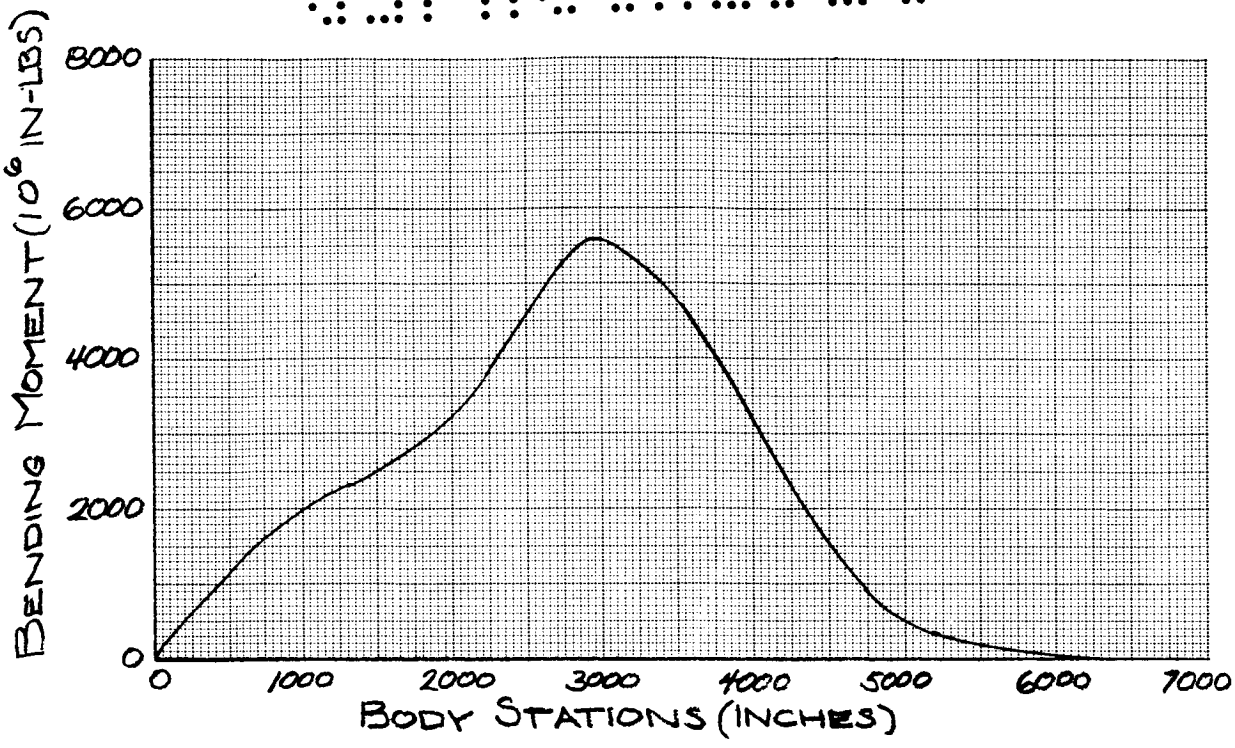

Figure 3.2.8-17 ULTIMATE BENDING MOMENT DUE TO 20-DEGREE ANGLE OF ATTACK CONDITION

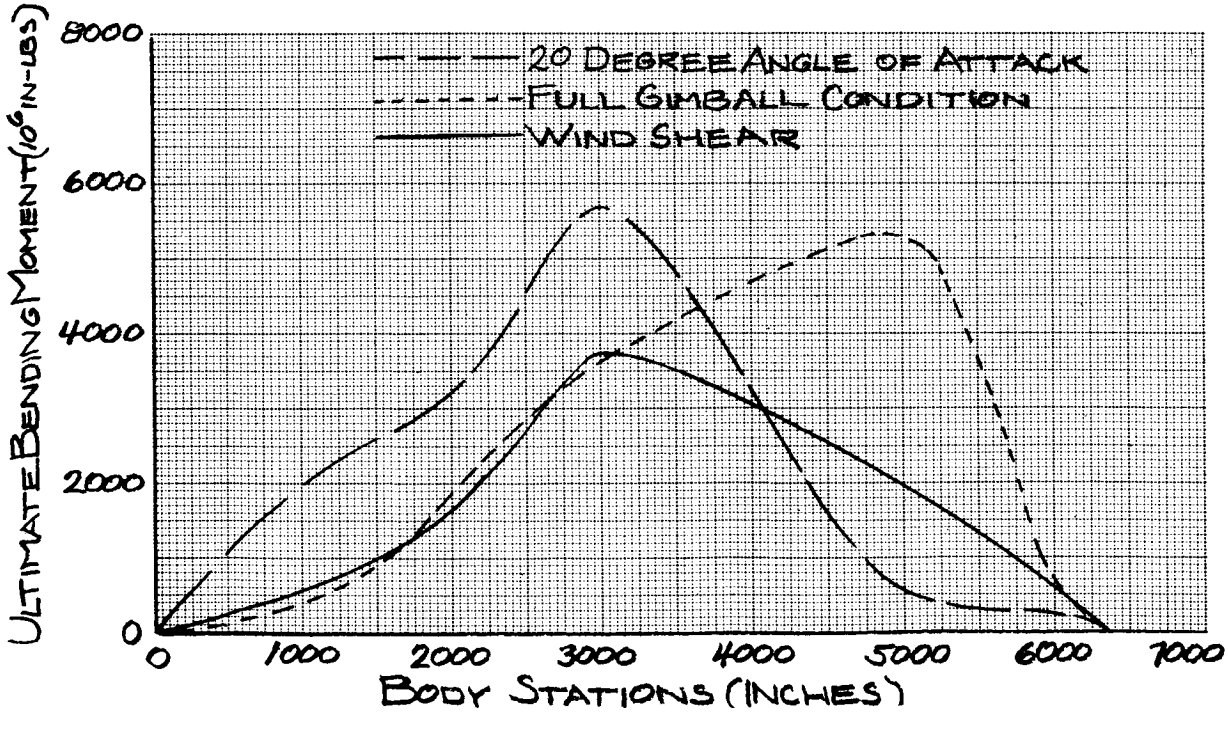

Figure 3.2.8-18 COMPARISON OF BENDING MOMENTS

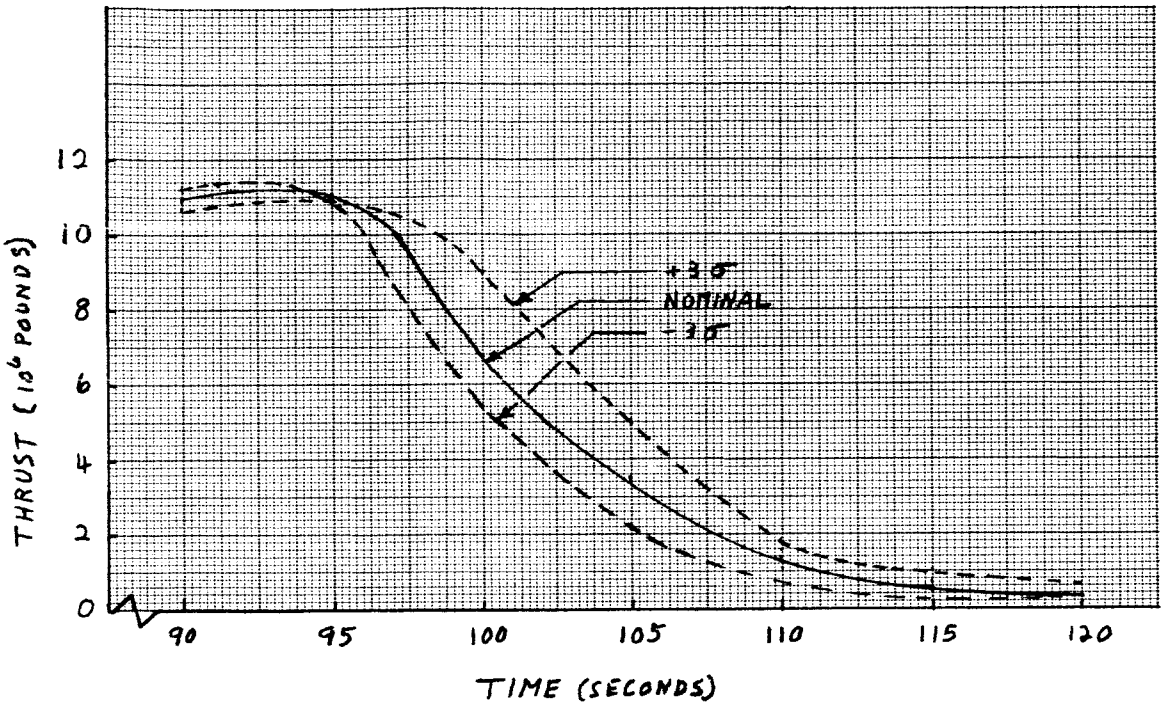

Figure 3.2.8-19 THRUST AT TAILOFF

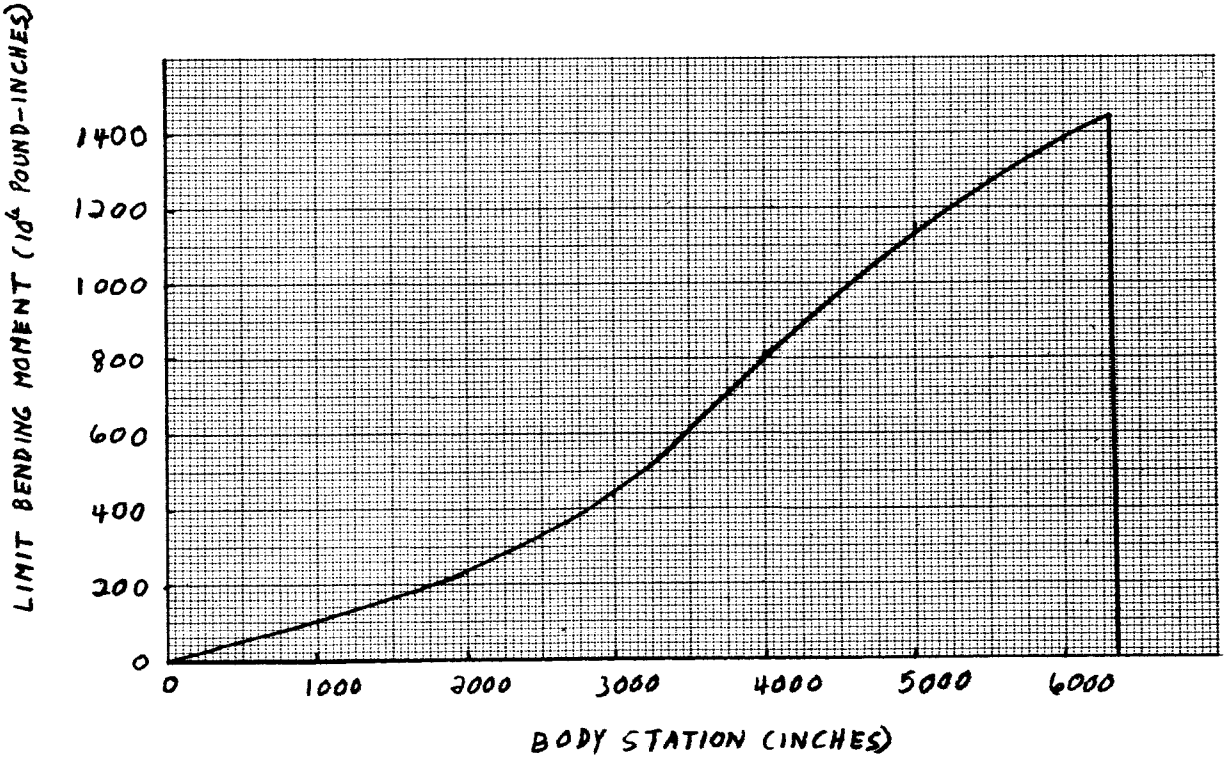

Figure 3.2.8-20 BENDING MOMENT DUE TO UNSYMMETRICAL THRUST TERMINATION

indicates a slow thrust decrease rate; during this time the nozzles could gimbal to trim the vehicle. However, in this analysis, the nozzles were assumed to remain in the null position. The bending loads shown in Figure 3.2.8-20 are, therefore, quite conservative.

Axial Loads — The axial loads were calculated from the tangential flight path accelerations resulting from a summation of thrust and drag forces. To simplify the presentation of axial loads, 100 percent of the thrust was assumed to be applied at the aft end of the vehicle. To determine the complete axial load distribution, the loads due to internal pressure must be superimposed on the axial loads shown.

The axial loads were determined at maximum q and burnout, and are shown in Figures 3.2.8-21 and 3.2.8-22.

3.2.8.6.2.2 Ground Wind Loads

In the ground wind load analysis, the vehicle support interface was located at an elevation of 100 feet. A NASA 99.9-percent ground wind profile with a 1.4 gust factor was used in determining the ground wind bending moment as shown in Figure 3.2.8-23. The vehicle was assumed rigid in this analysis and a dynamic magnification factor of 1.1 was applied to account for flexible body effects.

3.2.8.6.2.3 Loads for Base Heat Shield and Support Leg Fairing

A preliminary estimate of the acoustic environment associated with the launch of the reference vehicle has been made. The configuration is a six-nozzle cluster with the nozzle exit plane 100 feet above a 90-degree deflector. The exit diameter of each nozzle is 21.4 feet, and the equivalent nozzle diameter of the cluster is 52.5 feet. The maximum sound pressure levels during launch are predicted for the base of the vehicle as shown in Figure 3.2.8-24. The overall sound pressure level was predicted to lie within a range of 159 to 165 decibels. The 165-decibel level corresponds to an R.M.S. pressure level of 75 psf as given by the definition of decibel: $db = 20 \log 10\left(\frac{P}{P_{ref}}\right)$; where $P_{ref} = 4.2 \times 10^{-7}$ psf.

The important consideration in analyzing effects of acoustic loads is the resonance effect of the sound pressure on the structure. Experiments have been performed on flat plates subjected to acoustic environments with a frequency spread similar to that generated by a rocket motor. The results indicate that 80 percent of the plate deflections will be less than 10 times the plate deflections due to a static pressure of the same magnitude as the R.M.S. of the fluctuating pressure. On this basis, an equivalent static pressure of 750 psf was assumed for the acoustic load on the base heat shield.

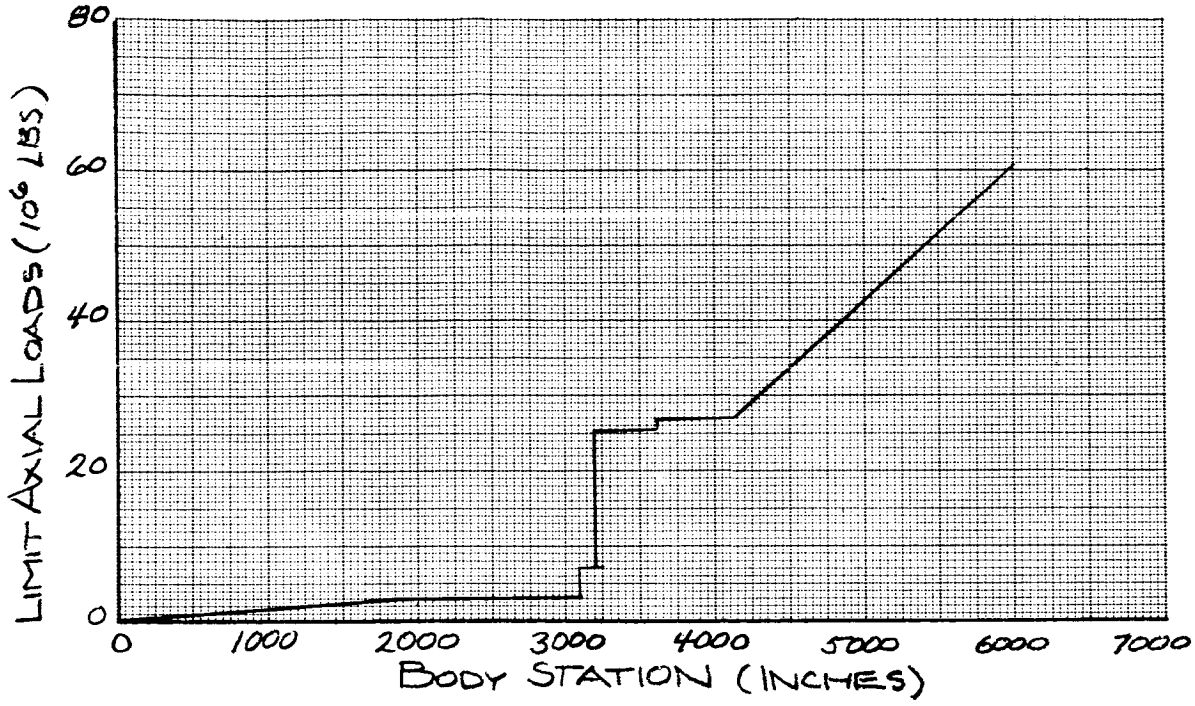

Figure 3.2.8-21 AXIAL LOADS AT MAXIMUM q
(2.55g Tangential Acceleration)

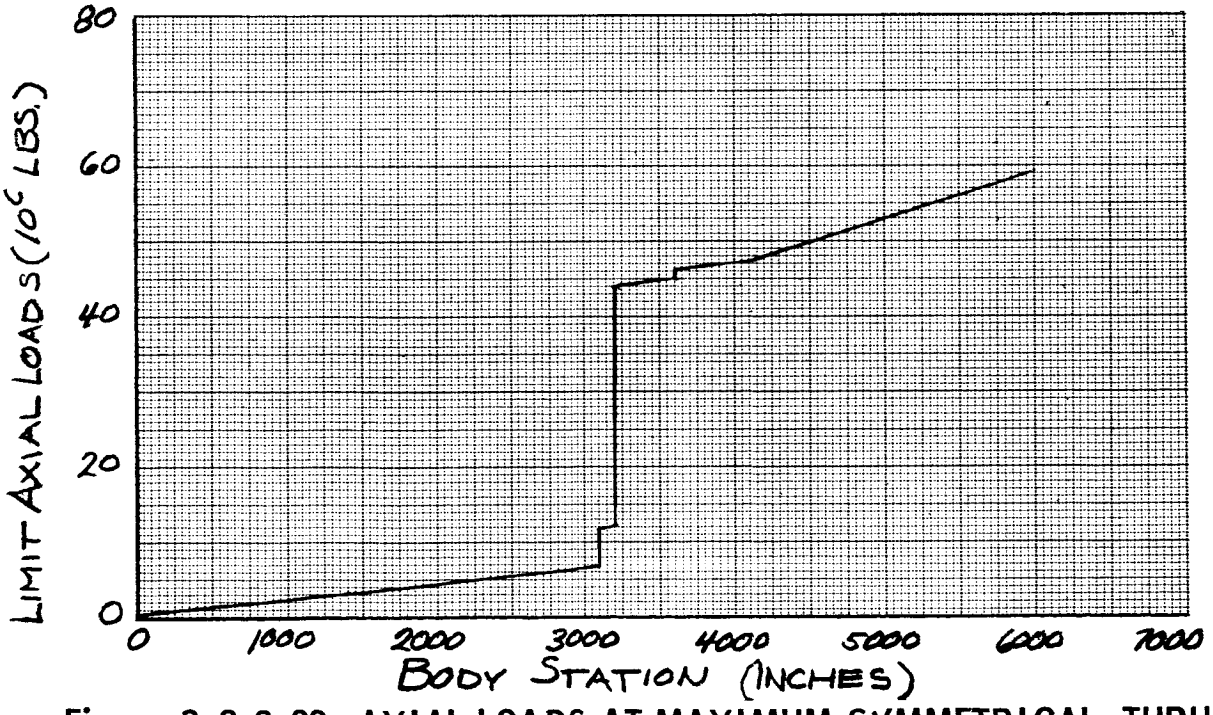

Figure 3.2.8-22 AXIAL LOADS AT MAXIMUM SYMMETRICAL THRUST
(4.5g Tangential Acceleration)

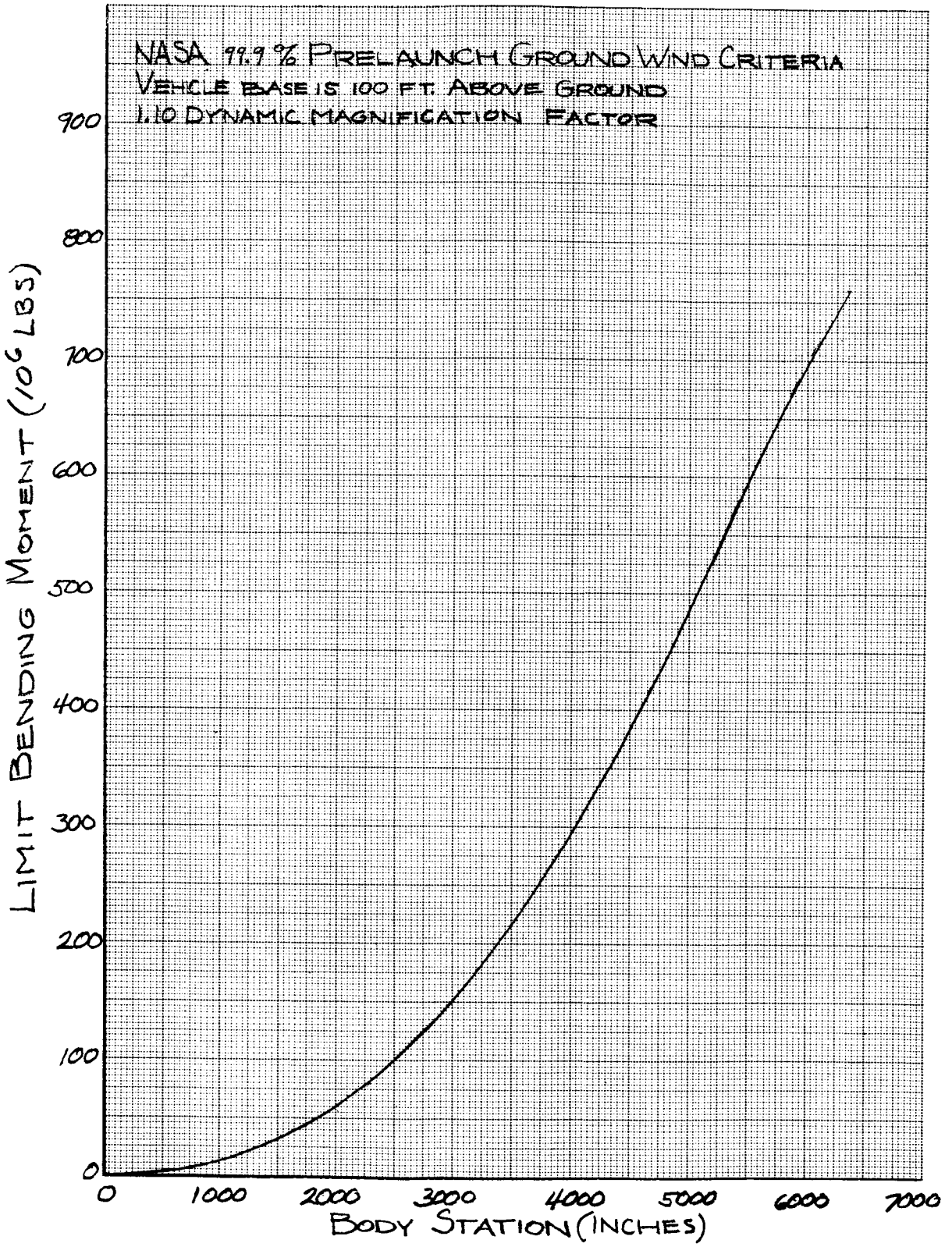

Figure 3.2.8-23 LIMIT BENDING MOMENT DUE TO GROUND WIND

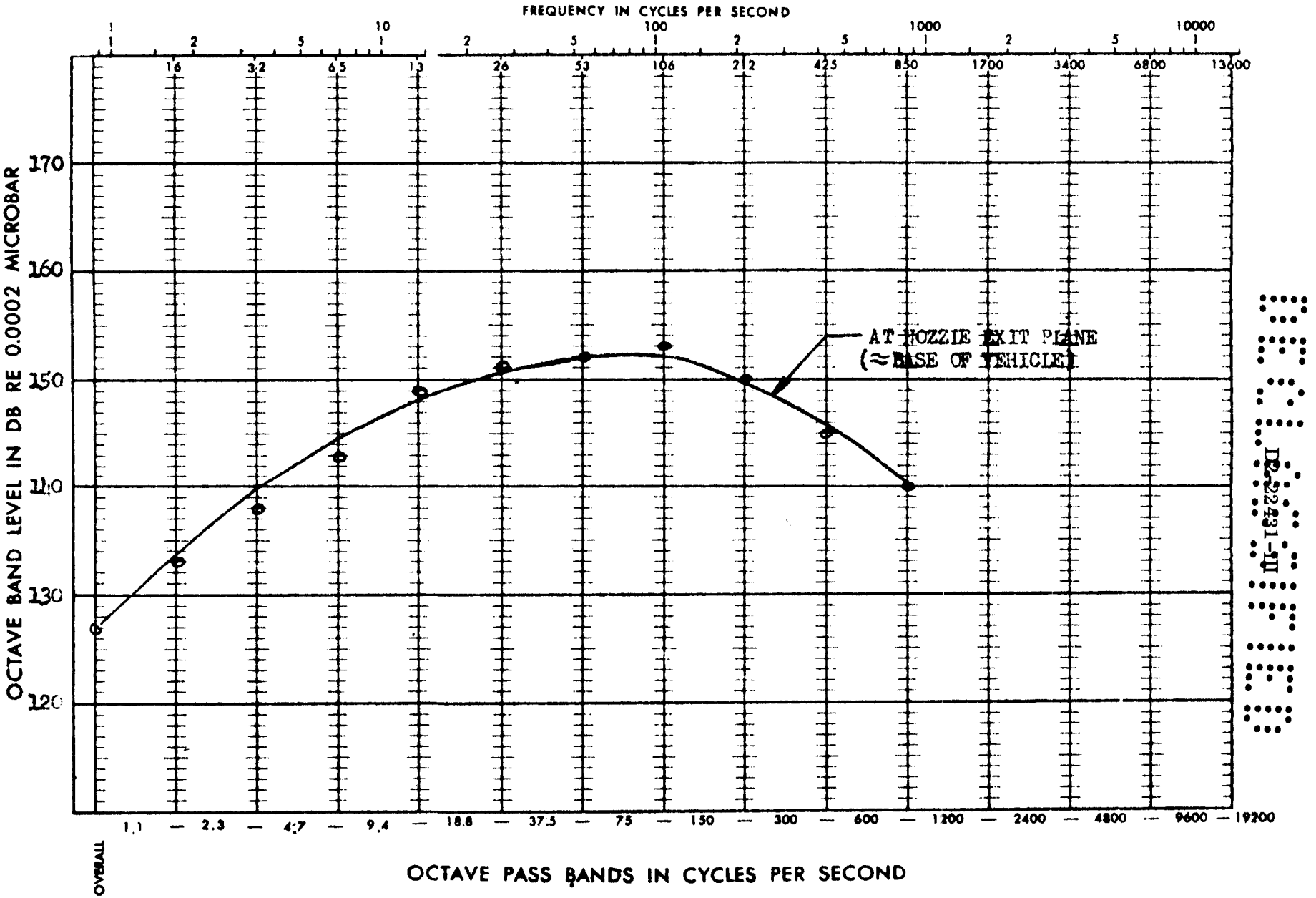

Figure 3.2.8-24 ESTIMATED MAXIMUM SOUND PRESSURE LEVELS AT BASE OF 59.5 x 10^6 lb. THRUST VEHICLE AT LAUNCH

The total aerodynamic pressure at maximum q on the support leg fairing was determined by shock expansion theory to be 967 psf. Since the vehicle velocity is well above Mach 1 at maximum q , the acoustic load due to the motors on the support leg fairing will be unimportant.

3.2.8.6.2.4 Bending Modes and Frequencies

The bending frequencies and mode shapes were obtained through the use of a digital program that determines bending mode shapes and frequencies for beams of variable mass and stiffness. The frequencies and mode shapes are determined by a Myklestad method of solution of the pertinent differential equations.

The composite stiffness of the six motors in the first-stage was assumed to be equal to the sum of the stiffnesses of the individual motors for the determination of the free-free mode shapes and frequencies of the baseline vehicle. The first- and second-mode frequencies for the baseline vehicle using the above assumption were 1.37 cps and 2.35 cps. A previous study (Reference 15, NAS8-2438) by Boeing on a smaller but similar vehicle indicated that the actual stiffness of the vehicle first-stage could be as low as one-fifth of the stiffness of the baseline vehicle first-stage as described above before a 10-percent reduction in the actual vehicle frequency would occur. This indicates that vehicle frequency is insensitive to first-stage stiffness variation, which in this case would be attributed to the neglect of cluster structure flexibility. The actual first-stage stiffness of the previous study vehicle was 43.4 percent of the baseline stiffness and resulted in a 4-percent reduction of the baseline stiffness. Assuming the present study vehicle to have similar characteristics because of the similar clustering concepts, the actual first-mode frequency of the present vehicle would be 1.31 cps.

The first-mode frequency of the individual motors in the first-stage booster were determined by single-beam theory to be 1.78 cps, which is larger than the first-mode frequency of 1.37 cps for the baseline vehicle. However, a more complete analysis is necessary to establish the effects of the coupled frequencies and mode shapes.

3.2.8.6.2.5 Ignition Transients

The effect of the ignition transients on vehicle loads was analyzed under a previous portion of Contract NAS8-2438 by Boeing for a smaller but similar vehicle using forehead ignition (Reference 15). The results of the above study indicate that the ignition transient does not present a problem if the rise time is greater than the natural period of the vehicle. However, since pad-mounted base ignition is to be employed, a potential problem area arises in the dissipation of the shockwave that impinges on the forward head. Further analysis may indicate limitations on the igniter pulse to avoid excessive vehicle loads.

3.2.8.6.3 Second-Stage Detail Analysis

3.2.8.6.3.1 Discussion

The second-stage structural layout drawings are shown in Section 3.2.11, Figures 3.2.11-4, -5, and -6. The trade study that led to selection of the second-stage separate-tank concept is discussed in 3.2.8.3.

The material used in the analysis of all-welded tankage was 2219-T87 aluminum because of its good fracture toughness and weldability. Material chosen for built-up structure was 7075-T6 because of its high-strength features.

The lower elliptical bulkheads posed a special problem in that they developed hoop compression stresses under the large pressure gradients associated with first-stage burnout loads. Skin thickness was increased to prevent instability in the upper 110 inches of the LO_2 bulkhead shell. It was noted that changing the dome contour to hemispherical was not sufficient to eliminate the compression problem.

External cork insulation sealed by a mylar film was chosen for the LH_2 tank (see 3.2.10.5). Cryogenic allowables were therefore used for the tank materials. This led to development of a room-temperature proof test that had to satisfy the strength requirements as well as the fracture toughness criteria using water as the pressurizing medium. Upper-head and sidewall gages were increased by proof-test requirements.

A silo proof test was proposed for the hydrogen tank that would provide a uniform internal proof pressure. The hydrogen tank was stiffened for the maximum q, 20-degree-angle-of-attack failure condition by integrally milled T-section stiffeners.

This method of stiffening was chosen to expedite forming procedures. The stringer panels were tapered to increase structural efficiency. With constant stringer spacing and skin gages fixed by pressure requirements, minimum-weight sections could not be obtained at both extremities of the tank. To obtain a near-optimum-weight design under these conditions, the section of maximum load was optimized and a positive margin of safety of 0.71 was accepted for compressive strength at the section of minimum load. Test work is required to evaluate the effect of pressure on the stability of the stringers with fixed frames to ensure a functional design under conditions of axial load plus pressure.

The intertank regions were designed of zee-stiffened panels. The temperature in this section at design load was 88°F resulting from aerodynamic heating.

The thrust structure contained four tapered longerons that redistributed the engine loads. These members were sized using a compatible-deflection shear-log analysis. The thrust structure design temperature was assumed to be 185°F.

3.2.8.6.3.2 Criteria and Loads (Second Stage)

The design conditions and criteria for the second stage are shown in Table 3.2.8-8. The load distributions for each structural component are included in the individual analyses.

The tank proof test requirements and design load comparisons are included in the following paragraphs.

Proof Pressure (Base Metal Only) — A room-temperature proof test that will test the propellant tank for equivalent cryogenic strength requirements as well as fracture toughness criteria is discussed herein (Table 3.2.8-13). The strength of a material increases with decrease in temperature. A proof test at room temperature with pressures reduced in proportion to the reduction in allowable strength from cryogenic operating temperature to room temperature would test the propellant container for strength. The room-temperature proof test would also test the container for fracture toughness if the stress level was sufficiently high to guarantee that the maximum flaw size existing in the container is equal to or less than 0.8 of the critical flaw size at operating temperature and operating stress.

Hydrogen-Tank Proof Test (Base Metal) — The maximum operating pressure in the LH_2 tank ranges from 38 psi to 50.58 psi at cryogenic temperatures (Figure 3.2.8-25). These pressures can be reduced for room-temperature proof test in proportion to the decrease in strength.

PROPERTIES OF 2219-T87 ALUMINUM		
Maximum Stresses	Cryogenic Temperature (423°F)	Room Temperature (70°F)
F_{tu}	93,000 psi	62,500 psi
F_{ty}	65,000 psi	50,000 psi
Operating Stress		
σ ultimate	93,000/1.4 = 62,200	62,500/1.4 = 44,600
σ yield	65,000/1.1 = 59,000	50,000/1.1 = 45,400
	Yield Critical	Ult. Critical

Table 3.2.8-13

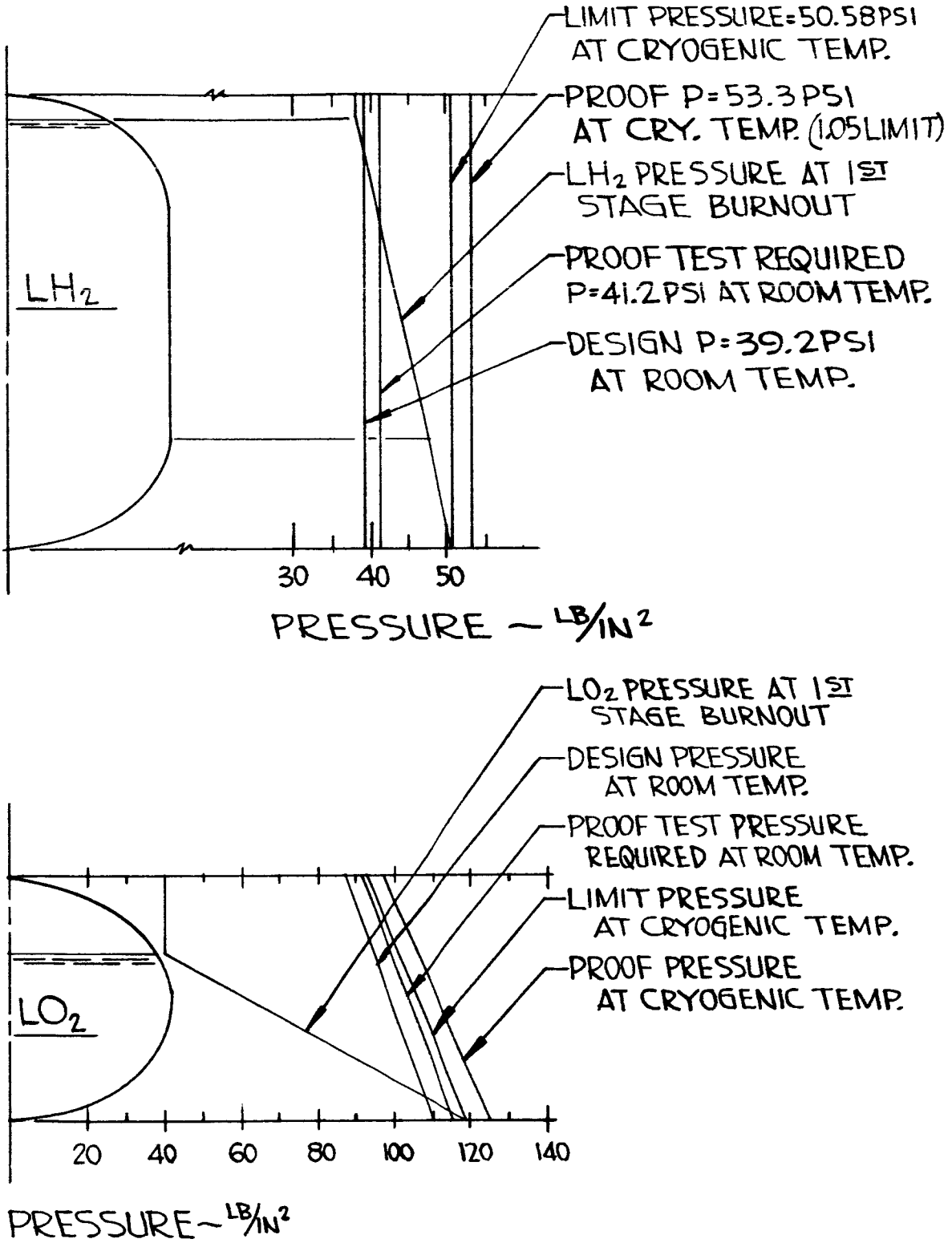

Figure 3.2.8-25 SECOND-STAGE TANK DESIGN PRESSURE

Assuming that proof testing at room temperature must guarantee $(a/Q)_{max}$ = 0.80 x $(a/Q)_{cr}$ at LH_2 operating stress (59,000 psi) (see Table 3.2.8-13) — based on 2219-T6 E46 data — it is presently estimated that a flaw that is less than 80-percent of critical at operating pressures will not propagate to failure under sustained loading during the estimated service life of the booster, where $(a/Q)_{cr}$ is the critical flaw size that would propagate at operating stress. The critical flaw size at cryogenic temperature is: $(a/Q)_{cr}$ = 0.14 inch (from Figure 3.2.8-26). The allowable crack size at room temperature is: $(a/Q)_{max}$ = (0.80) x (0.14 = 0.112 inch.

Room-temperature stress required to satisfy cryogenic fracture toughness criteria is:

σ = 48,000 psi (Figure 3.2.8-27)

σ = (45,400)(1.05) = 47,500 psi proof stress required for strength demonstration. (The required proof stress for strength is 47,500 psi and required stress for critical flaw-size criteria is 48,000 psi. Use 48,000 psi for proof test.)

The reduced pressure required for proof test of the hydrogen tank is as follows:

Pressure + head at bottom of the LH_2 tank at first-stage burnout = 50.58 psi

$$P_{proof} = \frac{50.58\ (48,000)}{50,000} = 41.2 \text{ psi}$$

$$P_{limit} = \frac{41.20}{1.05} = 39.2 \text{ psi}$$

Figure 3.2.8-25 indicates the required proof pressure versus tank height of the LH_2 tank for a room-temperature proof test.

Method of LH_2 Tank Testing —The hydrogen tank will be proof tested in a silo using water as the pressurizing medium and with water surrounding the tank to provide a uniform internal proof pressure. Upper head and sidewall gages were increased by this proof-test requirement. Other methods considered were proof testing with full operating pressure at room temperature and uniform internal pressure and proof testing with reduced pressure and water-pressure gradient. However, these conditions imposed greater skin-gage penalties.

LO_2 Tank Proof Pressure (Base Metal) — The proof pressure required for equivalent cryogenic fracture toughness is calculated in the following manner.

Proof stress required to demonstrate strength at room temperature: (operating stress x 1.05).

$$\sigma = 45,400 \text{ x } 1.05 = 47,500 \text{ psi}$$

From Figure 3.2.8-27, at 47,500 psi, the maximum flaw size existing in the material is (a/Q) = 0.115 inch.

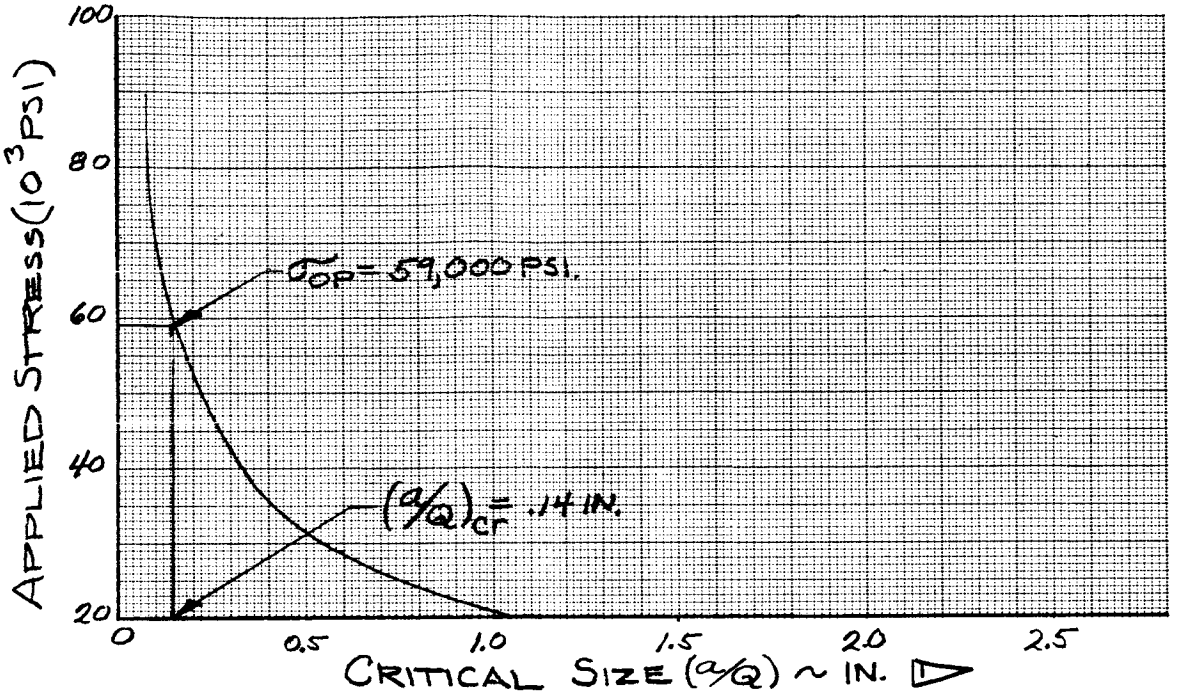

Figure 3.2.8-26 CRITICAL FLAW SIZE — 2219-T87 ALUMINUM
Liquid Hydrogen Temperature (-423°F)

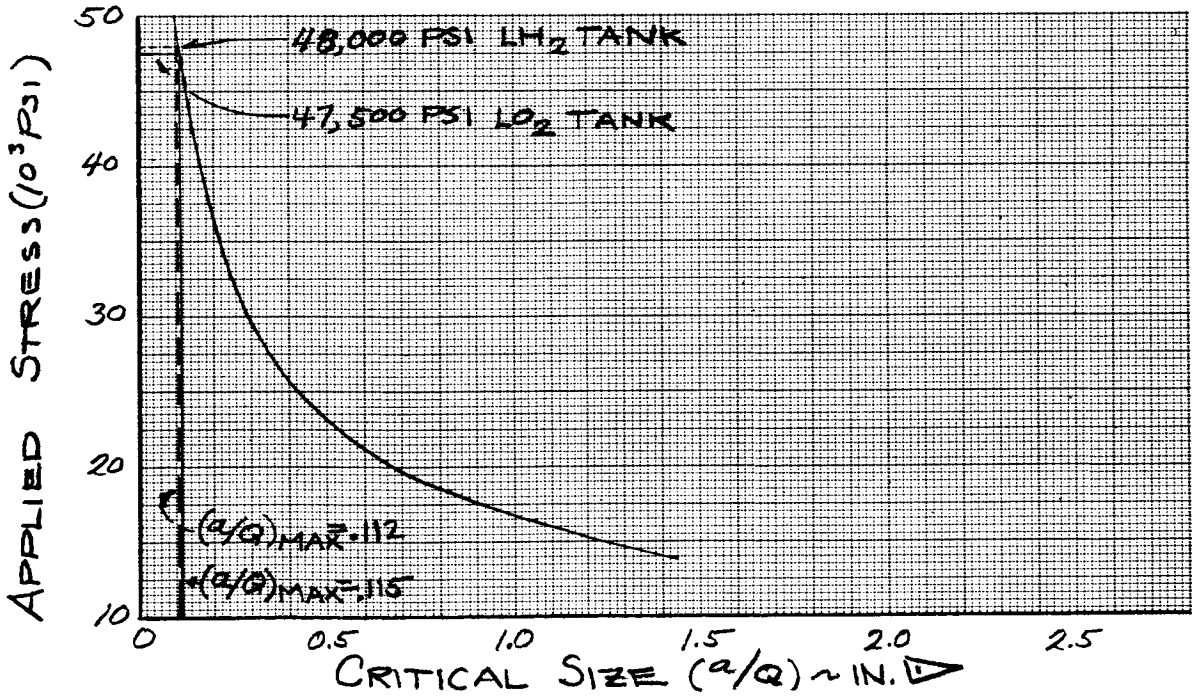

Figure 3.2.8-27 CRITICAL FLAW SIZE — 2219-T87 ALUMINUM
Room Temperature

Assume proof testing at room temperature must guarantee $(a/Q)_{max} = 0.80$ $(a/Q)_{cr}$ at LO_2 operating stress (see also LH_2 proof-test discussion).

Using the above equation with $(a/Q)_{max} = 0.115$ inch, the critical flaw size for hydrogen tank operating conditions can be defined as:

$$(a/Q)_{cr} = \frac{0.115}{0.8} = 0.144 \text{ inch}$$

With the critical flaw size defined, the maximum allowable operating stress at cryogenic temperature, obtained from Figure 3.2.8-28, is:

$$\sigma = 49,000 \text{ at } -320°F$$

The skin gage is sized by the operating stress = 49,000 psi and operating pressure plus head = 119.2 psi.

$$t = \frac{119.2 \times 600}{49,000 \times 2} = 0.73 \text{ inch (aft head)}$$

The required pressure for room-temperature proof pressure at $\sigma = 47,500$ psi is:

$$P_{proof} = \frac{0.73\ (47,500)\ 2}{600} = 115.8 \text{ psi}$$

$$P_{limit} = \frac{115.8}{1.05} = 110 \text{ psi}$$

Proof Pressure (Weld Zone) — The proof-test criteria used for design purposes in this study considered the properties of the base metal only. The weld-zone proof-test requirements, which may increase the proof pressure markedly, were not included. The following proof-test requirements were predicted for the weld zones using fracture toughness data that was considerably below that of the base metal. The fracture toughness properties of welds vary with process control and are a function of the inspection-acceptance specifications. The indicated weld-zone proof-test penalty will be required in addition to the base-metal proof test unless the fracture toughness properties of the welds are improved. This is a problem which is not well understood and additional effort should be devoted to weld toughness improvement.

The room-temperature proof test required in the weld zone for equivalent cryogenic strength is similar to the proof test required in the base material (see 3.2.8.6.3.2). However, to ensure equivalent cryogenic fracture toughness in the weld zone, the room-temperature proof-test pressure in the LH_2 tank must be increased above that necessary to ensure base-metal integrity. Weld-zone fracture toughness varies such that higher toughness is observed at -320°F than at -423°F. This produces a penalty for proof test of the welds at -423°F but not

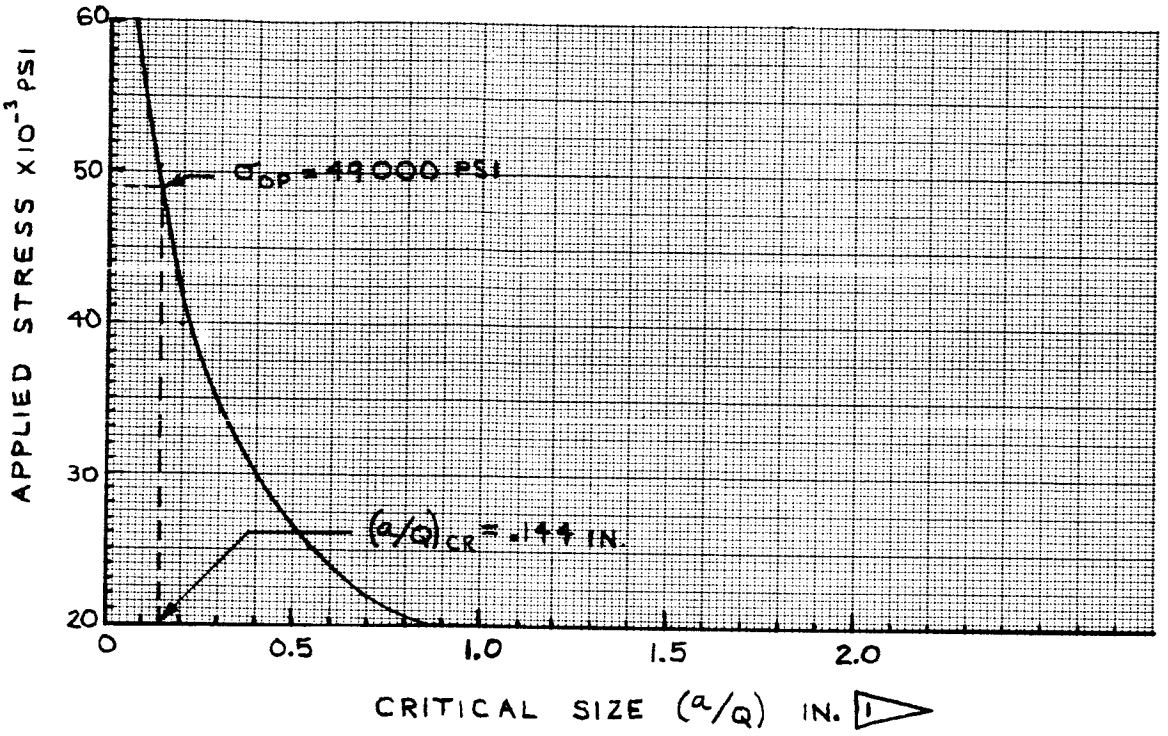

Figure 3.2.8-28 CRITICAL FLAW SIZE — 2219-T87 ALUMINUM
Liquid Oxygen Temperature (-320°F)

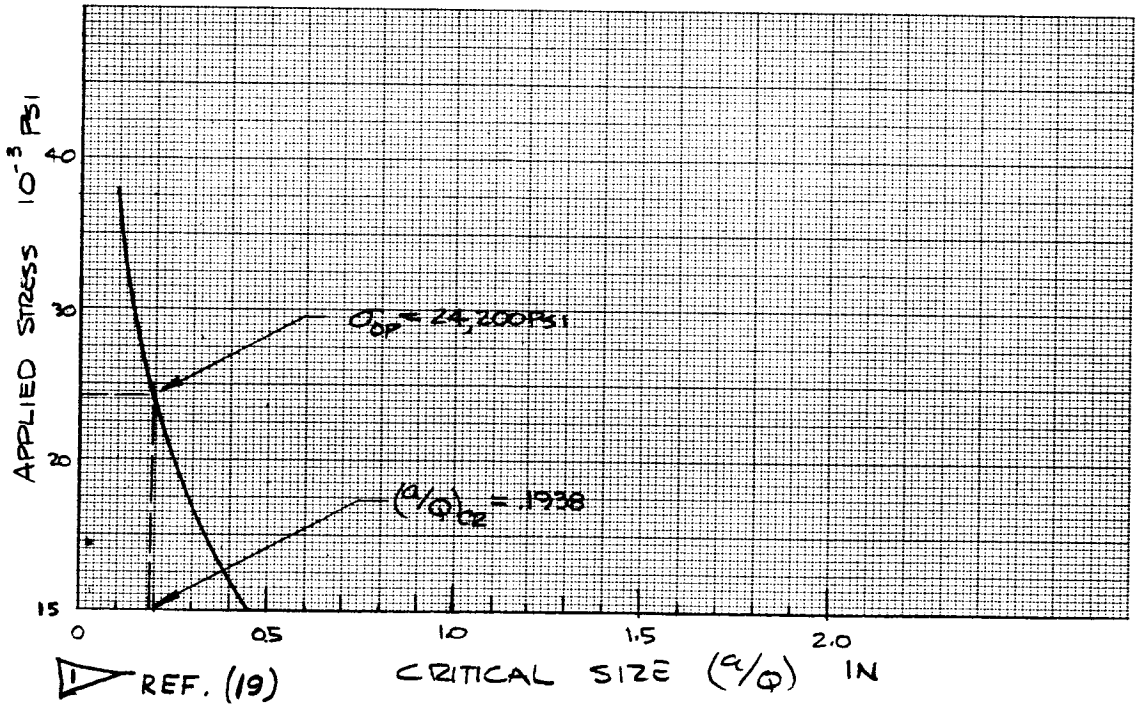

Figure 3.2.8-29 2219-T87 ALUMINUM WELD — 2319 FILLER
Liquid Hydrogen Temperature (-423°F)

at -320°F. A 21-percent increase in the proof pressure was required on the proof pressure was required on the LH_2 tank and a 1.37-percent reduction in the LO_2 tank.

The proof pressure required for equivalent cryogenic fracture toughness is calculated in the following manner.

Proof stress required to demonstrate strength at room temperature: (operating stress x 1.05).

$$\sigma = \frac{45,400 \times 1.05}{2} = 23,800 \text{ psi}^*$$

From Figure 3.2.8-30, at 23,800 psi, the maximum flaw size existing in the material is (a/Q) = 0.155 inch.

Assume proof testing at room temperature must guarantee $(a/Q)_{max} = 0.80$ $(a/Q)_{cr}$ at LH_2 operating stress (see also base-metal proof-test discussion).

Hydrogen Tank (Weld Zone) — Using the above equation with $(a/Q)_{max} = 0.155$ inch, the critical flaw size for hydrogen tank operating conditions can be defined.

$$(a/Q)_{cr} = \frac{0.155}{0.8} = 0.1938 \text{ inch}$$

With the critical flaw size defined, the maximum allowable operating stress at cryogenic temperature is obtained from Figure 3.2.8-29.

$$\sigma_{op} = 24,200 \text{ psi at } -423°F$$

The hydrogen-tank skin gage in the weld zone is sized by the operating stress = 24,200 psi and operating pressure plus head = 50.58 psi.

$$t = \frac{50.58 \times 1 \times 600}{24,200 \times 2} = 0.627 \text{ inch (aft head)}$$

The required pressure for room temperature proof pressure at σ = 23,800 psi is:

$$P_{proof} = \frac{0.627\ (23,800)\ 2}{1\ (600)} = 49.7 \text{ psi}$$

$$P_{limit} = 49.7/1.05 = 47.3 \text{ psi}$$

* The "as welded" joint strength was taken as 50 percent of the base-metal strength.

LO_2 Tank (Weld Zone) — The reduced pressures required for proof testing of the LO_2 tank were determined in a manner similar to that used for determining the reduced pressure required for the hydrogen tank.

Room-temperature properties from LH_2 tank analysis:

$$(a/Q)_{max} = 0.155 \text{ inch}$$

$$= 23,800 \text{ psi}$$

The critical flaw size for the LO_2 tank operating conditions was defined as:

$$(a/Q)_{max} = 0.80\ (a/Q)_{cr}$$

The allowable flaw at cryogenic temperature is:

$$(a/Q)_{cr} = \frac{0.155}{0.8} = 0.1938 \text{ inch}$$

With the critical flaw size defined, the maximum allowable operating stress, obtained from Figure 3.2.8-31 is:

$$\sigma_{op} = 25,000 \text{ psi at } -320°F$$

Skin gage required in the weld zone with the operating stress = 25,000 psi and operating pressure plus head = 119.2 psi:

$$t = \frac{119.2 \times 1 \times 525}{25,000 \times 2} = 1.25 \text{ inches (aft head)}$$

The required pressure for room-temperature proof pressure at σ = 23,800 psi:

$$P_{proof} = \frac{1.25\ (23,800)}{1\ (525)} = 114.2 \text{ psi}$$

$$P_{limit} = 114.2/1.05 = 108.8 \text{ psi}$$

Second-Stage Loads — Figure 3.2.8-32 presents the second-stage design loads versus station for ground-wind and flight-loading conditions (see 3.2.8.6.2). The ground-wind load condition was based on no internal pressure and propellant tanks filled. The ultimate first-stage maximum symmetrical thrust loads were determined by combining ultimate axial loads and minimum internal pressures. The maximum q 20-degree-angle-of-attack load condition is a failure condition and was considered as an ultimate load with minimum internal pressure in the hydrogen tank.

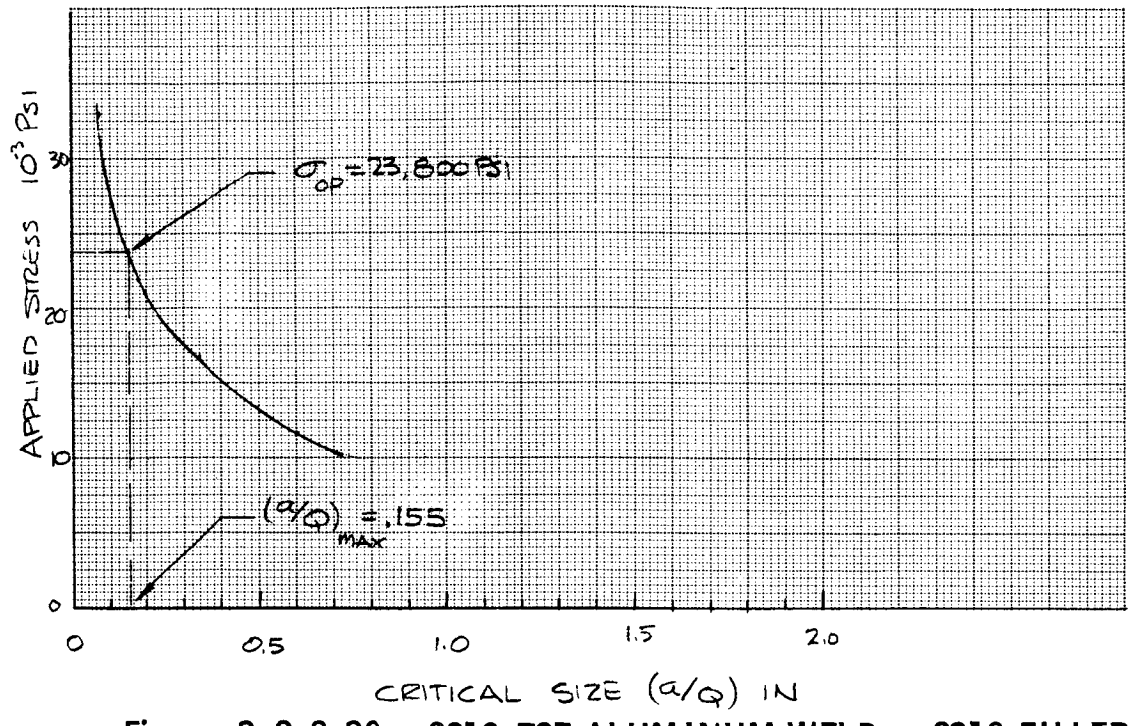

Figure 3.2.8-30 2219-T87 ALUMINUM WELD — 2319 FILLER
Room Temperature

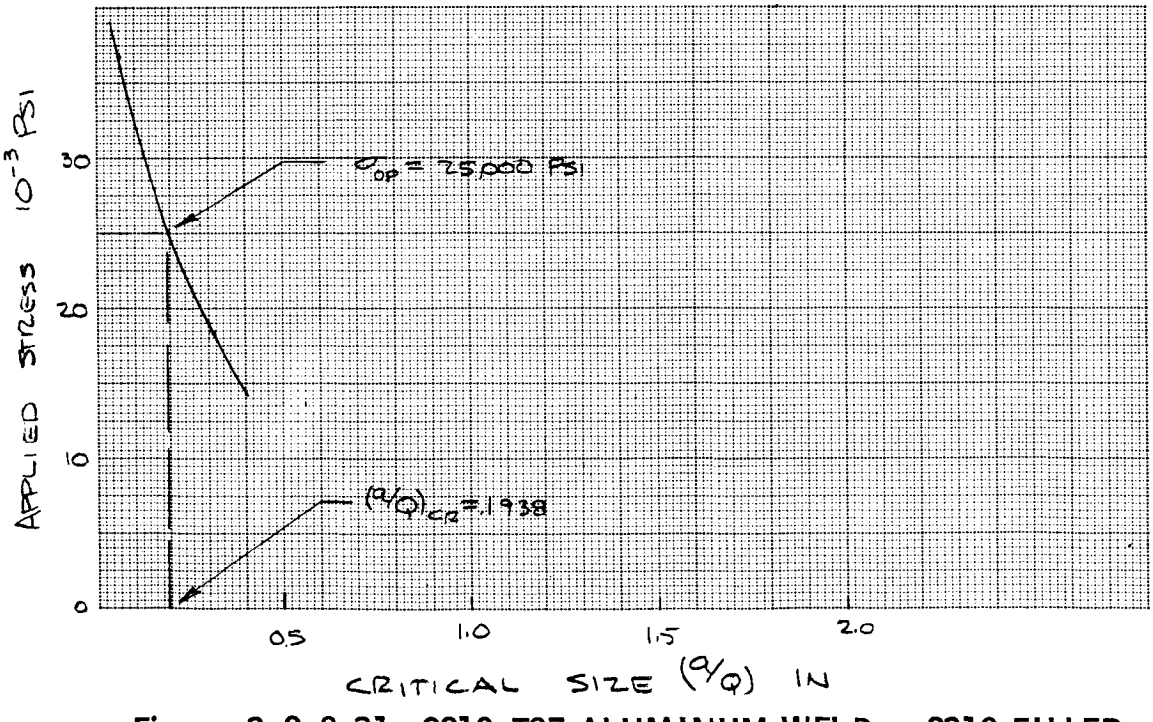

Figure 3.2.8-31 2219-T87 ALUMINUM WELD — 2319 FILLER
Liquid Oxygen Temperature (-320°F)

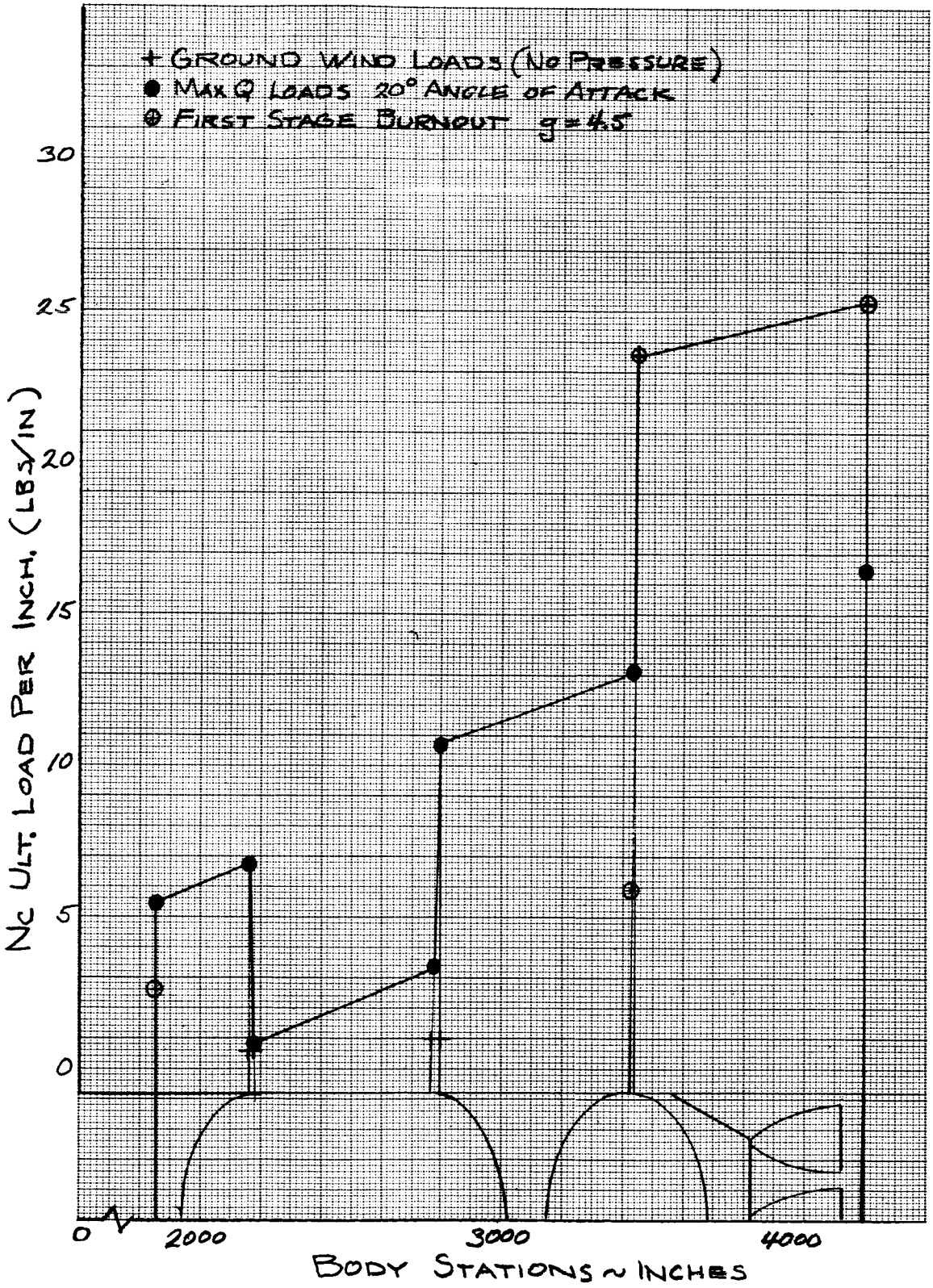

Figure 3.2.8-32 SECOND-STAGE ULTIMATE DESIGN LOADS

3.2.8.6.3.3 Second-Stage Materials

The analysis of all-welded cryogenic tankage used 2219-T87 aluminum allowables. This choice was based primarily on fracture toughness and weldability considerations. This alloy has excellent stress-corrosion resistance based on standard corrosion testing. The higher strength, comparable reliability, and successful performance at Boeing led to the selection of 2219-T87 over other alloys. The ultimate and yield strengths of 2219-T87 versus temperature are shown in Figure 3.2.8-33.

The analysis of the thrust structure and all-built-up unwelded structure used 7075-T6 aluminum allowables. The allowables are given in Reference 5.

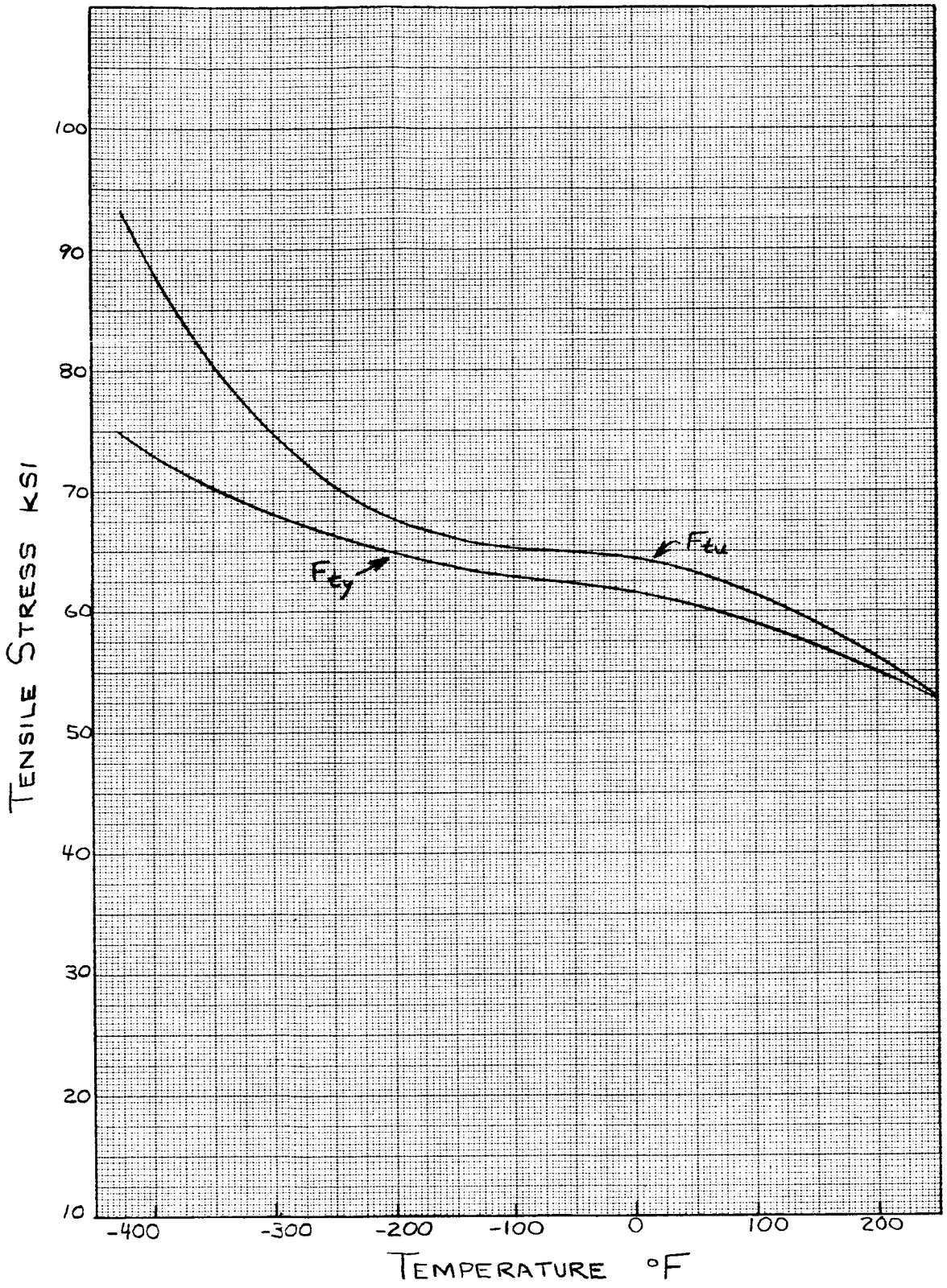

Figure 3.2.8-33 ALLOWABLE STRESS VERSUS TEMPERATURE 2219-T87 Aluminum Alloy

BLANK

3.2.8.6.3.4 Hydrogen Tank (Second Stage)

Forward Head (LH_2 Tank) — The forward hydrogen-tank bulkhead is a 0.707 ellipsoid terminating in a Y-ring sidewall joint. The bulkhead segments are tapered to the minimum required gage. The skin gage was designed by proof pressure.

FORWARD HEAD (LH_2 TANK)

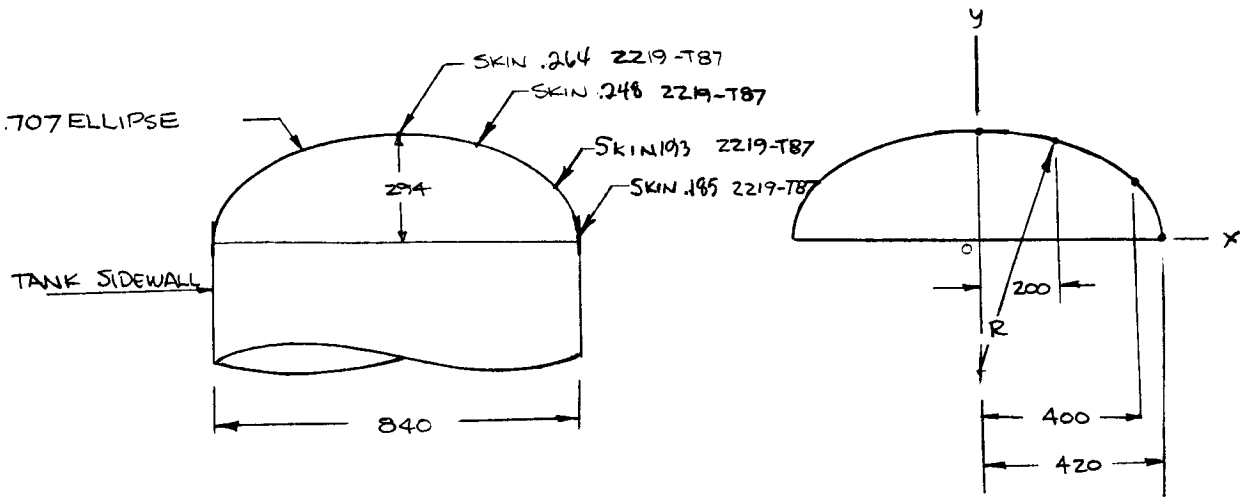

DESIGN CONDITION:

PROOF TEST PRESSURE REQUIREMENT

PRESSURE = 39.2 PSI, LIMIT AT ROOM TEMP. [1]

$$f_T = \frac{39.2\ (1.4)\ 600}{2\ (.264)} = 62{,}500\ \text{PSI} \qquad F_{TU} = 62{,}500\ [3]$$

M.S. = 0 ←

X	y	R RADIUS OF CURVATURE	t	M.S.	OPERATING CONDITION M.S.
0	294	m=600 H=600	.264	0	0.37
200	258	m=495 H=564	.248	0	0.37
400	89.7	m=237 H=440	.193	0	0.33
420	0	m=206 H=420	.185	0	0.30

[1] FIGURE 3.2.8-26

[2] FIGURE 3.2.8-33

Sidewall (LH_2 Tank) — The hydrogen tank sidewall consists of integrally milled T-stiffened panels. The skin was designed for room-temperature proof test pressure, and was checked at the forward and aft end of the sidewall for combined stresses at maximum q, 20-degree-angle-of-attack failure load conditions. The skin gage at the aft end of the sidewall required additional thickness to accommodate combined stresses. The stiffeners and skin panels were tapered to increase the structural efficiency, and frames were utilized to provide stability.

With constant stringer spacing and skin gages fixed by presssure requirements, minimum-weight sections could not be obtained at both extremities of the tank. To obtain a near-optimum-weight design under these conditions, the section of maximum load was optimized and a positive margin of safety was accepted at the section of minimum load.

FORWARD SIDEWALL (LH_2 TANK)

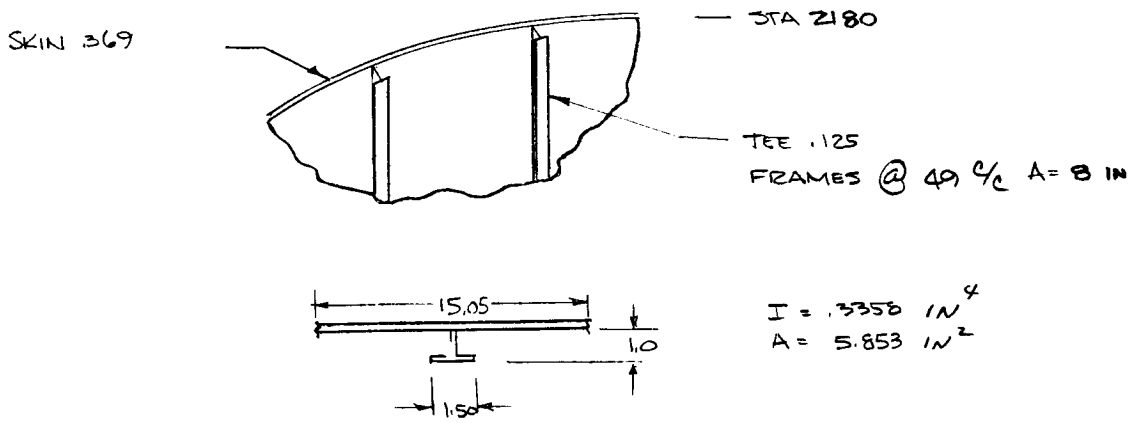

DESIGN CONDITION:

PROOF TEST PRESSURE REQUIREMENT

PRESSURE = 39.2 PSI LIMIT AT ROOM TEMP [1]
PRESSURE = 39.88 PSI @ 1ST STAGE B.O. STA 2180 AND CRYOGENIC TEMP.
ULTIMATE LOAD AT MAX Q, 20° ANGLE OF ATTACK [3]

$N_c = 810$ LB/IN

SKIN GAGE

ROOM TEMP

$$f_T = \frac{39.2\ (1.4)\ 420}{.369} = 62{,}500 \text{ PSI}$$

$F_{TU_{70°F}} = 62{,}500$ PSI [2]

M.S. = 0 AT ROOM TEMP PROOF TEST

CRYOGENIC TEMP

$$f_T = \frac{39.88\ (1.4)\ 420}{.369} = 63{,}500 \text{ PSI}$$

$F_{TU_{423°F}} = 93{,}000$ PSI [2]

$$f_c = \frac{810^{LB}/_{IN}\ (15.05)}{5.853} = 2080 \text{ PSI}$$

$F_S = \frac{1}{2} F_{t_u} = 46{,}500$ PSI [4]

$$f_{S\,MAX} = \frac{63{,}500 + 2080}{2} = 32{,}790 \text{ PSI}$$

$$M.S. = \frac{46{,}500}{32{,}790} - 1 = 0.40$$ @ MAX Q CRY. TEMP.

[1] FIGURE 3.2.8-25

[2] FIGURE 3.2.8-33

[3] FIGURE 3.2.8-32

[4] THE MAXIMUM SHEARING STRESS FAILURE THEORY IS ASSUMED APPLICABLE.

FORWARD SIDEWALL (LH_2 - TANK) — CON'T.

COMPRESSION STRENGTH OF HEAVY GAGE STIFFENED PANEL

ANALYSIS PER REFERENCE (10) SECTION 22.2.2

T- STIFFENER CRUSHING STRENGTH

$$A/t^2 = \frac{.3033}{(.125)^2} = 19.4$$

CRIPPLING ALLOWABLE FOR 7075-T6 AND INCREASED BY A RATIO OF YIELD STRENGTH.

$$F_{cc_{STIF}} = 27{,}700 \times \frac{65}{64} = 28{,}160 \text{ PSI}$$ ▷

SHEET BUCKLING STRESS

$$b/t = \frac{15.05}{.369} = 40.8$$

$$F_{c_{SKIN}} = 31{,}400 \text{ PSI}$$

CRUSHING STRENGTH OF PANEL

$$F_c = \frac{F_{cc_{STIF}} A_{STIF} + F_{c_{SKIN}} A_{SKIN}}{A_{STIF} + A_{SKIN}}$$

$$= \frac{28{,}160\,(.3030) + 31{,}400\,(5.55)}{5.853} = \underline{10{,}450 \text{ PSI}}$$

ULTIMATE STRENGTH OF PANEL

$$L/\rho\sqrt{c} = 49/.24(1.225) = 166.6$$

$$F_c = \frac{\pi^2 E}{(L'/\rho)^2} = \frac{\pi^2 10^7}{(166.6)^2} = 3550 \text{ PSI}$$

$$f_c = \frac{810 \text{ LB/IN } (15.05 \text{ IN})}{5.853} = 2080 \text{ PSI}$$

$$M.S. = \frac{3550}{2080} - 1 = \underline{.71} \leftarrow \text{M.S.}$$

▷ REFERENCE (3) SECTION 15

AFT SIDEWALL (LH_2 TANK)

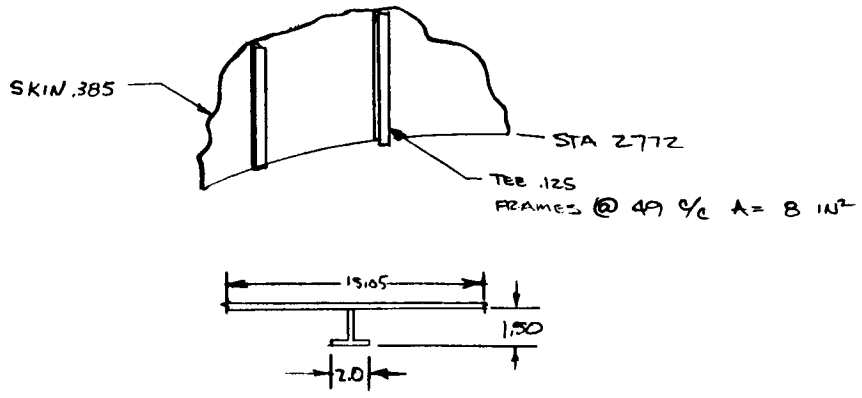

DESIGN CONDITION:

PROOF TEST PRESSURE REQUIREMENT

PRESSURE = 39.2 PSI LIMIT AT ROOM TEMP [1]

PRESSURE = 46.7 PSI @ 1ST STAGE B.O. STA 2772 AND CRY. TEMP.

ULTIMATE LOAD AT MAX Q, 20° ANGLE OF ATTACK

$N_c = 3290$ LB/IN [3]

SKIN GAGE

ROOM TEMP.

$$f_t = \frac{39.2(1.4)420}{.385} = 59{,}900 \text{ PSI} \qquad F_{tu} = 62{,}500 \text{ PSI} \text{ [2]}$$

$$MS = \frac{62{,}500}{59{,}900} - 1 = .06 \longleftarrow$$

CRYOGENIC TEMPERATURE

PRESSURE = 38 + 8.7 = 46.7 PSI

$$f_{t_{HOOP}} = \frac{46.7(420)1.4}{.385} = 71{,}300 \text{ PSI} \qquad F_s = \tfrac{1}{2} F_{tu} = 46{,}500 \text{ PSI} \text{ [4]}$$

$$f_c = \frac{3290(15.05)}{6.232} = 7940 \text{ PSI}$$

$$f_{s\,MAX} = \frac{71{,}300 + 7940}{2} = 39{,}620 \text{ PSI}$$

$$M.S. = \frac{46{,}500}{39{,}620} - 1 = .17 \longleftarrow$$

[1] FIGURE 3.2.8-25
[2] FIGURE 3.2.8-33
[3] FIGURE 3.2.8-32
[4] THE MAXIMUM SHEARING STRESS FAILURE THEORY IS ASSUMED APPLICABLE.

AFT SIDEWALL (LH_2 - TANK) - CONT.

COMPRESSION STRENGTH OF HEAVY GAGE STIFFENED PANELS

ANALYSIS PER REFERENCE (10) SECTION 22.2.2

T-STIFFENER - CRUSHING STRENGTH

$$A/t^2 = \frac{.432}{(.125)^2} = 27.6$$

CRUSHING ALLOWABLE FOR 7075-T6 AND INCREASED BY A RATIO OF YIELD STRENGTH.

$$F_{cc_{STIF.}} = 20{,}500 \frac{65}{60} = 20{,}800 \text{ PSI}$$

SHEET BUCKLING STRESS

$$b/t = \frac{15.05}{.385} = 39.1$$

$$F_{cc\,SKIN} = 33{,}000 \text{ PSI}$$

CRUSHING STRENGTH OF PANEL

$$F_c = \frac{F_{cc\,STIF} A_{STIF} + F_{cc\,SKIN} A_{SKIN}}{A_{STIF} + A_{SKIN}}$$

$$= \frac{20{,}800(.432) + 33{,}000(5.8)}{6.232}$$

$$= 32{,}000 \text{ PSI}$$

ULTIMATE STRENGTH OF PANEL

$$L/\rho\sqrt{c} = 49/.373(1.225) = 107.5$$

$$P/A = \frac{\pi^2 E}{(L/\rho)^2} = \frac{\pi^2 10^7}{(107.5)^2} = 8530 \text{ PSI}$$

$$f_c = \frac{3290\,(15.05)}{6.232} = 7940 \text{ PSI}$$

$$M.S. = \frac{8530}{7940} - 1 = +.07$$

FRAMES – LH_2 TANK

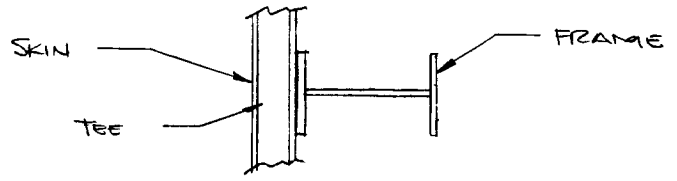

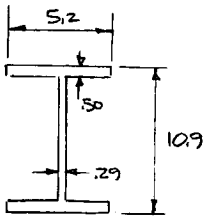

$I = 166.2$
$A = 8\ IN^2$

DESIGN CONDITION:

ULTIMATE LOAD AT MAX Q 20° ANGLE OF ATTACK

STA 2180 FWD END OF LH_2 TANK $N_c = 810\ LB/IN$ [1]

STA 2772 AFT END OF LH_2 TANK $N_c = 3290\ LB/IN$ [1]

$$\text{REQUIRED } I_{FWD} = \frac{.785\ R^4\ w}{E\ 1000\ L} \text{ [2]} = \frac{.785\ (420)^4\ 810}{10^{10}\ (49)} = 40.2$$

$$\text{REQUIRED } I_{AFT} = \frac{40.2}{810}(3290) = 163.2\ IN^4$$

FRAME USED:

$$I_{FRAME} = 166.2\ IN^4$$

[1] FIGURE 3.2.8-82

[2] REFERENCE 7, PAGE 590

Aft Head (LH_2 Tank) — The aft hydrogen-tank bulkhead was a 0.8 ellipsoid terminating in a Y-ring sidewall joint. The 0.8 ellipsoidal bulkhead was selected to minimize the stability problem associated with elliptical bulkheads and large pressure gradients. The bulkhead segments were tapered to the minimum required gage. The skin gage was designed for uniform internal proof pressure. The skin was checked for stability under hoop compression forces.

AFT HEAD - LH_2 TANK

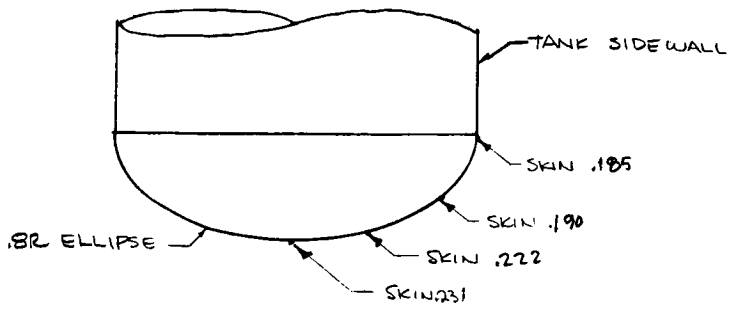

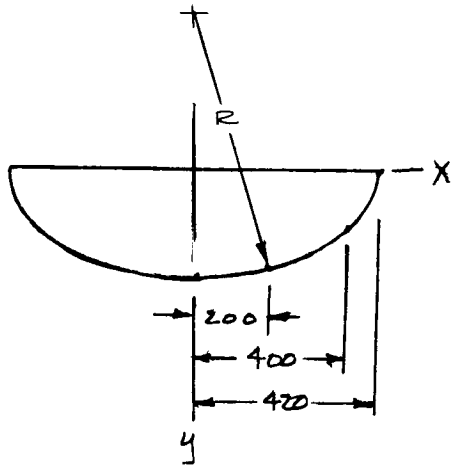

MATERIAL 2219 - T87

DESIGN CONDITION:

PROOF TEST PRESSURE REQUIREMENTS

PRESSURE = 39.2 PSI, LIMIT AT ROOM TEMP. [1]

$$f_t = \frac{39.2\ (1.4)}{2\ (.230)}\ \frac{525}{} = 62{,}500 \qquad F_{tu} = 62{,}500\ [2]$$

$$M.S. = \frac{62{,}500}{62{,}500} - 1 = 0$$

x	y	RADIUS OF CURVATURE		t	PROOF TEST M.S.	OPERATING M.S.
		HOOP	MERIDIAN			
0	336	525	525	.231	0	.11
200	296	504	465	.222	0	.09
400	102.5	431	290	.190	0	.04
420	0	420	269	.185	0	.03

[1] REFERENCE FIGURE 3.2.8-25

[2] REFERENCE FIGURE 3.2.8-33

3.2.8.6.3.5 Intertank Shell (Second Stage)

The intertank section is a stiffened-skin semimonocoque structure sized by the optimum design method of Reference 16 for the maximum load in the section. The maximum load occurs at the maximum q, 20-degree-angle-of-attack failure condition. Zee-section stringer-frame panels were used.

INTER TANK SHELL

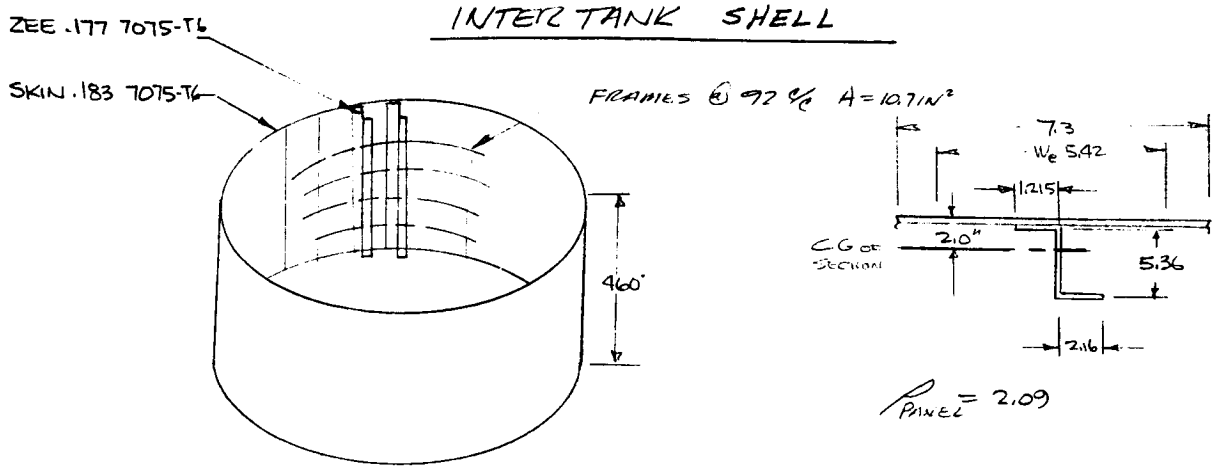

DESIGN CONDITION:

ULTIMATE LOAD AT MAX Q, 20° ANGLE OF ATTACK

$N_c = 13,040$ LB/IN [1]

COMPRESSION STRENGTH OF STIFFENED PANEL

ANALYSIS PER REFERENCE (10) SECTION 22.2.2

CRUSHING STRENGTH — Z-STIFFENER

$$A/t^2 = \frac{1.546}{.177^2} = 49.4$$

$$F_{cc\,STIF} = 41,000 \text{ PSI}$$

SHEET BUCKLING STRESS

$$b/t = \frac{7.3}{.183} = 40$$

$$F_{cc\,SKIN} = 33,500 \text{ PSI}$$

CRUSHING STRENGTH OF PANEL

$$F_c = \frac{F_{cc\,STIF}\, A_{STIF} + F_{cc\,SKIN}\, A_{SKIN}}{A_{STIF} + A_{SKIN}}$$

$$F_c = \frac{41,000(1.546) + 33,500(1.336)}{2.882} = 37,500 \text{ PSI}$$

[1] FIGURE 3.2.8-32

INTERTANK SHELL, CONT.

SKIN EFFECTIVE WIDTH

$$W_e = 1.7 t \sqrt{E/F_c}$$

$$= 1.7(.183)\sqrt{10^7/13{,}040} = 5.42$$

ULTIMATE STRENGTH OF PANEL

$$L/\rho\sqrt{c} = 92/209(1.225) = 35.9$$

$$F_c = 33{,}000 \text{ PSI}$$

$$f_c = \frac{13{,}040\ (7.3)}{2.882} = 33{,}000 \text{ PSI}$$

$$M.S. = \frac{33{,}000}{33{,}000} - 1 = \underline{0} \longleftarrow$$

FRAMES

REQUIRED $I_F = \dfrac{.785\ R^4 W}{1000\ L\ E} = \dfrac{.785(420)^4\ 13{,}040}{1000\ (92)\ 10^7} = 345 \text{ IN}^4$ [1]

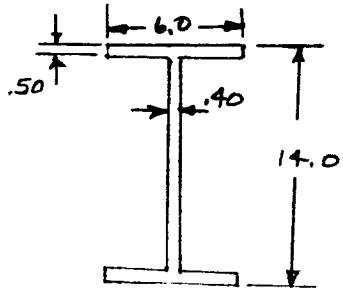

FRAME CROSS SECTION

MATERIAL: 7075-T6
$A = 11.2 \text{ IN}^2$
$I_F = 345 \text{ IN}^4$

[1] REFERENCE 1, PAGE 590

BLANK

3.2.8.6.3.6 Oxygen Tank (Second Stage)

Forward Head — The LO_2 tank configuration was selected on the basis of the second-stage tankage bulkhead trades (see 3.2.8.4). The resulting configuration used an off-loaded ellipsoidal tank. The forward LO_2 tank head is a 0.707 ellipsoid joined to the 0.8 elliptical bulkhead with a double Y-ring. The bulkhead segments are tapered to the minimum required gage. The skin gage was designed for hydrostatic proof pressure, room-temperature allowables, and water-pressure gradient.

Aft Head — The aft LO_2 tank bulkhead is a 0.8 ellipsoid. The head segments are tapered from the bottom of the bulkhead to a point 110 inches from the top of the lower bulkhead. The large pressure gradient associated with first-stage burnout loads produces compression stresses in the upper 110 inches of the aft LO_2 bulkhead shell. The skin thickness was increased in this area to prevent instability.

HEADS (LO_2 TANK)

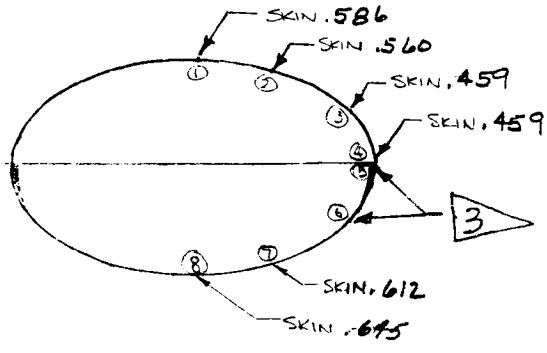

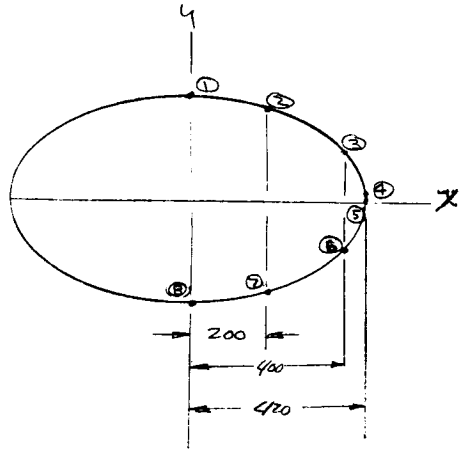

MATERIAL 2219-T87

DESIGN CONDITION:

PRESSURE TEST REQUIREMENT

LIMIT PRESURE = 87.25 @ POINT ① - ⑩; 110 @ POINT ⑧ [1]

POINT ①

$$f_{T①} = \frac{87.25(600)1.4}{2(.586)} = 62{,}500 \qquad F_{TU} = 62{,}500 \text{ [2]}$$

$$M.S. = \frac{62{,}500}{62{,}500} - 1 = 0$$

LOCATION	X	y	R_{HOOP}	$R_{MED.}$	PRESSURE	t	
①	0	336	600	600	87.25	.586	0
②	200	296	564	405	88.60	.560	0
③	400	102.5	440	237	93.80	.459	0
④	420	0	420	206	97.87	.459	0
⑤	420	0	420	269	97.87	[3]	
⑥	400	-102.5	431	290	101.57		
⑦	200	-296	504	465	108.55	.612	0
⑧	0	-336	525	525	110.00	.645	0

[1] FIGURE 3.2.8-25

[2] FIGURE 3.2.8-33

[3] CRITICAL HOOP COMPRESSION STRESS DESIGN CONDITION

AFT HEAD LO_2 TANK

INCREASED SKIN GAGE DUE TO HOOP COMPRESSION STRESS.

MATERIAL 2219 - T87

DESIGN CONDITION:

- 1ST. STAGE BURN OUT ($g = 4.5$)
- MINIMUM LOX PRESSURE ($P = 62$ PSI)

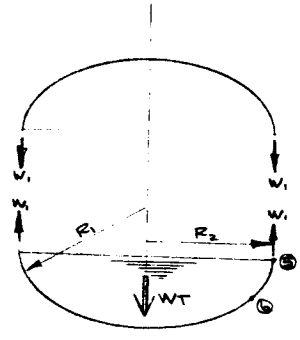

AT POINT ⑤
$W_2 = -13,450$ LB/IN COMPRESSION

AT POINT ⑥
$W_2 = -1,250$ LB/IN COMPRESSION

TANK HEAD COMPRESSIVE LOAD

SAMPLE CALCULATION

R_1 = MEDIAN RADIUS

R_2 = HOOP RADIUS

W_1 = LONGITUDINAL LOAD AT A POINT.

W_2 = LOAD AT A POINT IN THE HOOP DIRECTION

W_T = WEIGHT OF PROPELLANT BELOW THE POINT OF INTEREST

① $$\frac{W_1}{R_1} + \frac{W_2}{R_2} = P$$

② $$W_1 = \frac{W_T + PA}{C}$$

EQU. ②

$$W_1 = \frac{1.4(4.5)\,6,850,000\,\frac{71,750}{95,800} + (62)\,554,000}{2639}$$

$$W_1 = 25,300 \text{ LB/IN}$$

EQU. ①

$$\frac{25,300}{269} + \frac{W_2}{420} = 62$$

$$W_2 = -13,450 \text{ LB/IN COMPRESSION}$$

AFT HEAD LO_2 TANK

SKIN STABILITY IN THE AREA OF HOOP COMPRESSION

CRITICAL HOOP COMPRESSION STRESS

DESIGN CONDITION - FIRST STAGE BURN OUT

$$F_{cc} = K E \, t/R$$

$K = .2$ ▷

OR

$$W = K E \, t^2/R$$

$$t = \sqrt{\frac{WR}{KE}}$$

$$t = \sqrt{\frac{13,450(420)}{.2 \; 10^7}}$$

$$t = 1.68 \text{ IN.}$$

M.S. = 0

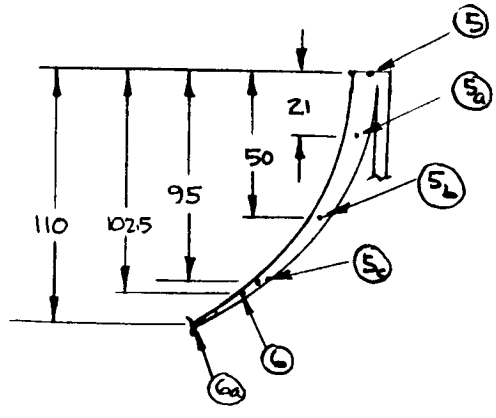

SKIN GAGE DETAIL

ADDED STABILITY OBTAINED FROM THE RESTRAINT OF THE Y-RING WAS NEGLECTED

LOCATION	x	y	R_m/R_H	t	W_2	M.S.
5	420	0	269/420	1.68	-13,450	0
5_a	419.2	-21	270/421	1.52	-11,000	0
5_b	415	-50	274/423	1.29	-7,860	0
5_c	404	-95	289/430	.725	-2,450	0
6	400	-102.5	299/431	.518	-1,250	0
6a	—	110	—	.614	0	TENSION DESIGNED

▷ USED ON SATURN S-IC

3.2.8.6.3.7 Thrust Structure (Second Stage)

The thrust-structure configuration was selected by the second-stage thrust structure trades (see 3.2.8.5). The thrust structure selected consisted of two aluminum shear-resistant thrust beams supporting a center engine with four equally spaced engines mounted on an aluminum ring. The engine thrust loads were transmitted through an aluminum cone-frustum structure, stiffened by four longerons and multiple stringers. The longerons were tapered to shear the load into the cone-frustum structure. A ring was placed at the cone-sidewall junction to react the kick loads caused by the slope. This ring is loaded by hoop tension because of the geometry and some bending because the thrust loads are not completely redistributed. The nonuniform load induced in the interstage structure by the second-stage engines is less than the design condition of the maximum axial acceleration during first-stage boost.

Description — The thrust structure consists of the following components.

- A thrust beam system that distributes the center-engine thrust load to four points on the engine-mount ring. The thrust beams also provide support for the engine actuators.

- An engine-mount ring capable of carrying the conservatively assumed uniform lateral kick load that results from thrust load and the geometry of the thrust cone.

- A stiffened cone-frustum consisting of a conical shell, four tapered longerons, and multiple stiffeners stabilized with rings.

- A forward thrust ring capable of carrying the thrust kick load that results from the cone-frustum geometry.

Design Loading Conditions — The thrust structure was designed by consideration of two loading conditions.

- Five-engine thrust at start-up with a dynamic factor of 1.4. This condition designed the majority of the thrust structure with the exception of the thrust beam.

- The four outside engines gimbaled 7.5 degrees radially outward with the center engine null. This condition was the critical load in designing the thrust beams as a beam column.

THRUST STRUCTURE (SECOND STAGE)

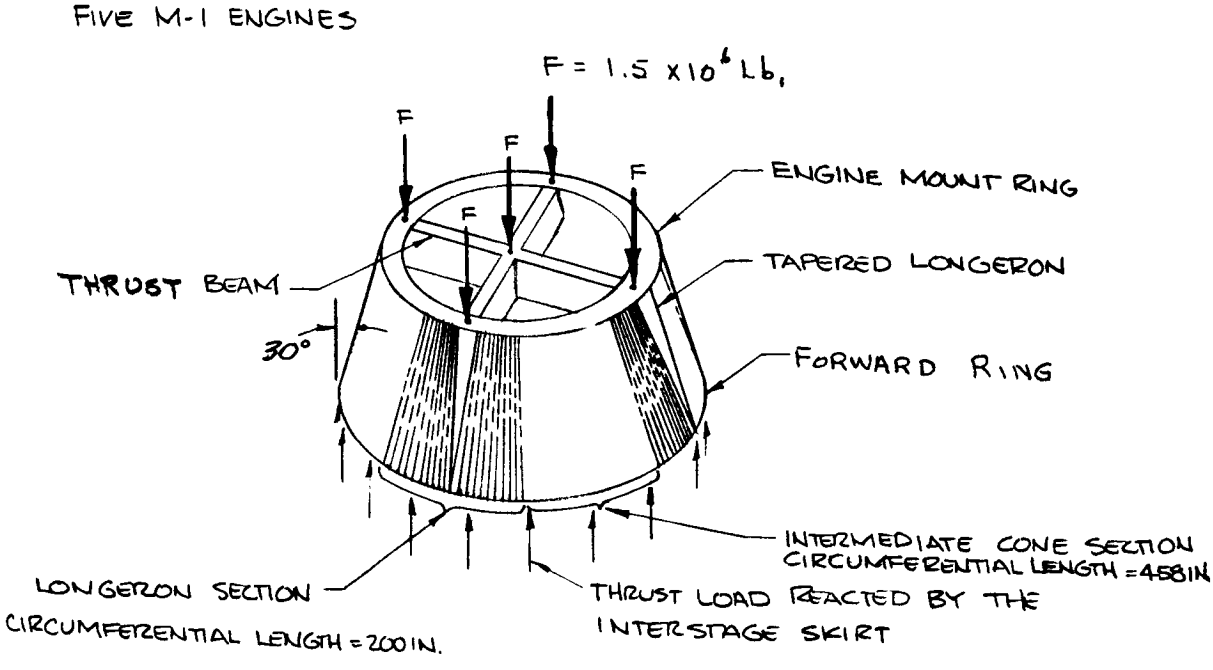

Figure 3.2.8-34

THRUST BEAM

THE CROSS BEAM SYSTEM DISTRIBUTES THE THRUST OF THE CENTER ENGINE TO FOUR POINTS ON THE ENGINE MOUNT RING OF THE THRUST STRUCTURE. THE BEAM ALSO REACTS THE KICK LOAD RESULTING FROM THE CONICAL FRUSTRUM GEOMETRY AND THE COMPRESSION LOAD RESULTING FROM THE OUTSIDE ENGINES GIMBALLED 7.5° RADIALLY OUTWARD.

THRUST STRUCTURE ANALYSIS (SECOND STAGE)

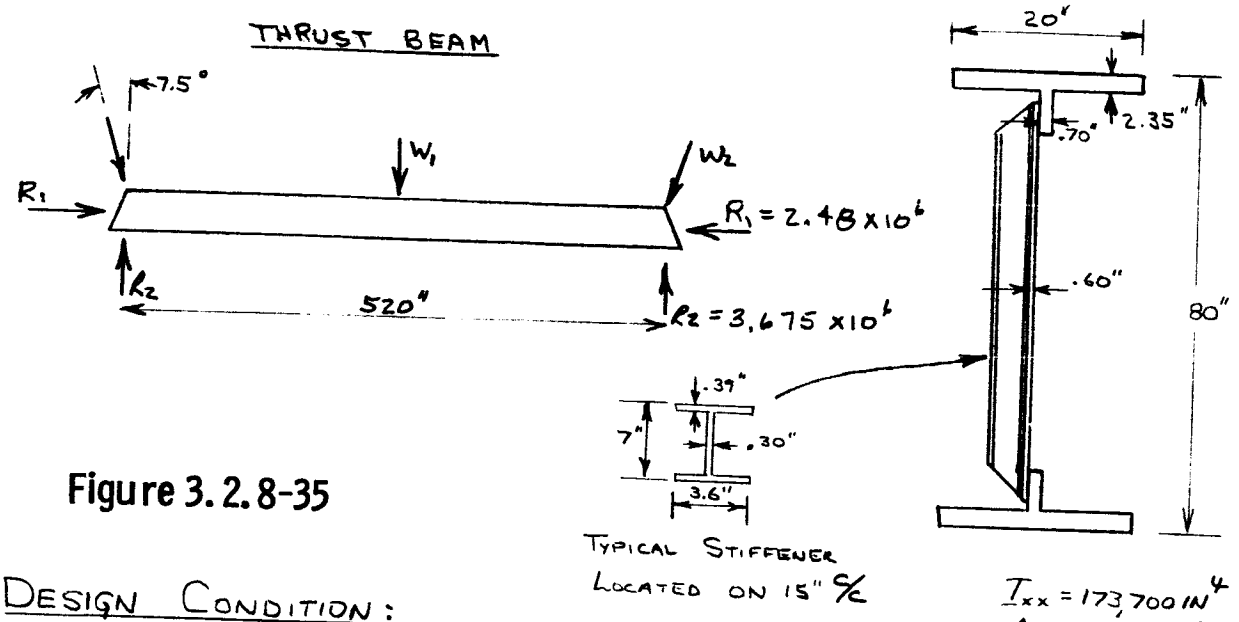

Figure 3.2.8-35

$I_{xx} = 173{,}700\ IN^4$

$A = 148.0\ IN^2$

MATERIAL: 7075-T6

DESIGN CONDITION:

ALL ENGINES FULL THRUST WITH OUTSIDE ENGINES GIMBALED 7.5 DEGREES RADIALLY OUTWARD.

THE ULTIMATE THRUST INCLUDES A 1.4 DYNAMIC LOAD FACTOR FOR THE EFFECT OF ENGINE START-UP

$$W_1 = \frac{1.5 \times 10^6}{2} \times 1.4 \times 1.4 = 1.47 \times 10^6 \text{ LB. ULTIMATE}$$

$$W_2 = 1.5 \times 10^6 \times 1.4 \times 1.4 = 2.94 \text{ LB. ULTIMATE}$$

$$R_1 = 1.5 \sin 7.5^\circ \times 1.4 \times 1.4 + 3.675 \times 10^6 \tan 30^\circ = 2.48 \times 10^6 \text{ LB.}$$

$$R_2 = \frac{1.47}{2} \times 10^6 + 1.5 \times 1.4 \times 1.4 \times 10^6 = 3.675 \times 10^6 \text{ LB. ULTIMATE}$$

THE CROSSBEAM WAS ANALYZED AS A BEAM COLUMN WITH A CONCENTRATED LATERAL LOAD AT THE CENTER AND COMPRESSIVE AXIAL LOADS AT THE ENDS.

$$M = C_1 \sin \frac{x}{j} + C_2 \cos \frac{x}{j} + f(\omega) \quad [1]$$

$$C_1 = -\frac{W_1 j}{2} \sec \frac{L}{2j} \qquad C_2 = 0 \qquad f(\omega) = 0$$

[1] REFERENCE 18 PAGE 90

THRUST STRUCTURE ANALYSIS (SECOND STAGE) – CONTINUED

$$j = \sqrt{\frac{EI}{R_1}}$$

ASSUME $E = E_T = 2.5 \times 10^6$ psi

$$M = -\frac{1.47 \times 10^6}{2}\sqrt{\frac{2.5 \times 10^6 \times 173{,}700}{2.48 \times 10^6}} \times \sec\left[2\sqrt{\frac{520}{\frac{2.5 \times 10^6 \times 173{,}700}{2.48 \times 10^6}}}\right] \times \sin\left[\sqrt{\frac{260}{\frac{2.5 \times 10^6 \times 173{,}700}{2.48 \times 10^6}}}\right]$$

$M = 220 \times 10^6$ IN-LB ULTIMATE

$f_b = \frac{220 \times 10^6 \times 40}{173{,}700} = 50{,}700$ psi $F_b = 1.25 F_{tu} = 91{,}300$ psi [1]

$f_c = \frac{2.48 \times 10^6}{148} = 16{,}700$ psi $F_c = F_{cy} = 65{,}000$ psi [2]

$R_b = \frac{50{,}700}{91{,}300} = .506$ $R_c = \frac{16{,}700}{65{,}000} = .257$

M.S. $= \frac{1}{R_b + R_c} - 1$ [2]

M.S. $= \frac{1}{.506 + .257} - 1$

M.S. $= .31$ ←

WEB STABILITY CHECK

$V = \frac{1.5 \times 10^6 \times 1.4 \times 1.4}{4} = .735 \times 10^6$ LB. ULTIMATE

[1] REFERENCE 5, PAGE 140

[2] REFERENCE 5

THRUST STRUCTURE ANALYSIS (SECOND STAGE) – CONTINUED

$$q = \frac{.735 \times 10^6}{80} = 9200 \text{ LB/IN}$$

$$f_s = \frac{9200}{.60} = 15,300 \text{ psi}$$

$$f_b = 51,600 \times \frac{32}{40} = 40,500 \text{ psi}$$

$$f_c = 16,700 \text{ psi}$$

THE ALLOWABLE STRESSES WILL BE COMPUTED FROM THE FORMULA:

$$F = K E_R \left(\frac{t}{b}\right)^2 \qquad a/b = \frac{64}{15}$$

ASSUME $E_R = \sqrt{E E_T} = 5 \times 10^6$ psi [1]

$$F_s = 5.0 \times 5 \times 10^6 \left(\frac{.7}{15}\right)^2 = 54,500 \text{ psi}$$

$\therefore$ USE $F_s = F_{su} = 46,000$ psi

$F_b = F_{cy} = 66,000$ psi $\qquad K \to \infty$ [2]

$$F_c = 3.62 \times 5 \times 10^6 \left(\frac{.70}{15}\right)^2 = 39,400 \text{ psi}$$

$$R_s = \frac{f_s}{F_s} = \frac{15,300}{46,000} = .332$$

$$R_b = \frac{f_b}{F_b} = \frac{40,500}{66,000} = .615$$

$$R_c = \frac{f_c}{F_c} = \frac{16,700}{39,400} = .424$$

[3]

$$MS = \frac{.63}{.615} - 1 = .02$$

THE FLANGES ARE NOT STABILITY CRITICAL

[1] REFERENCE 5
[2] REFERENCE 13 PAGE 394-395
[3] INTERACTION CURVES FOR FLAT PLATES IN BENDING, SHEAR AND LONGITUDINAL COMPRESSION.

ENGINE MOUNT RING - THRUST STRUCTURE

THE ENGING MOUNT RING OF THE SECOND STAGE THRUST STRUCTURE REACTS KICK LOADS RESULTING FROM THE SLOPE OF THE LONGERONS. THE DESIGN CONDITION OCCURS AT THE TIME OF ENGINE START UP. IT WAS CONSERVATIVELY ASSUMED THAT THE FOUR KICK LOADS APPLIED AT THE LONGERONS WOULD BE RESISTED BY A UNIFORMLY DISTRIBUTED LATERAL LOAD

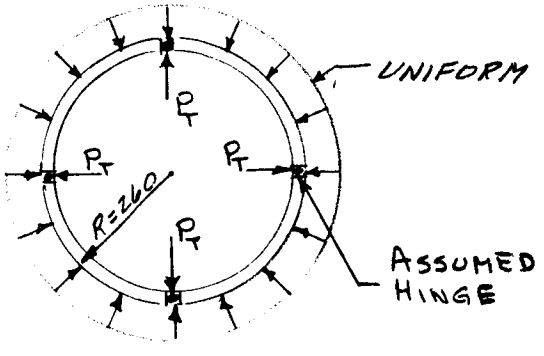

ENGINE MOUNT RING LOADS

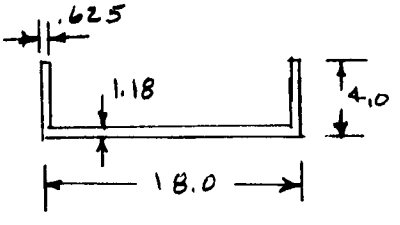

TYPICAL CROSS SECTION
$I = 828\ IN^4$
$A = 24.48\ IN^2$
MATERIAL: 7075-T6

ULTIMATE DESIGN LOADS:

P_T = (LONGITUDINAL LOAD) TAN 30°.

= (3.675×10^6) [1] .577 = 2.12×10^6 Lb.

[1] REFERENCE FIGURE 3.2.8-35

ENGINE MOUNT RING - THRUST STRUCTURE, CONTINUED.

$$p = \frac{4P_T}{\pi D} = \frac{4(2.12\times10^6)}{\pi(520)} = 5200 \text{ Lb/in}$$

RING STABILITY:

$$p_{CR} = \frac{EI}{R^3}\left(\frac{n^2}{\alpha^2} - 1\right) \quad [1]$$

$$= \frac{(10.5\times10^6)(828)}{(260)^3}\left(\frac{n^2}{.785} - 1\right) = 5720 \text{ Lb/in}^2$$

$$M.S. = \frac{5720}{5200} - 1 = \underline{.10}$$

MAXIMUM AXIAL LOAD $= pR = (5200)260 = 1.35\times10^6$

$$f_c = \frac{1.35\times10^6}{24.48} = 55,500 \text{ psi}$$

WEB CRIPPLING:

$$\frac{b}{t} = \frac{18 - 2(1.625)}{1.18} = 14.2$$

$$F_{cCR} = 67000 \quad [2]$$

$$M.S. = \frac{67000}{55500} - 1 = \underline{.20}$$

[1] REFERENCE (9) PAGE 307

[2] REFERENCE (10) SECTION 22.2.2

FORWARD RING - THRUST STRUCTURE

THE FORWARD RING REACTS KICK LOADS FROM THE SECOND STAGE THRUST STRUCTURE. CRITICAL LOADING OCCURS AT ENGINE START UP. A SINUSOIDAL PRESSURE DISTRIBUTION WAS ASSUMED.

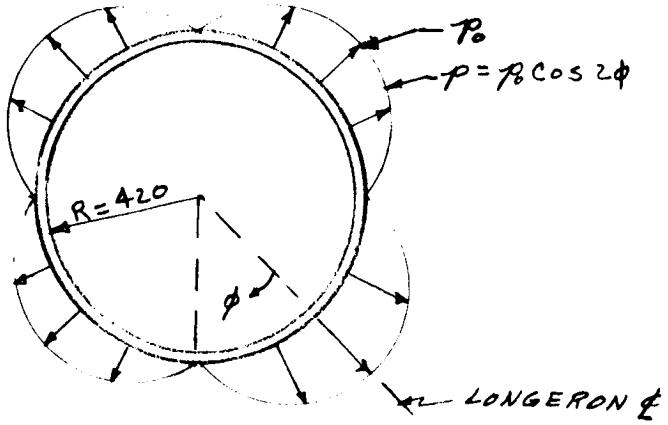

FORWARD RING
ASSUMED LOAD DISTRIBUTION

ULTIMATE DESIGN PRESSURE:

$$p_o = \frac{P_T}{.785R} = \frac{2.12 \times 10^4}{.785(420)} = 6440 \text{ Lb/IN}$$ [1]

[1] REFERENCE FIGURE 3.2.8-35

FORWARD RING - THRUST STRUCTURE (CONTINUED)

MATERIAL: 7075-T6
$I = 14,988 \text{ IN}^4$
$A = 67.73 \text{ IN}^2$

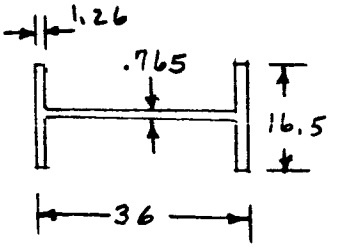

FORWARD RING - DESIGN CROSS SECTION

THE CRITICAL SECTION OCCURS AT $\phi = \frac{\pi}{4}$

$M = 34.1 \times 10^6$
$P = 1.8 \times 10^6$
$V = 0$

$$f = \frac{1.8 \times 10^6}{67.73} + \frac{(34.1 \times 10^6)18}{14988} = 67,400$$

$F_c = 68400$ [1]

$$M.S. = \frac{68400}{67400} - 1 = \underline{.01}$$

[1] REFERENCE (5). DESIGN TEMPERATURE = 185°F

Longerons and Shear Redistribution Structure (Thrust Structure) — The thrust-structure longerons and shear redistribution panels were analyzed by the numerical method of Reference 2 to determine the shear-lag effects. A detailed description of the method, including pertinent symbols and formulas is given in 3.2.8.6.4.5.

A width of 100 inches on each side of the longeron at the forward ring was assumed as an effective compression width.* The stringers provided in this width were assumed to carry all of the longitudinal load; the skin panels were utilized to redistribute the load applied at the engine mount ring. Since the panel width varies along the length of the cone, the "b_s" distance used in the calculations was varied.

Critical design condition: Engine start-up.

Ultimate longeron load:

$$P_o = \frac{3.675 \times 10^{6**}}{\cos 30^\circ} = 4240 \times 10^3 \text{ lb.}$$

One-half of the symmetrical structure was analyzed for an applied longeron load.

$$P' = \frac{1}{2} P_o = 2120 \times 10^3 \text{ lb.}$$

Tables 3.2.8-14 and 3.2.8-15 show the calculation of terms used in the shear-lag equations.

---

* Figure 3.2.8-35

** Figure 3.2.8-34

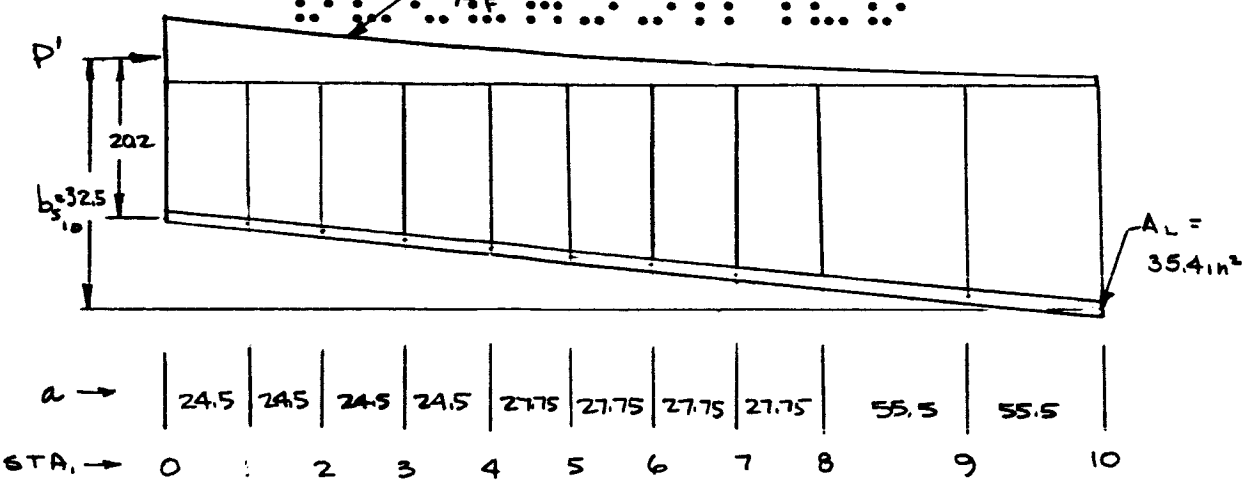

IDEALIZED HALF-PANEL

Table 3.2.8-14 CALCULATION OF $\bar{\gamma}$

STA.	A_F IN²	A_T IN²	$\frac{A_L}{A_T}$	$\Delta\left(\frac{A_L}{A_T}\right)$	a IN	b_s IN	$\bar{q}$ K/IN	t IN	$\bar{\gamma}$ X10⁵
0	36.0	71.40	.4958						
				.0855	24.5	20.7	7.4	.5	379.4
1	25.5	60.90	.5813						
				.0647	24.5	21.6	5.6	.5	287.1
2	19.4	54.80	.6460						
				.0599	24.5	22.6	5.2	.3	443.0
3	14.75	50.15	.7059						
				.0570	24.5	23.5	4.93	.3	421.5
4	11.00	46.40	.7629						
				.0528	27.75	24.5	4.03	.3	344.8
5	8.00	43.40	.8157						
				.0446	27.75	25.6	3.41	.3	291.2
6	5.75	41.15	.8603						
				.0336	27.75	26.6	2.57	.25	263.3
7	4.20	39.60	.8939						
				.0280	27.75	27.9	2.14	.25	219.4
8	3.00	38.40	.9219						
				.0196	55.5	29.3	.75	.20	96.0
9	2.20	37.60	.9415						
				.0114	55.5	31.4	.44	.15	74.3
10	1.75	37.15	.9529						

CALCULATION OF φ AND ψ

STA	A_F in^2	$\frac{G}{E}\frac{t}{b_s}$ $\times 10^3$	K	Ka	TANH Ka	SINH Ka	φ $\times 10^5$	ψ $\times 10^5$
0								
1	30.75	9.15	.0235	.576	.5197	.6084	2.32	1.98
2	22.45	8.76	.0252	.617	.5490	.6569	2.35	1.97
3	17.075	5.62	.0209	.512	.4715	.5347	3.79	3.34
4	12.875	4.83	.0226	.554	.5035	.5828	3.84	3.31
5	9.50	4.64	.0249	.691	.5986	.7473	3.56	2.85
6	6.875	4.44	.0277	.769	.6463	.8471	3.66	2.79
7	4.975	3.56	.0285	.791	.6590	.8761	4.44	3.34
8	3.60	3.42	.0323	.896	.7143	1.0208	4.64	3.25
9	2.60	2.58	.0327	1.815	.9483	2.9892	4.42	1.40
10	1.975	1.81	.0311	1.726	.9386	2.7201	5.66	1.95

SUBSTITUTION IN THE RECURRENCE FORMULA YIELDS TEN EQUATIONS DEFINING THE SHEAR LAG EFFECT.

Table 3.2.8-15

$$1.98(1051.1) - 4.67\chi_1 + 1.97\chi_2 = -92.3$$
$$1.97\ \chi_1 - 6.14\chi_2 + 3.34\chi_3 = 155.9$$
$$3.34\ \chi_2 - 7.63\chi_3 + 3.31\chi_4 = -21.5$$
$$3.31\ \chi_3 - 7.40\chi_4 + 2.85\chi_5 = -76.7$$
$$2.85\ \chi_4 - 7.22\chi_5 + 2.79\chi_6 = -53.6$$
$$2.79\ \chi_5 - 8.10\chi_6 + 3.34\chi_7 = -27.9$$
$$3.34\ \chi_6 - 9.08\chi_7 + 3.25\chi_8 = -43.9$$
$$3.25\ \chi_7 - 9.06\chi_8 + 1.40\chi_9 = -123.4$$
$$1.40\ \chi_8 - 10.08\chi_9 + 1.95\chi_{10} = -21.7$$
$$1.95\ \chi_9 - 5.66\chi_{10} + 0 = -74.3$$

THE VALUES OF χ DEFINED BY THE EQUATIONS ARE SHOWN IN TABLE 3.2.8-15

STA.	χ K	P_F K	σ_F KSI	σ_L KSI	τ_{MAX} KSI
0	1051.1	2120	58.9	0	72.6
1	343.5	1231.1	48.3	25.1	28.2
2	134.7	885.2	45.6	34.9	23.1
3	91.7	716.2	48.5	39.7	19.5
4	69.0	571.6	52.0	43.7	16.2
5	45.9	436.6	54.6	49.5	16.6
6	29.1	298.3	51.9	51.5	7.12
7	23.9	248.8	59.2	52.8	8.6
8	23.4	189.0	63.0	54.5	5.1
9	8.5	132.5	60.2	56.1	2.6
10	16.1	115.9	66.2	56.6	

Table 3.2.8-16 STRESSES IN LONGERON, SHEAR WEB AND SUBSTITUTE STRINGER.

LONGERON (THRUST STRUCTURE)

THE CRITICAL BUCKLING LOAD FOR A TAPERED COLUMN UNDER VARYING AXIAL LOAD IS GIVEN BY REFERENCE (1), PAGE 181 AS

$$P_{CR} = \frac{m E I_o}{L^2}$$ WHERE m DEPENDS ON THE VARIATION OF THE CROSS SECTION PROPERTIES,

$EI = (EI)_o \left(\frac{d}{L}\right)^n$ AND THE LOAD VARIATION,

$q = q_o \left(\frac{d}{L}\right)^p$ FOR THE LONGERON, p AND n WERE TAKEN AS BEING APPROXIMATELY 2 AND 1, RESPECTIVELY, FROM TABLE 2-14 OF REFERENCE (1), m = 23.1

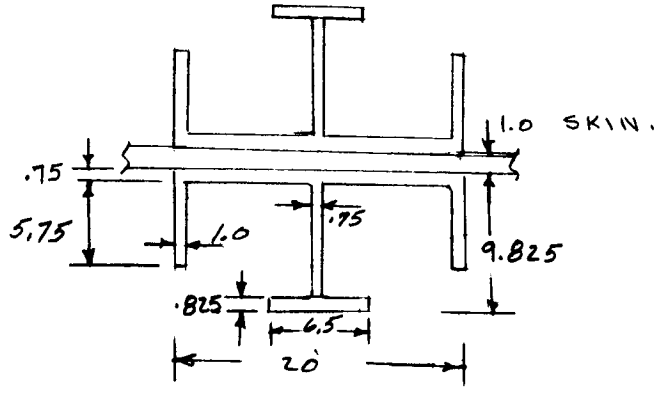

LONGERON CROSS SECTION AT THE ENGINE MOUNT RING, d = 0

A = 72 IN^2 I = 2017 IN^4

MATERIAL: 7075-T6

$$P_{CR} = \frac{23.1\,(10.5\times10^6)(2017)}{(320)^2} = 4.76\times10^6\ \text{Lb}$$

LONGERON - THRUST STRUCTURE - (CONTINUED)

$$M.S. = \frac{4.76 \times 10^6}{2(2.12 \times 10^6)} - 1 = .12$$

SINCE THE STABILIZING INFLUENCE OF THE INTERMEDIATE FRAMES WAS NOT CONSIDERED, THE INDICATED MARGIN OF SAFETY IS CONSERVATIVE.

SHEAR WEBS - THRUST STRUCTURE

MATERIAL: 7075-T6 CLAD SHEET

THE THICKNESS OF THE FIRST PANEL MUST BE INCREASED.

$$q = (72.6)(.5) = 36.3 \text{ K/in.}$$

USE $t = 1.0$, THEN

$$f = \frac{36.3}{1.0} = 36.3 \text{ ksi}$$

AVERAGE STRINGER SPACING = 5.7 IN.

PANEL ASPECT RATIO = $\frac{a}{b} = \frac{49}{5.7} = 8.1$

$K_s = 4.8 \quad F_s = 39$ [1]

$$M.S. = \frac{39.0}{36.3} - 1 = .07$$

THE CHANGE OF WEB THICKNESS IN THE FIRST TWO PANELS WILL HAVE ONLY A MINOR EFFECT ON THE SHEAR LAG ANALYSIS. THUS THE RESULTS ARE CONSIDERED TO BE VALID WITHOUT ITERATION.

ALL OTHER SHEAR WEBS ARE NON BUCKLING AT ULTIMATE LOAD.

[1] REFERENCE (3), SECTION 15.

STRINGERS - THRUST STRUCTURE - LONGERON SECTION

THE STRINGERS ARE DESIGNED TO CARRY THE FULL AXIAL LOAD AT START-UP. BASED ON THE RESULTS THE 'BASE SKIRT LONGERON ANALYSIS SECTION 3.2.8.6.4.5, THE LOAD WAS ASSUMED TO BE REDISTRUIBUTED UNIFORMLY INTO THE STRINGERS. EACH LONGERON SECTION CONTAINS TWENTY STRINGER, TEN ON EACH SIDE OF THE LONGERONS. (REFERENCE FIGURE 3.2.8-32)

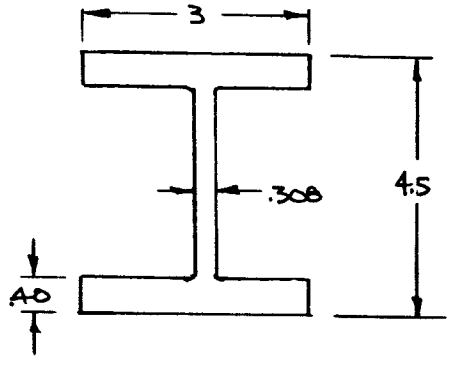

A = 3.54 IN^2

I = 11.38 IN^4

SPACING = 9.5 IN

TYPICAL STRINGER CROSS SECTION

$$f_{c_{STRINGER}} = \frac{2,120,000}{10\,(3.54)} = 59,900 \text{ PSI}$$

THE STRINGERS ARE SUPPORTED AT 55.5 IN. INTERVAL BY CIRCULAR FRAMES.

$$L'/\rho = L/\rho\sqrt{c} = 55.5/1.179(1.225) = 25.3$$

F_{cc} = 61,000 PSI [1]

[1] REFERENCE (3) SECTION 15.311

$$M.S. = \frac{61,000}{59,900} - 1$$

$$= \underline{.02}$$

STABILIZING FRAMES

CIRCULAR FRAMES SPACED AT 55.4 IN. ARE USED TO STABILIZE THE CONE PORTION OF THE THRUST STRUCTURE. THE MAXIMUM LOAD IS CONSERVATIVELY ASSUMED TO EQUAL THE ULTIMATE STRENGTH OF THE STRINGERS.

$$W = \frac{F_c A_{STRINGER}}{STRINGER\ SPACING} = \frac{61,000\,(3.54)}{9.5} = 22,700\ LB/IN$$

$$(I_F)_{REQUIRED} = \frac{.785\ R^4\ W}{1000\ E\ L}\ \triangleright 1$$

$$= \frac{.785\,(372)^4\ 22,700}{1000\ 10^7\ (55.5)}$$

$$= \underline{612\ IN^4}$$

FRAME SECTION

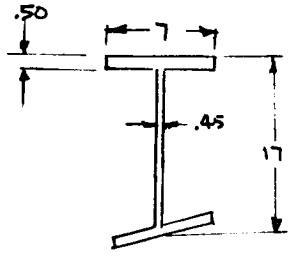

$A = 14.2\ IN^2$
$I = 611.5\ IN^4$

TYPICAL CROSS SECTION

$\triangleright 1$ REFERENCE (7) PAGE 590

THRUST CONE - INTERMEDIATE SECTION

THE THRUST CONE INTERMEDIATE SECTION CONSIST OF "I" STIFFENED SEMIMONOCOQUE PANELS. THE MAXIMUM LOAD OCCURS AT ENGINE START-UP WITH ENGINES GIMBALLED ONE DIRECTION 7.5°. THE SKIN AND STRINGERS ARE DESIGNED FOR THE RESULTING SHEAR LOADS. (REF. FIG. 3.2.8-34)

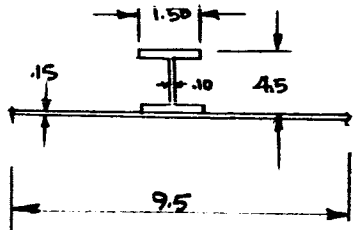

TYPICAL CONE SECTION

ULTIMATE SHEAR LOAD

$$V = 4[1.5\times10^6(1.4)^2 \sin 7.5^\circ] = 1.535\times10^6 \text{ LB.}$$

SHEAR FLOW

$$q = \frac{1535\times10^6}{TTR} = 1.163 \text{ LB/IN}$$

$$f_s = \frac{1.163}{.15} = 7,750 \text{ PSI}$$

SKIN STABILITY

$$F_{SCR} = 49\times10^6\left(\frac{.15}{9.5}\right)^2 = 12,280 \text{ PSI} \ [1]$$

$$M.S. = \frac{12,280}{7,750} - 1 = .58$$

[1] REFERENCE 13, PAGE 394

STRINGERS - THRUST STRUCTURE - INTERMEDIATE SECTION

THE STRINGERS ARE DESIGNED TO STABILIZE THE SKIN PANELS. THE MAXIMUM LOAD IS CONSERVATIVELY ASSUMED TO EQUAL THE ULTIMATE STRENGTH OF THE SKIN PANELS.

REQUIRED $I = \frac{\ell}{t}\left[\frac{h^2 t\, f_s}{11.8\, E}\right]^{4/3}$ [1]

$= \frac{9.5}{.15}\left[\frac{(55.5)^2(.15)\ 12{,}280}{11.8\ \ 10^7}\right]^{4/3}$

$= 1.1\ IN^4$

$A = .70\ IN^2$

$I = 1.52\ IN^4$

SPACING = 9.5 IN

MAT'L: 7075-T6

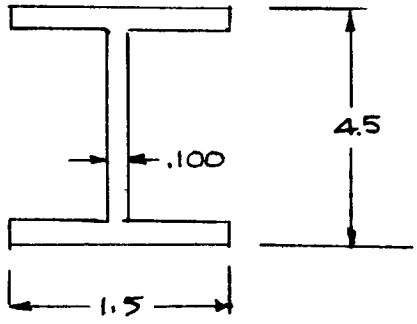

TYPICAL STRINGER CROSS SECTION

[1] REFERENCE 8, SECTION 15.6

[2] REFERENCE FIGURE 3.2.8-34.

3.2.8.6.3.8 Forward Interstage (Second Stage)

The interstage structure is a stiffened-skin semimonocoque shell sized by the optimum design method of Reference 16. The maximum load occurs at maximum q, 20-degree-angle-of-attack failure condition.

FORWARD INTERSTAGE (SECOND STAGE)

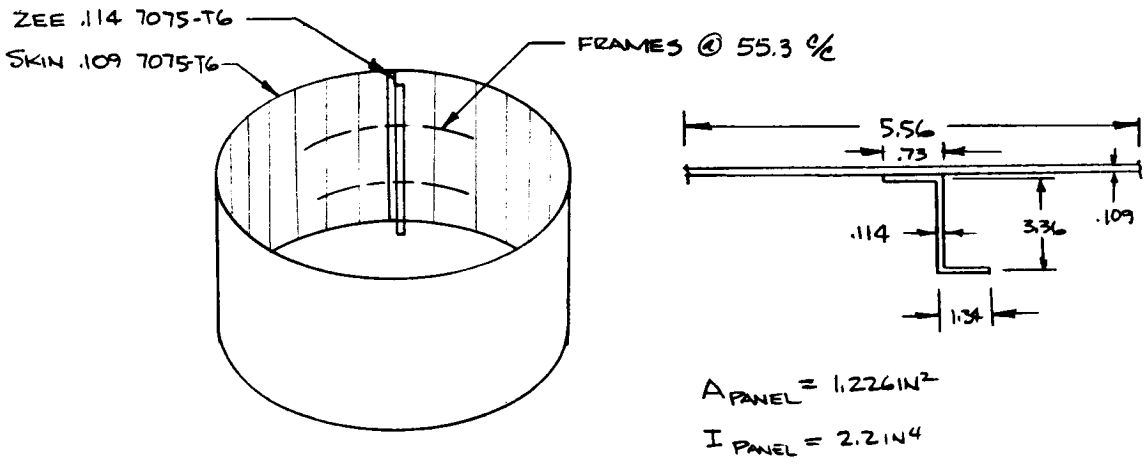

$A_{PANEL} = 1.226 IN^2$

$I_{PANEL} = 2.21 IN^4$

DESIGN CONDITION:

ULTIMATE LOAD AT MAX Q; 20° ANGLE OF ATTACK
FAILURE CONDITION
$N_c = 6740 \, LB/IN$ ▷

COMPRESSION STRENGTH OF STIFFENED PANEL

ANALYSIS PER REFERENCE (10) SECTION 22.2.2

CRUSHING STRENGTH – ZEE STIFFENER

$$A/t^2 = \frac{.619}{(.114)^2} = 47.6$$

$$F_{cc\,STIF} = 42{,}000 \text{ PSI}$$

SHEET BUCKLING STRESS

$$b/t = 5.56/.109 = 51$$

$$F_{cc\,SKIN} = 23{,}800 \text{ PSI}$$

CRUSHING STRENGTH OF PANEL

$$F_c = \frac{F_{ccSTIF} A_{STIF} + F_{ccSKIN} A_{SKIN}}{A_{STIF} + A_{SKIN}}$$

$$F_c = \frac{41{,}000(.619) + 23{,}800(.607)}{1.226} = 33{,}000 \text{ PSI}$$

▷ FIGURE 3.2.8-32

FORWARD INTERSTAGE (SECOND STAGE) - CONT.

ULTIMATE STRENGTH OF PANEL

$$L/\rho\sqrt{c} = 55.3/1.34(1.225) = 33.65$$

$$F_c = 30{,}600 \text{ PSI}$$

$$f_c = \frac{6740 \text{ LB/IN} \quad 5.56 \text{ IN}}{1.226 \text{ IN}^2} = 30{,}600 \text{ PSI}$$

$$\text{M.S.} = \frac{30{,}600}{30600} - 1 = \underline{0}$$

REQUIRED FRAMES

$$I = \frac{.785\ R^4\ W}{1000\ L\ E} \text{ [1]} = \frac{.785\ (420)^4\ 6740}{1000\ \ 55.3\ \ 10^7} = 298 \text{ IN}^4$$

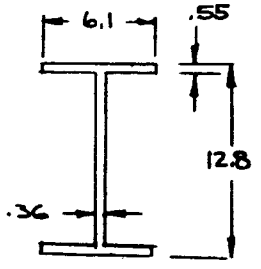

FRAME SECTION

MATERIAL: 7075-T6
A = 1092 IN²
I = 298 IN⁴

[1] REFERENCE (7) PG 5910

3.2.8.6.3.9 Slosh Provisions (Second Stage)

A slosh analysis was not performed during this study. Slosh structure has been indicated in the configurations and weight estimates have been made, based on previous experience.

The ring stiffeners in the hydrogen tank were incorporated with the slosh baffles to achieve an integrated design of greater efficiency.

3.2.8.6.4 First-Stage Detail Analysis

3.2.8.6.4.1 Discussion

The detailed layout drawings of the first stage are shown in Section 3.2.11, Figures 3.2.11-2 and 3.2.11-3.

The first stage has high L/d motors that are approaching the region where ground-wind loads design the case walls. Using 250,000-psi maraged steel, the resulting margin of safety for the ground-wind condition is 0.005.

The cluster structure (Figure 3.2.8-1) was designed for load conditions judged to be critical based on previous load-path work from Contract NAS8-2438. The referenced work contained a complete stiffness analysis of a structure similar to the present configuration. Externally applied loads of the present concept were compared with the external loads of the referenced concept and were noted to evidence similar trends. The maximum-q loads for this concept were slightly lower than the referenced concept. Therefore, the maximum-q load was not a critical design condition.

The indicated critical design conditions were maximum symmetrical acceleration and unsymmetrical thrust termination. The members by these load conditions are shown in Figure 3.2.8-1.

The major load path for longitudinal shear in the cluster structure is through the intercostals into the redistribution ring and motor-case skirt extensions. The crossbeam provides section stability and redistributes axial loads.

The base support concept was also developed under Contract NAS8-2438, which indicated it to be the lightest-weight approach. Three support points were recommended for each motor to permit alignment of the structure during erection and to minimize redundant loads in each motor.

The support-point locations were placed outboard of the motor sidewall centerline to clear the vehicle drift-cone envelope and to provide sufficient clearance for the ring structure between the nozzles and the skirt.

The location of the support points produced a bending moment in the skirt because of the eccentric load application. To react this moment, a pair of rings was incorporated in the base skirt and connected by sloping columns to force the moment to be reacted by kick loads in the rings. Tapered longerons were then used to redistribute the axial loads into the cylindrical skirt extension, which was of skin-stringer construction.

Analysis showed that 86.6 percent of the critical support point load was attributable to vehicle weight and 13.4 percent to ground wind loads.

The upper rings in the skirt were also used to redistribute the loads transmitted between motors by the clustering link ties.

Honeycomb structure was used in the aft portion of the skirt to carry distributed airloads.

3.2.8.6.4.2 Criteria and Loads (First Stage)

The design conditions and criteria for the first-stage are shown in Table 3.2.8-8.

The load distributions for each structural component are included in the individual analyses contained in the following sections.

3.2.8.6.4.3 Materials (First Stage)

The motor-case material selected for this study was 18N1-7CO-5MO maraged steel. Boeing test data indicate the following properties:

Ultimate strength	250,000 psi
Yield strength	240,000 psi
Elongation	12 percent
Modulus of elasticity	27×10^6 psi
Reduction of area	58 percent
Weld efficiencies (local aging)	98 percent*
Weld efficiencies (heat treat after welding)	97 to 98.7 percent*
K_{1C} fracture toughness parameter (welds)	77 to 81 ksi $\sqrt{in}$ **
K_{1C} fracture toughness parameter (base metal)	137 to 139 ksi $\sqrt{in}$ **

At the inception of this study, valid weld fracture toughness data were not available. On the basis of the base metal fracture toughness data, maraged steel exhibits good potential as a large booster case material, and was used for this study. The tabulated weld fracture toughness has subsequently been obtained in Boeing tests of TIG welded specimens. This data indicates a potentially serious toughness problem in the heat-affected zone. The critical crack depth at these toughnesses will be approximately 0.046 inch, which is considered marginal from an inspection standpoint. Data from other sources indicate that MIG welding and 12-hour aging produce even lower fracture toughness values.

* A 90-percent weld efficiency was assumed for this analysis.

** See Reference 19 for definition of fracture toughness.

In view of the weld toughness problem, development work should be performed to determine if variations in weld techniques can improve fracture toughness. Methods of reducing the operating stress in the weld zone by local thickness increase should be considered. Reduction of the alloy ultimate strength is another consideration. The investigation of other materials should also be intensified.

The alloy used for unwelded applications was 7075-T6 aluminum. The material properties were obtained from Reference 5.

BLANK

3.2.8.6.4.4 Clustering Structure (First Stage)

The clustering structure consists of stiffened motor-case skirt extensions tied together by intercostals and redistribution rings. Crossbeams were used to stabilize the structure and to redistribute axial loads (Figures 3.2.8-1, 3.2.8-36, and 3.2.11-3). The primary load path for the transfer of longitudinal shear between motors is through the intercostals. Approximately 98 percent of the moment on the individual motors is resisted by a couple composed of lateral shear forces in the clustering structure and in the link ties at the aft end of the motors.

Results from a previous study (NAS8-2438) were used as a guide for determining the design loads on the clustering structure. The loading conditions considered were symmetrical maximum thrust, unsymmetrical thrust termination, 20-degree angle of attack with null thrust vectoring at maximum q, 8-degree angle of attack with 3.5-degree thrust vectoring at maximum q, and the vehicle trimmed at maximum q.

Symmetrical Maximum Thrust Load Condition (Cluster Structure) — The assumed load distribution of the forward skirt extension and the interstage on the clustering structure beam network is shown in Figure 3.2.8-36. The longitudinal load distribution is shown above the centerline and the lateral load distribution is below the centerline. Both sets of loads are symmetrical about the centerline.

Approximately 98 percent of the moment due to 96.4 inches of eccentricity in the resultant interstage longitudinal load is resisted by bending in the motor cases. This was determined by requiring compatibility of the rotations in the plane of the clustering structure beam network (see Figure 3.2.8-36). The rotations induced in the clustering structure were calculated by conservatively assuming that all of the moment was resisted by bending in the solid motors. The proper load distribution to produce these rotations was then determined by iteration. A comparison of assumed quantities with the resulting calculated quantities is shown in Table 3.2.8-17.

The reaction of the lateral shear loads by the beam network and intercostals was determined by a load-path stiffness analysis. The stiffness of all direct shear paths was assumed to be inversely proportional to their length. Where the bending of free-spanning members was involved, the stiffness was assumed to be inversely proportional to the length cubed. The resultant reactions are shown in Figure 3.2.8-40.

The outer ties were analyzed as fixed-end beams with an elastic support (the crossbeam) at the center. The outer portion of the main crossbeam was designed for the elastic support loads resulting from the outer tie loads.

The rings mounted on the forward skirt extension were analyzed for the forward skirt loads, interstage loads, outer tie loads, and the reactions of the intercostals and main crossbeams. Because of symmetry of the ring and the loads, only one-half of the ring was considered. Longitudinal and lateral loads were analyzed separately and the results were superimposed. An energy solution was performed on the ring to solve for the redundant moments and forces. The resulting loads on the ring are tabulated in Table 3.2.8-18.

After the analysis was performed, the design was altered by removing the portion of the ring between the intercostals. The main crossbeam in this area was designed to resist these loads in addition to the loads from the outer tie and the loads induced by rotation in the plane of the beam network. (See Figure 3.2.8-41 for resultant loads.) The shape of the clustering structure was also modified. Curved rings were used around the inside and outside corners to improve the transition geometry of the forward skirt extension (Figure 3.2.8-1). The analysis was assumed to be valid for the modified structure.

The central portion of the main crossbeam was arbitrarily made the same size as the outer segment. Because of the length of these members, they are too flexible to constitute a significant load path. However, they have been included to supply lateral stability to the cross section and to redistribute lateral shear forces.

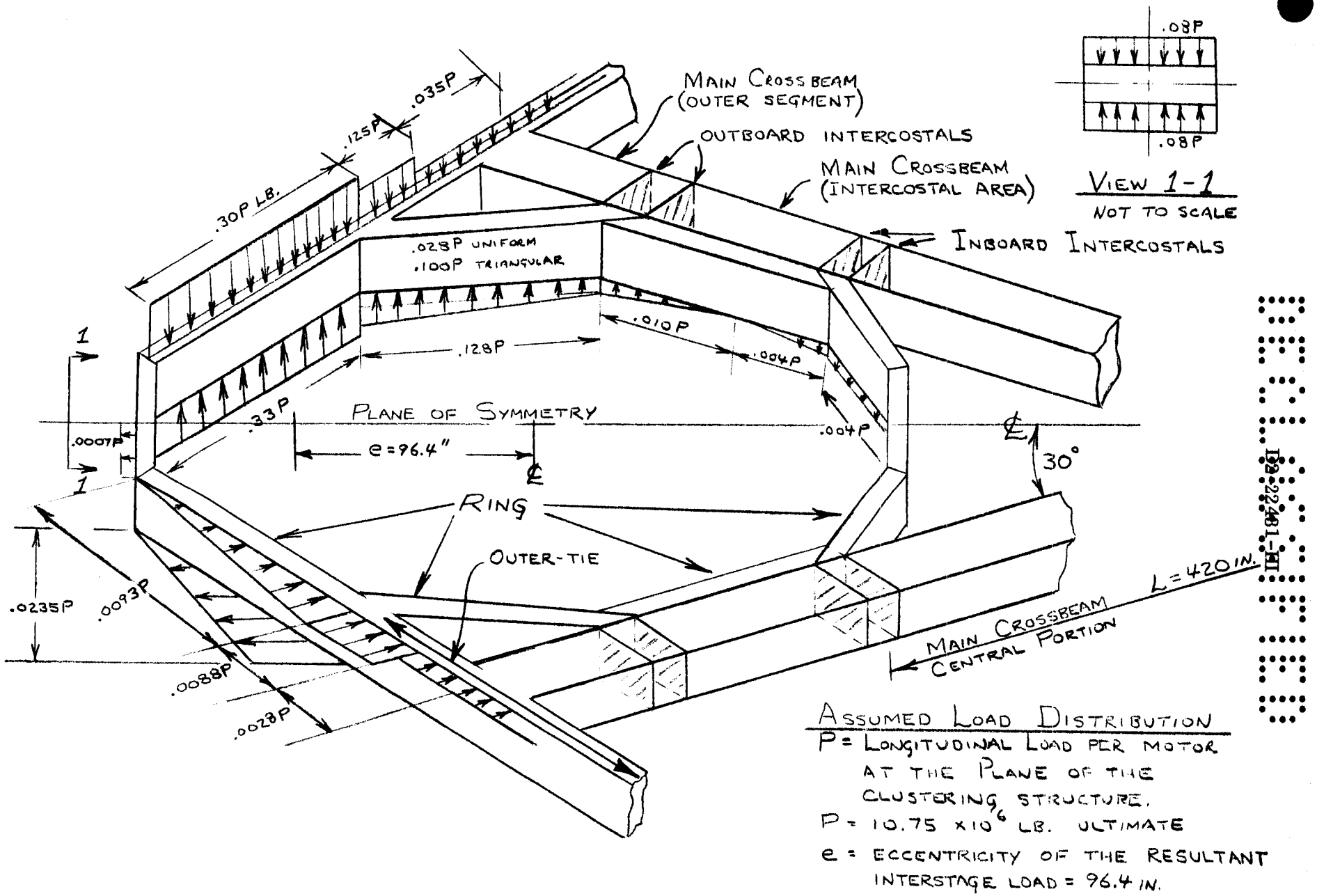

Figure 3.2.8-36 SYMMETRICAL MAXIMUM THRUST LOADS ANALYSIS
Typical First-Stage Clustering Structure Segment 1

Symmetrical Maximum Thrust Loads Analysis - Figure 3.2.8-37

Rotation of Forward Skirt Extension Due to Bending Moment in Solid Motors

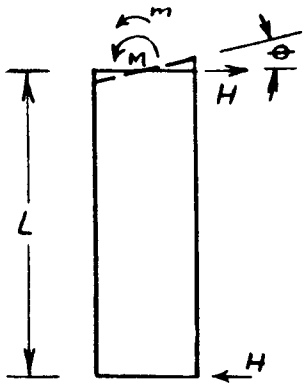

$$\theta = \int_0^L \frac{Mm\,dx}{EI} = \frac{ML}{3EI} = \frac{PeL}{3EI}$$

$$\theta = \frac{96.4 \times 10.75 \times 10^6 \times 2050}{3 \times 30 \times 10^6 \times 4.48 \times 10^6}$$

$$= 5250 \times 10^{-6} \text{ rad.}$$

Rotation of Main Cross Beam

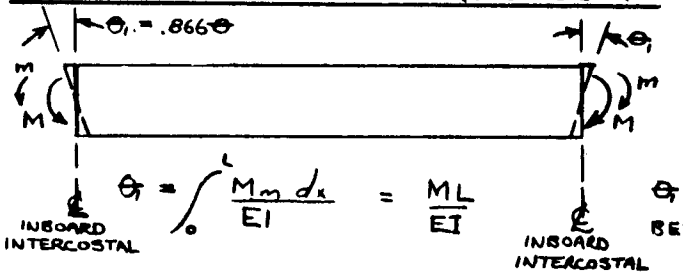

$$\theta_1 = \int_0^L \frac{Mm\,dx}{EI} = \frac{ML}{EI}$$

θ_1 = CHANGE IN SLOPE BETWEEN ENDS OF BEAM

$$M = \frac{\theta_1 EI}{L}$$

ASSUME I = 7500 IN⁴

$$M = \frac{2 \times .866 \times 5250 \times 10^{-6} \times 10 \times 10^6 \times 7500}{420} = 1.63 \times 10^6 \text{ IN-LB ULT.}$$

Rotation of Intercostals

$\theta_2 = \frac{ML}{EI}$ (SAME AS ABOVE) $\theta_2 = .500\,\theta$

$$M = \frac{EI\,\theta_2}{L} = \frac{10 \times 10^6 \times 25{,}000 \times 2 \times .5 \times 5250 \times 10^{-6}}{46}$$

$$= 28.6 \times 10^6 \text{ IN-LB ULT}$$

THESE NUMBERS DO NOT REFLECT THE EFFECT OF LOCAL DISPLACEMENTS. THE MODULI OF ELASTICITY FOR STEEL AND ALUMINUM WERE TAKEN AS 30×10^6 PSI AND 10×10^6 PSI RESPECTIVELY.

SYMMETRICAL MAXIMUM THRUST LOADS ANALYSIS

COMPARISON OF ASSUMPTIONS WITH RESULTS

Table 3.2.8-17

ITEM	MOTOR CASE	CROSS BEAM	INTERCOSTAL
ASSUMED I	4.48×10^6 IN^4	7500 IN^4	25,000 IN^4
RESULTANT I [4]	4.48×10^6 IN^4	10,600 IN^4	[1] 24,300 IN^4
ASSUMED M	1036×10^6 IN-LB	1.63×10^6 IN-LB	28.6×10^6 IN-LB
RESULTANT M [3]	[2] 1015×10^6 IN-LB	1.63×10^6 IN-LB	29.9×10^6 IN-LB

[1] DOES NOT INCLUDE STIFFNESS CONTRIBUTION OF FLANGES ON MAIN CROSS BEAM.

[2] MOMENT CORRESPONDING TO ASSUMPTION OF 98 PER CENT OF MOMENT BEING REACTED BY BENDING IN MOTOR CASES.

[3] LOADS RESULTING FROM THE CLUSTERING STRUCTURE LOADS ANALYSIS.

[4] SECTION PROPERTIES OF FINAL MEMBER SIZES BASED ON LOADS ANALYSIS.

Figure 3.2.8-38

OUTER TIE LOADS ANALYSIS
SYMMETRICAL MAXIMUM THRUST CONDITION

LONGITUDINAL LOADS

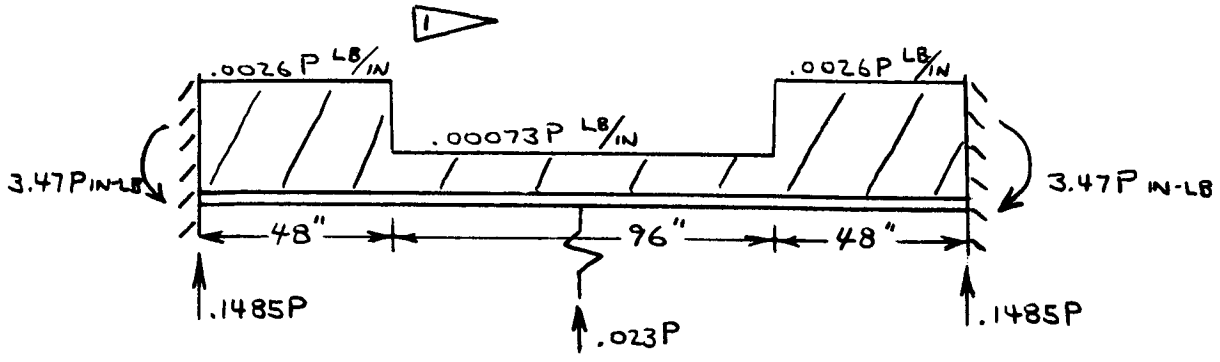

REACTIONS RESULT FROM ANALYZING THE OUTER TIE AS A FIXED END BEAM WITH AN ELASTIC SUPPORT AT THE CENTER. THE REACTION OF THE ELASTIC SUPPORT WAS BASED ON DATA FROM A PREVIOUS [2] STUDY BY COMPARING LOAD PATH STIFFNESSES OF THE TWO CONCEPTS.

$P = 10.75 \times 10^6$ LB. ULTIMATE

LATERAL LOADS

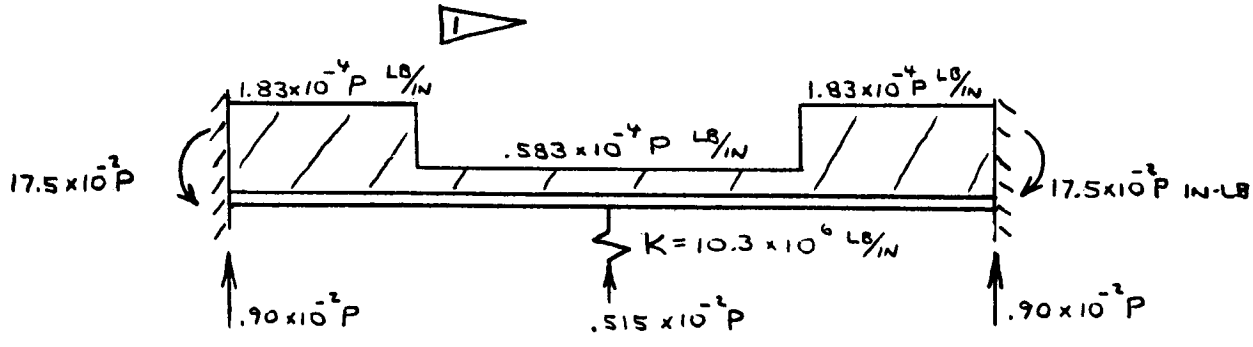

ASSUME AREA OF MAIN CROSS BEAM = 75 IN^2

$$K = \frac{AE}{L} = \frac{75\times10\times10^6}{73} = 10.3\times10^6 \text{ LB/IN}$$

[1] LOADS FROM FIGURE 3.2.8-36

[2] CONTRACT NAS8-2438

Figure 3.2.8-39

Loads Analysis For Ring – Symmetrical Max. Thrust Condition.

Longitudinal Loads

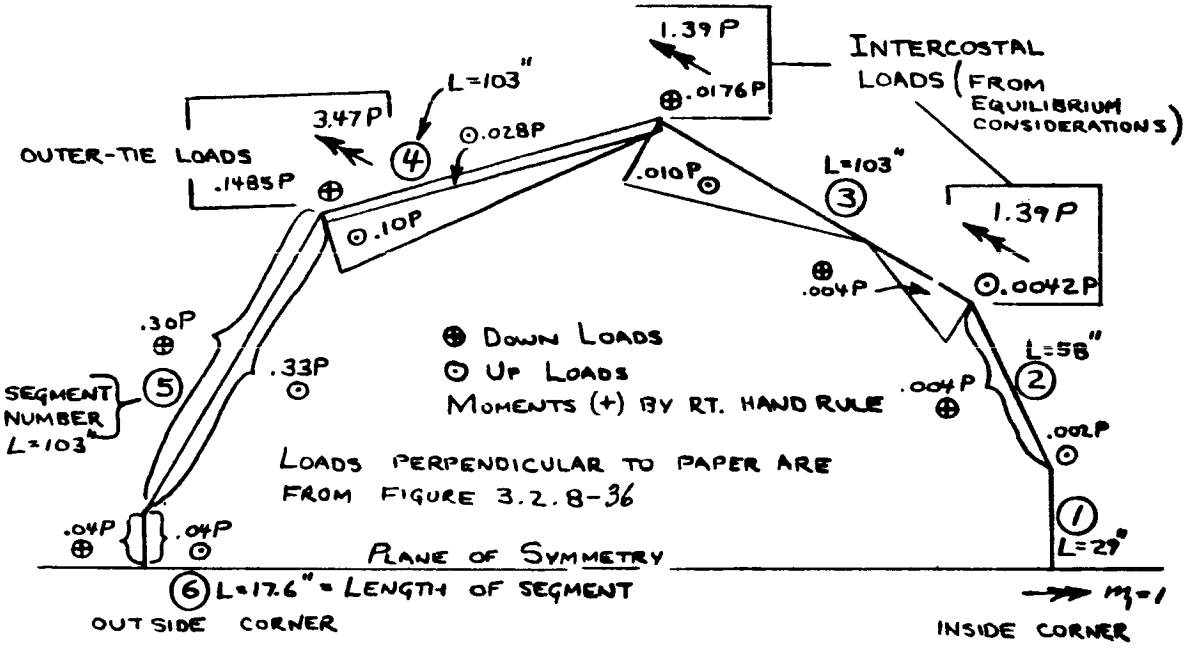

Only one half of ring was considered due to symmetry of loads and structure.

Structure was made statically determinant and stable by freeing inside corner and fixing outside corner.

By symmetry the shear, torsion, and the rotation in the m direction at the plane of symmetry are zero.

Θ = Rotation at inside corner for applied loads on base structure.

Θ_{11} = Rotation at inside corner for unit moment on base structure.

M = moment due to applied loads
T = torsion due to applied loads
M_I = redundant moment

$$\Theta = \int \frac{M m_1 dx}{EI} + \int \frac{T t_1 dx}{JG} \qquad \Theta_{11} = \int \frac{m_1^2 dx}{EI} + \int \frac{t_1^2 dx}{JG}$$

$$M_I \Theta_{11} + \Theta = 0 \qquad \text{(Elastic Equation)}$$

The resulting loads are tabulated in Table 3.2.8-18

Figure 3.2.8-40

LOADS ANALYSIS FOR RING – SYMMETRICAL MAX. THRUST CONDITION

LATERAL LOADS

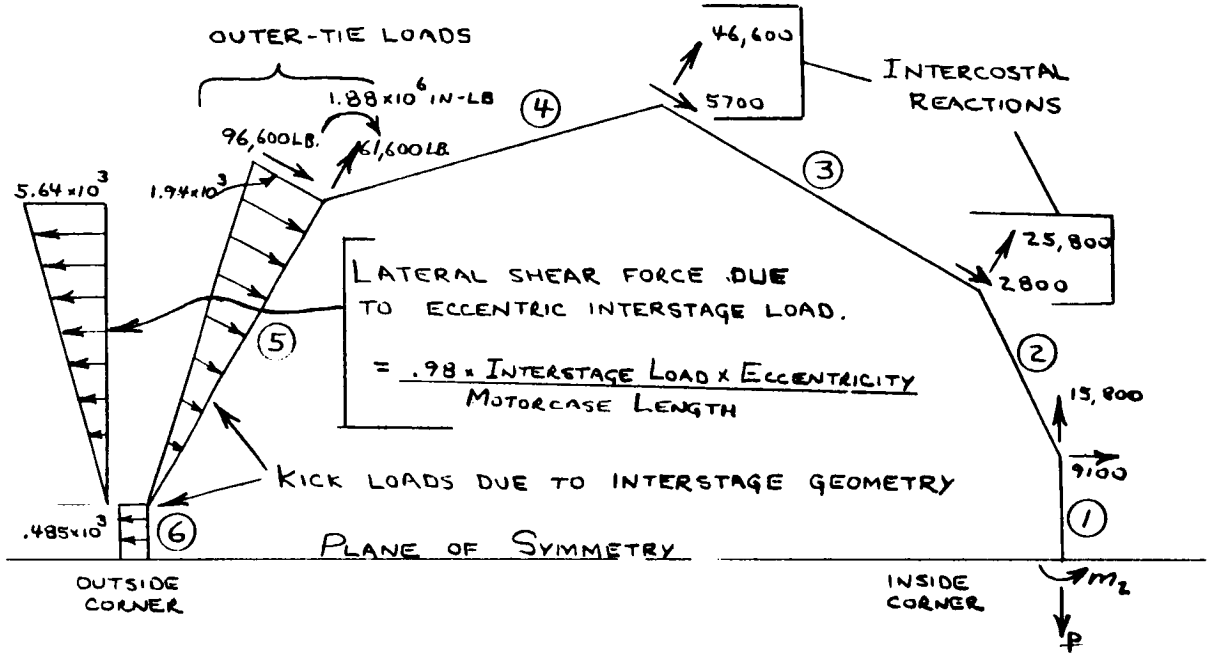

WILL ANALYZE ONE HALF OF RING BY SYMMETRY

SHEAR LOAD AT PLANE OF SYMMETRY IS ZERO

STRUCTURE WAS MADE STATICALLY DETERMINANT AND STABLE BY FIXING AT OUTSIDE CORNER AND FREEING AT INSIDE CORNER.

STRUCTURE IS TWO TIMES REDUNDANT
BY SYMMETRY : TRANSLATION AT $p' = 0$
ROTATION AT $m_2 = 0$

NEGLECT SHEAR AND AXIAL DEFLECTIONS

$$\left.\begin{aligned} P\delta_{pp} + M\delta_{pm} + \Delta = 0 \\ P\theta_{mp} + M\theta_{mm} + \Theta = 0 \end{aligned}\right\} \text{ELASTIC EQUATIONS}$$

P = REDUNDANT FORCE M = REDUNDANT MOMENT
Δ = DEFLECTION OF BASE STRUCTURE IN p DIRECTION
Θ = ROTATION OF BASE STRUCTURE IN m_2 DIRECTION
δ_{pp} = DEFLECTION AT p DUE TO A UNIT LOAD p
θ_{mm} = ROTATION AT m_2 DUE TO A UNIT MOMENT m_2
$\delta_{pm} = \theta_{mp}$ = DEFLECTION IN p DIRECTION DUE TO UNIT MOMENT m_2

THE RESULTING LOADS ARE TABULATED IN TABLE 3.2.8-18

Table 3.2.8-18

RESULTANT RING LOADS - SYMMETRICAL MAXIMUM THRUST CONDITION

SEGMENT	LONGITUDINAL LOADS		LATERAL LOADS	
	MOMENT-M_{xx}	TORSION	MOMENT-M_{yy}	AXIAL LOAD
(INSIDE CORNER) 1	2.21 P IN-LB	0	2.42×10^6 IN-LB	+61,300 LB
	2.21 P	0	2.42	61,300
2	2.01P	.93P	2.42	45,100
	2.01P	.93P	1.78	45,100
3	1.10P	.52P	1.78	33,600
	1.00P	.52P	.84	33,600
4	1.33P	.10P	.84	54,100
	-2.59P	.10P	.74	54,100
5	1.56P	-1.77P	-1.14	99,000
	3.11P	-1.77P	-4.69	-27,500
6 (OUTSIDE CORNER)	3.57P	0	-4.69	-38,300
	3.57P	0	-4.68	-38,300

POSITIVE MOMENTS ARE COMPRESSION IN BOTTOM FIBERS FOR LONGITUDINAL LOADS AND OUTSIDE FIBERS FOR LATERAL LOADS.

TORSION TENDING TO TWIST THE RING TOWARD INSIDE IS POSITIVE.

AXIAL LOADS ~ TENSION IS POSITIVE, COMPRESSION IS NEGATIVE.

SHEAR LOADS ARE RELATIVELY SMALL AND THEREFORE HAVE NOT BEEN TABULATED.

$P = 10.75 \times 10^6$ IN-LB ULTIMATE

Figure 3.2.8-41

Main Crossbeam (Intercostal Area) Loads Analysis
Symmetrical Maximum Thrust Condition

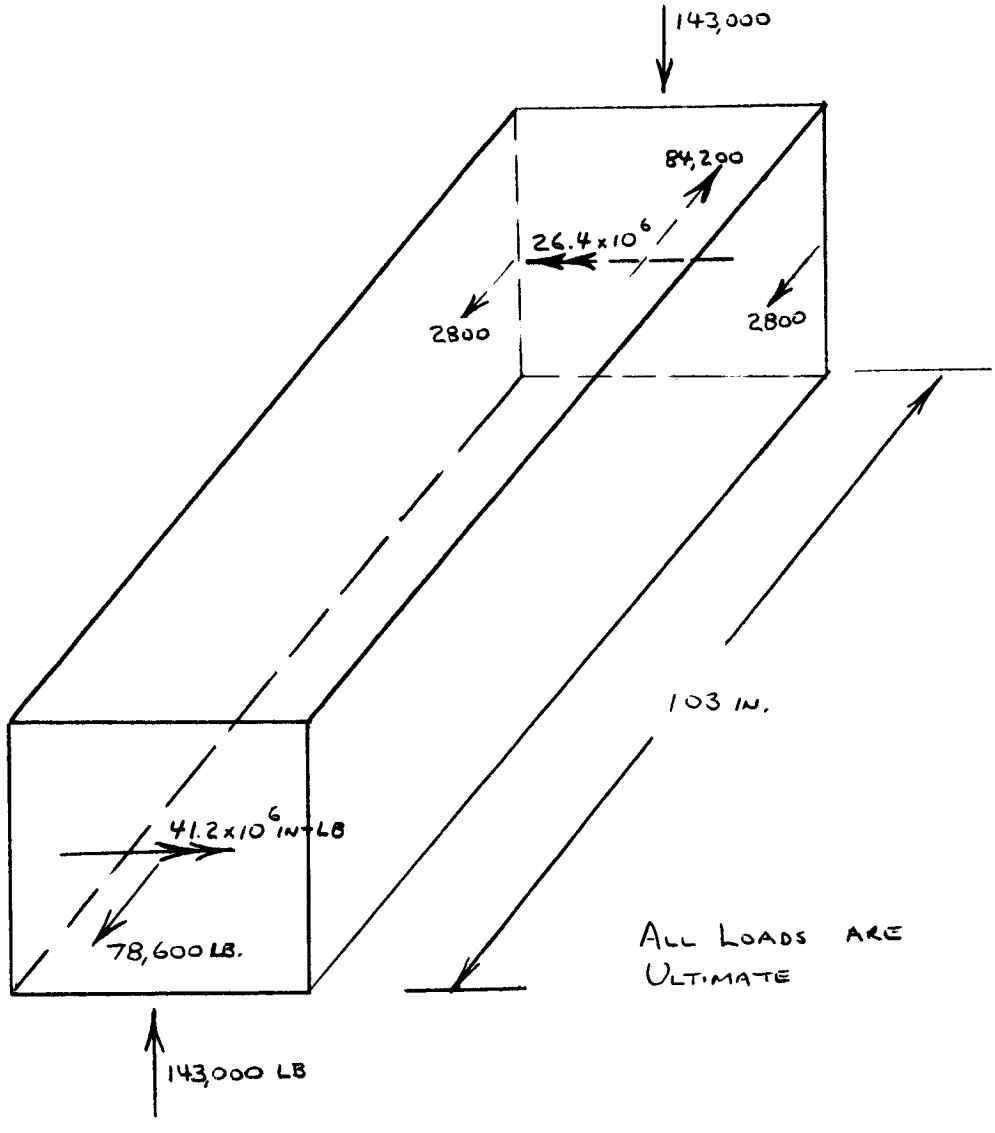

THE LOADS RESULT FROM A SUPERPOSITION OF THE CROSSBEAM LOADS AND THE CALCULATED RING LOADS FOR SEGMENT (3) FROM THE PRECEEDING PAGE. LATERAL LOADS HAVE BEEN OMITTED FOR CLARITY. SEE SYMMETRICAL MAXIMUM THRUST LOAD CONDITION DISCUSSION, 3.2.8.6.4.3.

OUTER-TIE STRESS ANALYSIS

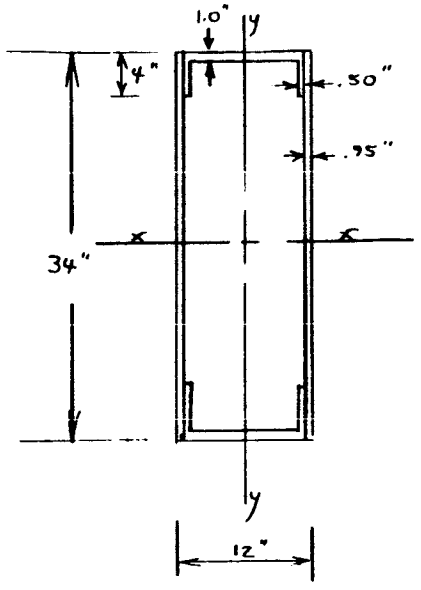

MATERIAL: 7075-T6

$A = 92.5\ IN^2$

$I_{xx} = 13{,}000\ IN^4$

$I_{yy} = 2275\ IN^4$

DESIGN CONDITION: SYMMETRICAL MAX THRUST

ULTIMATE DESIGN LOADS [1]

$M_{xx} = 37.3 \times 10^6\ IN\text{-}LB$

$M_{yy} = 1.88 \times 10^6\ IN\text{-}LB$

$V_y = 1.60 \times 10^6\ LB$

$V_x = .097 \times 10^6\ LB$

AXIAL LOAD = + 61,600 LB

MAXIMUM STRESS IN OUTER FIBERS

$$\sigma_{MAX} = \frac{37.3 \times 10^6 \times 17}{13{,}000} + \frac{1.88 \times 10^6 \times 6}{2275} + \frac{61{,}600}{92.5}$$

$$= +54{,}400\ psi$$

$$M.S. = \frac{76{,}000}{54{,}400} - 1 = .40$$

WEB STABILITY CHECK

$$f_B = \frac{37.3 \times 10^6 \times 14}{13{,}000} = 40{,}100\ psi$$

$$f_c = \frac{1.88 \times 10^6 \times 6}{2275} - \frac{61{,}600}{92.5} = 4300\ psi$$

$$f_s = \frac{1.60 \times 10^6}{2 \times 34 \times .95} = 24{,}800\ psi$$

CONSERVATIVELY ESTIMATE $E_R = \sqrt{E E_T}$ [2]

[1] FIGURE 3.2.8.38

[2] REFERENCE 11 PAGE 396-398 AND 402

OUTER-TIE STRESS ANALYSIS (CON'T)

ASSUME $f = 60{,}000$ psi $\quad E_T = 2.5 \times 10^6$ [1]

$E_R = \sqrt{10.3 \times 2.5 \times 10^6} = 5.10 \times 10^6$ psi

THE AMOUNT OF FIXITY OF THE EDGES OF THE WEB IS ASSUMED TO BE 45 % [2]

$F_{cr} = kE\left(\frac{t}{b}\right)^2$

$F_b = 21.6 \times 5.10 \times 10^6 \left(\frac{.95}{28}\right)^2 = 128{,}000$ [4]

∴ USE $F_b = F_{cy} = 66{,}000$ PSI [5]

$F_c = 4.85 \times 5.10 \times 10^6 \left(\frac{.95}{28}\right)^2 = 28{,}800$ psi [4]

$F_s = 6.35 \times 5.10 \times 10^6 \left(\frac{.95}{28}\right)^2 = 37{,}600$ psi [4]

$R_b = \frac{40{,}100}{66{,}000} = .609$

$R_c = \frac{4300}{28{,}800} = .150$

$R_s = \frac{24{,}800}{37{,}600} = .660$

[3] $MS = .01$ ←

LOCAL CRIPPLING OF THE FLANGE IS NOT CRITICAL

[1] REFERENCE 3 - SECTION 83
[2] REFERENCE 11, PAGE 336
[3] INTERACTION CURVES FOR FLAT PLATES LOADED IN BENDING, SHEAR AND LONGITUDINAL COMPRESSION.
[4] REFERENCE 13
[5] REFERENCE 5

RING STRESS ANALYSIS (CLUSTER STRUCTURE)

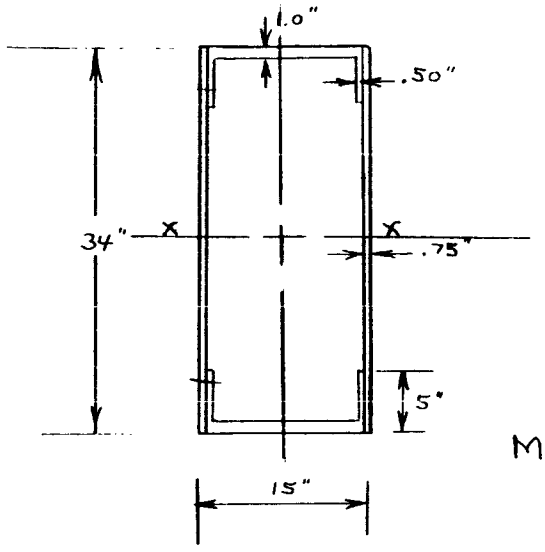

$A = 86.0\ IN^2$

$I_{xx} = 13,830\ IN^4$

$I_{yy} = 3330\ IN^4$

WEB STIFFENERS ARE $4 \times 4 \times 3/4$ ANGLES SPACED AT 26"

MATERIAL: 7075-T6

DESIGN CONDITION: SYMMETRICAL MAXIMUM THRUST

ULTIMATE DESIGN LOADS [1]

$M_{xx} = 33.4 \times 10^6\ IN\text{-}LB$

$M_{yy} = 4.69 \times 10^6\ IN\text{-}LB$

$T = 19.00 \times 10^6\ IN\text{-}LB$

$V_y = 0$

$V_x = 16,600\ LB$

AXIAL LOAD $= -27,500\ LB.$

MINIMUM STRESS IN OUTER FIBERS

$$\sigma_{min} = \frac{-33.4 \times 10^6 \times 17}{13,830} - \frac{4.69 \times 10^6 \times 7.5}{3330} - \frac{27,500}{86}$$

$$= -41,000 - 10,500 - 320$$

$$= -51,800\ psi$$

$$MS = \frac{66,000}{51,800} - 1 = .27$$

[1] TABLE 3.2.8-18, SEGMENT 5

[2] REFERENCE 5, $F_{cy} = 66,000\ PSI$

RING STRESS ANALYSIS (CON'T)

SHEAR FLOW

$$q = \frac{T}{2A} = \frac{19 \times 10^6}{2 \times 15 \times 34} = 18{,}600 \text{ LB/IN}$$

WEB STABILITY CHECK

$f_b = \frac{13}{17} \times 41{,}000 = 31{,}300$ psi

$f_s = \frac{18{,}600}{.75} = 24{,}800$ psi

$f_c = 10{,}500$ psi

CONSERVATIVELY ESTIMATE $E_R = \sqrt{E E_T}$ [1]

ASSUME $f = 60{,}000$ psi $\therefore E_T = 2.5 \times 10^6$ psi [2]

$E_R = \sqrt{10.3 \times 2.5} \times 10^6 = 5.10 \times 10^6$ psi

$$a/b = \frac{26}{26} = 1.0 \qquad \frac{t}{b} = \frac{.75}{26}$$

THE AMOUNT OF FIXITY OF THE EDGES OF THE WEB IS ASSUMED TO BE 55 PER CENT [3]

$F_{cr} = KE\left(\frac{t}{b}\right)^2$ [4]

$F_b = 21.6 \times 5.10 \times 10^6 \left(\frac{.75}{26}\right)^2 = 91{,}800$ [5]

$\therefore$ USE $F_b = F_{cy} = 66{,}000$ PSI

$F_s = F_{su} = 46{,}000$ PSI $\quad K \to \infty$ [4]

[4]

$F_c = 6.80 \times 5.10 \times 10^6 \left(\frac{.75}{26}\right)^2 = 28{,}806$ psi

[1] REFERENCE 11 PAGE 396 - 398 AND 402

[2] REFERENCE 3 - SECTION 83

[3] REFERENCE 11 PAGE 336

[4] REFERENCE 13

[5] REFERENCE 5

RING STRESS ANALYSIS (CON'T)

$R_B = \frac{31,300}{66,000} = .475$

$R_S = \frac{24,800}{46,000} = .540$

$R_c = \frac{10,500}{28,800} = .365$

[1]

M.S. = .02 ←

FLANGE STABILITY MS = .12 ←

[1] INTERACTION CURVES FOR FLAT PLATES LOADED IN BENDING, SHEAR AND LONGITUDINAL COMPRESSION

MAIN CROSSBEAM (OUTER SEGMENT) STRESS ANALYSIS

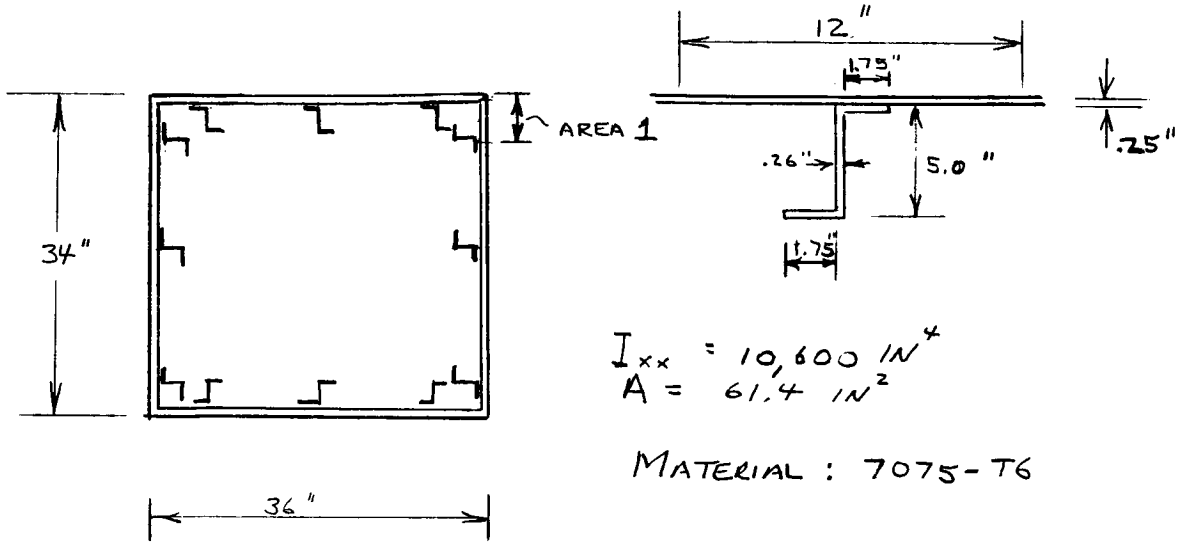

$I_{xx} = 10,600\ IN^4$

$A = 61.4\ IN^2$

MATERIAL : 7075-T6

DESIGN CONDITION : SYMMETRICAL MAXIMUM THRUST

ULTIMATE DESIGN LOADS

$M_{xx} = .023 \times 10.75 \times 10^6 \times 73 = 18.05 \times 10^6$ IN-LB ULTIMATE [1]

$V_y = .023 \times 10.75 \times 10^6 = .248 \times 10^6$ LB. ULTIMATE [1]

AXIAL LOAD $= .515 \times 10^{-2} \times 10.75 \times 10^6 = 55,300$ LB. ULTIMATE [1]

MINIMUM STRESS IN OUTER FIBERS

$$\sigma_{MIN} = \frac{-18.05 \times 10^6 \times 17}{10,600} - \frac{55,300}{61.4}$$

$$= -29,000 - 900 = -29,900\ psi$$

SHEAR STRESS IN WEB

$$\tau = \frac{V}{A} = \frac{.248 \times 10^6}{2 \times 34 \times .25} = 14,600\ psi$$

COMPRESSION STRENGTH OF STIFFENED FLANGE [2]

STIFFENER CRUSHING STRENGTH $F_c = 54,000\ psi$

SHEET $b/t = \frac{12}{.25} = 48$

[1] FIGURE 3.2.8-38

[2] REFERENCE 10

MAIN CROSSBEAM (OUTER SEGMENT) STRESS ANALYSIS - (CON'T)

SHEET BUCKLING STRESS = 26,500 PSI

PANEL CRUSHING STRENGTH $F_c = \frac{F_{c\,STIFF} A_{STIFF} + F_{c\,SKIN} A_{SKIN}}{A_{STIF} + A_{SKIN}}$

$= \frac{54,000 \times 2.21 + 26,500 \times 3.0}{5.21}$

$= 38,300$ psi

FIND THE RADIUS OF GYRATION OF STIFFENER-SHEET COMBINATION

$2w = 1.7t\sqrt{\frac{E}{f_c}} = 1.7 \times .25\sqrt{\frac{10.3 \times 10^6}{29,900}}$ [1]

$= 8.0$ IN

$\frac{We\,t'}{A_o} = \frac{8 \times .25}{2.21} = .94$ $\qquad \frac{s}{\rho_o} = \frac{2.62}{1.89} = 1.39$

$\left(\frac{\rho}{\rho_o}\right)^2 = 1.0$ $\qquad \therefore \rho = 1.89$

FOR STIFFENED PANEL $\left(\frac{L'}{\rho}\right) = \left(\frac{L}{\rho}\right) = \frac{73}{1.89} = 38.6$

ALLOWABLE PANEL ULTIMATE STRESS = 33,000 psi

$MS = \frac{33,000}{29,900} - 1 = .09$ ←

WEB STABILITY CHECK (AREA 1)

$f_c = 25,600$ psi (AVE. COMPRESSIVE STRESS ON AREA 1)

$f_s = 14,600$ psi $\qquad E = E_T = E_R$ [2]

$F_{cr} = k E \left(\frac{t}{b}\right)^2$ [3]

$F_s = 4.9 \times 10.3 \times 10^6 \left(\frac{.25}{5}\right)^2 = 12.6 \times 10^4$ $\qquad \therefore$ USE $F_s = F_{s_u} = 45,000$ [4]

[1] REFERENCE 3 - SECTION 15
[2] REFERENCE 3 - SECTION 83
[3] REFERENCE 13
[4] REFERENCE 5

MAIN CROSSBEAM (OUTER SEGMENT) STRESS ANALYSIS-(CON'T)

$$F_c = 3.6 \times 10.3 \times 10^6 \left(\frac{.25}{5}\right)^2 = 9.25 \times 10^4$$ [1]

$\therefore$ Use $F_c = F_{cy} = 66{,}000$ psi [2]

$$R_s = \frac{14{,}600}{45{,}000} = .33 \qquad R_c = \frac{25{,}600}{66{,}000} = .39$$

$$R_s^{1.5} + R_c = 1$$

$\therefore$ NOT CRITICAL

[1] REFERENCE 13
[2] REFERENCE 5

MAIN CROSSBEAM (INTERCOSTAL AREA) STRESS ANALYSIS

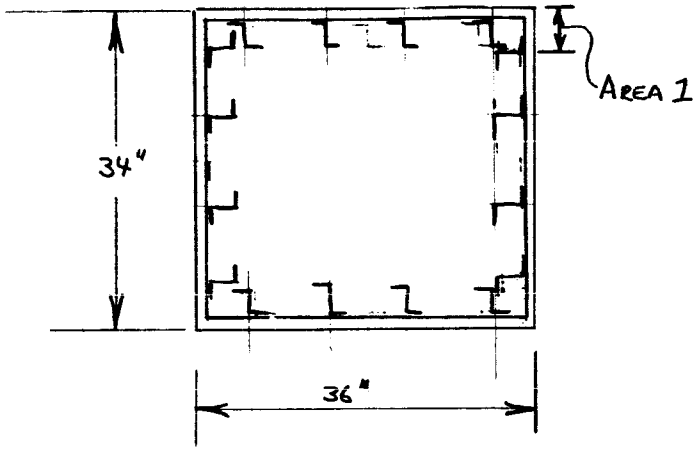

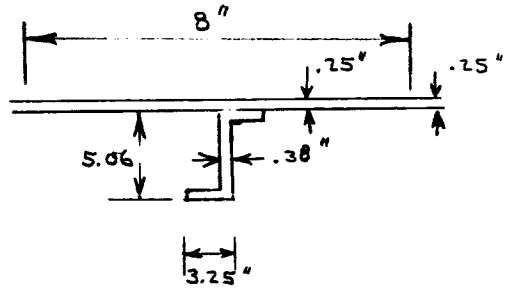

$A = 101.0\ IN^2$

$I_{xx} = 13,900\ IN^4$

MATERIAL - 7075-T6

DESIGN CONDITION: SYMMETRICAL MAXIMUM THRUST

ULTIMATE DESIGN LOADS [1]

$M_{xx} = 41.2 \times 10^6\ IN\text{-}LB$

$V_y = 143,000\ LB$

AXIAL LOAD = + 78,600 LB

STRESS IN OUTER FIBERS

$$\sigma_{MAX} = \pm \frac{41.2 \times 10^6 \times 17}{13,900} + \frac{-78,600}{101.0}$$

$= 50,400 + 780 = +51,180\ psi$

$= -50,400 + 780 = -49,620\ psi$

SHEAR STRESS IN WEB

$$\tau = \frac{V}{A} = \frac{143,000}{68 \times .25} = 8400\ psi$$

COMPRESSION STRENGTH OF STIFFENED PANELS [2]

STIFFENER CRUSHING STRENGTH $F_c = 65,000\ PSI$

SHEET $b/t = \frac{7.5}{.25} = 30$

SHEET BUCKLING STRESS = 42,000 PSI

[1] FIGURE 3.2.8-41

[2] REFERENCE 10

MAIN CROSSBEAM (INTERCOSTAL AREA) STRESS ANALYSIS - (CON'T)

PANEL CRUSHING STRENGTH $F_c = \frac{65{,}000 \times 4.12 + 42{,}000 \times 2.0}{4.12 + 2.0}$

$= 57{,}600$ PSI

FIND THE RADIUS OF GYRATION OF STIFFENER-SHEET COMBINATION

$2W = 1.7 \times .25 \sqrt{\frac{10.3 \times 10^6}{49{,}730}} = 6.15''$ [1]

$\frac{We\,t}{A_o} = \frac{6.15 \times .25}{4.12} = .373$ $\qquad \frac{s}{\rho_o} = \frac{2.65}{1.99} = 1.33$

$\left(\frac{\rho}{\rho_o}\right)^2 = 1.07$ $\qquad \rho = 2.07$

FOR STIFFENED PANEL $\left(\frac{L'}{\rho}\right) = \left(\frac{L}{\rho}\right) = \frac{62}{2.07} = 30.0$

PANEL ALLOWABLE ULTIMATE STRESS = 50,500 psi

$MS = \frac{50{,}500}{49{,}620} - 1 = .02$ ←

WEB STABILITY CHECK (AREA 1)

$f_c = 42{,}700$ psi (AVE. COMPRESSIVE STRESS ON PANEL)

$f_s = 8{,}400$ psi

CONSERVATIVELY ASSUME $E_R = \sqrt{E E_T}$ [2]

$E_R = \sqrt{10.3 \times 10} \times 10^6 = 10.2 \times 10^6$ psi [3]

$F_s = 4.9 \times 10.2 \times 10^6 \left(\frac{.25}{s}\right)^2 = 12.5 \times 10^4$ [3]

$\therefore$ USE $F_s = F_{su} = 45{,}000$ PSI [4]

$F_c = 3.6 \times 10.2 \times 10^6 \left(\frac{.25}{s}\right)^2 = 9.22 \times 10^4$ [3]

$\therefore$ USE $F_c = F_{cy} = 66{,}000$ PSI [4]

[1] REFERENCE 3 - SECTION 15
[2] REFERENCE 11, PAGE 396-398 AND 402
[3] REFERENCE 13
[4] REFERENCE 5

MAIN CROSSBEAM (INTERCOSTAL AREA) STRESS ANALYSIS - (CON'T)

$$R_s = \frac{8400}{45,000} = .187$$

$$R_c = \frac{42,700}{66,000} = .65$$

$$R_s^{1.5} + R_c = 1$$

∴ WEB BUCKLING IS NOT CRITICAL

Unsymmetrical Thrust Termination Load Condition (Cluster Structure) — The unsymmetrical thrust termination load condition consists of five motors at full thrust and one motor at partial thrust. The loads were determined for a ±3 sigma variation on the burn time for the thrust-time curve, Figure 3.2.8-19.

Since an exact solution of the loads distribution requires a complete stiffness analysis, the unsymmetrical thrust termination loads were determined by three independent approximate methods. Method I is based on data generated during a previous study under Contract NAS8-2438. This method breaks the intercostal longitudinal shear forces into two components. One component results from the inertia load of the partial-thrust motor and the other results from the portion of the second-stage inertia loads going into the partial-thrust motor. Since the motor is not at zero thrust for this vehicle, it was necessary to calculate symmetrical and unsymmetrical load components so that the previously generated data could be used.

Method II is based on breaking the load system into symmetrical and unsymmetrical components and superimposing the two. The symmetrical component is for symmetrical thrust on all motors. The unsymmetrical component is due to the bending moment introduced by the unbalance of thrust between a full-thrust motor and the partial-thrust motor. The basis for this method is theoretically exact for small deflections. It is limited by inelastic action and the assumptions regarding the distribution of the moment into the solid motors.

Method III is an arbitrary distribution and is included to illustrate the distribution of the unsymmetrical thrust loads on the overall vehicle. The structure was simplified to facilitate the analysis by representing the six motors with four motors arranged in a line. The two middle motors in the simplified structure each represent two motors in the actual structure. The partial-thrust motor is an end motor. Because of the complexity of the loads system, the method of superposition was used. The necessary assumptions are indicated on the individual distributions. The resulting load distribution shows the system in equilibrium.

The three methods considered yielded approximately the same design loads. The loads for Method II were used for analyzing the structure.

Intercostal loads were determined by superimposing the secondary loads induced by bending in the motor cases with the longitudinal shear loads due to unsymmetrical loading. The portionof the longitudinal shear load reacted by each intercostal was based on the rotation of the motor case at the plane of the clustering structure.

The forward skirt consists of semimonocoque structure with large stiffeners and frames. The structure was analyzed for out-of-plane bending due to the unsymmetrical thrust termination loads. The intercostal loads were reacted by the ring and the forward skirt extension. The portion of the moment equal

to the symmetrical maximum-thrust intercostal moment was reacted by the ring. The remaining portion of the moment was distributed by the ring to the forward skirt extension. The skin was designed to be nonbuckling to prevent panel flutter during flight.

Figure 3.2.8-42

UNSYMMETRICAL THRUST TERMINATION LOADS ANALYSIS METHOD I

BASED ON DATA FROM PREVIOUS VEHICLE STUDY [1]

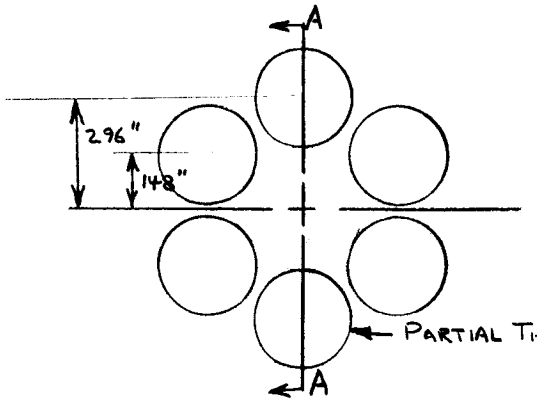

LENGTH OF INTERCOSTAL SHEAR LOAD PATH = 46 IN.

LENGTH OF INTERSTAGE SHEAR LOAD PATH = 400 IN.

[2]

THRUST ON EACH OF FIVE MOTORS = FULL THRUST = 14.12×10^6 LB. ULTIMATE

THRUST ON ONE MOTOR = PARTIAL THRUST = 7.60×10^6 LB ULTIMATE

INERTIA LOAD PER MOTOR = 3.11×10^6 LB. ULTIMATE

$$\text{ANTISYMMETRICAL INERTIA LOAD} = \left(\frac{14.12 - 7.60}{14.12}\right) 3.11 \times 10^6$$

$$= 1.44 \times 10^6 \text{ LB}$$

$$\text{LOAD THROUGH INTERCOSTALS} = \frac{400}{446} \times 1.44 = 1.30 \times 10^6 \text{ LB.}$$

$$\text{LOAD THROUGH INTERSTAGE} = \frac{46}{446} \times 1.44 = .14 \times 10^6 \text{ LB.}$$

ON PREVIOUS STUDY 17.8 % OF TOTAL SECOND STAGE INERTIA LOAD WENT INTO OUT MOTOR.

$\frac{4 \text{ MOTORS}}{6 \text{ MOTORS}} \times .178 = .118 = 11.8\%$ OF EXCESS SECOND STAGE INERTIA LOAD INTO MOTOR AT PARTIAL THRUST

$$\left[7.60 - (3.11 - 1.44)\right] \times 10^6 = 5.93 \times 10^6 \text{ LB}$$

PORTION OF SECOND STAGE INERTIA LOAD RESISTED SYMMETRICALLY BY EACH SOLID MOTOR

[1] CONTRACT NAS8-2438

[2] FIGURE 3.2.8-19

UNSYMMETRICAL THRUST TERMINATION LOADS ANALYSIS - (CON'T)

ANTISYMMETRICAL 2ND STAGE INERTIA LOAD = TOTAL SECOND STAGE INERTIA LOAD $-(6 \times 5.93 \times 10^6)$

$= 59.54 \times 10^6 - 35.58 \times 10^6$

$= 23.96 \times 10^6$ LB.

11.8 % OF THIS LOAD GOES THROUGH INTERCOSTALS

$.118 \times 23.96 \times 10^6 = 2.8 \times 10^6$ LB

TOTAL LOAD THROUGH INTERCOSTALS = 1.30×10^6
2.80×10^6
4.10×10^6 LB. ULTIMATE

UNSYMMETRICAL THRUST TERMINATION

METHOD II : BASED ON SUPERPOSITION OF SYMMETRICAL AND ANTI-SYMMETRICAL LOADS

SYMMETRICAL LOAD PER MOTOR = 2ND STAGE INERTIA LOAD (1/6)

$= (59.54)\,1/6 = 9.92 \times 10^6$ LB ULTIMATE

MOMENT = (FULL THRUST − PARTIAL THRUST) 296 (AT BASE OF VEHICLE)

$= (14.12 - 7.60)\,296 = 1930 \times 10^6$ IN-LB

ASSUMING NO GIMBAL ON NOZZLES THERE IS NO LATERAL ACCELERATION

THE BASE MOMENT WILL BE REDUCED BY ROTATIONAL INERTIA FORCES OF SOLID MOTORS AND EXCESS FIRST STAGE PROPELLANT.

$I = 1457 \times 10^{10}$

$\Sigma T = I\alpha \qquad \therefore \alpha = \frac{\Sigma T}{I} = \frac{1930 \times 10^6}{1457 \times 10^{10}} = 1.33 \times 10^{-4}$

$a_T = r\alpha$ ASSUMING 1ST STAGE INERTS TO BE CONCENTRATED AT MID POINT OF 1ST STAGE MOTORS

UNSYMMETRICAL THRUST TERMINATION LOADS ANALYSIS - (CON'T)

$$a_T = 110 \times 12 \times 1.33 \times 10^{-4} = .1755 \text{ g's}$$

REDUCTION IN MOMENT DUE TO INERTIA LOAD = M_R

$$M_R = (m a_T)\frac{L}{2} = 3.18 \times .1755 \times 1025$$

$$= 572 \times 10^6 \text{ IN-LB}$$

MOMENT AT CLUSTERING STRUCTURE

$$M = (1930 - 572)\,10^6 = 1358 \times 10^6 \text{ IN-LB ULTIMATE}$$

LOAD IN PARTIAL THRUST MOTOR

$$P = \frac{Md}{\Sigma d^2} = \frac{1358 \times 10^6 \times 296}{2 \times \overline{296}^2 + 4 \times \overline{148}^2}$$

$$P = 1.53 \times 10^6 \text{ LB. ULTIMATE}$$

ASSUMING STRESS TO BE PROPORTIONAL TO DISTANCE FROM NEUTRAL AXIS.

TOTAL LOAD FROM INTERSTAGE INTO PARTIAL THRUST MOTOR

P_{TOTAL} = SYMMETRICAL LOAD − LOAD DUE TO MOMENT

$$= (9.92 - 1.53) \times 10^6 = 8.39 \times 10^6 \text{ LB}$$

TOTAL LOAD THROUGH INTERCOSTALS

LOAD = (LOAD FROM INTERSTAGE + SOLID MOTOR INERTIA LOAD) − THRUST ON PARTIAL THRUST MOTOR

$$\text{LOAD} = (8.39 + 3.11) \times 10^6 - (7.60 \times 10^6)$$

$$= 3.90 \times 10^6 \text{ LB ULTIMATE}$$

UNSYMMETRICAL THRUST TERMINATION LOADS ANALYSIS

METHOD III : - BASED ON ASSUMED LOAD DISTRIBUTION FOR A SIMPLIFIED STRUCTURE

LONGITUDINAL LOAD DISTRIBUTION

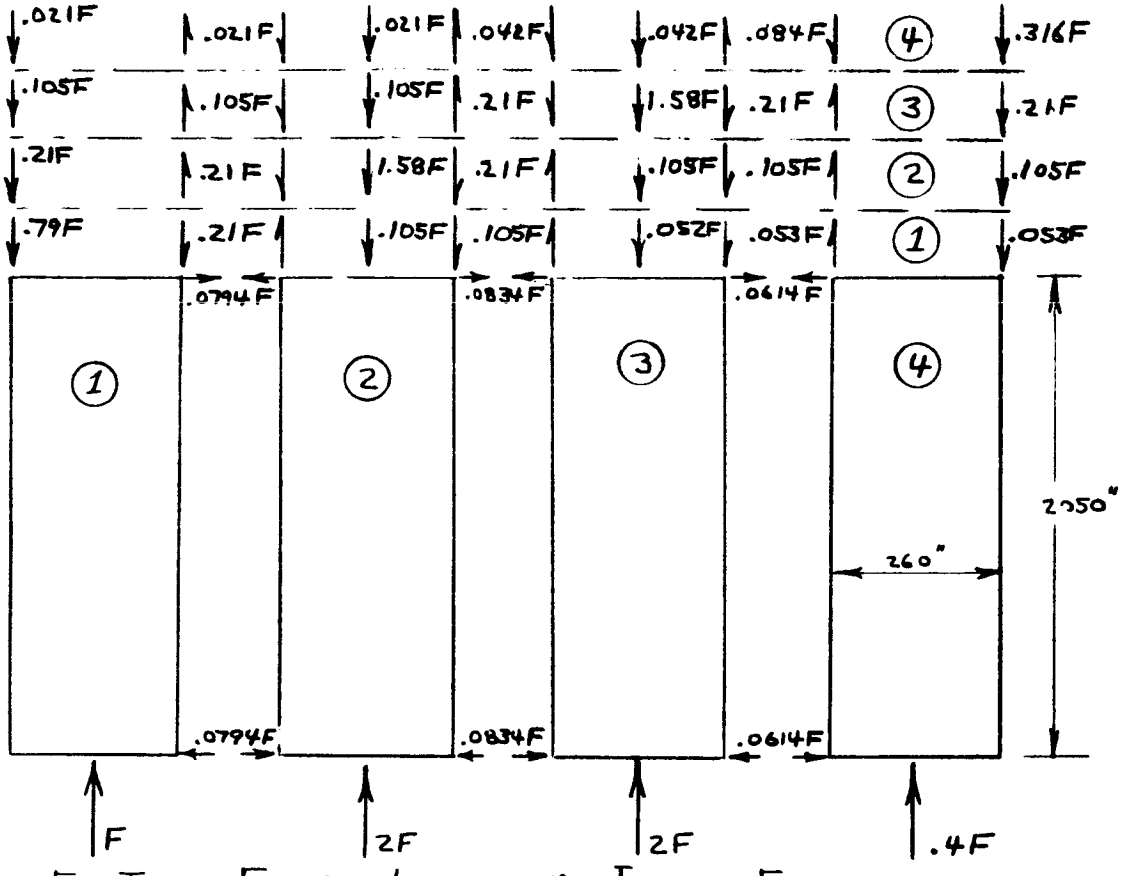

F = THRUST FORCE − LONGITUDINAL INERTIA FORCE

$F = (14.12 - 3.11) \times 10^6 = 11.01 \times 10^6$ LB. ULTIMATE

THE SIX MOTOR CLUSTER WAS ORIENTED AS INDICATED IN Fig. 3.2.8-40. THE STRUCTURE WAS SIMPLIFIED AS SHOWN ABOVE. ALL SHEAR FORCES WERE ASSUMED TO ACT AT THE EDGES OF THE MOTOR-CASES AND THE DISTANCE BETWEEN THE CASES WAS NEGLECTED. THE INTERSTAGE LOADS ON MOTORS (2) AND (3) WERE ASSUMED TO ACT IN THE CENTER OF THE CASES. ALL OF THE MOMENT ON THE INDIVIDUAL MOTORS WAS RESISTED BY BENDING OF THE MOTOR CASES.

EACH ROW IN THE DISTRIBUTION ARRAY ABOVE THE MOTORS RERESENTS THE DISTRIBUTION OF THE FORCE APPLIED AT THE BASE OF A SINGLE MOTOR. FOR EXAMPLE THE THRUST FORCE F ON MOTORCASE (1) IS DISTRIBUTED IN ROW (1). THE LATERAL FORCES ON THE MOTORCASES WERE DETERMINED BY EQUILIBRIUM CONSIDERATIONS.

UNSYMMETRICAL THRUST TERMINATION LOADS ANALYSIS - (CON'T)

(METHOD III - CON'T.)

INERTIA LOADS DISTRIBUTION

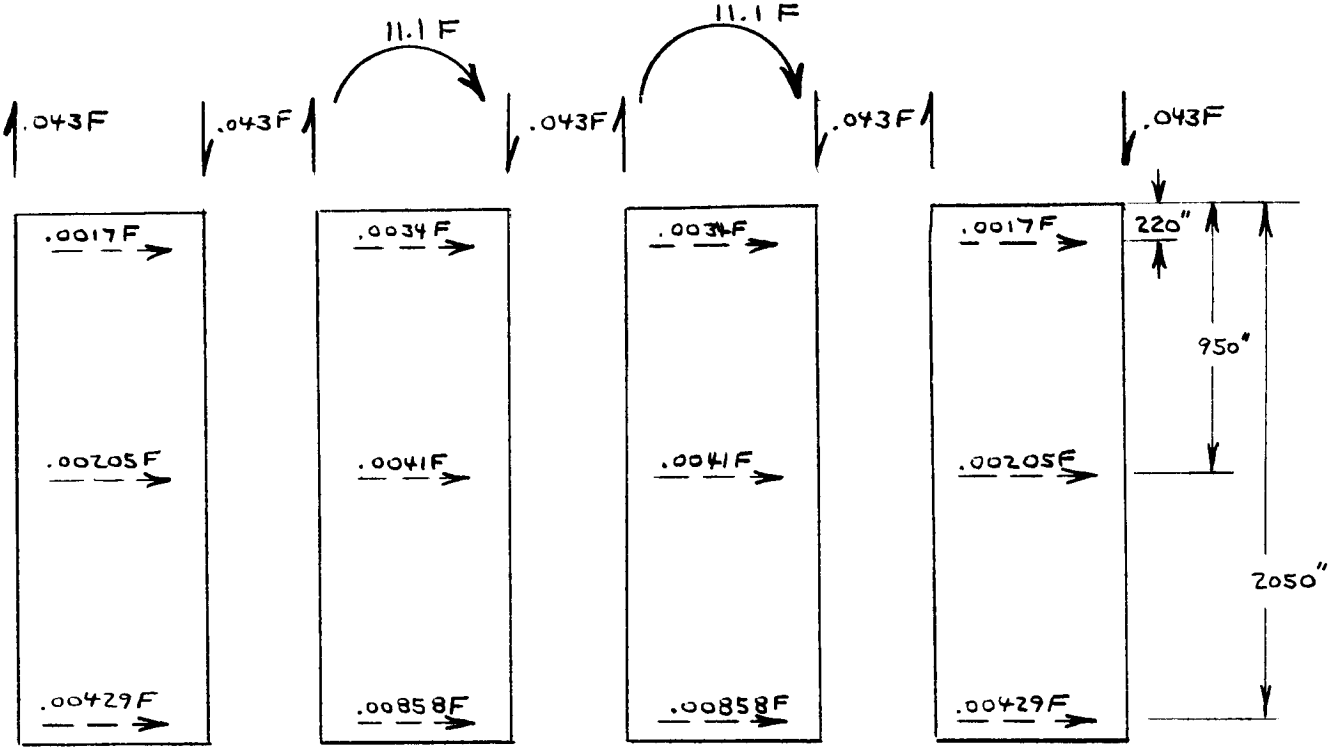

THE LATERAL INERTIA LOADS WERE DETERMINED FROM THE UNSYMMETRICAL THRUST TERMINATION LOADS ANALYSIS. ONE SIXTH OF THE INERTIA LOAD WAS APPLIED TO EACH OF THE TWO END MOTORS. ONE THIRD OF THE TOTAL LOAD WAS APPLIED TO EACH OF THE INTERIOR MOTORS BECAUSE THEY WERE ASSUMED TO REPRESENT TWO MOTORS IN THE ANALYSIS.

THE TOTAL MOMENT ON THE TWO END MOTORS WAS REACTED BY LONGITUDINAL SHEAR FORCES AT THE FORWARD END OF THE MOTORS.

ONE HALF OF THE MOMENT ON THE INTERIOR MOTORS WAS RESISTED BY LONGITUDINAL SHEAR FORCES AND ONE HALF WAS REACTED AS LOCAL BENDING IN THE INTERSTAGE.

UNSYMMETRICAL THRUST TERMINATION LOADS ANALYSIS - (CON'T)
(METHOD III CON'T)

RESULTANT LOADS ON STRUCTURE

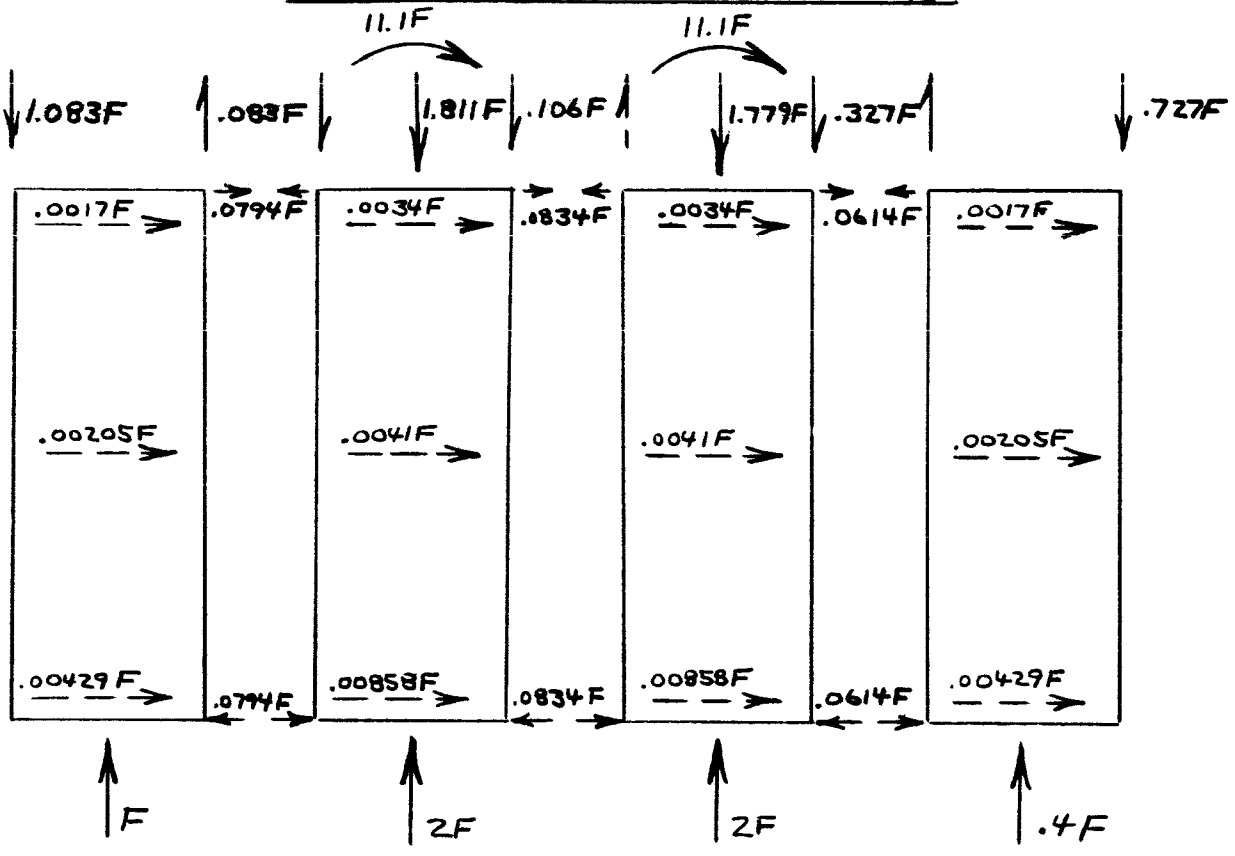

THE RESULTANT LOADS ON THE STRUCTURE WERE OBTAINED BY SUPERIMPOSING THE LONGITUDINAL THRUST DISTRIBUTION LOADS AND THE INERTIA LOADS RESULTING FROM THE ANTI-SYMMETRICAL DISTRIBUTION OF THE THRUST FORCES.

EQUILIBRIUM CHECK OF MOMENT AT PLANE OF CLUSTERING STRUCTURE

MOMENT OF INTERSTAGE LOADS

$$M = (1.083 - .727)F \times 2 \times 260 + (1.811 - 1.779)F \times 130 - 2 \times 11.1F$$

$$= 185.12F + 4.16F - 22.2F$$
$$= 167.1\ F \text{ IN-LB}$$

UNSYMMETRICAL THRUST TERMINATION LOADS ANALYSIS -(CON'T)
(METHOD III CON'T.)

MOMENT OF THRUST LOADS AND INERTIA LOADS

$$M = (1.0-.4)\,1.5\times 260\,F - (.02574F \times 2050 + .0123F \times 950 + .0102F \times 220)$$

$$M = 167.4F$$

$$167.4F \approx 167.1F \quad \text{CHECKS}$$

COMPARISON OF BENDING MOMENT AT PLANE OF CLUSTERING STRUCTURE WITH UNSYMMETRICAL BURNOUT LOADS. [1]

THE BENDING MOMENT FOR THE SIMPLIFIED STRUCTURE WILL BE MODIFIED TO REFLECT THE GEOMETRY OF THE ACTUAL STRUCTURE. THE ECCENTRICITY OF THE INTER-STAGE LOADS WILL BE ASSUMED TO BE 96.4 INCHES. (THE SAME AS FOR SYMMETRICAL BURNOUT)

$$M = 185.12F \times \frac{(296+96.4)}{520} + 4.16F \times \frac{196}{130} - 22.2F = 124F \text{ ULTIMATE}$$

FROM FIGURE 3.2.8-21 $M = 900 \times 10^6$ IN-LB LIMIT

$$M = 1.4 \times \frac{900 \times 10^6}{11 \times 10^6} = 115F \text{ ULTIMATE}$$

$$\text{PER CENT DIFFERENCE} = \frac{124-115}{\frac{1}{2}(124+115)} = 7.5 \text{ PER CENT}$$

MAXIMUM INTERCOSTAL SHEAR FORCE

$$V = .327 \times 11.0 \times 10^6$$

$$= 3.60 \times 10^6 \text{ LB.}$$

TOTAL LONGITUDINAL SHEAR FORCE TRANSFERRED FROM PARTIAL THRUST MOTOR THROUGH THE INTERCOSTALS

[1] FIGURE 3.2.8-20

INTERCOSTAL LOADS ANALYSIS

UNSYMMETRICAL THRUST TERMINATION CONDITION

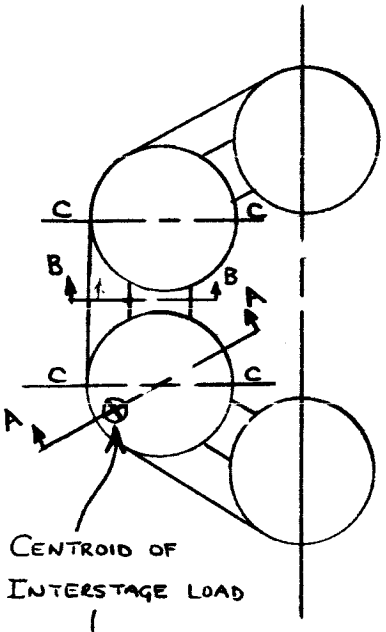

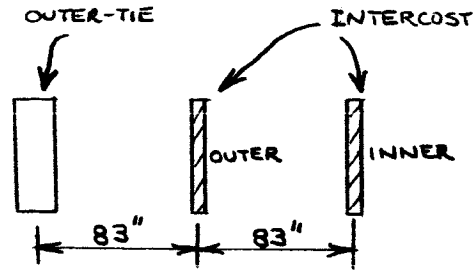

VIEW B-B
NOT TO SCALE

THE INTERCOSTAL LOADS CONSIST OF THE LONGITUDINAL SHEAR LOAD BETWEEN MOTORS AND THE LOADS INDUCED BY THE COMPONENT OF THE ROTATION AT THE PLANE OF THE CLUSTERING STRUCTURE ABOUT AXIS C-C. THE RESULTANT INTERCOSTAL LOADS WERE OBTAINED BY SUPERIMPOSING THE TWO COMPONENTS.

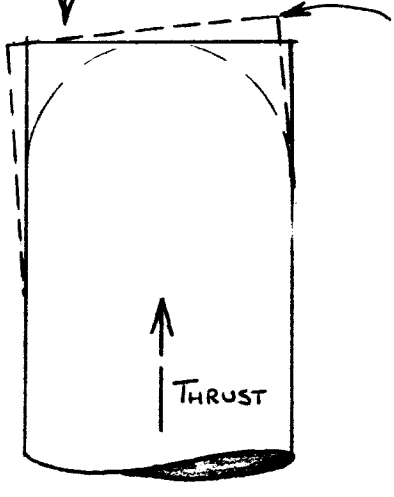

VIEW A-A
NOT TO SCALE

LONGITUDINAL SHEAR LOADS

BASED ON THE RELATIVE LOCATION OF THE INTERCOSTALS SHOWN IN VIEW B-B IT WILL BE ASSUMED THAT THE LONGITUDINAL SHEAR LOAD THROUGH EACH INTERCOSTAL IS PROPORTIONAL TO ITS DISTANCE FROM THE OUTER TIE.

$\therefore$ 1/3 OF LOAD GOES THROUGH OUTBOARD INTERCOSTAL

2/3 OF LOAD GOES THROUGH INBOARD INTERCOSTAL

INTERCOSTAL LOADS ANALYSIS (CONT)

THE SECONDARY LOAD INDUCED IN THE INTERCOSTALS BY BENDING OF THE MOTORCASES WAS ASSUMED TO BE PROPORTIONAL TO THE INTERCOSTAL LOAD INDUCED BY THE ECCENTRIC INTERSTAGE LOAD IN THE SYMMETRICAL MAXIMUM THRUST CONDITION. [2] THE AVERAGE OF THE ECCENTRIC LOAD FROM THE INTERSTAGE FOR THE PARTIAL THRUST MOTOR AND THE FULL THRUST MOTOR WAS ASSUMED TO ACT AT EACH END OF THE INTERCOSTAL.

OUTBOARD INTERCOSTAL LOADS [1]

LOAD INDUCED BY ROTATIONS

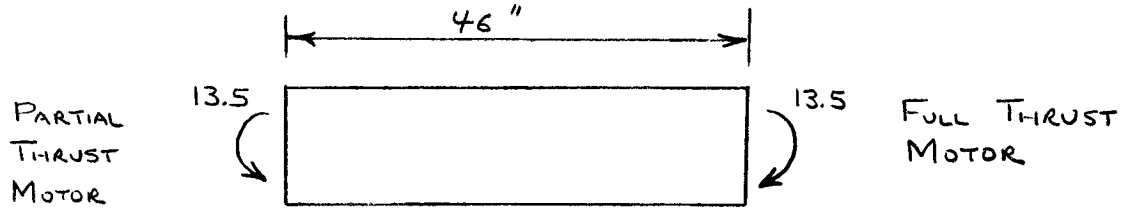

ALL LOADS ARE ULTIMATE $\times 10^{-6}$

$M = (\text{AVE. LOAD FROM INTERSTAGE})(1.39\,P)$

$= \left(\frac{8.39 + 11.01}{2}\right) 1.39 \times 10^{6} = 13.5 \times 10^{6}$ IN-LB

LOAD DUE TO LONGITUDINAL SHEAR FORCES

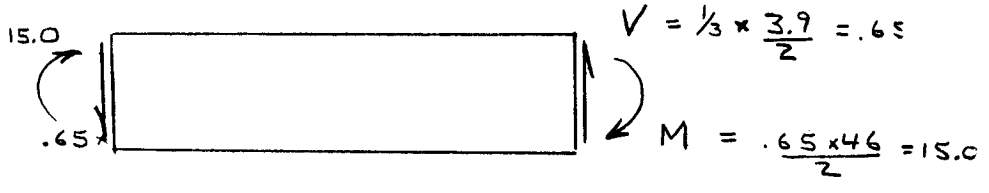

RESULTANT LOADS

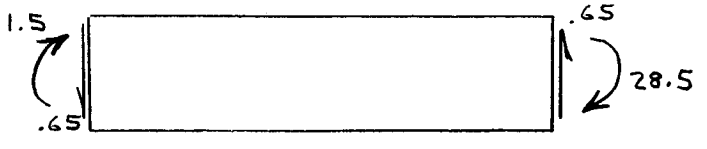

[1] ALL LOADS ARE REFERENCED TO METHOD II, UNSYMMETRICAL THRUST TERMINATION LOADS ANALYSIS.

[2] FIGURE 3.2.8-39, 1.39 P AT EACH INTERCOSTAL

INTERCOSTAL LOADS ANALYSIS - (CON'T.)

INBOARD INTERCOSTAL LOADS [1]

LOAD INDUCED BY ROTATIONS

SEE OUTBOARD INTERCOSTAL ANALYSIS FOR DETAILS

LOAD DUE TO LONGITUDINAL SHEAR FORCES

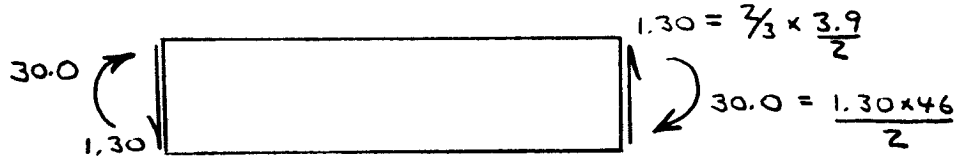

RESULTANT LOADS

[1] ALL LOADS ARE REFERENCED TO METHOD II UNSYMMETRICAL THRUST TERMINATION LOADS ANALYSIS.

FORWARD SKIRT LOADS ANALYSIS (CLUSTER STRUCTURE)

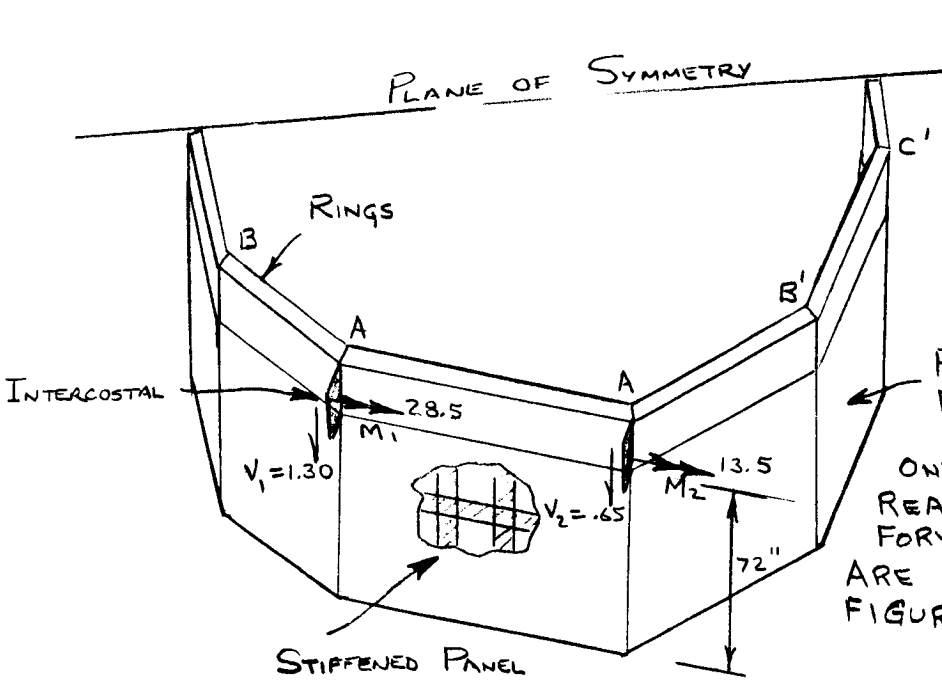

ONLY THOSE LOADS REACTED BY THE FORWARD SKIRT ARE SHOWN ON THE FIGURE.

ASSUME THAT THE PORTION OF THE INTERCOSTAL MOMENTS GREATER THAN THE SYMMETRICAL MAXIMUM THRUST MOMENT ARE REDISTRIBUTED BY THE RING INTO THE FORWARD SKIRT.

$M_2 = (28.5 - 1.39 \times 10.75) \times 10^6 = 13.5 \times 10^6$ IN-LB [1] [2]

$M_1 = (43.5 - 1.39 \times 10.75) \times 10^6 = 28.5 \times 10^6$ IN-LB [1] [2]

ASSUME 25 PER CENT OF THE TOTAL MOMENT DISTRIBUTED ALONG SIDE A-A':

$.25(28.5 + 13.5) \times 10^6 = .25(42 \times 10^6) = 10.5 \times 10^6$ IN-LB

$\left(\frac{28.5}{42.0}\right) 10.5 \times 10^6 = 7.10 \times 10^6$ IN-LB = PORTION OF M_1 REACTED ALONG SIDE A-A'

$(28.5 - 7.1) \times 10^6 = 21.4 \times 10^6$ IN-LB = PORTION OF M_1 REACTED ALONG SIDE A-B

[1] SEE PRECEDING INTERCOSTAL LOADS ANALYSIS

[2] REFERENCE FIGURE 3.2.8-39

FORWARD SKIRT LOADS ANALYSIS - CONT.

STRINGER ANALYSIS - PANEL A-B

LENGTH OF PANEL A-B = 58.4 IN
STRINGER SPACING = 11.0 IN

ASSUME THE LOAD TO BE DISTRIBUTED INTO PANEL A-B BY RING A-B

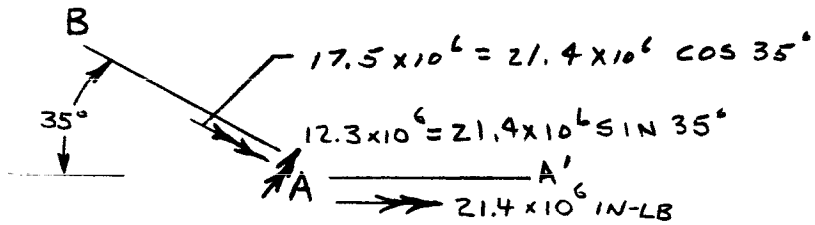

ASSUME TORSION LOAD TO BE UNIFORMLY DISTRIBUTED TO STRINGERS

ASSUME BENDING COMPONENT TO BE RESISTED BY FRAMES

$$\text{LOAD PER STRINGER} = 17.5 \times 10^6 \times \frac{11.0}{58.4} = 3.30 \times 10^6 \text{ IN-LB}$$

THE SHEAR LOADS V_1 AND V_2 WOULD BE DISTRIBUTED INTO THE SKIN AND STRINGERS BUT WOULD BE ZERO AT THE TOP OF THE STRINGER WHERE MOMENT IS MAXIMUM.

STRINGER ANALYSIS - PANEL A'-B'

LENGTH OF PANEL A'-B' = 103.3 IN.
STRINGER SPACING = 11.0 IN

MAKING THE SAME ASSUMPTIONS AS ABOVE

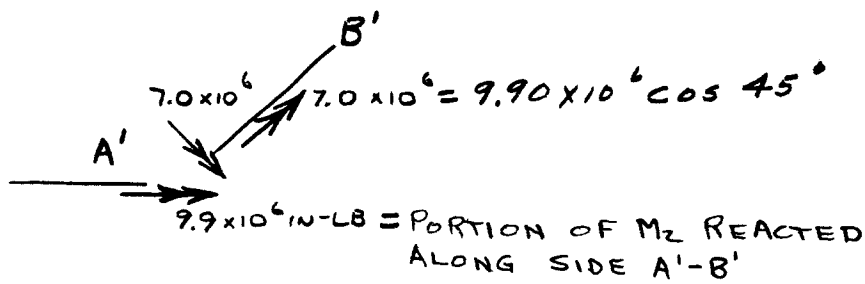

$$\text{LOAD PER STRINGER} = 7.0 \times 10^6 \times \frac{11.0}{103.3} = .75 \times 10^6 \text{ IN-LB}$$

FORWARD SKIRT LOADS ANALYSIS - CONT.

STRINGER ANALYSIS - PANEL B'-C'

CONSERVATIVELY ASSUME ALL OF FRAME LOADS IN PANEL B'-C' TO BE REACTED BY FIRST STRINGER

ASSUME LONGITUDINAL LOAD IN PANEL B'-C' TO BE THE SAME AS FOR SYMMETRICAL BURNOUT. [1]

LENGTH OF B'-C' = 103.3 IN.
STRINGER SPACING = 11 IN.

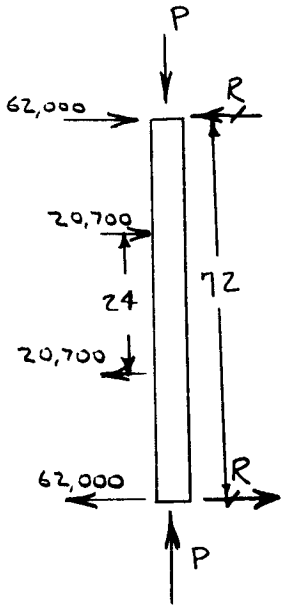

$$P = \text{LONGITUDINAL LOAD} = \frac{11}{103.3} \times .33 \times 10.75 \times 10^6 \quad [1]$$

$$= .378 \times 10^6 \text{ LB}$$

THIS LOAD MUST BE CARRIED BY THE STRINGER AND EFFECTIVE SKIN.

$$R = \frac{2(62{,}000 \times 36 + 20{,}700 \times 12)}{72}$$

$$R = 69{,}000 \text{ LB}$$

LATERAL SHEAR LOADS

SHEAR AT UNSYMMETRICAL THRUST TERMINATION DUE TO LATERAL INERTIA FORCE OF FIRST-STAGE INERTS = $.526 \times 10^6$ Lbs. ULTIMATE.

TOTAL SHEAR PER MOTOR = $\frac{.526}{6}$ + SHEAR DUE TO ECCENTRIC INTERSTAGE LOAD

$$= (.09 + .49) \times 10^6$$
$$= .580 \times 10^6 \text{ LB ULTIMATE}$$

[1] FIGURE 3.2.8-36

FORWARD SKIRT LOADS ANALYSIS - CONT.

FRAME ANALYSIS - PANEL A-B

ASSUME TWO INTERMEDIATE FRAMES AT A SPACING OF 24 IN.

FRAMES WILL BE SIZED FOR BENDING MOMENT = 12.3×10^6 IN-LB [1]

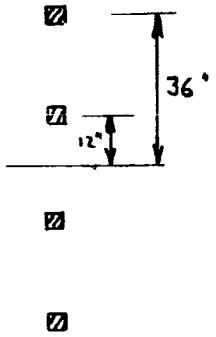

TYPICAL FRAME GEOMETRY FOR FORWARD SKIRT

$$\text{LOAD/FRAME} = \frac{M d_i}{\Sigma d_i^2}$$

$$\Sigma d_i^2 = 2\left[12^2 + 36^2\right] = 2878$$

$$\text{LOAD IN OUTER FRAME} = \frac{12.3 \times 10^6 \times 36}{2878}$$

$$= 154{,}000 \text{ LB}$$

$$\text{LOAD IN MIDDLE FRAMES} = \frac{12.3 \times 10^6 \times 12}{2878}$$

$$= 51{,}300 \text{ LB}$$

FRAME ANALYSIS - PANEL A'-B'

MOMENT = 7.0×10^6 IN-LB [1]

$$\text{LOAD IN OUTER FRAME} = \frac{7.0 \times 10^6 \times 36}{2878} = 88{,}000 \text{ LB.}$$

$$\text{LOAD IN MIDDLE FRAMES} = \frac{7.0 \times 10^6 \times 12}{2878} = 29{,}300 \text{ LB.}$$

FRAME ANALYSIS - PANEL B'-C'

BENDING IN PANEL A'-B' IS TRANSFERRED TO PANEL B'-C' AS BENDING AND TORSION

THE ANGLE BETWEEN A'-B' AND B'-C' IS 45 DEGREES.

$88{,}000 \cos 45^\circ = 62{,}000$ LB.
$29{,}300 \cos 45^\circ = 20{,}700$ LB.

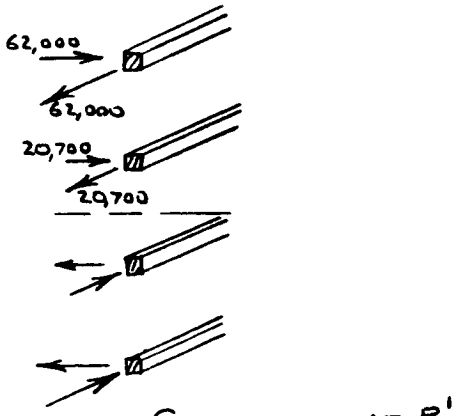

CROSS-SECTION AT B'

[1] SEE "STRINGER ANALYSIS" PANELS A-B AND A'-B'

FORWARD SKIRT LOADS ANALYSIS - CON'T.
FRAME ANALYSIS - PANEL B'-C' (con't)

IT WAS CONSERVATIVELY ASSUMED THAT THE FRAMES DISTRIBUTE ALL OF THE SIDE FORCES AT B' TO THE FIRST STRINGER IN PANEL B'-C' AS A CANTILEVER BEAM WITH THE FREE END AT B'.

THE LOWER FRAME IS CRTICAL

$M = 62{,}000 \times 11 = 680{,}000$ IN-LB

P = AXIAL LOAD = 62,000 LB. COMPRESSION

1 DISTANCE FROM B' TO FIRST STRINGER

INTERCOSTAL STRESS ANALYSIS (CLUSTER STRUCTURE)

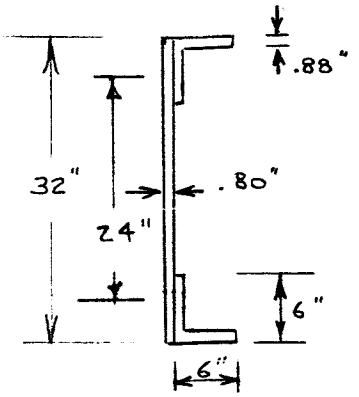

$A = 45.1\ IN^2$

$I = 6080\ IN^4$

$Q = 240\ IN^3$

MATERIAL: 7075-T6
UTILIZING TWO INTERCOSTALS AT EACH POINT [3]

DESIGN CONDITION : UNSYMMETRICAL THRUST TERMINATION

ULTIMATE DESIGN LOADS [1]

$V = 0.65 \times 10^6$ LB.
$M = 21.7 \times 10^6$ IN-LB
AXIAL LOAD = +63,500 LB

MAXIMUM STRESS IN OUTER FIBERS

$$\sigma_{MAX} = \frac{21.7 \times 10^6 \times 16}{6080} + \frac{63,500}{45.1}$$

$= 58,400$ psi , $F_{TU} = 76000$ [2]

$$MS = \frac{76000}{58400} - 1 = .30$$

WEB STABILITY CHECK

$$\frac{a}{b} = \frac{36}{24} = 1.5$$

$$f_b = \frac{21.7 \times 10^6 \times 12}{6080} = 42,700 \text{ PSI}$$

$$f_s = \frac{.65 \times 10^6}{.8(32)} = 24,400 \text{ PSI}$$

[1] SEE "INTERCOSTAL LOADS ANALYSIS"

[2] REFERENCE 5

[3] FIGURE 3.2.11-3

INTERCOSTAL STRESS ANALYSIS (CLUSTER STRUCTURE) - CONT.

CONSERVATIVELY ESTIMATE $E_R = \sqrt{E E_T}$ [1]

$f = \sqrt{f_b^2 + 3 f_s^2}$ [2]

$f = \sqrt{(42.7)^2 + 3(24.4)^2} \times 10^3 = 60{,}000 \text{ psi}$

$E_T = 2.8 \times 10^6$ [3]

$E_R = \sqrt{10.3 \times 2.8} \times 10^6 = 5.40 \times 10^6 \text{ psi}$

$F_b = 21.6 \times 5.40 \times 10^6 \times \left(\frac{.80}{24}\right)^2 = 130{,}000$ [4]

USE $F_b = 66{,}000 \text{ psi}$ [5]

$F_s = 5.9 \times 5.40 \times 10^6 \left(\frac{.80}{24}\right)^2 = 35{,}400 \text{ psi}$ [4]

$R_b = \frac{42{,}700}{66{,}000} = .65$ $\qquad R_s = \frac{24{,}400}{35{,}400} = .69$

$MS = \frac{1}{\sqrt{R_b^2 + R_s^2}} = \frac{1}{\sqrt{(.65)^2 + (.69)^2}} = .05$ [4] ←

FLANGE STABILITY CHECK

$b/t = \frac{5}{.88} = 5.7$ $\qquad F_{cc} = 66{,}000 \text{ psi}$ [5]

$MS = \frac{66{,}000}{55{,}600} - 1 = .18$ ←

[1] REFERENCE 11 PAGES 396-308, PAGE 402
[2] REFERENCE 12, SECTION D
[3] REFERENCE 3 SECTION 83
[4] REFERENCE 13
[5] REFERENCE 5

FORWARD SKIRT EXTENSION STRESS ANALYSIS

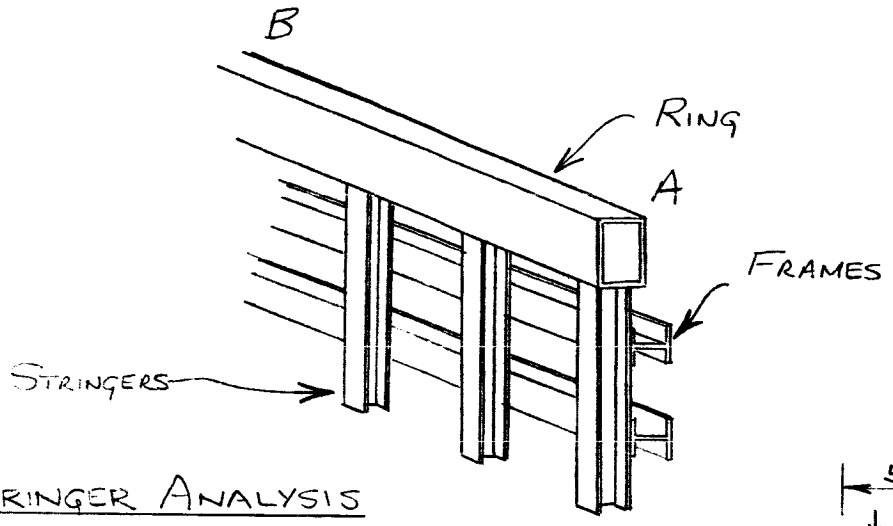

STRINGER ANALYSIS

PANEL A-B [1]

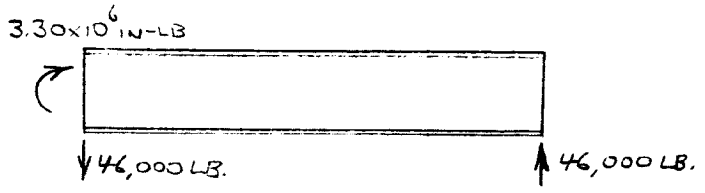

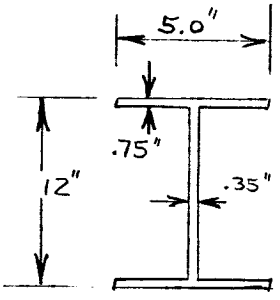

$I = 287\ IN^4$ $A = 11.15\ IN^2$

MATERIAL: 7075-T6

DESIGN CONDITION:
UNSYMMETRICAL THRUST TERMINATION

ULTIMATE DESIGN LOADS

$M = 3.30 \times 10^6$ IN-LB [1]
$V = 46,000$ LB.

$$\sigma = \frac{Mc}{I} = \frac{3.30 \times 10^6 \times 6}{287} = 69,000 \text{ PSI}$$

[2]

$$M.S. = \frac{76,000}{69,000} - 1 = .10$$

$$\tau = \frac{VQ}{It} = \frac{46,000 \times 27.3}{287 \times .35} = 12,500 \text{ PSI}$$

FLANGE STABILITY

$$b/t = \frac{2.25}{.75} = 3.0$$ [3] ∴ NOT STABILITY CRITICAL

[1] SEE FORWARD SKIRT LOADS ANALYSIS, PANEL A-B
[2] REFERENCE 5, $F_{tu} = 76,000$ PSI
[3] REFERENCE 3, SECTION 15

FORWARD SKIRT EXTENSION STRESS ANALYSIS - CONT.

WEB STABILITY

$f_b = \frac{4.75}{6.0} \times 69{,}000 = 54{,}800 \text{ psi}$

$f_s = 12{,}500 \text{ psi}$

$f = \sqrt{f_b^2 + 3f_s^2} = \sqrt{(54.8)^2 + 3(12.5)^2} \times 10^3 = 58{,}800 \text{ psi}$ [1]

$E_T = 3.3 \times 10^6 \text{ psi}$ [2]

$E_R = \sqrt{EE_T} = \sqrt{10.3 \times 3.3} \times 10^6 = 5.85 \times 10^6 \text{ psi}$ [3]

$F_b = 21.6 \times 5.85 \times 10^6 \times \left(\frac{.29}{9.5}\right)^2 = 11.8 \times 10^4 \text{ psi}$ [5]; USE $F_b = 76000$ [4]

$F_s = 4.9 \times 5.85 \times 10^6 \times \left(\frac{.29}{9.5}\right)^2 = 26{,}800$ [5]

$R_b = \frac{54800}{76000} = .72 \qquad R_s = \frac{12500}{26800} = .467$

$M.S. = \frac{1}{\sqrt{R_b^2 + R_s^2}} - 1$ [5] $= \frac{1}{\sqrt{(.72)^2 + (.467)^2}} - 1 = .14$

STRINGER ANALYSIS - PANEL B'-C'

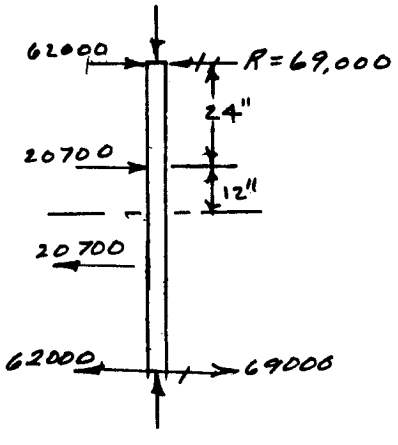

ULTIMATE DESIGN LOADS: [6]

$M = 7000(24) = 168000 \text{ IN-LB}$

AXIAL LOAD = 378,000 Lb.

$\rho = \sqrt{\frac{I}{A}} = \sqrt{\frac{287}{11.15}} = 5.09 \text{ IN.}$

$\frac{L}{\rho} = \frac{72}{5.09} = 14.12$

[1] REFERENCE 12 SECTION D

[2] REFERENCE 3 SECTION 83

[3] REFERENCE 11, PAGES 396 - 398, PAGE 402.

[4] REFERENCE 5

[5] REFERENCE 13

[6] SEE "FORWARD SKIRT LOADS ANALYSIS"

FORWARD SKIRT EXTENSION (STRESS ANALYSIS) CONT.

MAXIMUM STRESS IN OUTER FIBERS

NEGLECTING THE EFFECT OF SECONDARY BENDING

$$\sigma = \frac{.168 \times 10^6 \times 6}{287} + \frac{378 \times 10^3}{11.15} \quad \text{(ASSUMING NON EFFECTIVE SKIN)}$$

$$= 3500 + 32{,}900$$

$$= 36{,}400 \text{ psi}$$

$F_{cy} = 66000$ PSI [2]

$$MS = \frac{66{,}000}{36{,}400} - 1 = .81$$

SKIN ANALYSIS

PANEL WIDTH = 11.0 − 4.0 = 7.0 INCHES

SKIN THICKNESS = .22"

SHEAR LOAD = $.580 \times 10^6$ LB ULTIMATE [1]

$$q_{MAX} = \frac{V}{\pi R} = \frac{.580 \times 10^6}{\pi \times 130} = 1430 \text{ LB/IN}$$

$$f = \frac{1430}{.22} = 6{,}500 \text{ psi}$$

FOR NON-BUCKLED SKIN $f_c = 3500 + \frac{378 \times 10^3}{11.15 + 11 \times .22}$

$= 3500 + 27900$

$= 31400$ PSI

[3] $F_{sCR} = 4.90 \times 10.3 \times 10^6 \times \left(\frac{.22}{7}\right)^2 = 50{,}000$ PSI

USE $F_s = F_{su} = 45000$ PSI [2]

[3] $F_c = 3.62 \times 10.3 \times 10^6 \left(\frac{.22}{7}\right)^2 = 36900$ PSI

$R_c = \frac{31400}{36900} = .85$ $\qquad R_s = \frac{6500}{45000} = .144$

[3] $R + R_s^{1.5} = .85 + .144^{1.5} = .85 + .06 = .91$

$MS = \frac{1}{.91} - 1 = .10$

[1] SEE FORWARD SKIRT LOADS ANALYSIS - (LATERAL SHEAR LOADS)

[2] REF. 5

[3] REF. 13

FORWARD SKIRT EXTENSION (STRESS ANALYSIS) - CONT.

FRAME STRESS ANALYSIS

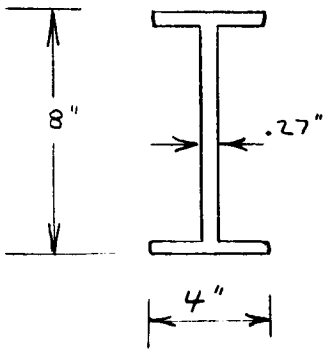

AMERICAN STANDARD I-SECTION

$I = 57.55 \ IN^4$
$A = 5.40 \ IN^2$

DESIGN CONDITION: UNSYMMETRICAL THRUST TERMINATION

ULTIMATE DESIGN LOADS [1]

$M = .68 \times 10^6 \ IN\text{-}LB$

AXIAL LOAD = 62,000 LB. COMPRESSION

$$\sigma = -\frac{Mc}{I} - \frac{P}{A} = -\frac{.68\times10^6\times4}{57.55} - \frac{62,000}{5.40}$$

$$= -47,000 - 11,500$$

$$= -58,500 \ psi$$

$$MS = \frac{66,000}{58,500} - 1 = .13$$ [2] ←

THE FLANGES AND THE WEB ARE NOT STABILITY CRITICAL

[1] SEE FORWARD SKIRT LOADS ANALYSIS (FRAME ANAL.- PANEL B-C)

[2] REF. 5 $F_{cy} = 66000$ PSI

Maximum Dynamic Pressure Load Condition (Cluster Structure) — Three conditions at maximum dynamic pressure were considered. The conditions for a 20-degree angle of attack with null thrust vectoring and for an 8-degree angle of attack with a 3.5-degree thrust vectoring were treated as failure conditions. The condition for the vehicle trimmed at maximum dynamic pressure was analyzed for a factor of safety of 1.40 on the limit loads. In all cases, the equivalent axial load was calculated and the ratio of equivalent axial load at symmetrical burnout to equivalent axial load at maximum dynamic pressure was computed. This ratio was then compared with the similar ratio for the previous study, Contract NAS8-2438. In all cases, the ratio was less critical than for the previous study. Therefore, this is not a design condition for the clustering structure. (The maximum dynamic pressure loads were only 68 percent of the design loads of the previous study.)

MAXIMUM DYNAMIC PRESSURE LOADS ANALYSIS

20 DEGREE ANGLE OF ATTACK WITH NULL THRUST VECTORING AT MAXIMUM DYNAMIC PRESSURE

THIS IS A FAILURE CONDITION. THEREFORE NO FACTOR OF SAFETY WAS APPLIED TO THE LOADS.

$M_{MAX} = 2950 \times 10^6$ IN-LB [1]

$P_{MAX} = 26.8 \times 10^6$ LB [2]

ASSUME THE EQUIVALENT AXIAL LOAD FOR BENDING = $\frac{2M}{R}$

$$P_{EQ} = \left(26.8 + \frac{2 \times 2950}{420}\right) \times 10^6$$

$$= 40.8 \times 10^6 \text{ LB}$$

FOR SYMMETRICAL MAXIMUM THRUST

$P_{EQ} = 64.5 \times 10^6$ LB. ULT [3]

T65 ISTUDY VEHICLE

$$\frac{P_{EQ\ MAXT}}{P_{EQ.\ MAX\ q}} = \frac{64.5 \times 10^6}{40.8 \times 10^6}$$

$$= 1.58$$

PREVIOUS VEHICLE

$\frac{P_{EQ\ MAXT}}{P_{EQ.\ MAX\ q}} = 1.23$ [4]

∴ THIS CONDITION IS NOT CRITICAL

[1] FIGURE 3.2.8-19

[2] FIGURE 3.2.8-21

[3] FIGURE 3.2.8-22 ; INCLUDES SAFETY FACTOR OF 1.4

[4] CONTRACT NAS8-2438

MAXIMUM DYNAMIC PRESSURE LOADS ANALYSIS - CONT.

EIGHT DEGREE ANGLE OF ATTACK WITH 3.5 DEGREE THRUST VECTORING AT MAXIMUM DYNAMIC PRESSURE

THIS IS A FAILURE CONDITION. THEREFORE NO FACTOR OF SAFETY WAS APPLIED TO THE LOADS.

$M_{MAX} = 4750 \times 10^6$ IN-LB [1]

$P_{MAX} = 26.8 \times 10^6$ LB

$$P_{EQ.} = \left(26.8 + \frac{2 \times 4750}{420}\right) \times 10^6$$

$$= 49.3 \times 10^6 \text{ LB.}$$

T65 STUDY VEHICLE	PREVIOUS VEHICLE
$\frac{P_{EQ\ MAX\ T}}{P_{EQ.\ MAX.\ q}} = \frac{64.5 \times 10^6}{49.3 \times 10^6}$	$\frac{P_{EQ.\ MAX\ T}}{P_{EQ.\ MAX.\ q}} = 1.23$ [3]
$= 1.31$	

∴ THIS CONDITION IS NOT CRITICAL

VEHICLE TRIMMED AT MAXIMUM DYNAMIC PRESSURE

$M_{MAX} = 3100 \times 10^6$ IN-LB ULTIMATE [2]

$P_{MAX} = 26.8 \times 1.4 \times 10^6 = 37.4 \times 10^6$ LB. ULTIMATE

$$P_{EQ.} = \left(37.4 + \frac{2 \times 3100}{420}\right) \times 10^6 = 52.15 \times 10^6 \text{ LB}$$

T65 STUDY VEHICLE	PREVIOUS VEHICLE
$\frac{P_{EQ.\ BO}}{P_{EQ\ MAX\ q}} = \frac{64.50}{52.15}$	$\frac{P_{EQ\ BO}}{P_{EQ\ MAX\ q}} = 1.23$ [3]
$= 1.24$	

∴ THIS CONDITION IS NOT CRITICAL

[1] FIGURE 3.2.8-16

[2] FIGURE 3.2.8-15

[3] CONTRACT NAS8-2438

BLANK

3.2.8.6.4.5 Interstage Structure

THE INTERSTAGE IS DESIGNED FOR THE MAXIMUM LONGITUDINAL LOAD WHICH OCCURS DURING THE SYMMETRICAL MAXIMUM THRUST CONDITION.

$w_1 = 31{,}200$ Lb/in AT THE PLANE OF THE FIRST STAGE CLUSTER STRUCTURE [1]

$\frac{.30 \times 10.75 \times 10^6}{103.3} = 31{,}200^{\#}/_{IN}$ SEGMENT LENGTH = 103.3 IN.

$w_2 = 24{,}500$ Lb/in AT THE STAGE SEPERATION PLANE [2]

THE SEMIMONOCOQUE STRUCTURE WAS SIZED BY THE OPTIMUM DESIGN METHOD OF REFERENCE (7) FOR THE MAXIMUM LOAD, w_1. THE SKIN WAS TAPERED FROM .36 IN. THICKNESS AT THE FIRST STAGE CLUSTER STRUCTURE TO .29 IN. AT THE STAGE SEPERATION PLANE. THE DESIGN TEMP. WAS 125° F. SEE FIGURE 3.2.10-10.

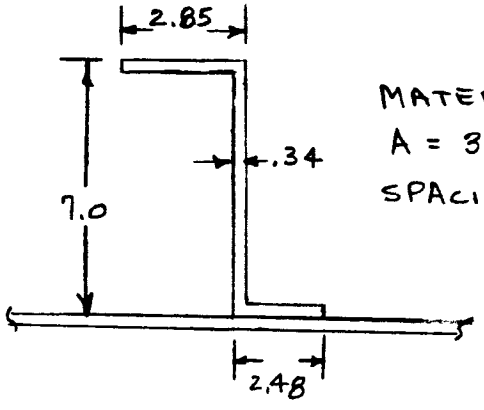

MATERIAL: 7075-T6
A = 3.96 IN²
SPACING = 10.5 IN.

STRINGER CROSS SECTION

[1] FIGURE 3.2.8-36

[2] FIGURE 3.2.8-32

INTERSTAGE STRUCTURE — CONT.

COMPRESSION CRIPPLING OF OUTSTANDING FLANGE:

$$\frac{b}{t} = \frac{2.51}{.34} = 7.38$$

$F_{CCR} = 53000$ [1]

MAXIMUM STRESS OCCURS AT THE PLANE OF THE FIRST STAGE CLUSTER STRUCTURE.

$$\text{EFFECTIVE AREA} = \left[(10.5)(.36) + 3.96\right]\frac{1}{10.5} = .735 \text{ IN}^2/\text{IN}$$

$$f = \frac{31,200}{.735} = 42,500$$

$$\text{M.S.} = \frac{53000}{42500} - 1 = .25$$

COMPRESSION BUCKLING OF SKIN:

$$\frac{a}{b} = \frac{114}{10.5} = 10.45$$ [2]

$K_c = 3.6 \qquad F_{CCR} = 45000$ [1]

$$\text{M.S.} = \frac{45000}{42500} - 1 = .06$$

[1] REFERENCE (3) SECTION 15

[2] FRAME SPACING = 114 IN.

3.2.8.6.4.6 Base Skirt

The base skirt supports the vehicle in the flight-ready prelaunch condition.

The vehicle is supported prior to launch at three points on each motor skirt (see Figure 3.2.8-43). Two aluminum I-section support columns extend from each support point to tapered aliminum T-section longerons. Loads experienced during the prelaunch condition are redistributed by the six longerons in an aluminum semimonocoque structure, resulting in an approximately uniform distribution at the interface of the base skirt and the motor-case stub skirt. Lateral loads from the support columns are reacted by the forward ring and the pad interface ring, which are steel I sections. Aluminum box sections serve as clustering links connecting adjacent motors. The link attach points are located at the forward ring.

The base skirt fairing and the base heat shield are designed to resist local airloads. Aluminum honeycomb construction is used for both components because of its light weight and rigidity.

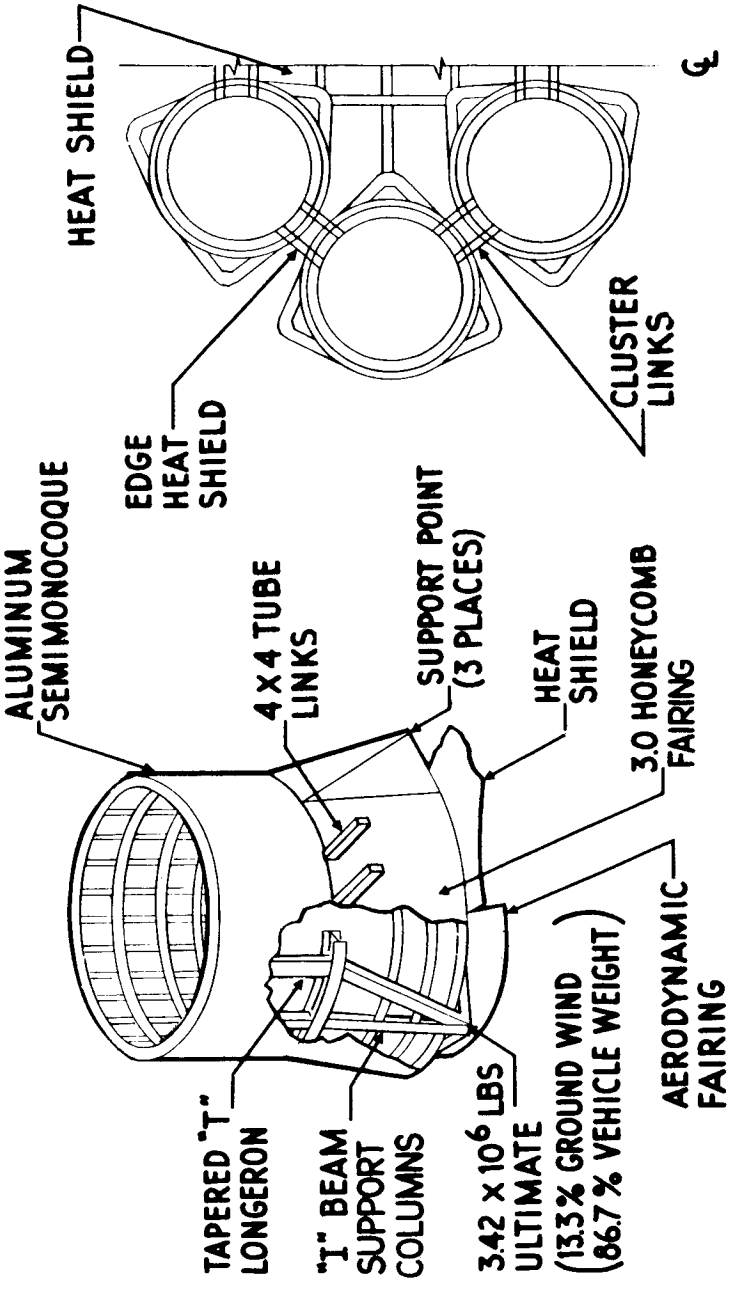

Figure 3.2.8-43 SUPPORT STRUCTURE

Design Loading Conditions — Base Skirt (First Stage) — The base skirt and base heat shield were designed by three loading conditions:

- prelaunch ground wind
- unsymmetrical thrust termination
- maximum q

Prelaunch Ground Wind — The prelaunch ground-wind condition was analyzed by considering one-sixth of the vehicle bending moment to be reacted by each motor. This results in a maximum support-point load that is 3 percent greater than if the moment were reacted by the vehicle acting as a unit. Secondary bending moments resulting from nonuniform distribution of upper-stage weight at the plane of the cluster structure were reacted by a lateral couple at the cluster structure and the aft clustering links (see Figure 3.2.8-44).

Loads applied at the vehicle support points are carried by six support columns on each motor skirt to the forward ring joint. The longitudinal components are transferred to the longerons and redistributed by skin panels to produce an approximately uniform load distribution at the motor-case joint. A bending moment at the forward ring joint, caused by eccentricity of longitudinal loads, was assumed to be carried by the support columns and reacted at the forward ring and the pad interface ring by a couple (see Figure 3.2.8-45).

Unsymmetrical Thrust Termination — Critical loading for the clustering links occurs at the time of unsymmetrical thrust termination. It was conservatively assumed that five motors operate at maximum thrust with nozzles at the full-gimbal position while one motor operates at one-half maximum thrust. The resultant lateral load was assumed to be redistributed by the clustering links to produce equal shears in all six motors. The resulting link load was added to the load required to react the bending moments caused by nonumiform distribution of longitudinal loads at the interstage (see 3.2.8.6.4.3).

Maximum q — Air pressures occuring at the time of maximum q represent critical loading for the base-skirt fairing and for the base heat-shield structure. The heat-shield support structure was conservatively designed for maximum limit pressure of 950 psf at an operating temperature of 200° F (see 3.2.10.2.3).

DESIGN LOADING CONDITION (BASE SKIRT) - CONT.

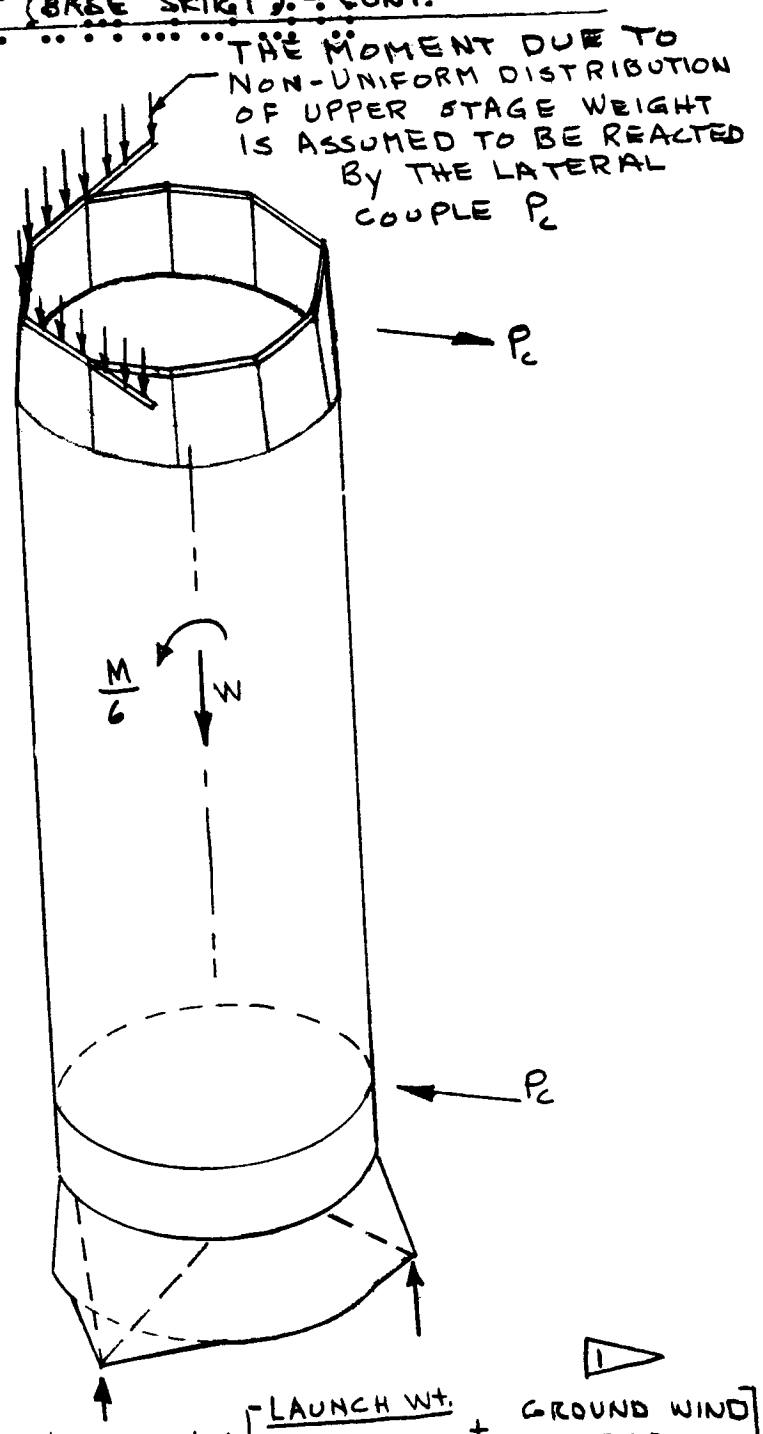

MAXIMUM ULTIMATE SUPPORT POINT LOAD $= 1.4\left[\frac{\text{LAUNCH WT.}}{18} + \text{GROUND WIND LOAD}\right]$ (1)

$= 3.42 \times 10^6$ LB

(1) FIG 3.2.8-23

Figure 3.2.8-44 VEHICLE SUPPORT LOAD FOR PRELAUNCH GROUND WIND CONDITION

DESIGN LOADING CONDITIONS (BASE SKIRT) — CONT.

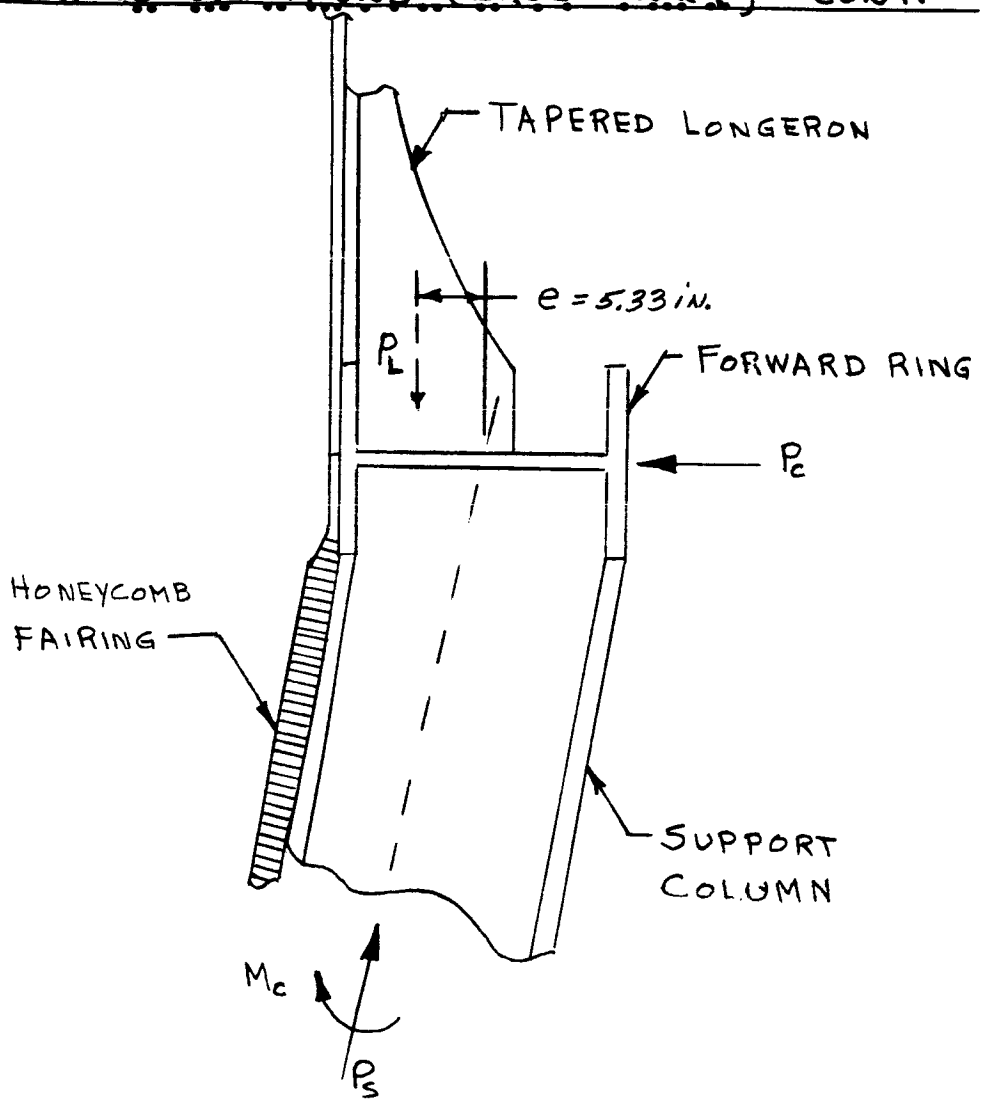

ULTIMATE SUPPORT POINT LOAD = 3.42×10^4 Lb.

LONGITUDINAL COMPONENT: $P_L = \frac{1}{2}(3.42 \times 10^4) = 1.71 \times 10^4$ Lb./COLUMN

$P_s = (1.71 \times 10^4)\left(\frac{169}{141}\right) = 2.05 \times 10^4$ Lb.

SUPPORT COLUMN LENGTH = $\sqrt{(141)^2 + (64)^2 + (67)^2} = 169$ IN.

Figure 3.2.8-45 LOADS AT THE FORWARD RING JOINT
Prelaunch Ground Wind Condition

SUPPORT COLUMN
(BASE SKIRT)

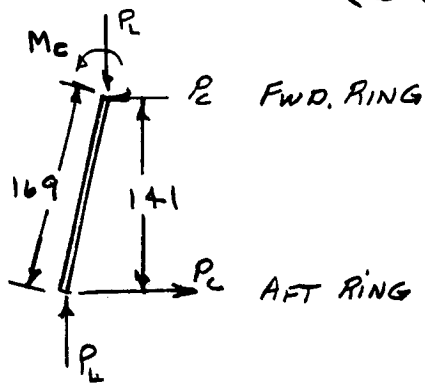

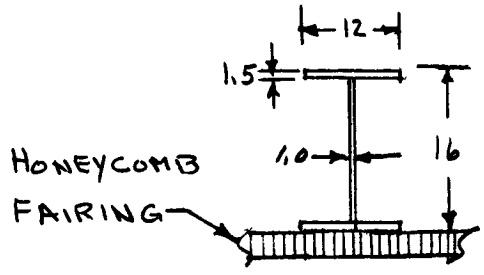

COLUMN CROSS SECTION
$I = 2109\ IN^4$ $A = 49\ IN^2$
MAT'L: 7178-T6

DESIGN CONDITION:
PRELAUNCH GROUND WIND
LOAD = 3.42×10^6 Lb PER JACK, ULTIMATE

$P_L = \frac{3.42 \times 10^6}{2} = 1.71 \times 10^6$ Lb $\quad M_c = (1.71 \times 10^6)5.33 = 9.12 \times 10^6$ IN.Lb. [1]

COLUMN AXIAL LOAD: $P_S = 1.71 \times 10^6 \left(\frac{169}{141}\right) = 2.05 \times 10^6$ Lb

MAX. BENDING MOMENT:

$\alpha = \frac{L}{2}\sqrt{\frac{P}{EI}} = .82$ [2] $\quad M_{MAX} = \frac{9.12 \times 10^6}{2 \sin .82 \cos .82} =$

$= 9.12 \times 10^6$ IN.Lb.

$f_b = \frac{(9.12 \times 10^6)8}{2109} = 34{,}600 \quad F_b = 86{,}000$ (REF. 5 CHAP. 3)

$f_c = \frac{2.05 \times 10^6}{49} = 41{,}800 \quad \frac{L}{e} = 26.2$ [4] $\quad F_c = 72{,}000$ [3]

$R_b = \frac{34{,}600}{86{,}000} = .401 \quad R_c = \frac{41800}{72000} = .580$

$M.S. = \frac{1}{.401 + .580} - 1 = \underline{\underline{.02}}$ ←

[1] REF. FIGURE 3.2.8-45

[2] BEAM COLUMN CONSTANT. REF. (3), SECTION 14.3

[3] REF. (3) SECTION 15

[4] THE SECTION IS ASSUMED STABILIZED BY THE 3 INCH HONEYCOMB FAIRING.

WEB CRIPPLING M.S. = 0.11

FLANGE CRIPPLING M.S. = 0.11

TENSION STRUTS (BASE SKIRT)

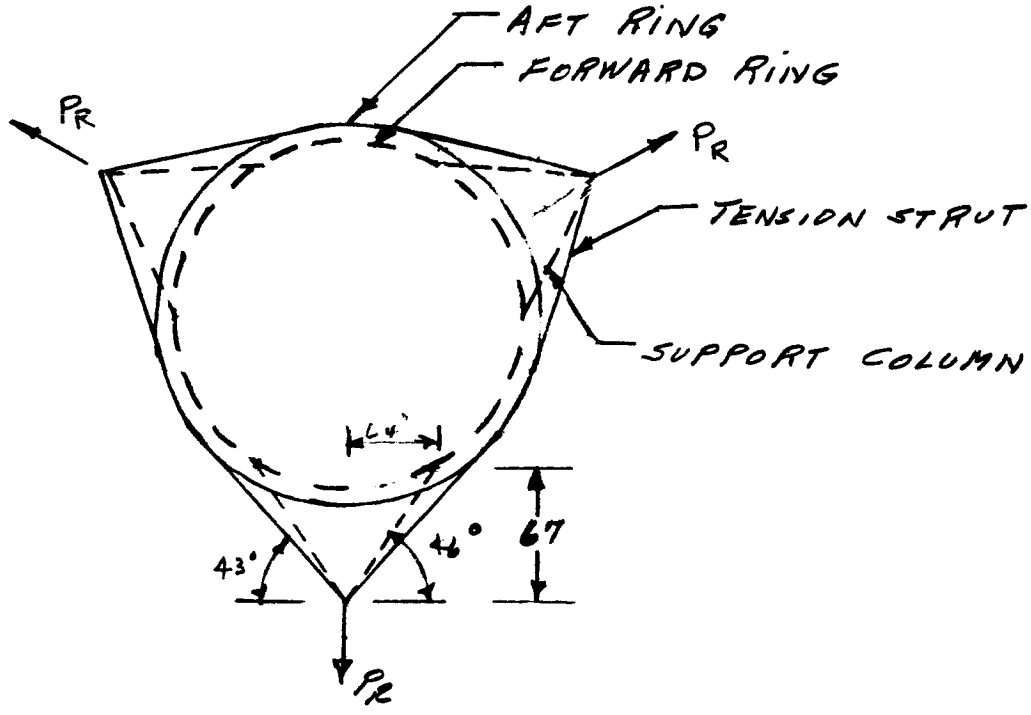

DESIGN CONDITION: PRELAUNCH GROUND WIND

$$P_R = 2(\text{COLUMN AXIAL LOAD})\frac{67}{169} - \frac{2(\text{COLUMN MOMENT})\cos 44°}{141}$$

$$= 2(2.05\times10^6)\frac{67}{169} - \frac{2(9.12\times10^6)}{141}(0.719) = 1.529\times10^6 \text{ Lb. ULTIMATE}$$

$$\text{TENSION STRUT LOAD} = \frac{P_R}{2\cos 47°}$$

$$= \frac{1.529\times10^6}{2(.682)} = 1.12\times10^6 \text{ Lb ULTIMATE}$$

[1] SEE FIGURE 3.2.8-45 FOR LOADS.

TENSION STRUTS (BASE SKIRT) - CONT.

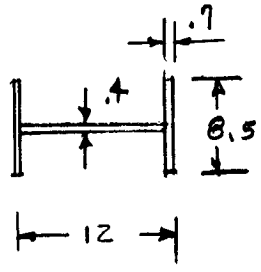

CROSS SECTION OF TENSION STRUT
MATERIAL: 7075-T6
AREA = 16.4 in²

$F_{TU} = 80{,}000$ [1]

ALLOWABLE AXIAL LOAD = (80,000)16.4 = 1.31×10^6 Lb.

$$M.S. = \frac{1.31 \times 10^6}{1.12 \times 10^6} - 1 = .17$$

PAD INTERFACE RING (BASE SKIRT)

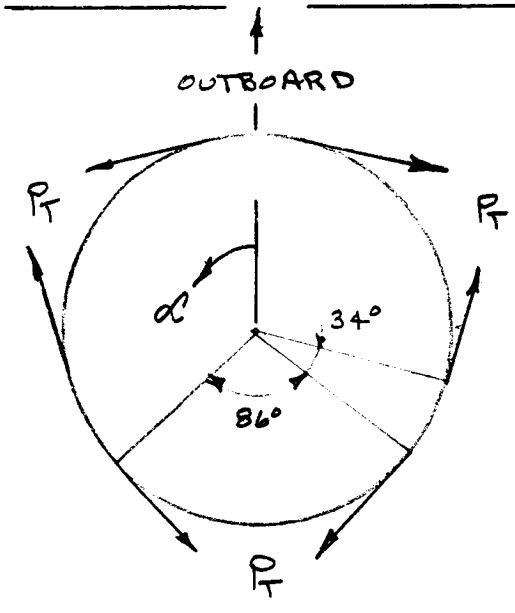

RING LOADS

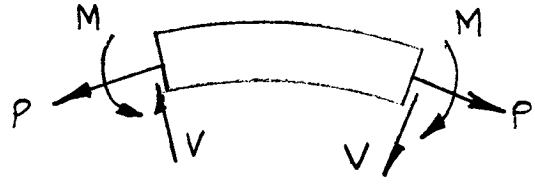

POSITIVE DIRECTIONS OF SHEAR, V, AXIAL LOAD, P AND BENDING MOMENT, M.

[1] REF. (5) TABLE 3.2.7.0 (f)

PAD INTERFACE RING (BASE SKIRT) - CONT.

IT IS CONSERVATIVELY ASSUMED THAT THE AFT RING LOADS ARE SYMMETRICAL AND EQUAL TO THE MAXIMUM TENSION STRUT LOAD.

$P_T = 1.12 \times 10^6$ Lb ULTIMATE

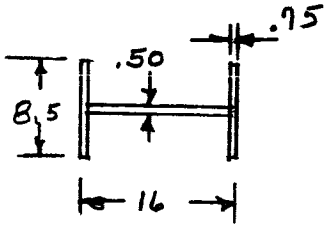

AFT RING CROSS SECTION

$I_x = 867$ in^4

$I_y = 76.8$ in^4

$A = 20$ in^2

$J = 3.03$

MATERIAL: 4340 STEEL

$F_{TU} = 180{,}000$ [1]

CRITICAL SECTIONS

LOADS SHOWN ARE ULTIMATE

(I) $\alpha = 0°, 120°, 240°$

$M = -11.71 \times 10^6$ IN-Lb

$V = 0$

$P_{AXIAL} = .937 \times 10^6$ Lb

(II) $\alpha = 60°, 180°, 300°$

$M = 7.85 \times 10^6$ IN. Lb.

$V = 0$

$P = -.402$ Lb.

SECTION (I)

$$f_T = \frac{(11.71 \times 10^6)8}{867} + \frac{.937 \times 10^6}{20.0} = 154{,}900 \text{ psi}$$

$$M.S. = \frac{180{,}000}{154{,}900} - 1 = .16$$ ←

THE COMPRESSION FLANGE IS ASSUMED TO BE STABALIZED BY THE HONEYCOMB FAIRING.

[1] REFERENCE (5). TABLE 2.2.2.0.(b)

PAD INTERFACE RING (BASE SKIRT) — CONT.

SECTION (II)

$$f_c = -\frac{(7.85 \times 10^4)8}{867} - \frac{.402 \times 10^6}{20.0} = -92{,}600 \text{ psi}.$$

LOCAL CRIPPLING OF THE INNER FLANGE:

$$\frac{b}{t} = \frac{\frac{1}{2}(8.5 - .50) - .50}{.75} = 4.67$$ [1]

$F_{CLR} = 179{,}000$ [2] M.S. $= \frac{179{,}000}{92{,}600} - 1 = .93$

LATERAL STABILITY OF INNER FLANGE

THE BENDING MOMENT AT WHICH A RING WILL BUCKLE LATERALLY WHEN LOADED IN PURE BENDING IS GIVEN BY THE EQUATION

$$M_{CR} = \frac{EI_x + C}{2R} \pm \frac{\pi}{L}\sqrt{EI_y C}$$ [3], (WHERE $C = JG$)

WHICH RESULTS IN A MAXIMUM FLANGE STRESS OF

$$\sigma_{CR} = \frac{M_{CR}\,\bar{y}}{I_x}$$ [4]

[1] DESIGN FILLET RADIUS

[2] REFERENCE (3), SECTION 15

[3] REFERENCE (1), Equation (7-34)

[4] REFERENCE (1), EQUATION (6-11) (f)

PAD INTERFACE RING (BASE SKIRT) — CONT.

IT IS ASSUMED THAT THE LENGTH OF THE RING SUBJECT TO BUCKLING IS EQUAL TO THE PORTION OF THE UNSTABILIZED FLANGE WHICH IS IN COMPRESSION, i.e., 70°.

$$L = \frac{\pi}{180}(70)139 = 170 \text{ in.}$$

$$M_{CR} = \frac{(29\times10^6)(76.8)+(3.03)(11\times10^6)}{2(139)} + \frac{\pi}{170}\sqrt{(29\times10^6)(76.8)(3.03)(11\times10^6)}.$$

$$= 13.15\times10^6$$

$$\sigma_{CR} = \frac{(13.15\times10^6)8}{867} = 121{,}000 \text{ psi}$$

$$M.S. = \frac{121{,}000}{92{,}600} - 1 = \underline{.30} \longleftarrow$$

SINCE M_{CR} WAS CALCULATED BY NEGLECTING THE INCREASE OF TORSIONAL RIGIDITY ($C = JG$) DUE TO THE STABILIZING EFFECT OF THE HONEYCOMB FAIRING, THE INDICATED MARGIN OF SAFETY IS CONSERVATIVE.

CLUSTERING LINKS (BASE SKIRT)

SEE FIGURE 3.2.8-43

DESIGN CONDITION: UNSYMMETRICAL BURNOUT

ULTIMATE LINK LOAD = $.434 \times 10^6$ LB.

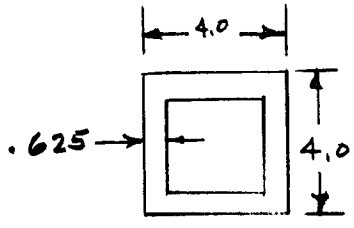

$\frac{L}{\rho} = 32.6$

$F_c = 62000$ [1]

LINK CROSS SECTION

$A = 8.55$ IN.^{2}

$\rho = 1.38$ IN.

$L = 45$ IN.

MATERIAL: 7075-T6

$$f_c = \frac{.434 \times 10^6}{8.55} = 50,700 \text{ psi}$$

$$M.S. = \frac{62000}{50700} - 1 = .22$$

[1] REF. (2) SECTION 15

FORWARD RING (BASE SKIRT)

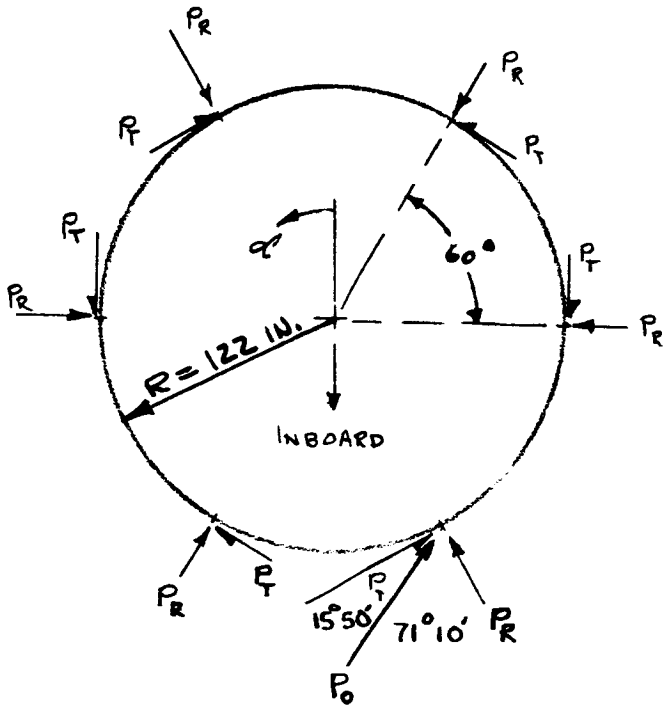

FORWARD RING LOADS

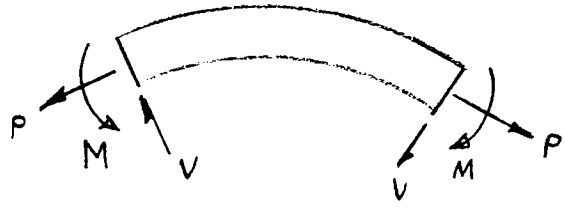

POSITIVE DIRECTIONS OF SHEAR, V, AXIAL LOAD, P AND BENDING MOMENT, M.

FORWARD RING (BASE SKIRT) - CONT.

DESIGN CONDITION: PRELAUNCH GROUND WIND.

ULTIMATE LOADS: $P_o = (2.05 \times 10^6$ [1]$)(.520$ [4]$) = 1.065 \times 10^6$ LB.

$P_T = P_o \cos(15°50') = .318 \times 10^6$ LB.

$P_R = P_o \cos(74°10') = 1.12 \times 10^6$ LB.

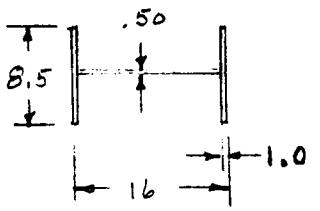

RING CROSS SECTION

$I_x = 1070$ IN^4

$I_y = 103$ IN^4

$A = 24$ IN^2

$J = 6.3$ IN^4

MATERIAL: 4340 STEEL

$F_{TU} = 180{,}000$

THE CRITICAL SECTIONS OCCUR AT $\alpha = 0°, 120°, 240°$

$M = 12.3 \times 10^6$ IN. LB.

$P = -.968 \times 10^6$ LB

$V = 0$

$$f_{bc} = \frac{-.968 \times 10^6}{24} - \frac{(12.3 \times 10^6)8}{1070} = -132{,}400 \text{ PSI}$$

LOCAL CRIPPLING: [2]

$$\frac{b}{t} = \frac{\frac{1}{2}(8.5 - .5) - .5}{1.0} = 3.5 \qquad F_{CCR} = 179{,}000$$ [3]

[1] SUPPORT COLUMN LOAD. SEE FIGURE 3.2.8-45

[2] DESIGN FILLET RADIUS = $\frac{1}{2}$ IN.

[3] REFERENCE (3), SECTION 15

[4] SLOPE OF SUPPORT COLUMN. LOAD ASSUMED AT ℄ RING

FORWARD RING (BASE SKIRT) - CONT.

$$M.S. = \frac{179,000}{132,400} - 1 = .35$$

LATERAL STABILITY OF INNER FLANGE:

THE BENDING MOMENT AT WHICH A RING WILL BUCKLE LATERALLY WHEN LOADED IN PURE BENDING IS

$$M_{CR} = \frac{EI_y + C}{2R} \pm \frac{\pi}{L}\sqrt{EI_y C} \quad [1] \quad \text{WHERE } C = JG$$

WHICH RESULTS IN A MAXIMUM FLANGE STRESS OF

$$\sigma_{CR} = \frac{M_{CR}\,\bar{y}}{I_x} \quad [2]$$

IT WAS ASSUMED THAT THE LENGTH OF THE RING SUBJECT TO BUCKLING IS EQUAL TO THE LENGTH OF UNSUPPORTED FLANGE IN COMPRESSION, i.e., 70°

$$L = \frac{\pi}{.80}(70)(122) = 149 \text{ IN.}$$

$$M_{CR} = \frac{(25.5\times10^6)(103) + (6.3)(9.85\times10^6)}{2(122)} + \frac{\pi}{149}\sqrt{(25.5\times10^6)(103)(6.3)(9.85\times10^6)}$$

$$= 19.52\times10^6 \text{ IN. LB.}$$

$$\sigma_{CR} = \frac{(19.52\times10^6)8}{1070} = 146,000 \text{ PSI}$$

[1] REFERENCE (1), EQUATION 7-34
[2] REFERENCE (1), EQUATION 6-11 (f)
[3] $E_T = 25.5$, $G_T = 25.5/2(1+.3) = 9.85$

FORWARD RING (BASE SKIRT) — CONT.

$$M.S. = \frac{146,000}{132,400} - 1 = .10$$

SINCE THE CALCULATED CRITICAL BENDING MOMENT NEGLECTS THE STABILIZING INFLUENCE OF THE SKIN WHICH IS ATTACHED TO THE OUTER FLANGE, THE INDICATED MARGIN OF SAFETY IS CONSERVATIVE.

Longerons (Base Skirt) — The longerons were tapered to unload into the skin panels over a length of 120 inches. The stringers were conservatively assumed to carry all of the longitudinal load with none of the skin considered effective. The skin panels were used to redistribute shear loads from the longerons to the stringers.

The load distribution in the region of the longeron was estimated by the numerical method of shear-lag analysis described in Chapter 4 Reference 2. The analysis requires idealization of the actual stringers into a "substitute single stringer" with an area equal to the sum of the actual stringer areas. The panel width between the longeron and the substitute stringer is determined by an empirical equation. The idealized structure is divided into a number of fictitious bays in which the longeron is assumed to have a constant area equal to its average area in each bay. The skin gages used in the idealized structure are the same as for the actual structure. The shear-lag stresses are determined from a system of simultaneous equations and added to the stresses determined by elementary theory. The shear-lag equations are determined by requiring consistent deformations between bays of the idealized structure and by satisfying the known end conditions.

One-half of the symmetrical structure was analyzed.

LONGERONS (BASE SKIRT) — CONT.

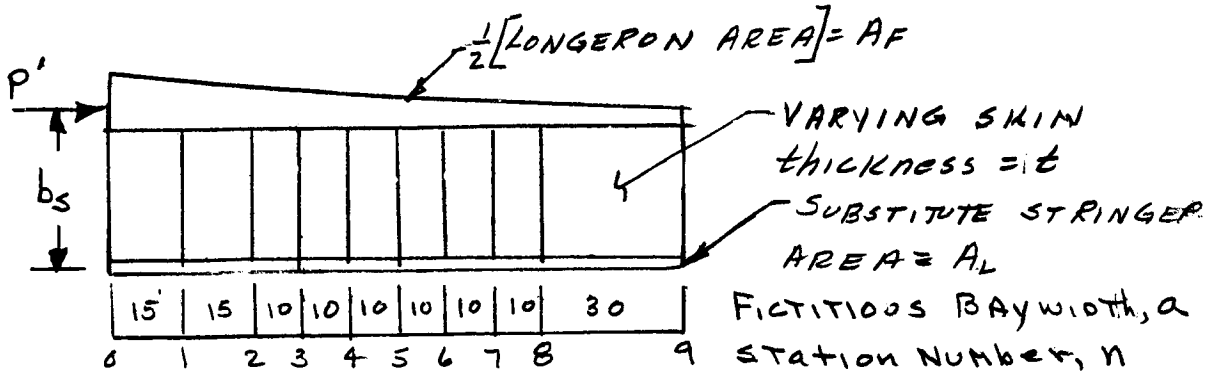

IDEALIZED STRUCTURE

EQUATIONS AND SYMBOLS USED IN THE ANALYSIS

$$\bar{q} = \frac{P' \Delta \left(\frac{A_L}{A_T}\right)}{a}$$ = SHEAR FLOW GIVEN BY ELEMENTARY THEORY

$$\bar{\gamma} = \frac{\bar{q}}{Gt}$$ = SHEAR STRAIN GIVEN BY ELEMENTARY THEORY

$$K = \frac{Gt}{E\, b_s}\left(\frac{1}{A_F} + \frac{1}{A_L}\right)$$ = SHEAR LAG PARAMETER

X = MAGNITUDE OF COUPLE DUE TO SHEAR LAG

b_c = DISTANCE FROM LONGERON TO AREA CENTROID OF STRINGER IN THE ACTUAL HALF PANEL.

$b_s = b_c\left(.65 + \frac{.35}{n/2}\right)$ = WIDTH OF IDEALIZED PANEL

n = NUMBER OF ACTUAL STRINGERS CONTRIBUTING TO A_L

$A_T = A_L + A_F$

$$P = \frac{K}{Gt \tanh Ka}$$ = MAGNITUDE OF SHEAR DEFORMATION AT ONE END OF A BAY DUE TO A UNIT X COUPLE ACTING AT THE SAME END OF THE BAY

LONGERONS (BASE SKIRT) — CONT.

$$q = \frac{K}{Gt \sinh Ka}$$ = MAGNITUDE OF SHEAR DEFORMATION AT ONE END OF A BAY DUE TO A UNIT X COUPLE ACTING AT THE OPPOSITE END OF THE BAY.

THE RECURRENCE FORMULA FOR SHEAR LAG EFFECT RESULTING FROM THE PRINCIPLE OF CONSISTENT DEFORMATIONS:

$$q_n \chi_{n-1} - (p_n + p_{n+1}) \chi_n + q_{n+1} \chi_{n+1} = -\bar{r}_n + \bar{r}_{n+1}$$

THE SUBSTITUTE SINGLE STRINGER AREA WAS DETERMINED BY ADDING THE AREAS OF THE ACTUAL STRINGERS IN THE HALF PANEL:

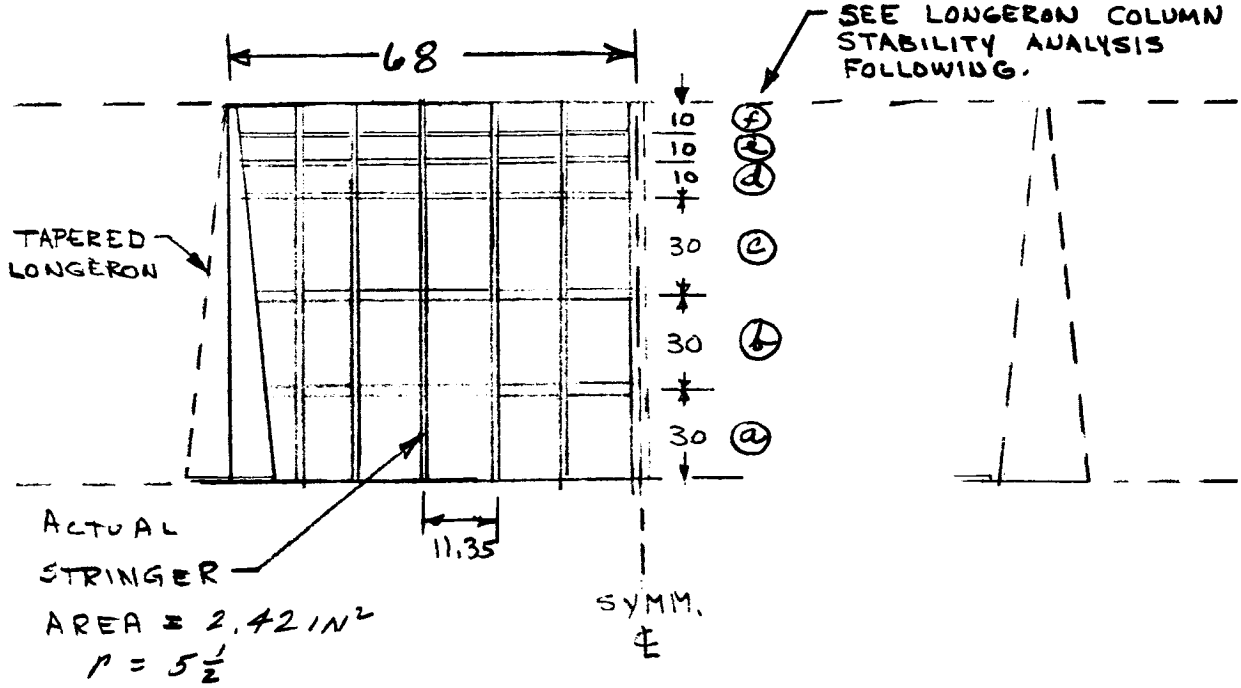

AREA = 2.42 IN²

$\rho = 5\frac{1}{2}$

$b_c = 37.2$ IN.

ACTUAL STRUCTURE SHOWING TYPICAL HALF PANEL

LONGERON (BASE SKIRT) – CONT.

DESIGN CONDITION : PRELAUNCH GROUND WIND.

ULTIMATE APPLIED LONGERON LOAD :

$$P_o = \frac{1}{2}(3.42 \times 10^6) = 1.71 \times 10^6 \text{ Lb.}$$ (1)

ONE HALF OF THE SYMMETRICAL STRUCTURE WAS ANALYZED FOR $P' = \frac{1}{2}(1.71 \times 10^6) = .855 \times 10^6$ Lb.

(1) MAXIMUM LOAD PER SUPPORT POINT. – FIGURE 3.2.8-45

LONGERON (BASE SKIRT) — CONT.

$A_L = (2.42)(5\frac{1}{2}) = 13.3 \text{ in}^2$

$b_s = 37.2\left(.65 + \frac{.35}{(5.5)^2}\right) = 24.6 \text{ in.}$

$G = 3.9 \times 10^6$

THE CALCULATION OF $\bar{r}$, ρ AND q IS SHOWN IN TABLES I AND II.

STA.	A_F IN^2	A_T IN^2	$\frac{A_L}{A_T}$	$\Delta\left(\frac{A_L}{A_T}\right)$	a IN	$\bar{q}$ K/IN	t IN	$\bar{\sigma}$ $\times 10^5$
0	14.0	27.3	.487					
				.0957	15	5.45	.50	279.5
1	9.52	22.82	.583					
				.0930	15	5.30	.50	271.8
2	6.38	19.68	.676					
				.0631	10	5.39	.30	460.7
3	4.70	18.0	.739					
				.0637	10	5.45	.30	465.8
4	3.27	16.57	.803					
				.0532	10	4.55	.30	388.9
5	2.24	15.54	.856					
				.0332	10	2.84	.25	291.3
6	1.66	14.96	.889					
				.0276	10	2.36	.25	242.0
7	1.21	14.51	.917					
				.0260	10	2.22	.25	227.7
8	.81	14.11	.943					
				.0142	30	.40	.17	61.0
9	.60	13.90	.957					

CALCULATION OF $\bar{\sigma}$

Table 3.2.8-19

LONGERONS (BASE SKIRT) — CONT.

STA.	A_F IN^2	$\frac{G}{E}\frac{t}{b_3}$ $\times 10^2$	K	Ka	TANH Ka	SINH Ka	p $\times 10^5$	q $\times 10^5$
6								
	11.76	.769	.0351	.5265	.483	.551	3.73	3.27
1								
	7.95	.769	.0394	.591	.530	.625	3.81	3.23
2								
	5.54	.462	.0344	.344	.327	.346	8.99	8.50
3								
	3.98	.462	.0388	.388	.371	.400	8.95	8.30
4								
	2.75	.462	.0450	.450	.422	.465	9.12	8.28
5								
	1.95	.385	.0476	.476	.438	.487	11.14	10.02
6								
	1.43	.385	.0546	.546	.493	.567	11.36	9.88
7								
	1.01	.385	.0641	.641	.565	.685	11.63	9.59
8								
	.70	.261	.0625	1.875	.954	3.200	9.90	2.95
9								

CALCULATION OF p AND q

SUBSTITUTION IN THE RECURRENCE FORMULA YIELDS THE SYSTEM OF SIMULTANEOUS EQUATIONS DEFINING THE SHEAR LAG EFFECT.

Table 3.2.8-20

LONGERONS (BASE SKIRT) — CONT.

$$
\begin{array}{llllll}
3.27(416) - 7.54\,\chi_1 & + 3.23\,\chi_2 & = & -7.7 \\
3.23\,\chi_1 - 12.80\,\chi_2 & + 8.50\,\chi_3 & = & 188.9 \\
8.50\,\chi_2 - 17.94\,\chi_3 & + 8.30\,\chi_4 & = & 5.1 \\
8.30\,\chi_3 - 18.07\,\chi_4 & + 8.28\,\chi_5 & = & -76.9 \\
8.28\,\chi_4 - 20.26\,\chi_5 & + 10.02\,\chi_6 & = & -97.6 \\
10.02\,\chi_5 - 22.50\,\chi_6 & + 9.88\,\chi_7 & = & -49.3 \\
9.88\,\chi_6 - 22.99\,\chi_7 & + 9.59\,\chi_8 & = & -14.3 \\
9.59\,\chi_7 - 21.53\,\chi_8 & + 2.95\,\chi_9 & = & -166.7 \\
3.56\,\chi_8 - 9.90\,\chi_9 & + 0 & = & -61.0
\end{array}
$$

2.95

SOLUTION OF THE EQUATIONS YIELDS THE VALUES OF χ AS SHOWN IN FIGURE 3.2.8-21. LONGERON STRESSES, WEB SHEARS AND STRINGER STRESSES WERE CALCULATED FROM THE EQUATIONS:

$$\sigma_F = \frac{P'}{A_T} + \frac{\chi}{A_F} \quad \text{(STRESS IN LONGERON)}$$

$$\tau = \frac{\Delta P_F}{t} \quad \text{(SHEAR STRESS IN SKIN)}$$

$$\sigma_L = \frac{P'}{A_T} - \frac{\chi}{A_L} \quad \text{(STRESS IN SUBSTITUTE STRINGER)}$$

LONGERONS (BASE SKIRT) — CONT.

STA.	χ Lb x 10^{-3}	P_F Lb x 10^{-3}	σ_F psi x 10^{-3}	Y psi x 10^{-3}	σ_L (1) psi x 10^{-3}
0	416.0	855.0	61.0		0
				37.6	
1	215.7	572.7	60.1		21.2
				28.7	
2	80.2	357.7	56.0		37.4
				24.5	
3	61.0	284.2	60.5		43.0
				21.7	
4	50.4	219.1	67.0		47.9
				18.8	
5	39.6	162.8	72.5		52.0
				15.8	
6	28.8	123.3	74.5		55.0
				12.6	
7	20.4	91.7	75.7		57.4
				10.7	
8	17.7	64.8	80.0		59.5
				1.33	
9	10.9	47.8	79.6		60.5

(1) STRESS IN SUBSTITUTE STRINGER

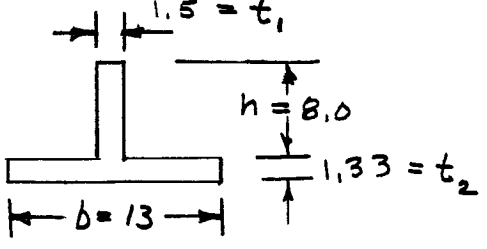

CROSS SECTION OF THE TAPERED LONGERON AT THE FORWARD RING JOINT. $A_{FO} = 28\ IN^2$ $I_{FO} = 176\ IN^4$
MATERIAL: 7178-T6

Table 3.2.8-21

LONGERON COLUMN STABILITY ANALYSIS

SECTION NUMBER [1]	A_F	t_1	h	t_2	b	I_F
a	20.38	1.5	8.00	1.33	6.3	169.7
b	8.62	1.0	5.47	.50	6.3	31.4
c	3.05	.6	3.00	.312	4.0	3.38
d	1.41	.3	1.50	.24		.32
e						
f	1.41	.3	1.50	.24	4.0	.32

SECTION NUMBER	L	L/ρ	F_c [2]	σ_c	M.S.
a	30	10.4	81	58.5	.38
b	30	15.7	81	64.2	.26
c	30	28.6	76	76.2	0
d	10	14.6	81	79.8	.01
e					
f	10	14.6	81	79.8	.01

[1] PROPERTIES AND STRESSES ARE FOR THE MID POINT OF EACH SECTION

[2] REFERENCE 3, SECTION 15 (COLUMN STABILITY CURVES)

SHEAR WEBS (BASE SKIRT)

SHEAR WEBS ARE CRITICAL FOR THE PRELAUNCH GROUND WIND CONDITION. THE MINIMUM MARGIN OF SAFETY OCCURS IN THE AFT PANEL.

ULTIMATE SHEAR STRESS = 37,600 PSI

(SEE TABLE 3.2.8-21 FOR LOAD)

SHEAR BUCKLING AT ULTIMATE LOAD

PANEL ASPECT RATIO = $\frac{a}{b} = \frac{30}{11.35} = 2.64$

$K_s = 5.2$ [1]

$f_{cr} = 46{,}000$ psi

MATERIAL:
7075-T6
CLAD SHEET

$M.S. = \frac{46000}{37600} - 1 = .122$

STRINGERS (BASE SKIRT)

THE STRINGERS ARE DESIGNED TO CARRY THE FULL AXIAL LOAD. THE VARIATION OF PANEL SHEAR FLOWS IN THE CIRCUMFERENTIAL DIRECTION WAS ESTIMATED BY THE PROCEDURE OF REFERENCE (2), FIGURE 18. TO DETERMINE THE LOAD IN THE STRINGER CLOSEST TO THE LONGERON, THE AVERAGE SHEAR FLOWS IN THE PANELS ON EITHER SIDE WERE CALCULATED AT 10 INCH LONGITUDINAL INTERVALS.

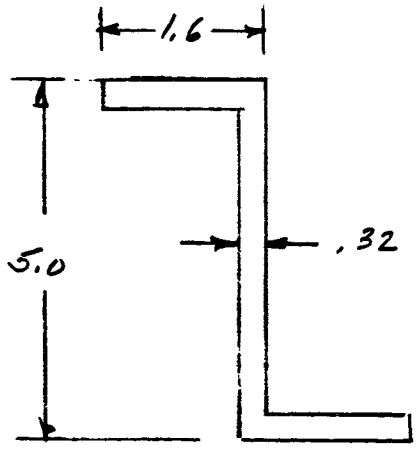

$A = 2.42$ in^2
$I = 7.83$ in^4
SPACING = 13.35 in.

TYPICAL STRINGER
CROSS SECTION

[1] REF. (3), SECTION 15

STRINGERS (BASE SKIRT) — CONT.

DISTANCE FROM FWD RING, d	AVG. SHEAR FLOW q_1	q_2	Δl	$\Delta q \cdot \Delta l$
10	14.8	12.5	15	64.5
20	14.5	11.8	10	27.0
30	9.2	8.2		10.0
40	6.8	6.2		6.0
50				6.0
60				
70	FOR d 740 IN. THE			
80	VALUES OF $(q_1 - q_2)$ REMAIN			
90	APPROXIMATELY CONSTANT.			
100	THE ACCURACY OF THE METHOD			
110	DOES NOT JUSTIFY MORE		10	60
120	PRECISE CALCULATION.		5	3.0
			Σ =	152.5

$$\sigma_{L\,MAX} = \frac{P}{A} = \frac{152.5}{2.42} = 63{,}000 \text{ psi}$$

THE STRINGERS ARE SUPPORTED AT 30 IN. INTERVALS BY CIRCOLAR FRAMES.

$$\frac{L}{\rho} = \frac{30}{\sqrt{\frac{783}{2.42}}} = 16.8$$

$F_c = 69{,}000$ [1]

$$M.S. = \frac{69000}{63000} - 1 = .09$$

[1] REF (3), SECT. 15.3

STABILIZING FRAMES (BASE SKIRT)

CIRCULAR FRAMES SPACED AT 30 IN. ARE USED TO STABILIZE THE SEMIMONOCOQUE PORTION OF THE BASE SKIRT STRUCTURE. THE MAXIMUM LOAD IS CONSERVATIVELY ASSUMED TO EQUAL THE ULTIMATE STRENGTH OF THE STRINGERS

$$w = \frac{(F_c)\, A_{STRINGER}}{STRINGER\ SPACING} = \frac{(69000)(2.42)}{13.35} = 12{,}650\ lb/in$$

$$(I_F)_{REQUIRED} = \frac{.785}{1000}\left(\frac{R^4}{E}\right)\frac{w}{d}$$ [1]

$$= \frac{.785}{1000}\left(\frac{\overline{130}^4}{10.3 \times 10^6}\right)\frac{12650}{13.35} = 9.06\ IN.^4$$

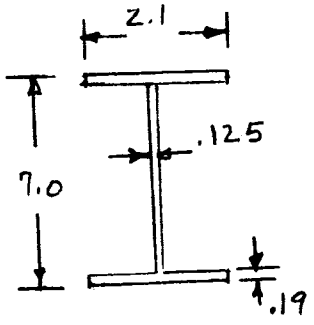

DESIGN CROSS SECTION
MATERIAL: 7075-T6
$I = 12.1\ IN^4$
$A = 1.61\ IN^2$

$$M.S. = \frac{12.1}{9.06} - 1 = \underline{.33}$$

[1] REFERENCE (7).

FAIRING BASE SKIRT

THE BASE SKIRT FAIRING WAS DESIGNED BY THE METHOD OF REFERENCE (4) TO WITHSTAND A MAXIMUM ULTIMATE PRESSURE OF 5.45 P.S.I WHICH OCCURS AT MAXIMUM q.

AN ALUMINUM HONEYCOMB STRUCTURE STIFFENED BY INTERMEDIATE FRAMES WAS SELECTED BECAUSE OF THE HIGH STIFFNESS TO WEIGHT RATIO. THE PROCEDURE OF REFERENCE (4) IS BASED ON BUCKLING OF A CYLINDER UNDER UNIFORM LATERAL PRESSURE.

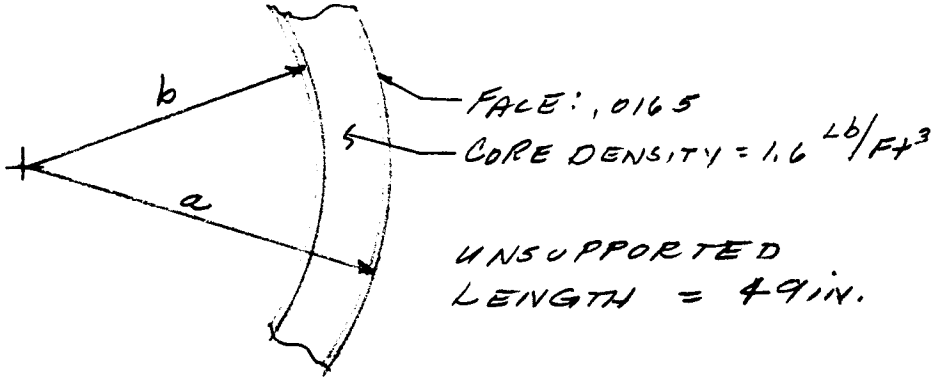

$$\frac{b}{a} = \frac{143.08}{146} = .98$$

$$\frac{l}{a} = \frac{49}{146} = .336$$

$$q_{CR} = \frac{E t \alpha}{a(1-\mu^2)} = \frac{(10.3\times10^6)(.0165).0044}{(146)(1-.09)} = 5.65 \text{ PSI}$$ [1]

$$M.S. = \frac{5.65}{5.45} - 1 = .03$$

[1] REF. (4), FIGURE 6.

3.2.8.6.4.7 Base Heat Shield (First Stage)

THE BASE HEAT SHIELD IS DESIGNED TO WITHSTAND THE 9.25 PSI ULTIMATE PRESSURE WHICH OCCURS AT THE TIME OF MAXIMUM q. AIR LOADS ARE CARRIED LOCALLY BY THE ALUMINUM HONEYCOMB HEAT SHIELD TO "I"-SECTION SUPPORT BEAMS. SUPPORT BEAM LOADS ARE REACTED AT SIX VEHICLE SUPPORT POINTS ON THE BASE SKIRT. REFERENCE FIGURES 3.2.11-2 AND 3.2.11-43 FOR HEAT SHIELD LOCATION.

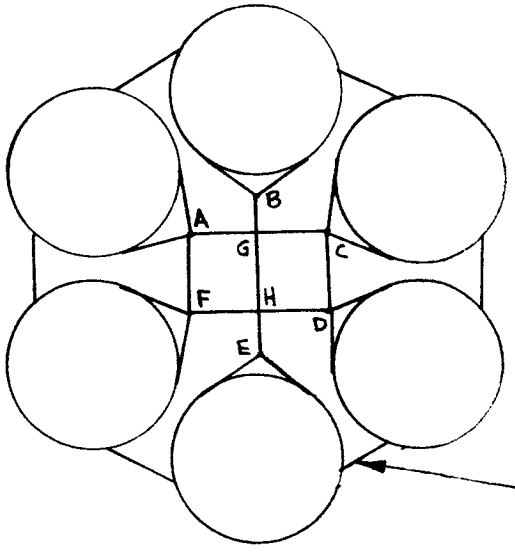

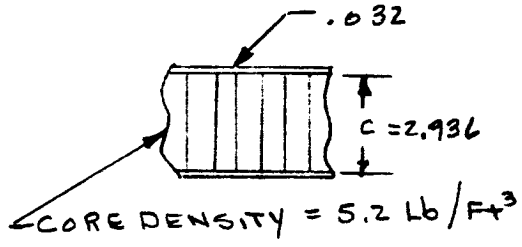

TYPICAL CROSS SECTION OF HONEYCOMB HEAT SHIELD.
MATERIAL: 2024-T86

BASE HEAT SHIELD SUPPORT BEAM NOTATION. BEAMS ARE 2024-T86

DESIGN TEMPERATURE AT THE FORWARD SURFACE OF THE HEAT SHIELD IS 200°F. [1] BEAM DESIGN IS SUMMARIZED IN TABLE 3.2.8-22.

[1] REFERENCE SECTION 3.2.10.2.3

BASE HEAT SHIELD (FIRST STAGE)

SUMMARY OF HEAT SHIELD SUPPORT STRUCTURE DESIGN

BEAM NUMBER	ASSUMED ULTIMATE LOAD DISTRIBUTION	ULTIMATE BENDING MOMENT	DESIGN SECTION	f_b	F_b	M.S.
B-G E-H	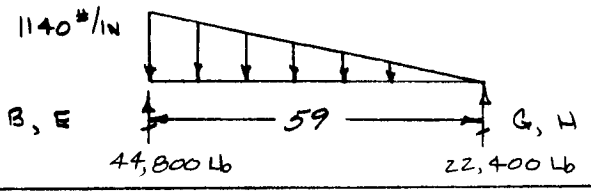	508,000 IN-Lb.	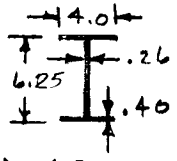 A = 4.72 I = 31.7	50,300	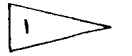 61,000	.22
C-D A-F	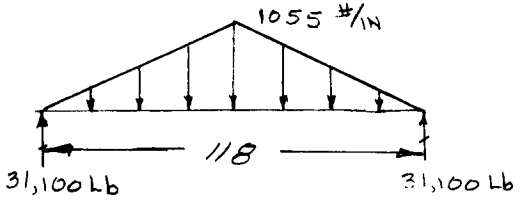	1,220,000 IN-Lb.	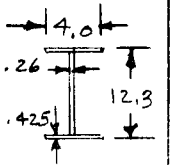 A = 6.47 I = 155.7	48,200	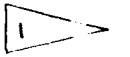 61,000	.27
G-H	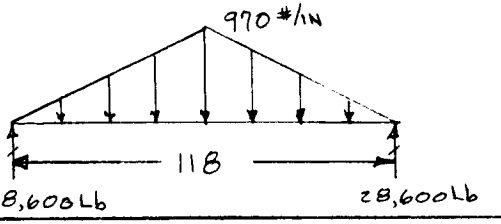	1,120,000 IN-Lb	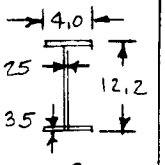 A = 5.79 I = 130.1	52,300	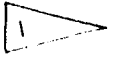 61,000	.17
A-G-C F-H, D	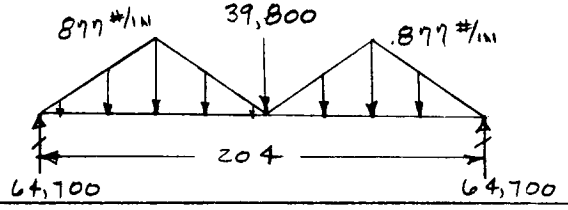	4,320,000 IN-Lb	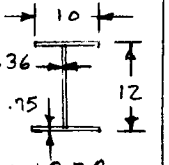 A = 18.78 I = 509.8	51,000	 53,000	.04

SEE EXPLANATION OF NOTES ON NEXT PAGE

Table 3.2.8-22

BASE HEAT SHIELD (FIRST STAGE) - CONT.

NOTES FOR TABLE 3.2.8-22

1 ALLOWABLE STRESS IN BENDING FOR 2024-T86 AT 200 F. REFERENCE (5).

2 ALLOWABLE STRESS BASED ON CRIPPLING OF COMPRESSION FLANGE.

$$\frac{b}{t} = \frac{5 - \frac{1}{2}(.36) - .32}{.15} = 6.0$$

$F_{ccR} = 53{,}000$, REFERENCE (3), SECTION 15.

HONEYCOMB PANELS (BASE HEAT SHIELD)

THE HEAT SHIELD WAS DESIGNED BY THE PROCEDURE OF REFERENCE (6), REFERENCE PAGE 167 FOR GEOMETRY. THE MAXIMUM SPAN BETWEEN SUPPORTS OF 102 IN. by 118 IN. WAS USED FOR DESIGN.

$$S_x = \frac{\pi^2 E_c t_1 t_2}{G_{xz}\, a^2 (1-\mu^2)(t_1 + t_2)} = \frac{\pi^2 (10.5\times10^6)(.032)(.032)}{(22{,}000)(102)^2(1-.09)(.032+.032)}$$

$$= 7.95 \times 10^{-3}$$

$$S_y = \frac{\pi^2 E_c t_1 t_2}{G_{yz}\, a^2 (1-\mu^2)(t_1 + t_2)} = \frac{\pi^2 (10.5\times10^6)(.03)(.03)}{(44{,}000)(102)^2(1-.09)(.03+.03)}$$

$$= 3.97 \times 10^{-3}$$

$$\rho = \frac{a}{b} = \frac{102}{118} = .865$$

HONEYCOMB PANELS (BASE HEAT SHIELD)- CONT.

$$K = \frac{16 q a (1-\mu^2)}{\pi^6 E I} = \frac{16(9.25)(102)(1-.09)}{\pi^6 (10.5\times10^6)(.1410)} = 9.67$$

[1]

$$K_1 = \left(\frac{\pi^2 K}{a^2}\right)\left(\frac{E}{1-\mu^2}\right)\left(\frac{t_1 t_2}{t_1+t_2}\right)\left(c + \frac{t_1+t_2}{2}\right)$$

$$= \left(\frac{(\pi^2)(9.67)}{(102)^2}\right)\left(\frac{10.5\times10^6}{1-(.3)^2}\right)\left(\frac{(.032)^2}{2(.032)}\right)\left(2.936 + \frac{2(.032)}{2}\right) = 5020$$

$$K_2 = \frac{16 q a}{\pi^2 [c + \frac{1}{2}(t_1+t_2)]} = \frac{16(9.25)(102)}{\pi^2 [2.936 + \frac{1}{2}(2)(.032)]} = 516$$

USING THE QUANTITIES CALCULATED ABOVE AND REFERRING TO TABLE I OF REFERENCE (6.):

$N_x = K_1(C_2 + \mu C_3)$

$N_y = K_1(C_3 + \mu C_2)$

} MAXIMUM NORMAL FORCES PER UNIT LENGTH OF FACES IN THE X AND Y DIRECTIONS

$C_2 = .29$

$C_3 = .22$

[1] $I = \left(\frac{t_1 t_2}{t_1+t_2}\right)\left(c + \frac{t_1+t_2}{2}\right)^2 = \left(\frac{(.032)(.032)}{.032+.032}\right)\left(2.936 + \frac{.032+.032}{2}\right)^2$

$= .1410 \text{ IN}^4$

HONEYCOMB PANELS (BASE HEAT SHIELD) - CONT.

THE MAXIMUM FACE STRESS IS GIVEN BY:

$$\sigma_{MAX} = \frac{N_x}{t} = \frac{(5020)(.29 + (.3).22)}{.03} = 56{,}000 \text{ psi}$$

INTERCELL BUCKLING ALLOWABLE:

$$\sigma_{CR} = \frac{\pi^2 K E_T}{12(1-\mu^2)} \left(\frac{t}{b_c}\right)^2 = \frac{\pi^2 4 (5.7 \times 10^4)}{12(1-.09)} \left(\frac{.032}{.25}\right)^2 \geq F_{cy} \quad [1]$$

$$F_{cy} = 63000 \quad [2]$$

$$M.S. = \frac{63000}{56000} - 1 = .12$$

[1] REFERENCE (8) ~ b_c = WIDTH OF HONEYCOMB CELL

[2] REFERENCE (5) ; 2024-T86 AT 200°F

BLANK

3.2.8.6.4.8 Motor Cases (First Stage)

Discussion — The motor cases were analyzed for the following load conditions:

- Ground wind condition
- Internal pressure condition
- Combined flight load conditions
- Ground-handling condition

The results of the analysis indicate that the ground-wind and internal-pressure conditions design the case wall. Using 250,000 psi maraged steel, the resulting margin of safety for both conditions are approximately zero. The analysis also indicates that the combined flight load conditions were not critical for the motor-case-wall design.

Ground Wind Condition (Motor Case) — The analysis procedure used in this solution is an approximate method that has not been substantiated by test. The basic approach involves an assumed treatment of the length/radius effect in cylinder buckling. This effect is applied to a motor case under a nonuniform axial load which increases linearly with length. It was assumed that a motor case of a given length will be sized for a certain percent of the average load rather than for the load applied at the upper end. It was further assumed that any finite length of the motor case could be sized on the same assumptions.

GROUND WIND CONDITION (MOTOR CASE) - CONT.

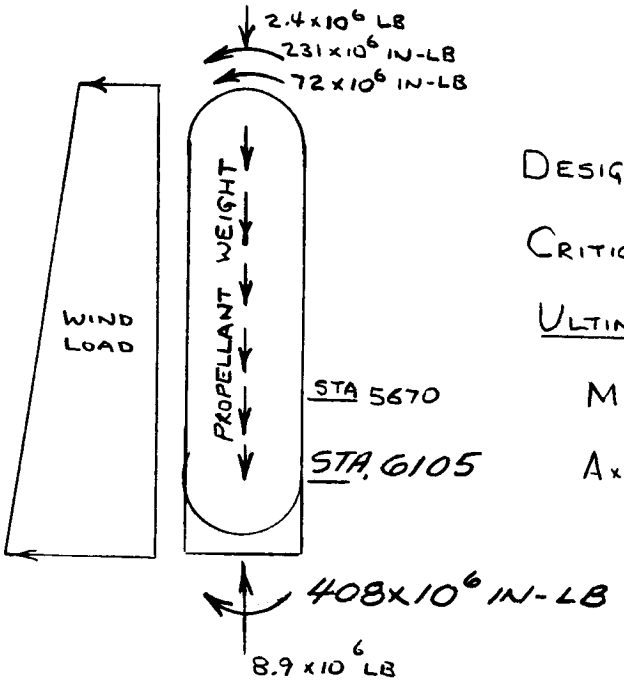

DESIGN CONDITION IS GROUND WIND

CRITICAL SECTION - STATION 5670

ULTIMATE DESIGN LOADS

$M = 231 + 131 = 362 \times 10^6$ IN-LB

AXIAL LOAD = 6.8×10^6 LB

THE MOTORCASE WAS ANALYZED FOR BUCKLING AS A THIN WALLED CYLINDER UNDER COMBINED BENDING AND AXIAL LOAD. THE LOADS AT THE MIDPOINT OF THE CYLINDRICAL SECTION UNDER CONSIDERATION WERE ASSUMED TO ACT OVER THE ENTIRE LENGTH OF THE SECTION. 95 PER CENT PROBABILITY, 95 PER CENT CONFIDENCE BUCKLING CURVES WERE USED AND THE STABILITY EFFECT OF THE PROPELLANT WAS NEGLECTED.

THE CRITICAL SECTION WAS 870 INCHES LONG WITH ITS MIDPOINT AT STATION 5670.

$$L/R = 870/130 = 6.7$$

$$R/t = 130/.65 = 200$$

$F_b = KE$ $\quad K = .94 \times 10^{-3}$ [1]

$F_b = .94 \times 10^{-3} \times 27 \times 10^6 = 25{,}400$ psi

[1] REFERENCE (17)

GROUND WIND CONDITION (MOTOR CASE) - CONT.

$F_c = KE$ $\quad K = .815 \times 10^{-3}$ [1]

$= 815 \times 10^{-3} \times 27 \times 10^{6}$

$= 22{,}000$ psi

$$f_b = \frac{362 \times 10^{6} \times 130}{\pi (130)^3 \times .65} = 10{,}500 \text{ psi}$$

$$f_c = \frac{6.8 \times 10^{6}}{2\pi \times 130 \times .65} = 12{,}800 \text{ psi}$$

$R_b + R_c = 1$

$$\frac{10{,}500}{25{,}400} + \frac{12{,}800}{22{,}000} = .413 + .582 = .995$$

$$MS = \frac{1}{.995} - 1 = .005$$

[1] REFERENCE (17)

INTERNAL PRESSURE CONDITION MOTOR CASE ANALYSIS

THE MAXIMUM EXPECTED OPERATING PRESSURE IS 804 PSIA [1].

MOTORCASE SIDEWALL: .65 MARAGED STEEL [3]

$$\sigma_{ULT.} = \frac{(PRESSURE)(RADIUS)(F.S.)}{(WELD\ FACTOR)(THICKNESS)} \quad [1]$$

$$\sigma_{ULT.} = \frac{804 \times 130 \times 1.4}{.90 \times .65} = 250{,}000\ PSI$$

[2]

$$M.S. = \frac{250{,}000}{250{,}000} - 1 = 0$$

MOTORCASE HEMISPHERICAL: .325 MARAGED STEEL FORWARD HEAD [3] [1]

$$\sigma_{ULT.} = \frac{804 \times 1.30 \times 1.4}{2 \times .90 \times .325} = 250{,}000\ PSI$$

[2]

$$M.S = \frac{250{,}000}{250{,}000} - 1 = 0$$

[1] SEE 3.2.8.6.1, TABLE 3.2.8-8

[2] SEE 3.2.8.6.4.3

[3] CONDITIONS VALID IN FREE STRESS FIELD — LOCAL BENDING STRESSES ARE NOT SHOWN.

COMBINED FLIGHT LOAD CONDITONS
MOTORCASE ANALYSIS

THE MAXIMUM STRESS IN THE MOTOR CASES WAS DETERMINED BY CALCULATING AN "EQUIVALENT AXIAL LOAD"; I.E., THE UNIFORM AXIAL LOAD WHICH WOULD PRODUCE A UNIFORM STRESS EQUAL TO THE MAXIMUM STRESS CAUSED BY BENDING. THUS

$$P_{EQ} = A\frac{MR}{I} = \frac{MR}{\pi R^3 t}(2\pi R t) = \frac{2M}{R}$$

MINIMUM TENSION LOADING FOR MOTOR CASES OCCURS AT THE MAX. Q, 20° ANGLE OF ATTACK CONDITION. [1] SINCE NO COMPRESSION LOAD OCCURRED, MOTOR CASE BUCKLING WAS NOT CRITICAL FOR FLIGHT LOADING CONDITIONS

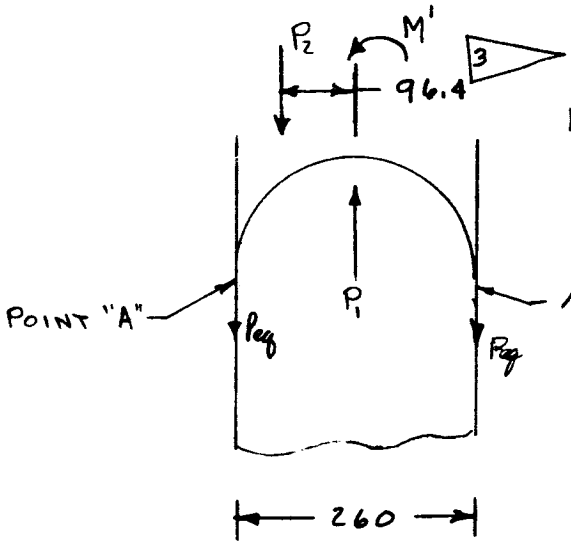

LIMIT PRESSURE AT THE FORWARD HEAD = 722 psi [2]

MOTOR CASE THICKNESS = .65

LOADS AT THE FORWARD MOTOR CASE HEAD.

[1] FAILURE CONDITION

[2] REFERENCE SECTION 3.2.B.6.2

[3] REFERENCE SECTION 3.2.B.6.4.3

COMBINED FLIGHT LOAD CONDITIONS (MOTORCASE)-CONT.

THE VEHICLE BENDING MOMENT WAS ASSUMED TO BE REACTED AS M/6 IN EACH MOTOR.

$$P_2 = \frac{1}{6}(\text{WEIGHT OF } 2^{nd} \text{ STAGE AND PAYLOAD})(\text{LOAD FACTOR})$$

$$= \frac{1}{6}(10.13 \times 10^6)(2.55) \quad [1]$$

$$= 4.30 \times 10^6 \text{ Lb.}$$

EQUIVALENT AXIAL LOAD:

$$P_{EQ} = P_1 - P_2 \pm \frac{2M' + (96.4 P_2)2}{R}$$

$$= (722)\left(\frac{\pi (260)^2}{4}\right) - 4.3 \times 10^6 \pm \frac{2}{130}\left(\frac{2585 \times 10^6}{6} + (96.4)4.3 \times 10^6\right) \quad [1]$$

AT POINT "B" $= +46.8 \times 10^6$
AT POINT "A" $= +21.0 \times 10^6$
} TENSION

GROUND HANDLING CONDITIONS (MOTOR CASE)

THE UNPRESSURIZED MOTOR CASE WAS ASSUMED TO BE LOADED BY ITS OWN WEIGHT WHILE IN A HORIZONTAL POSITION AND SUPPORTED BY SADDLE RINGS SIXTY FIVE INCHES WIDE. THE NUMBER OF SUPPORT POINTS REQUIRED TO PREVENT BUCKLING AT THE RINGS WAS CALCULATED BY THE METHOD OF REFERENCE (14) WHICH NEGLECTS THE INFLUENCE OF THE SOLID PROPELLENT. ALTHOUGH THE METHOD IS NOT

[1] REFERENCE SECTION 3.2.8.6.2

GROUND HANDLING CONDITIONS (MOTOR CASE) - CONT.

STRICTLY APPLICABLE, IT PROVIDES A FIRST ORDER APPROXIMATION OF THE NUMBER OF SUPPORTS REQUIRED.

$$\frac{a}{h} = \frac{\text{CASE RADIUS}}{\text{WALL THICKNESS}} = \frac{130}{.65} = 200$$

FROM FIGURE 5 OF REFERENCE (14):

$$\frac{p_{cr}\, a}{E\, h} = 3.9 \times 10^{-4}$$

$$p_{cr} = 52.5 \text{ PSI}$$

IF THE LOAD DISTRIBUTION AT EACH SUPPORT RING IS ASSUMED UNIFORM OVER ONE HALF OF THE CIRCUMFERENCE,

$$p = \frac{W}{n \pi R L}$$

FOR THE LOADED MOTOR, $W = 4.3 \times 10^6$ LB. THE MINIMUM NUMBER OF SUPPORT RINGS REQUIRED TO SUPPORT THE MOTOR CASE FOR A LOAD CONDITION WOULD BE:

$$n = \frac{4.3 \times 10^6 (1.4)}{\pi (130)(52.5)(65)} = 5$$

ALLOWABLE BENDING MOMENT (MOTOR CASE)

WHEN THE MOTOR CASES ARE SUPPORTED AT THE FORWARD AND AFT STUB SKIRTS A BENDING-TYPE

ALLOWABLE BENDING MOMENT (MOTOR CASE) - CONT.

FAILURE CAN OCCUR. THE COMPRESSIVE BUCKLING STRESS FOR THE UNSUPPORTED LENGTH OF 1740 INCHES IS DEFINED AS FOLLOWS.

$$F_{BCR} = KE$$

FOR $\frac{L}{R} = \frac{1740}{130} = 13.4$ AND $\frac{R}{t} = \frac{130}{.65} = 200$

$K = .60 \times 10^{-3}$ [1] $\quad F_{BCR} = (27 \times 10^6)(.60 \times 10^{-3})$

$= 16{,}200$ PSI

THE ULTIMATE ALLOWABLE BENDING MOMENT AT BUCKLING WILL BE:

$$M_{CR} = \frac{\pi R^2 t F_{CCR}}{1.4} = \frac{\pi (130)^2 (.65)(16{,}200)}{1.4}$$

$= 400 \times 10^6$ IN. Lb.

ALLOWABLE AXIAL LOAD (MOTOR CASE)

THE ULTIMATE ALLOWABLE LOAD IN AXIAL COMPRESSION FOR THE 1740 INCH UNSUPPORTED LENGTH IS DEFINED AS FOLLOWS:

[1] $K = .45 \times 10^{-3}$ $\quad F_{CCR} = (27 \times 10^6)(.45 \times 10^{-3}) = 12{,}100$ PSI

THE ULTIMATE ALLOWABLE COMPRESSIVE LOAD AT BUCKLING IS:

$$P_{CR} = \frac{A F_{CCR}}{1.4} = \frac{(130) 2\pi (12{,}100)(.65)}{1.4} = 4.6 \times 10^6 \text{ Lb}$$

[1] REFERENCE (17)

REFERENCES

1. Timoshenko, S., Theory of Elastic Stability, McGraw Hill Book Company, Inc., New York, 1961.
2. Kuhn, P., Stresses in Aircraft and Shell Structures, McGraw Hill Book Company, Inc., New York, 1956.
3. Boeing Airplane Company, "Design Manual," D-5000.
4. Forest Products Laboratory Report No. 1844-B, "Buckling of Sandwich Cylinders Under Uniform External Pressure," May, 1955.
5. Military Handbook -5, "Strength of Metal Aircraft Elements," Armed Forces Supply Support Center, Washington, D.C.
6. Forest Products Laboratory Report No. 1847, "Deflection and Stresses in a Uniformly Loaded, Simply Supported, Rectangular Sandwich Plate," December, 1955.
7. Shanley, F. R., "Simplified Analysis of General Instability of Stiffened Shells in Pure Bending," Journal of the Aeronautical Sciences, October, 1949, Page 590.
8. Boeing Airplane Company, "Structural Development Note No. 9 — Sandwich Material," D-11165.
9. Roark, J. J., Formulas for Stress and Strain, McGraw Hill Book Company, Inc., New York, 1954.
10. The Boeing Company, "Stress Manual," D-13330
11. Bleich, F., Buckling Strength of Metal Structures, McGraw Hill Book Company, Inc., New York, 1952.
12. Boeing Airplane Company, "Structural Development Note No. 7 — Design of Sheet Structures for Shear," D-14504.
13. Peery, J. D., Aircraft Structures, McGraw Hill Book Company, Inc., New York, 1950.
14. Brush, D. O., and Field, F. A., "Buckling of a Cylindrical Shell Under a Circumferential Band Load," Journal of the Aerospace Sciences, December, 1959, Page 825.
15. The Boeing Company, "Study of Large Launch Vehicles Using Solid First-Stages," SSD-TDR-62-144, Contract AF04(611)-8186 and NAS8-2438, Vol. III and IV, December, 1962 (Confidential).
16. Yusuff, S., "Design for Minimum Weight," Aircraft Engineering, October, 1960, Pages 288 - 294.
17. Convair Astronautics, "Development of Design Curves for the Stability of Thin Pressurized and Unpressurized Circular Cylinders," Report AZS-27-275, May 8, 1959.

18. Niles, Alfred S., and Newell, Joseph, Airplane Structure, John Wiley and Sons Inc., New York, 1955.

19. The Boeing Company, "An Approach to the Prediction of Pressure Vessel Minimum Fatigue Life Based upon Applied Fracture Mechanics," D2-22437.

3.2.9 Weight Analysis

3.2.9.1 Summary

The following weights analysis parallels closely the iterative design procedure for the 1000K payload vehicle. The early phases of the study relied heavily on data developed during Tasks I and II. A matrix of both parallel- and tandem-staged vehicles was investigated using parametric second-stage mass-fraction data combined with a constant first-stage mass fraction. Six vehicles (three tandem-staged, two parallel-staged, and one stage and one-half concept) were chosen for further evaluation, and weights statements were prepared for these configurations. From this group, a tandem-staged vehicle (six 260-inch-diameter solid motors in the first stage and five M-1 engines in the LO_2/LH_2 second stage) was chosen as subject of a preliminary design exercise. Major weight trade studies were undertaken for second-stage tank configuration and for first-stage case material.

The entire preliminary design process was predicated on keeping first- and second-stage propellant weight constant. Changes in inert weight were accounted for by appropriate adjustments in payload weight. The final vehicle has the following characteristics:

	Propellant	Inerts	Mass Fraction	Total Weight
Payload (225-kilometer orbit)				1,165,000
LO_2/LH_2 Second Stage	8,064,000	873,060*	0.902	8,982,000**
Solid-Propellant First Stage	24,821,000	3,093,870	0.889	27,915,000
Launch Weight				38,062,000

* Includes 154,000 pounds ΔV reserve propellant
** Includes weight expended prior to ignition

3.2.9.2 Conclusions

The following general conclusions may be drawn from a weights standpoint.

- Tandem-staged vehicles possess slightly better mass fractions than a corresponding vehicle designed to a parallel staging concept; however, the differences are not extreme.
- The multicell tank configuration results in a noticeable, but not significant weight reduction as compared with the single tank configuration.

BLANK

3.2.9.3 Selection of Candidate Vehicles

The initial vehicle matrix included several representative vehicles of two general classes: (1) tandem staged, and (2) parallel staged. First-stage motor diameter, number of motors, M-1 engine thrust, and number of M-1 engines were taken as parameters. Data developed during Tasks I and II were utilized to provide depth in areas where detailed study was not possible.

3.2.9.3.1 Mass Fraction Data

First-Stage Mass Fractions — For initial parametric vehicle sizing, first-stage mass fraction was held constant at 0.875. This value was chosen as representative of the optimum mass fraction obtainable for reasonable combinations of motor diameter, number of motors, first-stage thrust, and propellant weight at 600 psi chamber pressure (as indicated in Task II). This mass fraction was used for the first stage of both tandem-staged and parallel-staged vehicles.

Second-Stage Mass Fraction Data (Tandem Staged) — Vehicle staging ratios and launch weights are a strong function of second-stage mass fraction and thrust level; therefore, parametric mass fraction data over a range of second-stage propellant weights were developed. The significant criteria used to determine second-stage mass fractions are listed in Table 3.2.9-1.

Second-stage mass fractions for 70-foot-diameter stages are shown as a function of propellant weight in Figure 3.2.9-1.

The effects of changing the stage diameter to 60 feet or to 80 feet is indicated in Figure 3.2.9-2. The significant weight items affected are tankage, interstages, and thrust structure. The configuration concept involves keeping the LO_2 tank diameter equal to the stage diameter, resulting in off-loaded LO_2 tanks as follows:

60-foot stage	$W_{p_2} < 7.06 \times 10^6$ pounds
70-foot stage	$W_{p_2} < 11.2 \times 10^6$ pounds
80-foot stage	$W_{p_2} < 16.7 \times 10^6$ pounds

Alternate tank configurations with fully loaded LO_2 tanks were not considered at this time. The inset plot on Figure 3.2.9-2 gives an indication of the geometric effects on tankage weight efficiency. These trends are reflected in the larger plot of mass fraction alteration. In general, the larger changes in each band reflect stages with the larger number of engines due to the relatively large weight of the thrust structure in addition to the other components. Some of these configuration combinations entail difficulties that were not assessed in terms of weight penalties. For example, a cluster of eight M-1 engines cannot be completely contained in a 60-foot-diameter stage envelope. However, the engine

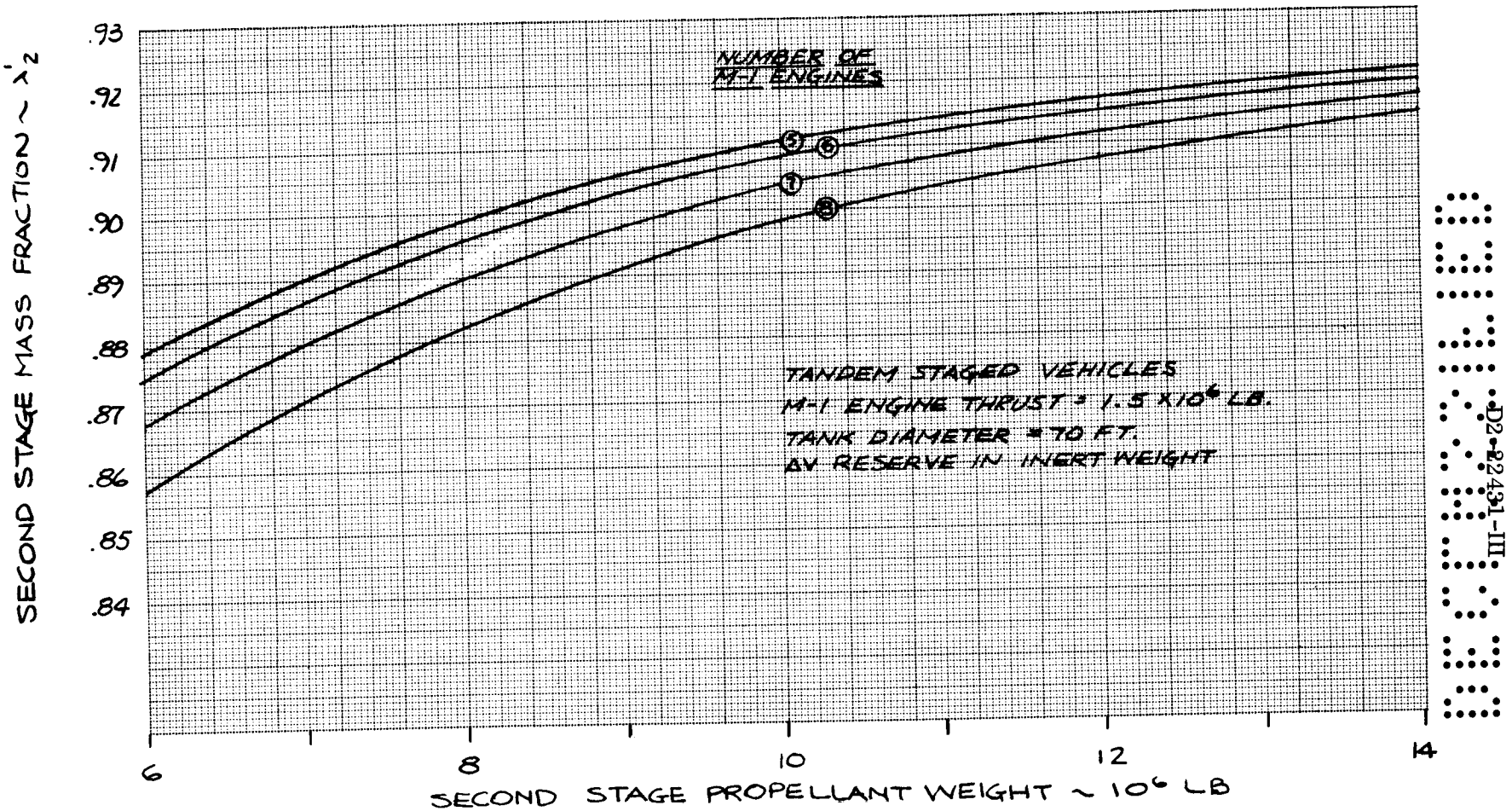

Figure 3.2.9-1 SECOND-STAGE MASS FRACTIONS
Tandem-Staged Vehicles

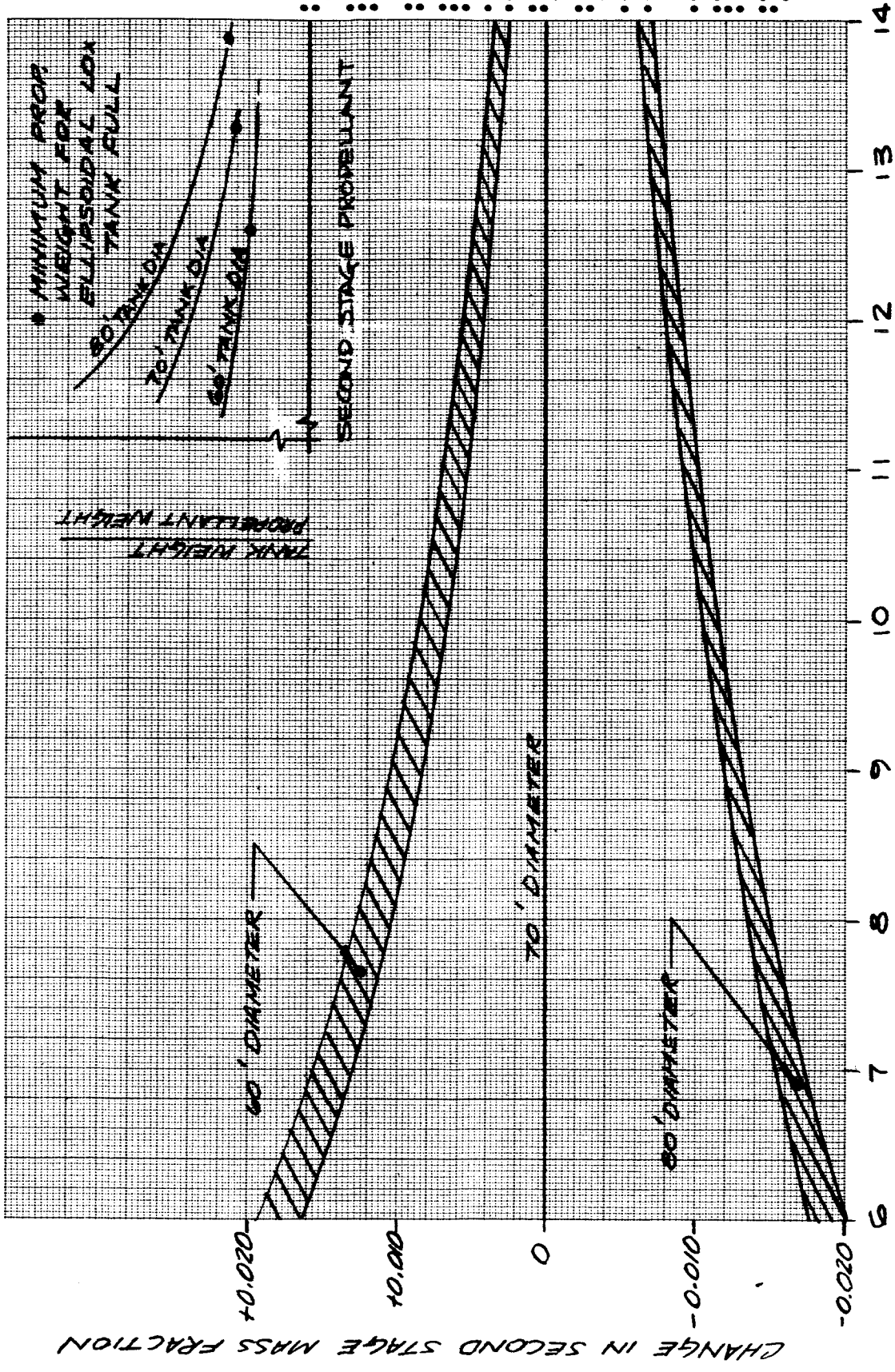

Figure 3.2.9-2 SECOND-STAGE DIAMETER EFFECT ON MASS FRACTIONS

PARAMETRIC SECOND-STAGE MASS FRACTION CRITERIA

Propellants	LO_2/LH_2
LO_2 Location	Aft
Tankage Concept	Nested Tanks
Bulkhead Shape	LO_2 Aft Bulkhead 0.8 b/a ellipsoid Other bulkheads 0.7 b/a ellipsoid
Separation Mode	Single Plane
Separation Plane	Engine Gimbal Plane
Thrust Structure	Cone Type
Tank Material	2219 Aluminum
Tank Construction	Waffle
Allowable Tensile Yield Strength	55,000 psi (cryogenic temperature)
M-1 Engine Thrust (vac)	1.5×10^6 pounds
M-1 Engine Weight (dry)	20,000 pounds
LO_2 Tank Ullage Pressure, 0.1 g start	39 psi
LH_2 Tank Ullage Pressure, 0.1 g start	36 psi
LO_2 Tank Ullage Pressure, 1.0 g start	29
LH_2 Tank Ullage Pressure, 1.0 g start	27
Thrust Decay Propellants	2500 pounds per engine
Parallel Staging Concept	Solid stage slides aft on parallel rail system

Table 3.2.9-1

mounting ring can be fitted into this diameter if a portion of the outboard engine bell extends outside the 60-foot diameter.

Parallel and Stage and One Half Concepts — Second-stage inert weight changes associated with the parallel concept and with the stage and one half concept are shown in Figure 3.2.9-3. The separation concept involves sliding the solid first stage aft from the second stage with the motors retaining their original relationship with the second stage (i.e., the solid motor axes remain parallel to, and the same distance from, the LO_2/LH_2 stage centerline). The weight penalty to the second stage includes rails for first-stage separation, structural provisions for rail attachment, and longerons and additional material in aft skirt for load distribution.

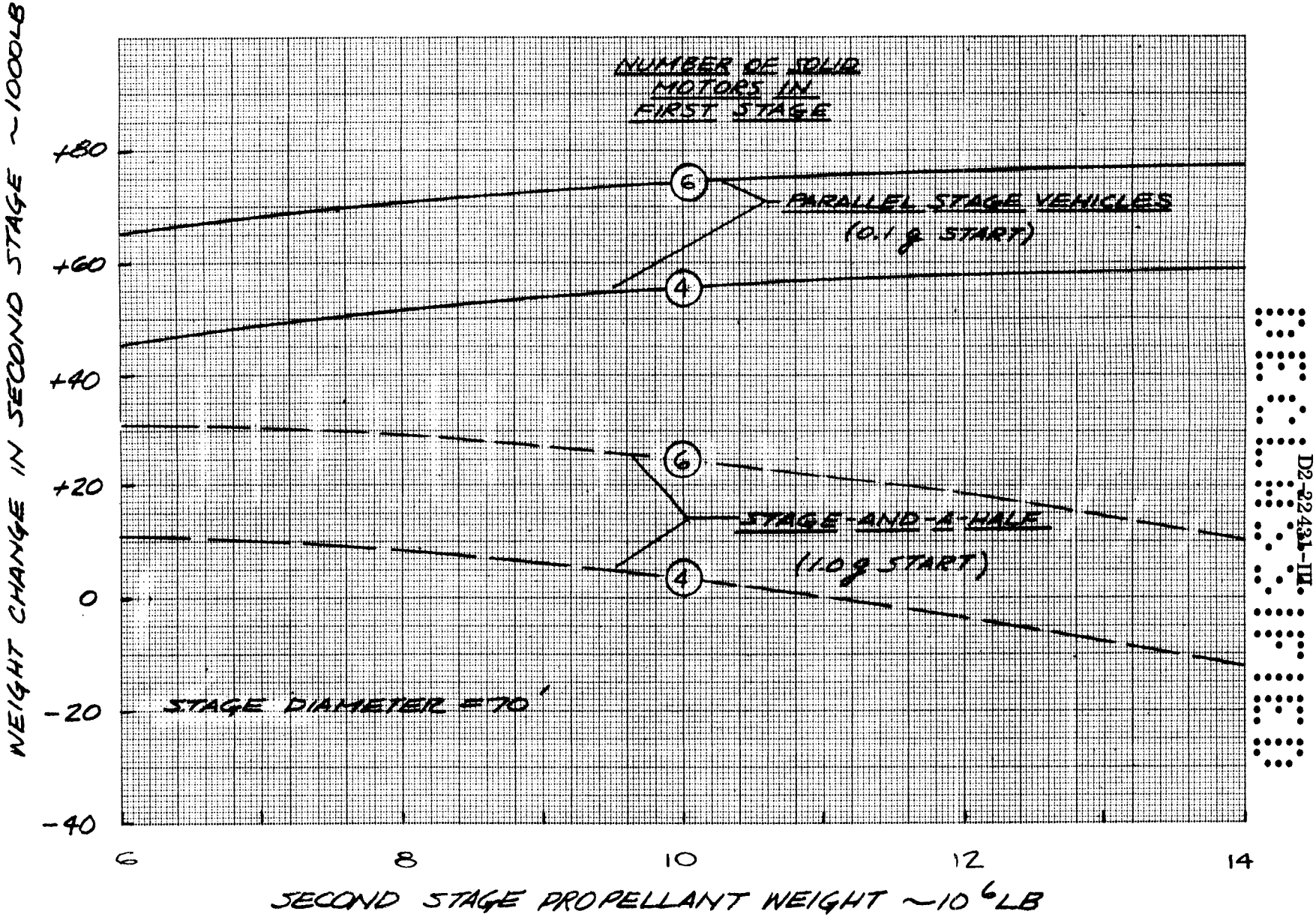

Figure 3.2.9-3 WEIGHT CHANGE IN SECOND STAGE DUE TO CHANGE FROM TANDEM TO PARALLEL STAGE CONCEPT

The first stage-second stage separation plane is the same for the parallel-staged vehicles as for the tandem staged. Second-stage configuration is, therefore, not altered in changing from tandem to parallel staging, except for the structural modifications above. It is also possible that some of the added structural weight may be jettisoned after separation.

The stage and one half concept incorporates ground start of the second stage engines. Because of the increased propellant head pressures at engine ignition (1.0 g compared to 0.1 g for tandem and parallel), a reduction in ullage pressure and therefore in tank weight is realized. This reduction, combined with the increases noted above, gives the net weight changes shown in Figure 3.2.9-3.

3.2.9.4 Candidate Configurations

From the general parametric data described 3.2.9.3, a group of six vehicles was chosen for further evaluation. Vehicle designations were assigned as follows:

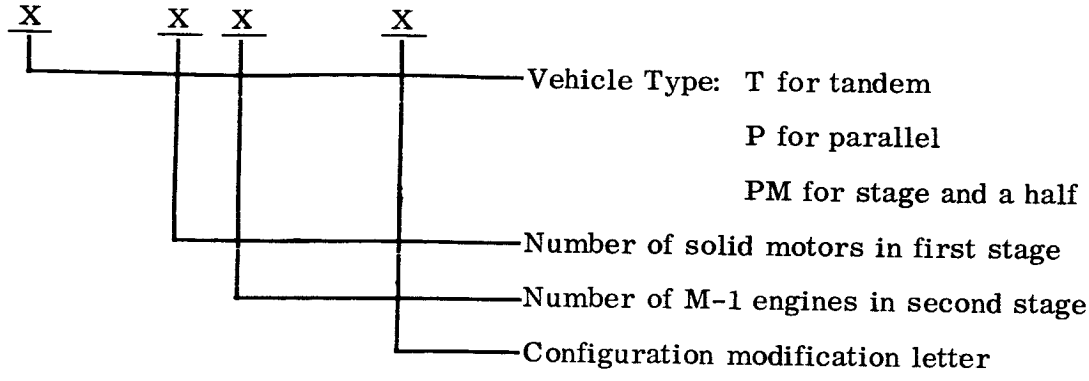

Vehicles chosen for analysis are identified in Table 3.2.9-2.

Outline configurations of these vehicles are shown in Figure 3.2.9-4.

3.2.9.4.1 Weights Analysis, Tandem Stages

Solid Stages — Solid stage weights and mass fractions are based on the following criteria and design ground rules.

Solid Motor — The basic motor consists of the motor case, nozzle, case liner, and bulkhead internal insulation.

Motor Case — Motor cases are cylindrical with hemispherical ends. Motor nominal chamber pressure is 600 psi and MEOP is 720 psi. The case material is 4430 steel, with ultimate tensile strength of 200,000 psi, and the ultimate factor of safety is 1.4. Motor volumes are based on the cross-sectional loadings shown in Table 3.2.9-2 and straight-through propellant ports in the hemispherical bulkheads.

In addition to the case shell, the following local structural provisions are included in case weight: cylinder extensions past the forward and aft bulkhead, joint rings for handling and structural attachment, a boss on the aft bulkhead for nozzle attachment and propellant porting purposes, and build-up joints in the sidewall to provide for manufacturing limitations.

Nozzle — Nozzle weights are based on Boeing estimates and lie between the optimistic and conservative extremes of industry data. The weight of the nozzle gimbal ring is included in the nozzle weight and is 30 to 40 percent of the total.

Case Liner — Liner weights are based on the total inner surface of the motor case being coated with 0.30-inch-thick rubber-based liner with a density of 0.042 pound per cubic inch.

CANDIDATE VEHICLE CHARACTERISTICS

	Tandem Vehicles			Parallel Vehicles		
	T45	T67	T65	P67	P65	PM67
First Stages						
Total Thrust at S. L. (10^6 lb)	(53.1)	(48.9)	(53.1)	(48.9)	(53.1)	(54.10)
Solid Motors (10^6 lb)	53.1	48.9	53.1	48.9	53.1	45.56
M-1 Engines (10^6 lb)						8.44
Total Propellant (10^6 lb)	(24.9)	(20.5)	(24.9)	(20.5)	(24.9)	(22.703)
Solid Propellant (10^6 lb)	24.9	20.5	24.9	20.5	24.9	20.132
LO_2/LH_2 Expended (10^6 lb)						2.571
Solid Motor Nozzle Area Ratio, ϵ	5.4	5.8	4.8	5.8	4.8	6.2
Motor Cross-Sectional Loading, η_{cs}	0.695	0.732	0.718	0.732	0.718	0.752
LO_2/LH_2 Stages						
Propellant Weight (10^6 lb)	8.1	9.5	8.1	9.5	8.1	9.648
M-1 Engine Thrust (at alt, 10^6 lb)	1.5	1.5	1.5	1.5	1.5	1.38
M-1 Engine Expansion ratio, ϵ	40.0	40.0	40.0	40.0	40.0	20.0
Estimated Payload in 225-kilometer orbit 10^6 lb	1.1	1.1	1.1	1.1	1.1	1.1

Table 3.2.9-2

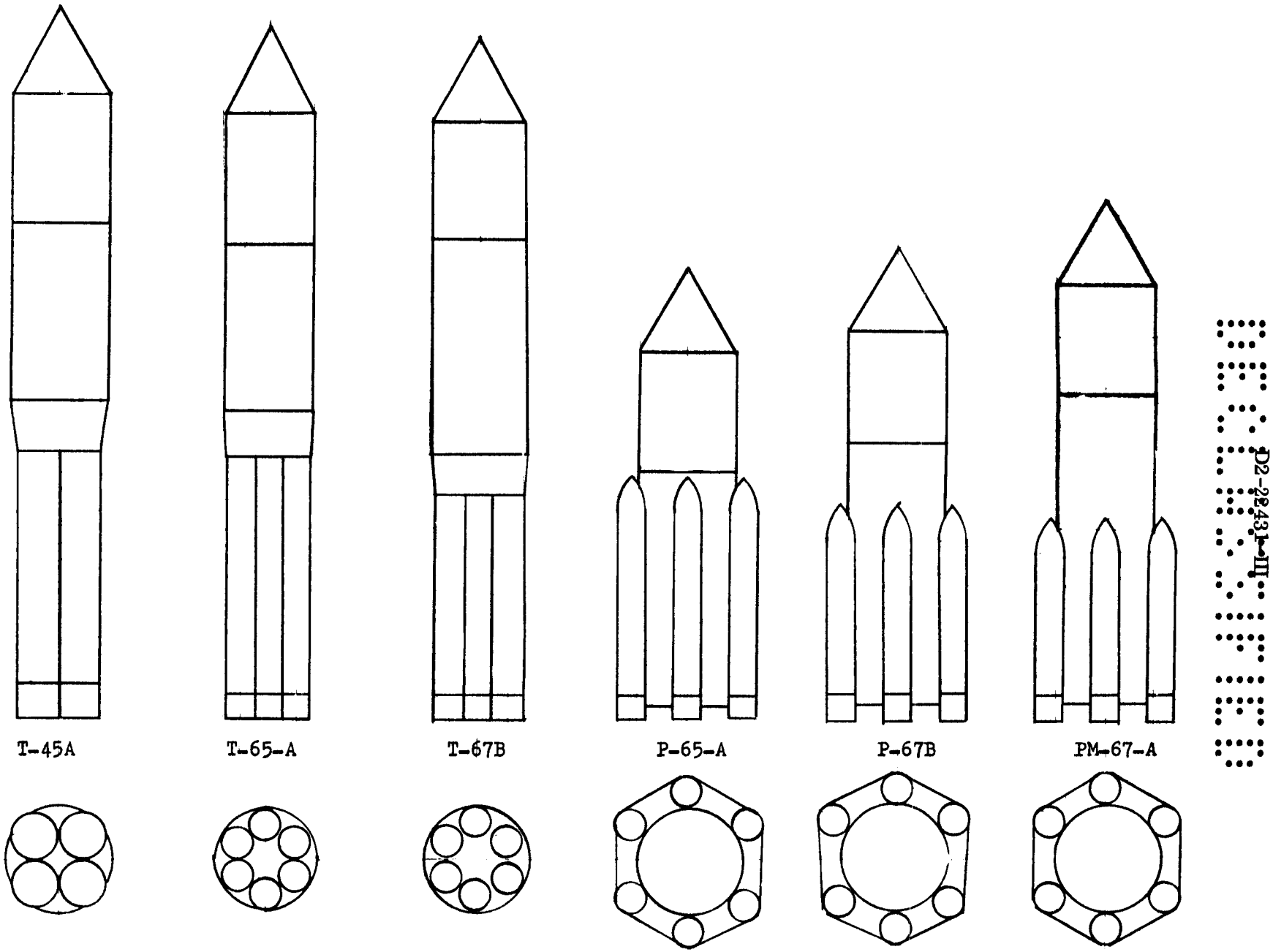

Figure 3.2.9-4 CANDIDATE VEHICLE CONFIGURATIONS

Internal Insulation, Bulkheads — Motors have phenolic-based insulation (ρ = 0.063 lb/in^3) for the forward and aft bulkheads. The insulation weight for the forward bulkhead is based on an average thickness of 0.10 inch. The aft head insulation weight is a function of chamber pressure and burn time and the average thickness is about 0.70 inch.

Thrust Vector Control — A thrust-vector-control system utilizing closed loop hydraulically actuated gimbaled nozzles is included. The weights were extrapolated from data developed during Task I of the current contract.

Equipment — Equipment weight includes such items as control elements, telemetry, environmental control provisions, power supply and electrical network, range safety, and stage separation systems.

Forward Interstage (Structure forward of tanks) — The forward interstage is a semimonocoque structure. The surface is the transition between the first-stage cross section and the circular second stage. The interstage extends from the first-stage clustering structure to the first stage-second stage separation plane at the second-stage engine gimbal plane. These interstages were designed according to first-stage burnout loads.

Cluster Structure — The clustering structure is a cross-beam type. Weights are extrapolated from the data of Task I.

Aft Skirt (Structure aft of tanks) — The aft skirt consists of a structural semimonocoque cylinder on each motor extending from the motor handling skirt to the ground support plane.

Aft Fairing (Structure aft of tanks) — The aft fairing consists of a nonstructural cone frustum on each motor extending from the aft skirt to the nozzle exit plane; its purpose is to protect the nozzles from the aerodynamic loads which would be imposed by the airstream. The weight is 2.0 pounds per square foot of surface area.

Base Heat Protection — Base heat protection consists of a structural shield and ablation material on exposed surfaces. Weights are based on estimated heating rates and shield area requirements, as extrapolated from Task I.

Retrorockets — Retrorocket capability is 5 g's for 1 second plus 2 g's for 2 seconds, based on first-stage grain designs similar to those developed during the Task I effort. The retro mass fraction is 0.65, and an additional 25 percent of inert weight is added for attachment provisions.

Sliver Residuals — Sliver residuals are extrapolated from Task I since the grain designs are similar.

LO_2/LH_2 Tandem Stage Criteria — Structure — Structure consists of tanks, antislosh provisions, tank insulation, forward and aft interstages, thrust structures, and separation provisions.

Propellant Tanks — Tank weights are based on a nested tank LO_2 aft configuration with the aft LO_2 bulkhead a 0.80 b/a semi-ellipsoid and the other three 0.70 b/a ellipsoids. An average cryogenic temperature allowable (F_{ty} = 55,000 psi) was used for all components. The tank sidewalls are aluminum waffle pattern and designed by the 0.4 psi overpressure requirement on the pad. As compared with the same tank designed for ground wind conditions, this criterion imposes a weight penalty of about 2 percent of tank weight or about 0.8 percent of stage burnout weight. The forward domes are designed by the ullage pressure at ignition — 43 psi for the LH_2, and 45 psi for the LO_2. Aft domes are designed by the sum of the ullage pressure at startburn and the propellant head pressure at first-stage burnout. A 20-inch clearance space is provided between the aft dome of the LH_2 tank and the forward dome of the LO_2 tank to ensure against LH_2 seepage.

Antislosh and Antivortex Provisions — In lieu of definitive criteria, slosh suppression provisions consist of a beaded lightened cylinder in each propellant compartment with unit weights based on extrapolated data. Vortex suppression is supplied by a covered cruciform baffle mounted in each line inlet.

Tank Insulation — Insulation has a unit weight of 0.35 psf and is applied to all propellant compartment external surfaces.

Forward Interstage (Structure forward of tanks) — The forward interstage is an aluminum semimonocoque cylinder designed according to second-stage burnout loads.

Aft Interstage (Structure aft of tanks) — Single plane separation is at the second-stage engine gimbal plane. The structure is a semimonocoque aluminum shell designed by first-stage burnout loads.

Thrust Structure — Thrust structure is a 60-degree cone frustum with the odd engine mounted on cross beams in the center.

Propulsion System — Engines and Thrust Vector Control — Engine weights for an expansion rate of 40 are based on a dry M-1 engine weight of 20,000 pounds. The thrust-vector control system weight per engine is 1500 pounds. The center engine is fixed and requires no thrust vector control.

Propellant Distribution System — Weight includes lines and bellows, prevalve insulation, and miscellaneous hardware. Engine feedlines are 19 inches in diameter.

Pressurization System — Pressurization is accomplished by a bleed system. The propellants are vaporized in the engines and returned to the tanks as heated gases.

Fill and Drain — The fill and drain system includes the fill and drain lines, valves, bellows, insulation, and disconnects.

Vent System — There are four vent valves at 75 pounds each.

Equipment — Equipment includes control elements, telemetry, environmental control provisions, power supply and electrical network, range safety systems, engine malfunction detection system, and separation and ullage rocket systems.

Retrorockets — Retrorocket capability is 3 g's deceleration for one second. The retro mass fraction is 0.65 and an additional 25 percent of inert weight was added for attachment provisions.

Ullage Rocket Attachment Provisions — Ullage rocket weights are based on 0.1 g for 3 seconds. The ullage rocket motor has a mass fraction of 0.65. The motor case is jettisonned after firing and an additional 40 percent of ullage rocket inert weight was included for the portion of the attachment and separation provisions that are carried with the second stage.

Residual and Reserve Propellants —

- Propellant Trapped in Engines — For the M-1 engine, 1200 pounds of trapped propellant per engine is included.
- Propellant in Lines — Trapped propellant weights are based on total line volumes.
- Gaseous Residuals — Gaseous residuals are based on the following burnout conditions:

LO_2 tank mean temperature (°R)	270
LH_2 tank mean temperature (°R)	160
LO_2 tank pressure (psia)	29
LH_2 tank pressure (psia)	39

- Helium Slugs — Helium slugs are used for prepressurization to the start-up ullage pressures (45 psi for LO_2 and 43 for LH_2).
- Thrust Decay Residual — An allowance of 2500 pounds per M-1 engine was made for shutdown time variances.
- P.U. Residual — P.U. residual weights were:

  0.375 percent total propellant weight for five engines
  0.345 percent total propellant weight for seven engines

3.2.9.4.2 Parallel-Stage Weights Analysis

Criteria and analysis are the same as for the tandem-staged vehicles, except for the following items.

Solid Stages — The forward interstage is an aluminum semimonocoque cylinder that transmits the solid-stage thrust loads from the aft end of the solid stage to the aft end of the LO_2/LH_2 stage. It requires longerons and shear-out plates for load distribution since the loads are fed into it at six points along the periphery.

Cluster Structure — Two circumferential rings are fastened to the interstage. In the aft skirts of the solid motors are matching circumferential rings. In addition, there are tension ties between the solid motors. The two rings act as the upper and lower chords of a truss, the upper one being in compression and the lower one in tension.

Aft Skirt — The aft skirt, in addition to acting as support structure, must also carry the moments associated with the truss-type structure described above.

Nose Fairings — Nose fairings are aerodynamic fairings on the forward end of the solid motors. Ogive surfaces with unit weight of 2.5 psf were used for weights purposes.

Separation Rails — The stage separation concept involves sliding the solid propellant motors aft on parallel "rails," while retaining the original relationship between the centerlines of the solid and liquid stages. The rails are aluminum I-beams fixed to the LO_2/LH_2 stage; built-up channels mate with them on the solid stage. Included in the weight are allowances for bearing surfaces and attachment provisions.

Second Stage —

- Tankage — Tankage for the stage and one-half concept only is designed for somewhat lower ullage pressures than the tandem stages. Since this concept involves ground start of the engines, use can be made of the 1.0-g static head available, thus reducing the ullage pressure requirement at startup. The tank design pressure is then the ullage pressure at burnout — 29 psi for the LO_2 and 39 psi for the LH_2.
- Separation Rails — Separation rails are the built-up I sections mentioned above. The forward end is at the forward end of the solid motor case and the aft end is at the separation plane.
- Rail Attachment Provisions — Circumferential rings are required at both the forward and aft ends of the LO_2/LH_2 stage for structural stability during separation.

- Engines — M-1 engines for the stage and one-half concept have an expansion ratio of 20. The weight of 17,430 pounds was determined by removing the portion of the nozzle bell aft of the $\epsilon = 20$ plane and keeping the remaining weight fixed.
- Ullage Rockets — Ullage rockets are unnecessary for the stage and one-half concept since LO_2/LH_2 engines are ignited on the ground.
- Weight Statements and Mass Fractions — Solid propellant stage weight statements are shown in Table 3.2.9-3. The calculated mass fractions compare favorably with the estimated value of 0.875, on which the propellant weights are based.
- Semidetailed weight statements for the LO_2/LH_2 stages appear in Table 3.2.9-4. The mass fractions are noticeably lower than those in Figure 3.2.9-1, largely because of the increase in required ullage pressures due to further information regarding propellant vapor pressures and gas venting tolerances. The same weight statement is shown for the second stage of the T45 and T65 vehicles, since the only difference between the design criteria is a slight difference in first-stage burnout thrust-to-weight ratio.

			T45A
W3	Structure		2,541,25
3.4	Solid Propellant Container		2,208,15
3.6	Structure Forward of Tanks		257,00
	3.6.1	Forward Interstage	66,00
	3.6.11	Cluster Structure	191,00
3.8	Structure Aft of Propellant Containers		45,00
	3.8.11	Aft Support Structure	35,00
	3.8.12	Aft Aerodynamic Fairing	10,00
3.10	Nose Fairing		- - -
3.14	Base Heat Protection		15,30
3.26	Miscellaneous		15,80
W4	Propulsion System		606,50
4.2	Nozzle (Gimbaled)		590,00
	4.10.1	Thrust-Vector-Control Hardware	16,50
W6	Equipment and Instrumentation		180,00
	6.2-12	Electrical, Telemetry, etc.	5,70
	6.17	Separation System Hardware	174,30
	6.17.1,2	Installed Rocket Cases	174,00
	6.17.5	Explosive Devices	30
	6.17.8	Separation Rails	- - -
Ws 1d Dry Stage			3,327,75
W7	Residual Propellants and Service Items		301,20
	7.9.13	Separation System Propellants	174,00
	7.11	Solid Propellant Slivers	127,20
Ws 1c Stage Weight at Cutoff			3,628,95
W8	Propellant Consumption		24,900,00
	8.5	Solid Propellant	24,900,00
ABEE	8.12	LO_2/LH_2 Expended	- - -
Ws 1g Stage Weight at Ground Ignition			28,528,95
	Stage Mass Fraction, λ' (Total expended propellant)		0.8728
	Stage Mass Fraction, λ' (Solid propellant only)		0.8728

1

Vehicle Configurations

	Parallel Vehicles		Stage and One-Half
T65A	P67B	P65A	PM67A
2,470,800	2,122,390	2,535,000	2,052,200
2,070,300	1,679,690	2,070,800	1,621,500
293,500	225,200	237,200	206,300
70,500	87,200	87,200	77,300
223,000	138,000	150,000	129,000
68,000	139,000	150,000	139,800
50,000	129,000	140,000	140,000
18,000	10,000	10,000	9.800
- - - -	15,000	15,000	15,000
20,000	42,000	40,000	38,600
19,000	21,500	22,500	21,000
551,000	491,200	551,000	537,500
530,000	471,000	530,000	518,000
21,000	20,200	21,000	19,500
168,900	154,700	179,300	158,750
6,100	6,400	6,100	6,250
162,800	148,300	173,200	152,500
162,500	139,500	165,000	144,000
300	500	500	500
- - - -	8,300	7,700	8,000
3,190,700	2,768,290	3,265,300	2,748,450
287,900	237,900	290,400	238,800
162,500	139,500	165,000	144,000
125,400	98,400	125,400	94,800
3,478,600	3,006,190	3,555,700	2,987,250
24,900,000	20,500,000	24,900,000	22,703,000
24,900,000	20,500,000	24,900,000	20,132,000
- - - -	- - - -	- - - -	2,571,000
28,378,600	23,506,190	28,455,700	25,690,250
0.8773	0.8720	0.8749	0.8846
0.8773	0.8720	0.8749	0.8707

Table 3.2.9-3

SEMIDETAILED WEIGHT STATE

Candidate Vehi

			Tandem Vehicl	
			T67A	T45A
W3	Structure		609,940	52
	3.1.3.2.3.7	Tankage	366,400	33
	3.6	Structure Forward of Tanks	41,000	3
	3.8	Structure Aft of Tanks	74,000	7
	3.9	Thrust Structure	107,700	6
	3.14	Base Heat Protection	5,000	
	3.26	Miscellaneous	11,840	1
W4	Propulsion System and Accessories		179,200	12
	4.1	M-1 Engines and Accessories	140,000	10
	4.7	Fuel System	9,900	
	4.8	Oxidizer System	14,800	1
	4.10	Control System Hardware	9,000	
	4.26	Miscellaneous	5,500	
W6	Equipment and Instrumentation		17,800	1
	6.2-12	Electrical, Telemetry, etc.	7,900	
	6.17	Separation System	8,400	
	6.17.1,2	Installed Retro Hardware	8,100	
	6.17.5	Explosive Devices	300	
	6.17.8	Separation Rails	- - - -	-
	6.18	Ullage System Mounting Hardware	1,500	
Ws 2d Dry Stage			802,940	67
W7	Residual and Reserve Propellants		351,200	31
	7.1	LH_2 Pressurants	16,400	1
	7.2,6	ΔV Reserve	167,000	15
	7.3.7	Thrust Decay Propellants	17,500	1
	7.4.8	Trapped Propellants	37,800	2
	7.5	LO_2 Pressurants	61,800	6
	7.9	Retrorocket Propellant	12,000	1
	7.11	Maximum Propellant Utilization Residual (LO_2)	33,400	3
	7.26	Miscellaneous	5,800	
Ws 2c Stage Weight at Cutoff			1,154,140	99
W8	Propellant Consumption		9,333,000	7,94
Ws 2i Stage Weight at Ignition			10,487,140	8,93
	Stage Mass Fraction, λ'		0.8899	0.8

* Burned after Separation of Solid Stage

Table

es T65B	Parallel Vehicles P67B	P65A	Stage and One-Half PM67A
),490	636,160	559,150	649,200
),050	360,260	332,550	408,900
3,600	41,000	33,600	30,000
4,000	106,200	106,200	83,600
3,400	107,700	68,400	104,000
4,000	8,000	7,000	9,500
),400	13,000	11,400	13,200
7,800	178,600	128,100	163,800
),000	140,000	100,000	122,000
7,200	9,900	7,300	11,000
),800	14,800	10,900	16,600
5,000	9,000	6,000	9,000
3,800	4,900	3,900	5,200
5,300	43,300	38,600	41,200
5,800	7,900	6,800	8,200
7,300	33,800	30,500	33,000
7,000	8,500	7,200	8,700
300	300	300	300
- - -	25,000	23,000	24,000
1,200	1,600	1,300	- - - -
2,550	858,060	725,850	854,200
7,660	356,700	323,460	389,230
4,000	16,400	14,000	21,300
4,000	172,000	159,000	174,000
2,500	17,500	12,500	16,800
5,200	37,300	26,200	37,750
4,520	61,800	64,520	76,700
),000	12,500	10,800	12,500
1,200	33,400	31,200	43,400
5,240	5,800	5,240	6,780
0,210	1,214,760	1,049,310	1,243,430
6,000	9,328,000	7,941,000	9,474,000*
6,210	10,542,760	8,990,310	10,717,430
892	0.8848	0.8833	0.8839

3.2.9-4

3.2.9.5 Study Baseline Vehicle — T65C

3.2.9.5.1 Criteria and Analysis

The T65 vehicle was chosen from the candidate matrix for preliminary design effort. This vehicle, which is reflected in the weight statements, is also shown in Figure 3.2.9-5. Configuration modifications from the T65 candidate include:

- Separation of orbital transfer stage from payload
- Reversal of LH_2 tank aft dome to form two tanks with convex bulkheads
- Change of LH_2 aft bulkhead from 0.7 b/a ellipsoid to 0.8 b/a ellipsoid
- Moving the first stage-second stage separation plane forward to a point 24 feet forward of the gimbal plane.

Pertinent criteria are listed in Table 3.2.9-5 for the solid first stage and in Table 3.2.9-6 for the liquid propellant stages.

Semidetailed weight statements for the total vehicle and the individual stages are included in Tables 3.2.9-7 through 3.2.9-10.

3.2.9.5.2 Mass and Inertia Data

Mass distributions for the first and second stages, respectively, of the T65C vehicle are shown in Figures 3.2.9-6 and 3.2.9-7. Center of gravity, mass moment of inertia, and vehicle weight are shown as a function of first-stage burn time in Figure 3.2.9-8.

BLANK

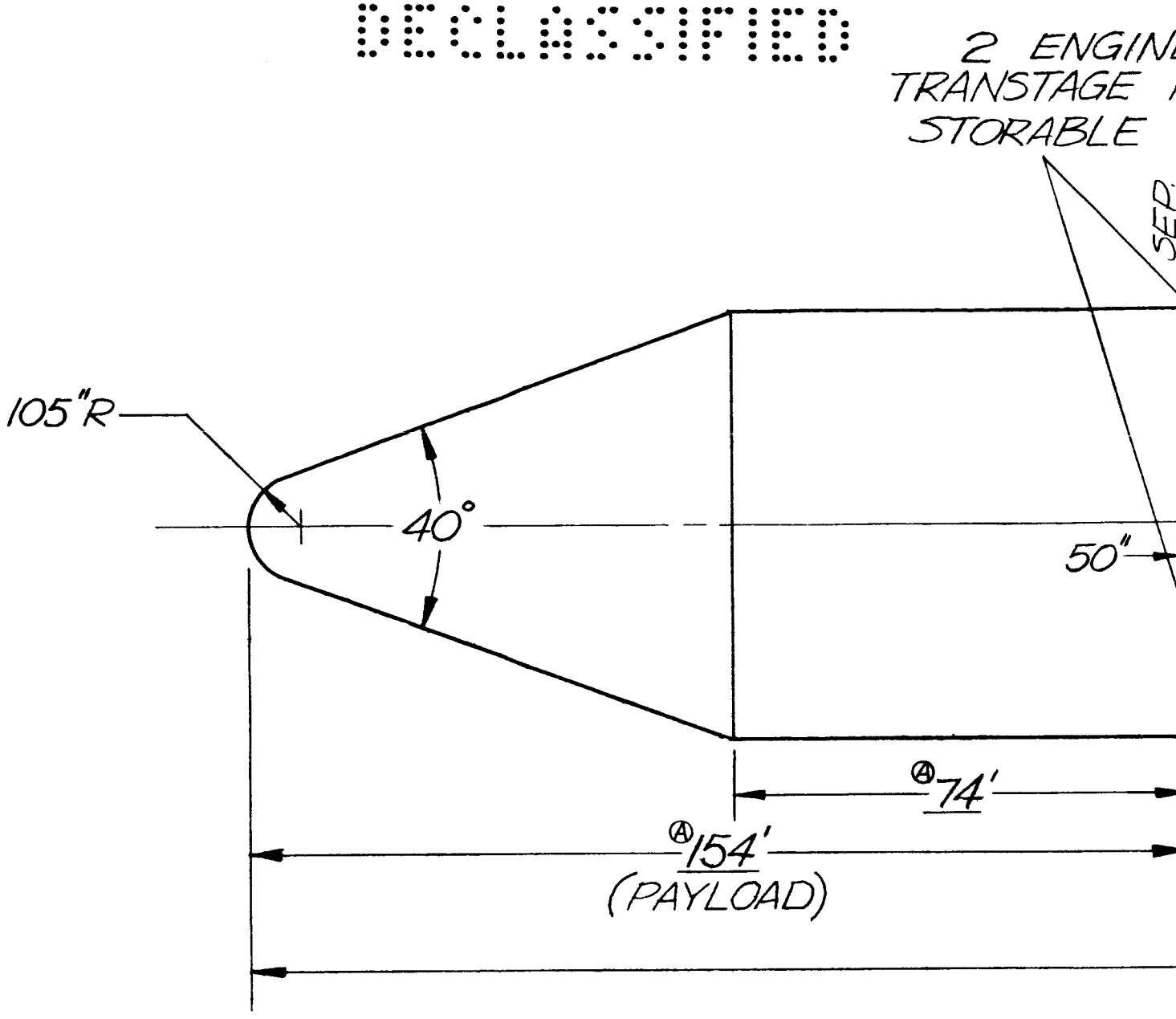

PAYLOAD TO 567KM

1,021,000#@

TRANST

W_{P_3} = 75,5

F_3 = 100,

λ'_3 = .75

ES
PROP. SYSTEM
PROPELLANTS

FIVE M-1 ENGINES
$\epsilon = 40$

YPLANES

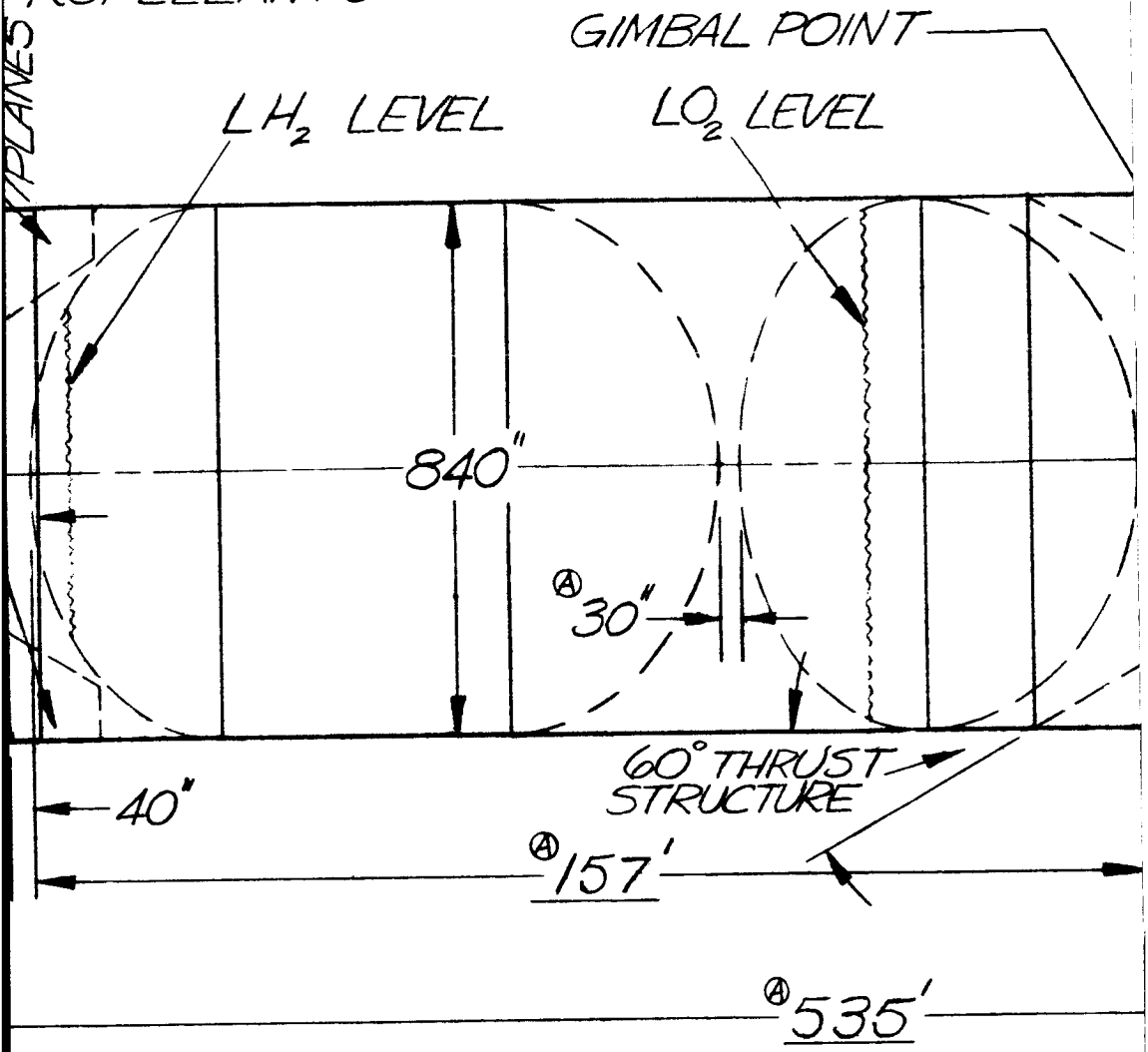

AGE

00# Ⓐ (INCL. RES.)

000#

Ⓐ

SECOND STAGE

W_{P_2} = 8,218,000# (IN

F_2 = 7,500,000#

λ_2' = .9136 Ⓐ

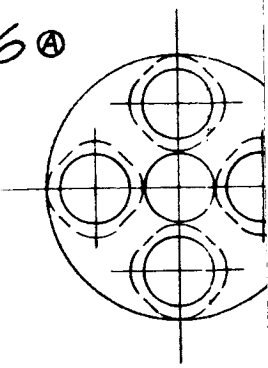

2

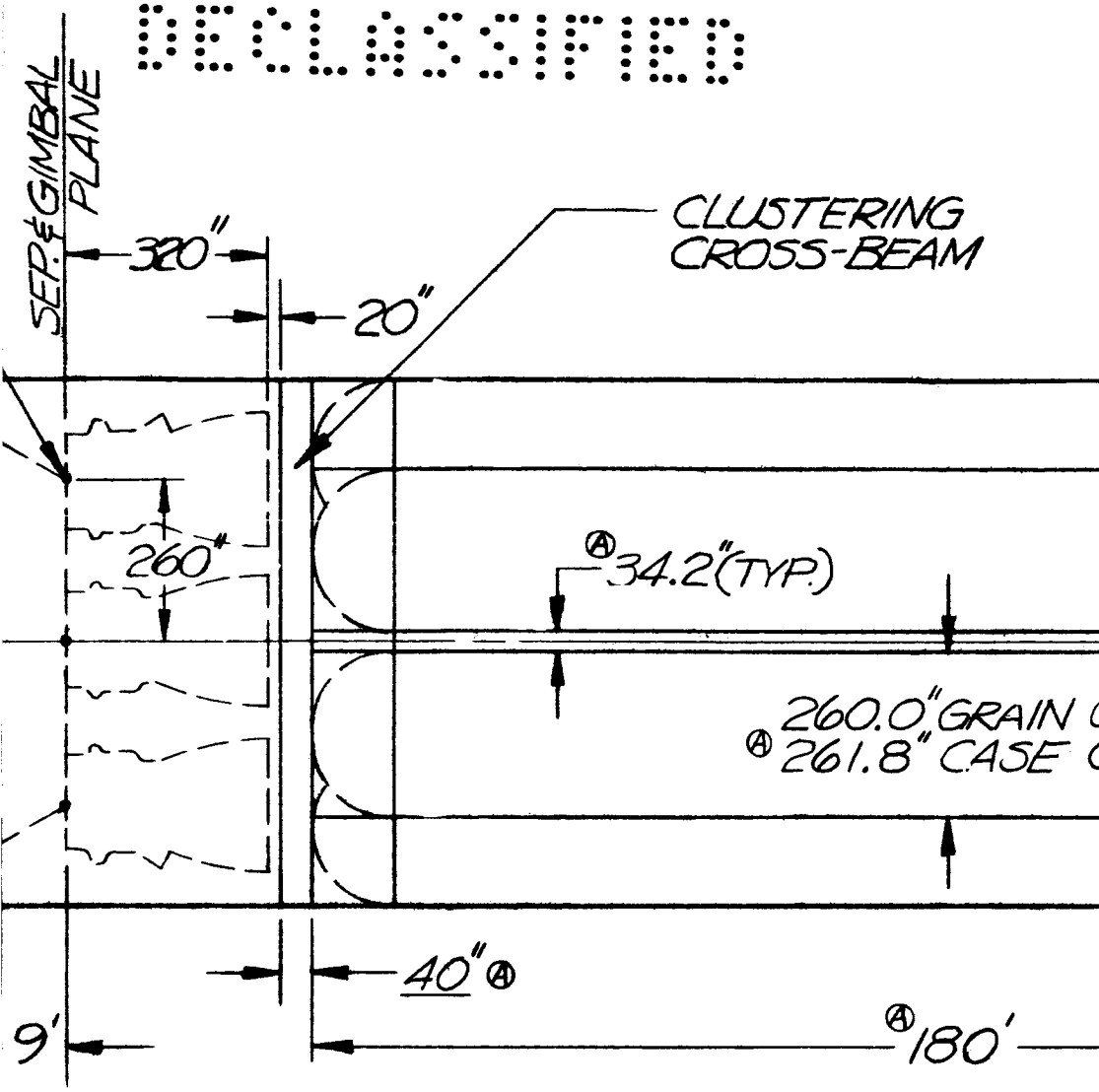

IC. RES.)

FIRST STAGE

W_{P_1} = 24,820,0

F_{o_1} = 54,900,0

X_1 = .888 Ⓐ

M-1 ENGINE PATTERN
CENTER ENGINE FIXED-
OUTBOARD ENGINES
GIMBAL 7½° MAX.

VEHICLE LAUNCH WT

Figure 3.2.9-5 BASELINE CONFIGURATION T65C 1000K Nominal Payload to 567 km Orbit

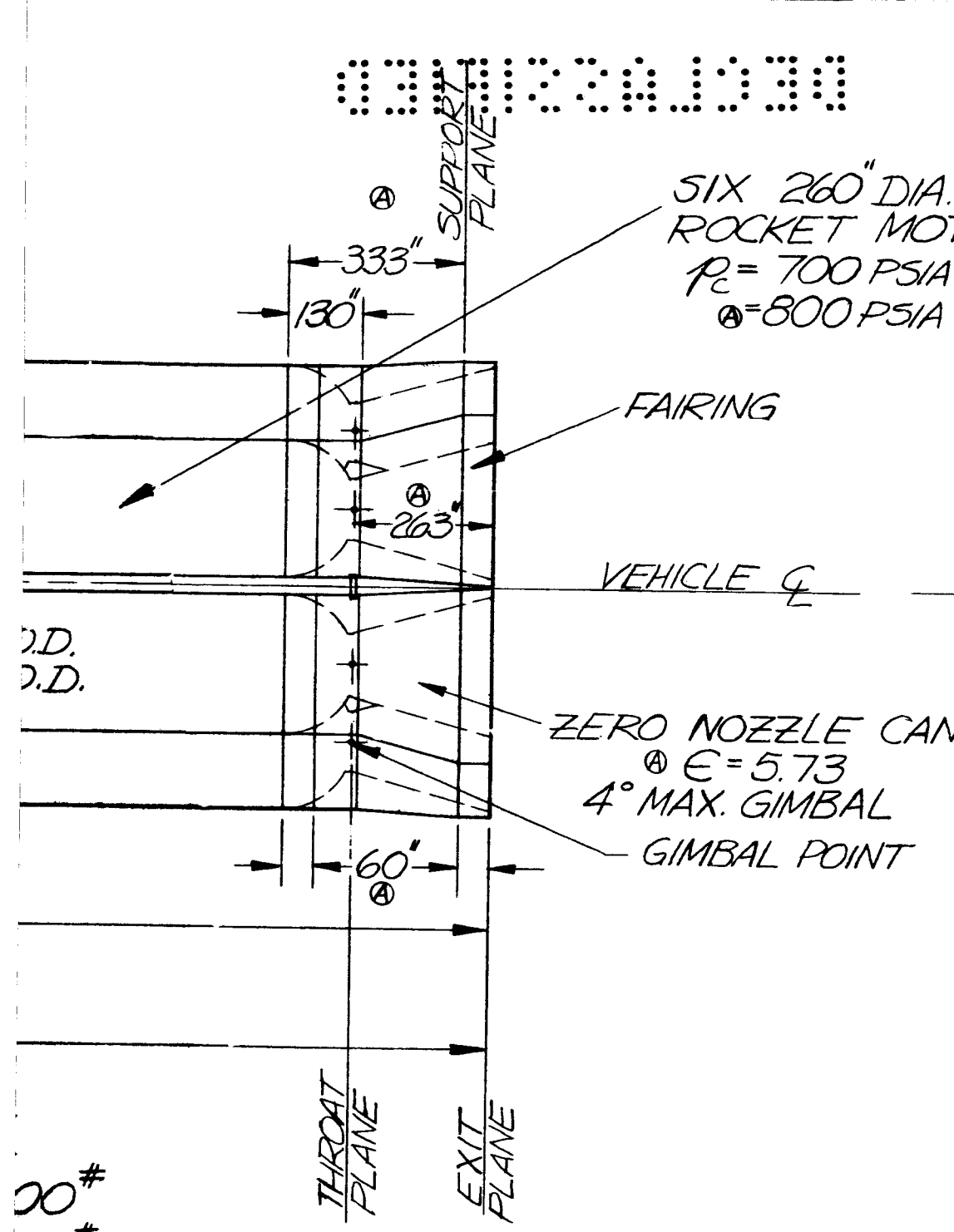

00#

00#

= 38,074,000#Ⓐ

4

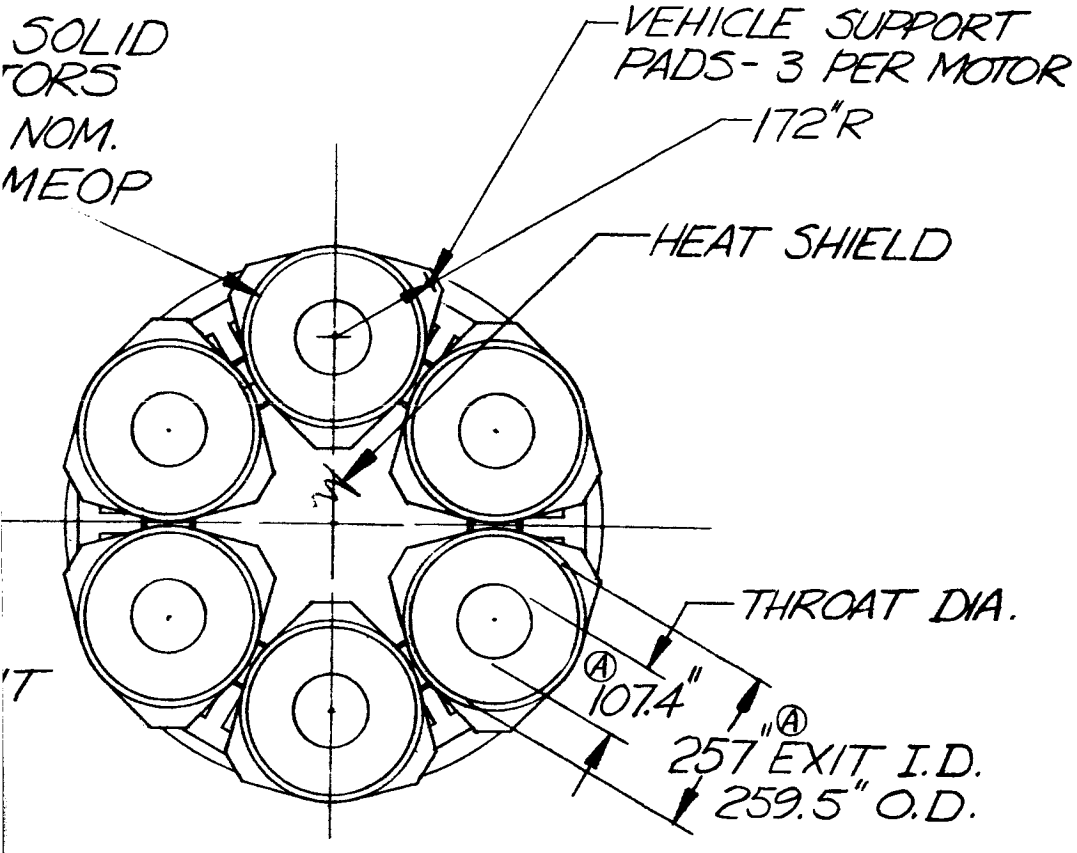

5

SOLID STAGE CRITERIA

T65C Vehicle

Number of Motors/Diameter	6/260 inches
Total Thrust at Launch (10^6 lb)	54.9
Total Propellant Weight (10^6 lb)	24.82
Nominal Chamber Pressure (psi)	698
Grain Cross-Sectional Loading, η_{cs}	0.693
Motor Volumetric Loading, η_v	0.684
Aport/Athroat	1.80
Nozzle Area Ratio, ϵ	5.7
TVC	Gimbaled Nozzles
Case Limit Design Pressure, MEOP (psi)	799
Case Material	18-percent Ni Marage Steel
Case Ultimate Strength (psi)	250,000
Weld Factor	0.90
Retrorocket Capability	0.5 g for 3 seconds
Slivers	Inert
Clustering Concept	Cross Beams
Igniter	Aft-End Ignition

Table 3.2.9-5

LIQUID STAGE CRITERIA

T65C Vehicle

LO_2/LH_2 Second Stage	
Engines	Five M-1 at 1.5×10^6 lb
Propellant Weight (10^6 lb)	8.218
Tank Diameter (feet)	70
Tank Material/Construction	2219-T87 Aluminum/Waffle
Tank Stiffening Design Criteria	Failure at 20-degree Angle of Attack at maximum q
Ullage Pressures (Startburn/Burnout)	LO_2 45/29 LH_2 43/39
Pressurization Concept	Bleed: 160°R GH over LH_2 270°R GO_2 over LO_2
Ullage Rocket Capability	0.1 g for 3 seconds
Retrorocket Capability	1 g for 3 seconds
Reserve Velocity Capability	3.5 percent of 225-kilometer ΔV
Separation Plane	24 feet forward of engine gimbal plane
N_2O_4/Aerozine-50 Orbit Transfer Stage	
Engines	Two at 50,000-pound thrust
Engine Chamber Pressure (psi)	300
Propellant Weight, including 2300-pound ΔV reserve	75,500 pounds
Propellant Supply	Pressure fed
Ullage Pressure (psi)	430
Pressurization Concept	Helium Blowdown
Helium Storage Pressure (psi)	3000
Ullage Rockets	Not Required
Retrorocket Capability	0.1 g for 3 seconds
Reserve Velocity Capability	3.5-percent of ($\Delta V_{567\text{-km Orbit}} - \Delta V_{225\text{-km Orbit}}$)

Table 3.2.9-6

VEHICLE WEIGHT STATEMENT

T65C Vehicle

	Payload (567-km)	1,021,000
Ws 3c	ORBIT TRANSFER STAGE AT CUTOFF	20,350
Ws 3d	Stage Dry Weight	17,180
W7*	Unusable Propellants and Gases	755
W7.2,6	ΔV Reserve Propellant	2,300
W7.11	Maximum P.U. Residual	115
Wv 3c	Vehicle Weight at Transorbit Stage Cutoff	1,041,350
W8	Orbit Transfer Stage Propellant	73,200
Ws 2c	SECOND-STAGE WEIGHT AT CUTOFF	869,890
Ws 2d	Stage Dry Weight	590,250
W7*	Unusable Propellant and Gases	94,440
W7.2,6	ΔV Reserve Propellant	154,000
W7.11	Maximum P.U. Residual	31,200
Wv 2c	Vehicle Weight at Second-Stage Cutoff	1,984,440
W8	Second-Stage Propellant	8,064,000
Wv 2i	Vehicle Weight at Second-Stage Ignition	10,048,440
W9	Second-Stage Weight Loss During Sep./Start	26,100
Ws 1c	FIRST-STAGE WEIGHT AT BURNOUT	2,970,420
Ws 1d	Stage Dry Weight	2,890,920
W7	Unused Propellant and Slivers	79,500
Wv 1c	Vehicle Weight at First-Stage Burnout	13,044,960
W8	First-Stage Propellant	24,823,400
Wv 1L	Vehicle Weight at Liftoff	37,868,360

*W7, less 7.2, 7.6, and 7.11

Table 3.2.9-7

SEMIDETAILED WEIGHT STATEMENT
SOLID PROPELLANT FIRST-STAGE

T65C Vehicle

W3	STRUCTURE			2,276,210
	3.4	Solid Propellant Container		1,884,990
		3.4.1	Cylinder	1,481,400
		3.4.4	Forward Bulkhead	46,200
		3.4.5	Y Rings	83,400
		3.4.6	Nozzle Boss	24,120
		3.4.8	Container Wall Liner	39,400
		3.4.9	Forward Bulkhead Insulation	14,600
		3.4.15	Aft Bulkhead	40,260
		3.4.16	Aft Bulkhead Insulation	81,550
		3.4.18	Cylinder Extensions	36,960
		3.4.26	Miscellaneous	37,100
	3.6	Structure Forward of Tanks		282,220
		3.6.1	Forward Interstage	129,000
		3.6.11	Cluster Structure	153,220
			3.6.11.1 Rings and Outer Ties	27,800
			3.6.11.2 Cross Beams	6,800
			3.6.11.3 Intercostals	4,100
			3.6.11.4 Motor Case Extensions	114,000
			3.6.11.5 Aft Ties	520
	3.8	Structure Aft of Propellant Containers		70,300
		3.8.11	Aft Support Structure	66,200
		3.8.12	Aft Aerodynamic Fairing	4,100
	3.14	Base Heat Protection		20,000
	3.26	Miscellaneous		18,700
W4	PROPULSION SYSTEM			595,000
	4.2	Nozzle (gimbaled)		562,000
		4.10.1	Thrust-Vector-Control Hardware	21,900
			4.10.1.1 Support Structure	1,050
			4.10.1.2 Power Unit	11,250
			4.10.1.3 Actuators	9,600
	4.26	Miscellaneous		11,100

Table 3.2.9-8

SEMIDETAILED WEIGHT STATEMENT
SOLID PROPELLANT FIRST-STAGE

T65C Vehicle

W6	EQUIPMENT AND INSTRUMENTATION		19,710
	6.1	Support Structure	550
	6.2	Environmental Control System	100
	6.5	Control System Electronics	
	6.7	Navigation and Tracking	
	6.8	Telemetering and Measuring	1,550
	6.11	Electrical System	3,160
	6.12	Range Safety	750
	6.17	Separation System	13,600
		6.17.1 Mounting Hardware	2,600
		6.17.2 Rocket Cases	10,500
		6.17.5 Explosive Devices	500
Ws 1d	DRY STAGE		2,890,920
W7	RESIDUAL PROPELLANTS AND SERVICE ITEMS		79,500
		7.9.13 Separation System Propellants	19,500
	7.11	Solid Propellant Slivers (Inert)	60,000
Ws 1c	STAGE WEIGHT AT CUTOFF		2,970,420
W8	PROPELLANT CONSUMPTION		24,823,400
	8.1	Solid Propellant	24,820,000
	8.4	TVC Drive Propellant	3,400
Ws 1g	STAGE WEIGHT AT GROUND IGNITION		27,793,820
Ws 1f	STAGE MASS FRACTION, λ'		0.8931

Table 3.2.9-8 (Cont.)

SEMIDETAILED WEIGHT STATEMENT
LO_2/LH_2 SECOND STAGE

T65C Vehicle

W3	STRUCTURE		449,100
	3.1	LH_2 Container	136,720
		3.1.1,2 Skin, including Stiffening	76,050
		3.1.4 Forward Bulkhead	23,280
		3.1.5 Aft Bulkhead	21,080
		3.1.10 Container Wall Insulation, Outer	3,790
		3.1.12 Forward Bulkhead Insulation, Outer	2,160
		3.1.14 Aft Bulkhead Insulation, Outer	2,360
		3.1.15 Antislosh Devices	4,000
		3.1.26 Miscellaneous	4,000
	3.2	LO_2 Container	100,540
		3.2.4 Forward Bulkhead	28,470
		3.2.5 Aft Bulkhead	61,750
		3.2.12 Forward Bulkhead Insulation, Outer	2,160
		3.2.14 Aft Bulkhead Insulation, Outer	2,360
		3.2.15 Antislosh Devices	2,900
		3.2.26 Miscellaneous	2,900
	3.6	Structure Forward of Tanks	22,600
	3.7	Structure Between Tanks	68,400
	3.8	Structure Aft of Tanks	34,500
	3.9	Thrust Structure	68,400
	3.14	Base Heat Protection	4,000
	3.26	Miscellaneous	13,940
W4	PROPULSION SYSTEM AND ACCESSORIES		125,350
	4.1	Engines and Accessories	100,000
	4.7	Fuel System	11,665
		4.7.3 Fill and Drain System	400
		4.7.4 Distribution System	8,750
		4.7.7 Vent System	150
		4.7.8 Tank Pressurization System	1,400
		4.7.10 Antivortex Devices	125
		4.7.26 Miscellaneous	840

Table 3.2.9-9

SEMIDETAILED WEIGHT STATEMENT
LO_2/LH_2 SECOND STAGE

T65C Vehicle

	4.8	Oxidizer System	7,685
	4.8.3	Fill and Drain System	400
	4.8.4	Distribution System	5,850
	4.8.7	Vent System	150
	4.8.8	Tank Pressurization System	600
	4.8.10	Antivortex Devices	125
	4.8.26	Miscellaneous	560
	4.10	Control System Hardware (TVC)	6,000
W6	EQUIPMENT AND INSTRUMENTATION		15,800
	6.1	Support Structure	600
	6.2	Environmental Control System	140
	6.8	Telemetering and Measuring	1,900
	6.10	Propellant Utilization System	1,300
	6.11	Electrical System	3,200
	6.12	Range Safety	160
	6.17	Separation System	6,800
	6.17.1	Mounting Hardware	1,300
	6.17.2	Rocket Cases	4,200
	6.17.5	Explosive Devices	300
	6.18	Ullage System (Attach Provisions)	1,700
Ws 2d	DRY STAGE		590,250
W7	RESIDUAL AND RESERVE PROPELLANTS		279,640
	7.1	LH_2 Pressurants	14,600
	7.2	LH_2 for ΔV Reserves	25,600
	7.3	LH_2 for Thrust Decay	2,100
	7.4	LH_2 Trapped	6,350
	7.4.3	In Lines	4,500
	7.4.6	In Engine	1,850
	7.5	LO_2 Pressurants	31,840
	7.6	LO_2 for ΔV Reserves	128,400

Table 3.2.9-9 (Cont.)

SEMIDETAILED WEIGHT STATEMENT
LO_2/LH_2 SECOND STAGE

T65C Vehicle

7.7	LO_2 for Thrust Decay	10,400
7.8	LO_2 Trapped	16,150
7.8.3	In Lines	12,000
7.8.6	In Engines	4,150
7.9	Retrorocket Propellant	9,500
7.11	Maximum Propellant Utilization Residual (LO_2)	31,200
7.26	Miscellaneous	3,500
Ws 2c	STAGE WEIGHT AT CUTOFF	869,890
W8	PROPELLANT CONSUMPTION	8,064,000
8.1	LH_2	1,341,950
8.2	LO_2	6,709,750
Ws 2i	STAGE AT IGNITION	8,933,890
W9	WEIGHT LOSS PRIOR TO IGNITION	26,100
9.1	Fuel for Start	1,300
9.2	Oxidizer for Start	6,500
9.3	Ullage System Propellants	11,900
9.7	Ullage Rocket Cases	6,400
Ws 2s	STAGE AT SEPARATION	8,959,990
	Stage Mass Fraction, λ' *	0.9026

* $\lambda' = \frac{\text{Propellant Consumption}}{\text{Stage Weight at Ignition}}$

Table 3.2.9-9 (Cont.)

SEMIDETAILED WEIGHT STATEMENT
ORBIT TRANSFER STAGE

T65C Vehicle

W3	STRUCTURE		10,080
	3.1	Aerozine-50 Container	1,850
		3.1.4 Forward Bulkhead	820
		3.1.5 Aft Bulkhead	820
		3.1.7 Support Structure Brackets	210
	3.2	N_2O_4 Container	1,500
		3.1.4 Forward Bulkhead	670
		3.1.5 Aft Bulkhead	670
		3.1.7 Support Structure Brackets	160
	3.6	Structure Forward of Tanks	5,410
	3.9	Thrust Structure	350
	3.14	Base Heat Protection	350
	3.17	Tank Support Structure	130
	3.26	Miscellaneous	490
W4	PROPULSION SYSTEM AND ACCESSORIES		6,315
	4.1	Engines and Accessories (including TVC)	1,700
	4.7	Fuel System	4,205
		4.7.1 Fill and Drain	15
		4.7.4 Distribution System	60
		4.7.7 Vent System	20
		4.7.8 Tank Pressurization System (including N_2O_4)	4,100
		4.7.10 Antivortex Devices	10
	4.8	Oxidizer System	110
		4.8.3 Fill and Drain System	15
		4.8.4 Distribution System	65
		4.8.7 Vent System	20
		4.8.8 Tank Pressurization	(included in 4.7.8)
		4.8.10 Antivortex Devices	10
	4.26	Miscellaneous	300
W6	EQUIPMENT AND INSTRUMENTATION		785
	6.1	Support Structure	50

Table 3.2.9-10

SEMIDETAILED WEIGHT STATEMENT
ORBIT TRANSFER STAGE

T65C Vehicle

6.2	Environmental Control	30
6.4	Guidance System	200
6.8	Telemetering and Measuring	240
6.11	Electrical System	50
6.17	Separation System	215
6.17.1	Mounting Hardware	5
6.17.2	Rocket Cases	10
6.17.5	Explosive Devices	200
Ws 3d	DRY STAGE	17,180
W7	RESIDUAL AND RESERVE PROPELLANTS	3,170
7.1,5	Residual Propellants	590
7.2	Aerozine-50 for ΔV Reserves	770
7.4	Aerozine-50 Trapped	30
7.6	N_2O_4 for ΔV Reserves	1,530
7.8	N_2O_4 Trapped	45
7.9	Retrorocket Propellant	20
7.11	Maximum Propellant Utilization Residual (N_2O_4)	115
7.26	Miscellaneous	70
Ws 3c	STAGE WEIGHT AT CUTOFF	20,350
W8	PROPELLANT CONSUMPTION	73,200
8.1	Aerozine-50	24,400
8.2	N_2O_4	48,800
Ws 3i	STAGE WEIGHT AT IGNITION	93,550
Ws 3f	STAGE MASS FRACTION, λ'	0.7825

Table 3.2.9-10 (Cont.)

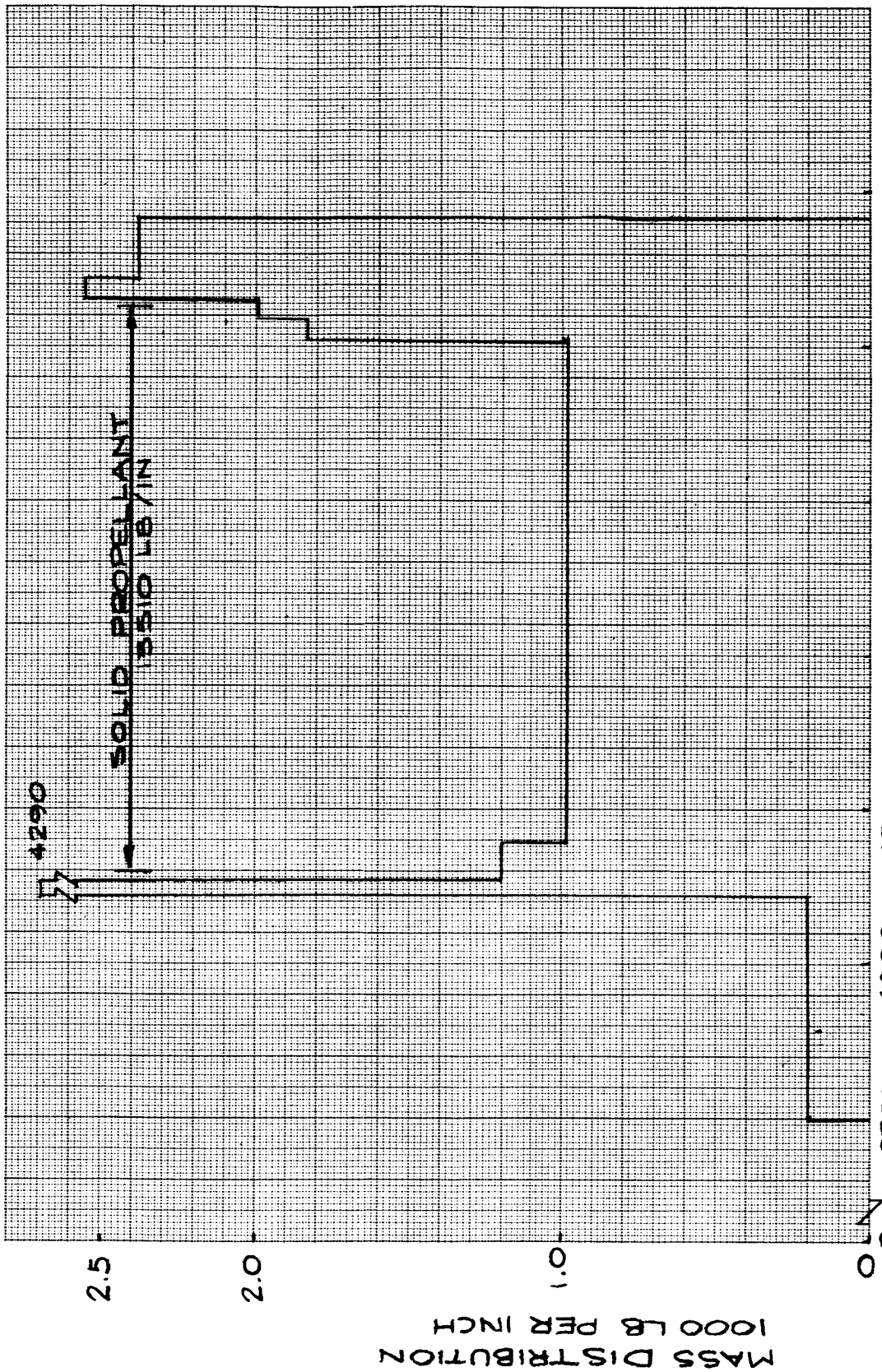

Figure 3.2.9-6 FIRST-STAGE MASS DISTRIBUTION
T65C Vehicle

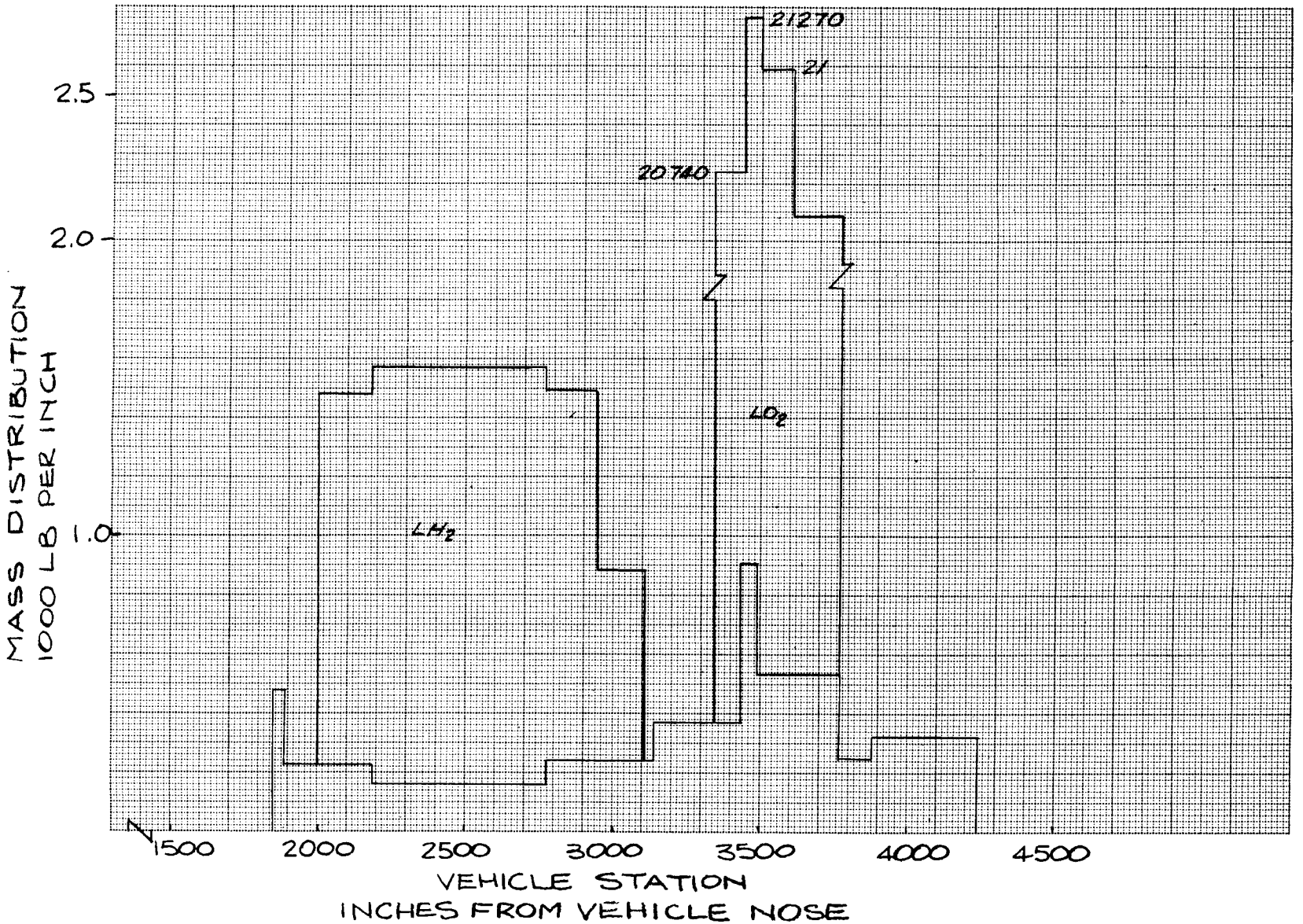

Figure 3.2.9-7 SECOND-STAGE MASS DISTRIBUTION
T65C Vehicle

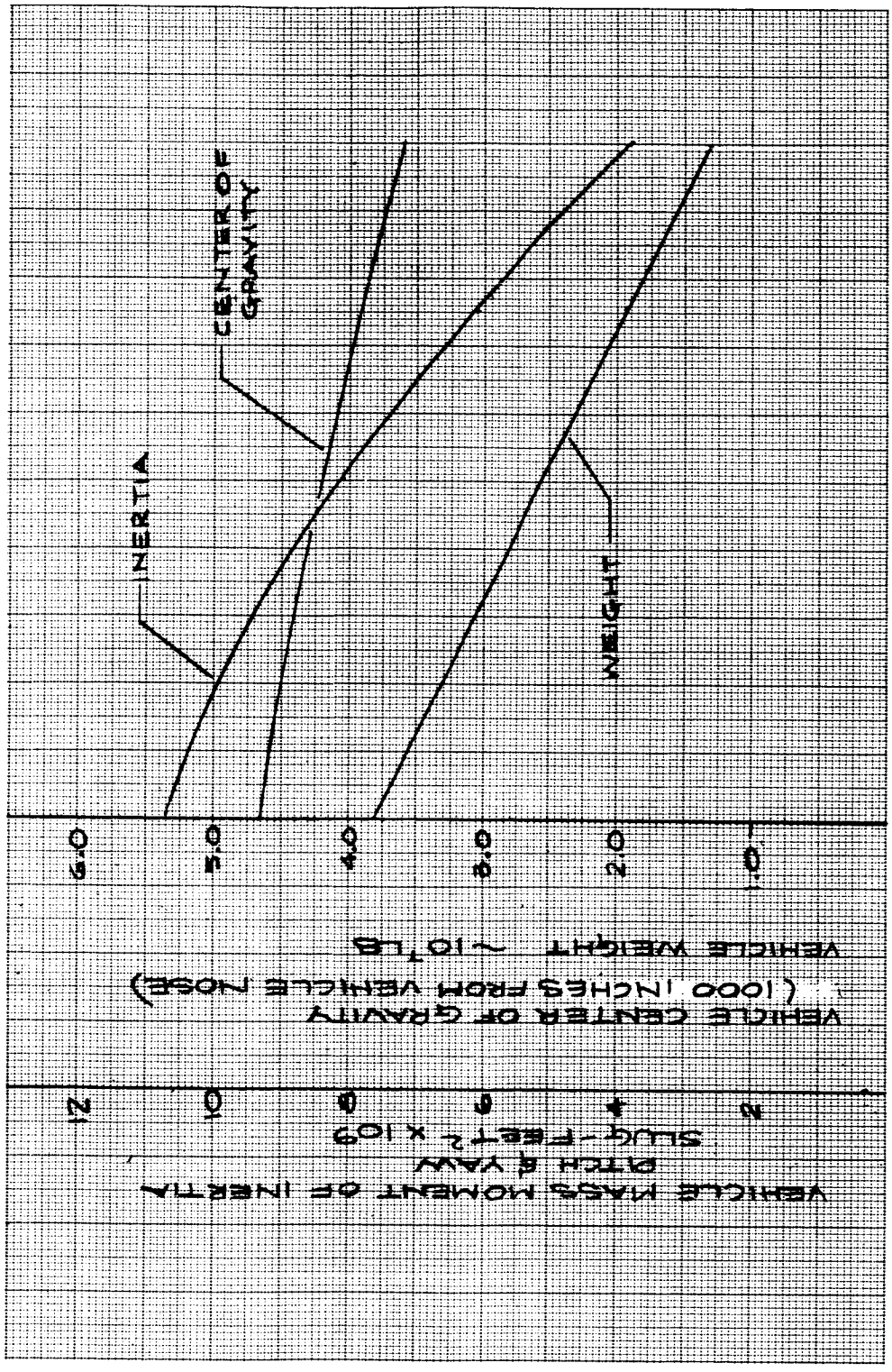

Figure 3.2.9-8 INERTIA DATA—FIRST-STAGE BURNING
T65C Vehicle

BLANK

3.2.9.6 Vehicle Trade Studies

Two vehicle trade studies were conducted on a weight basis — second stage tankage concept, and first stage case material.

3.2.9.6.1 Second-Stage Tank Concept

To select a tank configuration most suitable to the NOVA vehicle second stage, three candidates were evaluated on a weight basis.

- A single tank with separate propellant containers (tank diameter = 70 feet),
- A cluster of five 25-foot-diameter tanks with separate propellant containers,
- An eight-cell tank (shell radius = 17.5 feet, tank diameter = 70 feet).

All configurations have a usable propellant capacity of 8,064,000 pounds (+ ΔV reserve = 154,000) of LO_2/LH_2 and five M-1 engines. The general arrangement of the tank configurations is shown in Figure 3.2.9-9 and weight statements for all three second stages are shown in Table 3.2.9-11.

Weight Analysis —

- Structure — The single- and multicell tanks are constructed of aluminum waffle pattern, and the clustered tanks are constructed of an integrally milled sheet-stringer pattern. Outside insulation was used, and cryogenic temperature allowables for 2219-T87 aluminum were used wherever possible. Tankage weight is allocated to weld lands based on weld lengths defined by manufacturing. Interstage and intertank structure is integral sheet-and-stringer construction.
- The dome (tank and closure) weight for the single tank is considerably higher than for either of the others; however, the propellant capacity is also higher ($V \propto D^3$). Skin gages and areas for these components are lower on the multicell and multiple tanks, since they are composed of a number of sections of small radius. The sidewall weight for the single tank is slightly higher than for the multicell configuration, even though the area is smaller. However, an equitable comparison must include the weight of the radial webs in the multicell configuration, since they carry the hoop tension loading that is removed from the side wall by the smaller diameter of the side wall segments as compared to the single tank. The clustered tanks suffer severely in the side walls, since the light pressure shell obtained from the 25-foot diameter must be stiffened substantially to carry the axial loads.
- Figure 3.2.9-10 is a bar chart showing a breakdown of structural weights for the three tankage concepts. Note that the weight advantage of the multicell tank lies in the sharp decrease in the amount of interstage-type structure required. The diagonally shaded areas to the right of the weight breakdown divide the total propellant volume into the portion carried by each structural

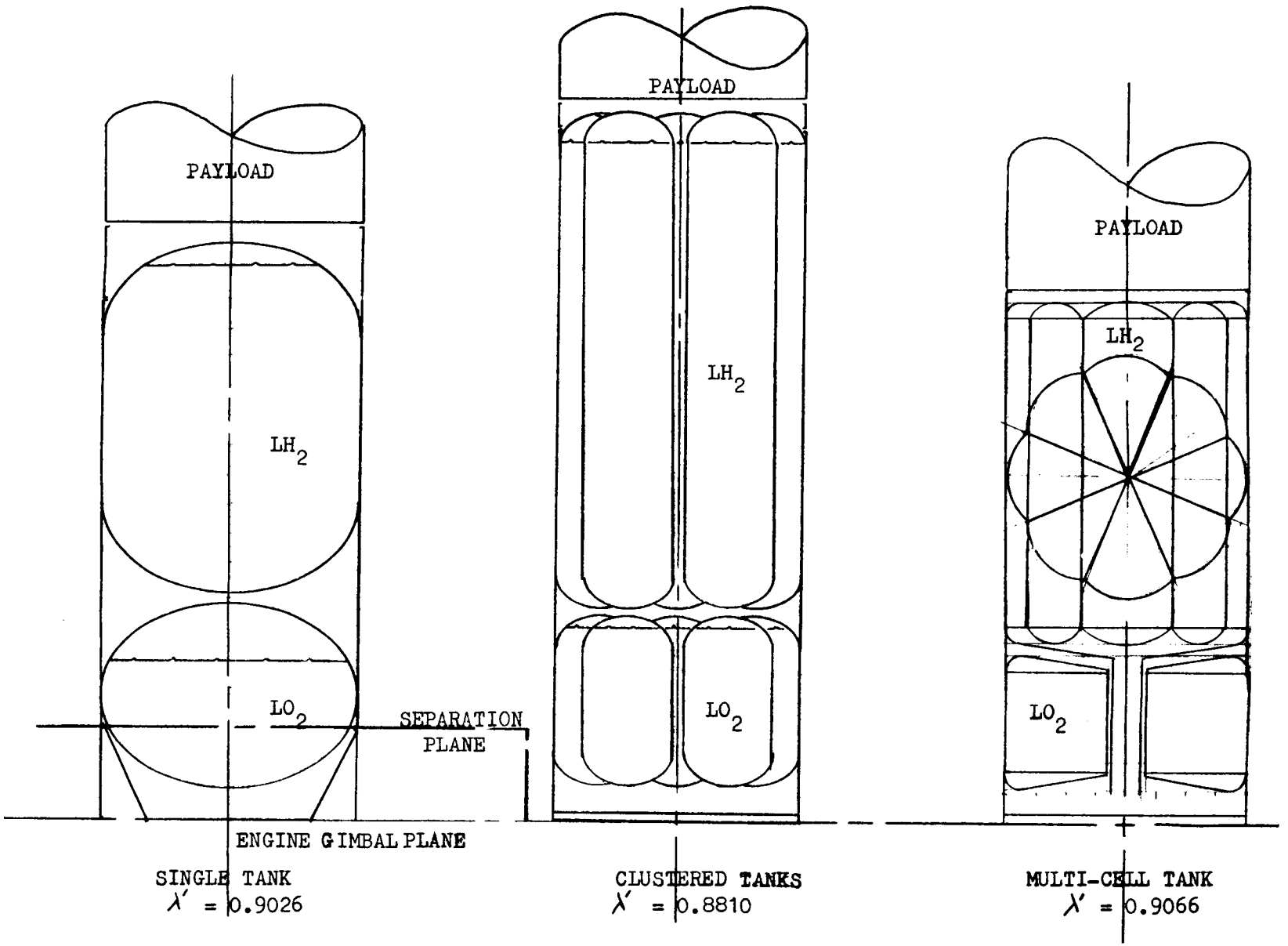

PROPELLANT WEIGHT = 8,218,000 lb (inc. V Reserve)
FIVE M-1 ENGINES

Figure 3.2.9-9 SECOND-STAGE TANK CONFIGURATIONS

SEMIDETAILED WEIGHT STATEMENT
TANK CONFIGURATION TRADE

T65C Baseline Vehicle

			Single Tank	Cluster of Five	Multicell Tank
W3	STRUCTURE		449,100	659,790	410,720
3.1	LH_2 Container		120,620	240,300	141,620
3.1.1,2		Skin, including Stiffening	58,850	191,220	51,300
3.1.3		Radial Webs	- - - -	- - - -	60,800
3.1.4		Forward Bulkhead	23,280	4,850	7,010
3.1.5		Aft Bulkhead	21,080	5,700	8,210
3.1.10-14		Insulation	8,310	27,400	9,500
3.1.15		Antislosh Devices	4,000	630	- - - -
3.1.26		Miscellaneous	5,100	10,500	5,000
3.2	LO_2 Container		102,040	107,090	162,370
3.2.2,2		Skin, including Stiffening	- - - -	66,430	29,850
3.2.3		Radial Webs	- - - -	- - - -	63,300
3.2.4		Forward Bulkhead	28,470	5,400	8,520
3.2.5		Aft Bulkhead	61,750	15,800	18,900
3.2.10-14		Insulation	4,520	14,700	5,000
3.2.15		Antislosh Devices	2,900	260	- - - -
3.2.16		Center Tube	- - - -	- - - -	32,000
3.2.26		Miscellaneous	4,400	4,500	4,800
3.6	Structure Forward of Tanks		30,400	40,400	5,050
3.6.1		Forward Interstage	30,400	25,400	5,050
3.6.11		Forward Cluster Structure	- - - -	15,000	- - - -
3.7	Structure Between Tanks		78,000	54,400	10,420
3.8	Structure Aft of Tanks		34,500	165,200	31,700
3.8.1		Aft Skirt	34,500	122,000	31,700
3.8.11		Aft Cluster Structure	- - - -	43,200	- - - -
3.9	Thrust Structure		68,400	34,400	46,500
3.14	Base Heat Protection		4,000	5,000	5,000
3.26	Miscellaneous Structure		11,140	13,000	8,060
W4	PROPULSION SYSTEM		125,350	127,350	123,350
4.1	M-1 Engines and Accessories		100,000	100,000	100,000

Table 3.2.9-11

SEMIDETAILED WEIGHT STATEMENT
TANK CONFIGURATION TRADE

T65C Baseline Vehicle

		Single Tank	Cluster of Five	Multicell Tank
4.7,8	Propellant Systems	17,950	17,950	16,300
4.10	TVC System	6,000	7,500	6,000
4.26	Miscellaneous	1,400	1,900	1,050
W6	EQUIPMENT AND INSTRUMENTATION	15,800	17,900	14,800
Ws 2d	Dry Stage	590,250	805,040	548,870
W7	RESIDUALS AND RESERVE PROPELLANTS	279,640	283,310	281,890
7.2,6	ΔV Reserve	154,000	154,000	154,000
7.3,7	Thrust Decay	12,500	12,500	12,500
7.4,8	Trapped Propellant	22,500	24,800	26,780
7.5	LO_2 Pressurants	32,140	31,010	31,010
7.9	Retrorocket Propellants	9,500	12,000	8,500
7.11	Maximum Propellant Utilization Residual	31,200	31,200	31,200
7.26	Miscellaneous	3,500	3,500	3,600
Ws 2c	Stage Weight at Cutoff	869,890	1,088,350	830,760
W8	PROPELLANT CONSUMPTION	8,064,000	8,064,000	8,064,000
Ws 2i	Stage Weight at Ignition	8,933,890	9,152,350	8,894,760
Ws 2f	Stage Mass Fraction, λ'	0.9026	0.8810	0.9066

Table 3.2.9-11 (Cont.)

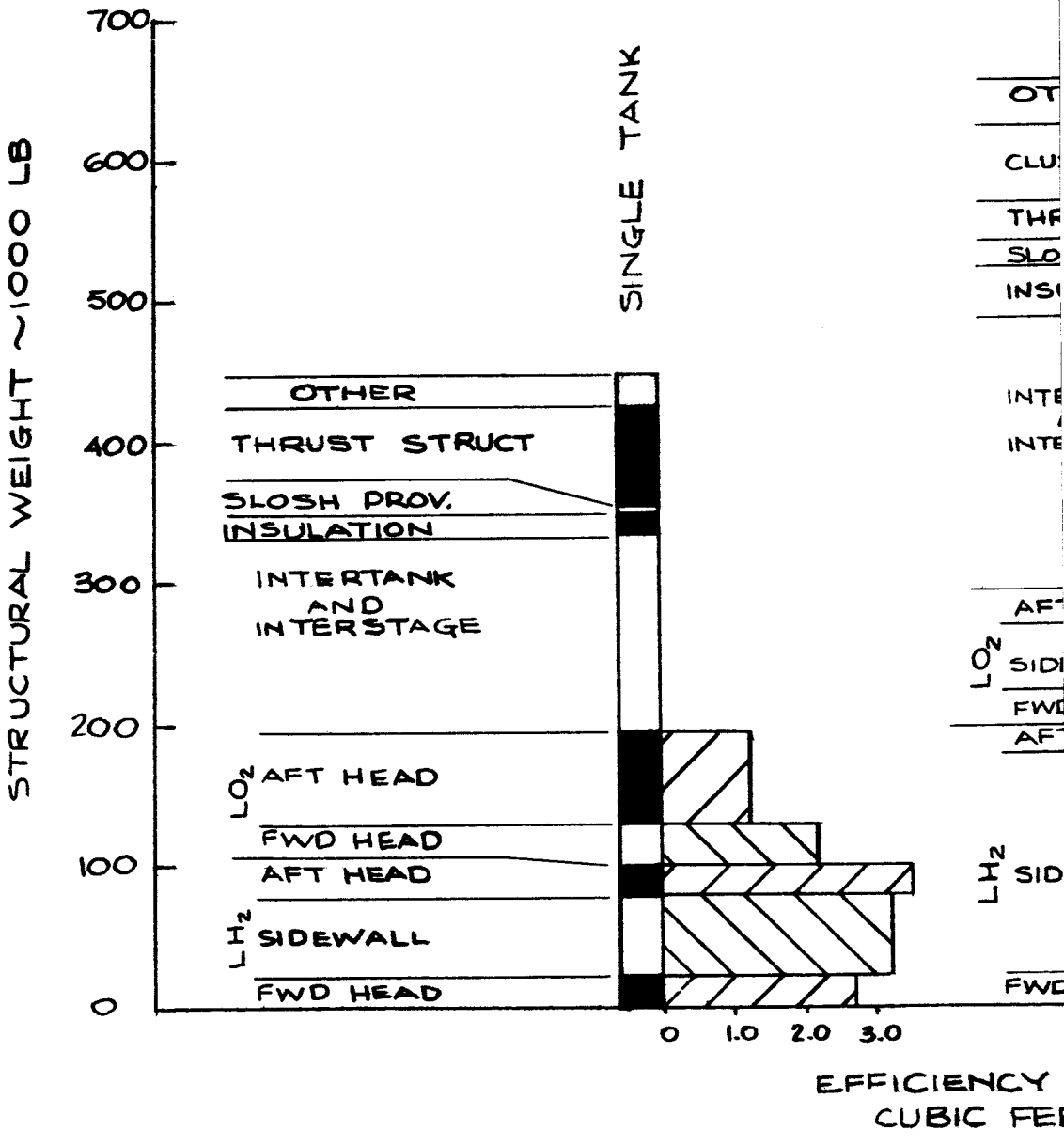

Figure 3.2.9-10
Tank Conf

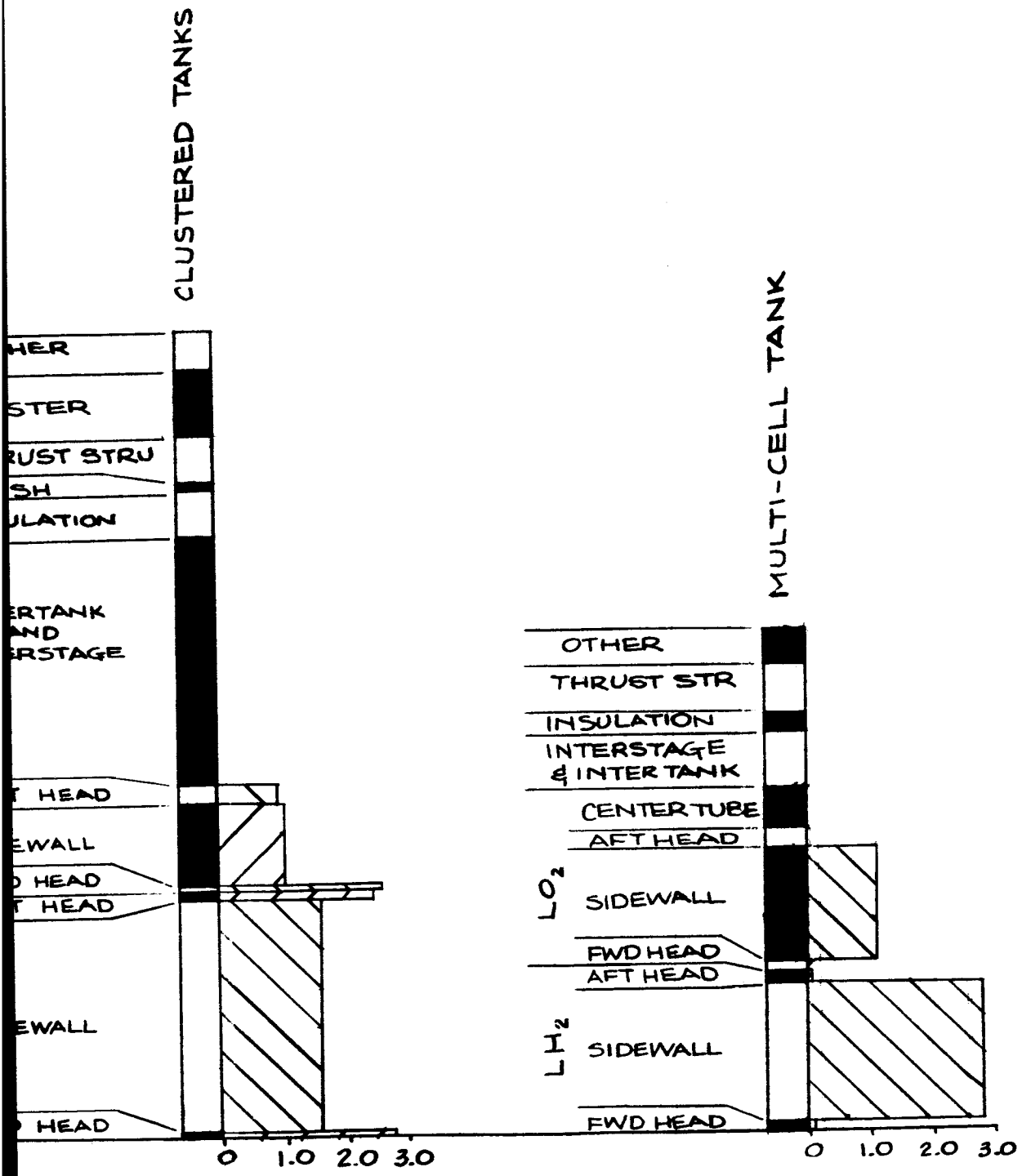

OF STRUCTURE FOR CONTAINING VOLUME
ET OF PROPELLANT CAPACITY / LB OF STRUCTURE

WEIGHT COMPARISON
iguration Trade

member. The further to the right that each block extends, the more efficient the component is in containing the volume. The propellant containers of the single-tank configuration are quite efficient, but the connecting structure is a heavy item and contains no propellant. Conversely, the cylindrical sidewalls of the clustered tanks are quite inefficient due to the sidewall thickness required by the clustering loads.

- The weight statements shown in Table 3.2.9-11 reflect stage separation at the engine gimbal plane for the multiple and multicell tanks and at a point approximately 24 feet forward of the gimbal plane for the single-tank configuration.
- Tank insulation weights are based on total tank areas of both propellants.
- Slosh suppression provisions consist of a beaded, lightened cylinder in each propellant compartment with unit weights based on extrapolated data. The radial webs of the multicell tanks were assumed to provide the same function.
- Thrust structure for the single tank is a 60-degree thrust-cone frustum with four M-1 engines mounted on the periphery and one on a cross-beam structure in the center. The multiple tank concept has one engine mounted on cross beams on the aft end of each tank module. The multicell tank concept has beams running from the center post to the web-sidewall joint, with one engine mounted between alternate pairs of beams and a single engine at the center of the cluster. In the single-tank and clustered-tank configurations, the thrust loads are carried by the tank sidewall. The multicell utilizes both the external sidewall and the LO_2 tank center tube.
- The cluster structure for the clustered-tank configuration is a cross-beam arrangement similar to that used on the solid propellant stage. Note that the weight allocated as "structure aft of tanks — aft skirt" is also largely a clustering penalty. A more efficient second-stage clustering concept might be designed if the number of second-stage tank-engine modules equaled the number of first-stage motors.
- As anticipated, the propellant container weight of the single tank and the multicell tank are comparable. The net weight reduction of about 40,000 pounds in the multicell tank as compared to the single tank is largely a result of eliminating the inefficiencies involved in the interstage structures that must transmit loads but have no propellant capacity.
- Propulsion System — The variation in propellant feed system weights depends on the length of the lines in the various configurations. The LH_2 lines are taken to be outside the LO_2 tank for the single-tank configuration, between the LO_2 tanks for the clustered tanks, and to run through the LO_2 tank center tube in the multicell configuration. In addition, level-equalizing manifolding is provided for the clustered-tank concept.
- Retrorocket and ullage rocket weights are functions of the inert weight of the stage.

- Residuals — Line residuals were based on total line volumes in each case. It was assumed there would be no residual propellant in the tanks for any configuration. Level-equalizing manifolding for the clustered tanks and holes in the radial webs of the multicell configuration maintain liquid levels and pressures such that the P.U. residual is treated as that of a single tank.

3.2.9.6.2 First-Stage Case Material Trade

To evaluate the effect of case material allowable on vehicle weight, a motor constructed of HP 150 (F_{tu} = 150,000 psi) was compared with one of 18-percent Ni marage (F_{tu} = 250,000 psi). The pertinent criteria are listed in Table 3.2.9-12, and a summary of the weight effects is shown in Table 3.2.9-13. The weight increase of 814,510 pounds associated with the change from 18-percent Ni marage to the HP 150 results in a payload decrease of approximately 98,000 pounds (with no change in propellant weight).

Weights Analysis — Table 3.2.9-12 lists the criteria involved. The 0.65-inch sidewall thickness for the maraged steel was obtained from ground load stability considerations rather than hoop tension. The motor chamber pressure was adjusted to give a maximum expected operating pressure that would require the same thickness for the pressurized condition. Since no such limitation existed for the thicker HP 150 case, the motor nominal chamber pressure was 600 psi, and the MEOP was 720 psi.

WEIGHTS CRITERIA: First-Stage Solid-Propellant Case Materials		
	Type of Steel	
	18 Ni Marage	HP 150
Ultimate Tensile Strength (psi)	250,000	150,000
Density (lb/in3)	0.290	0.283
Weld Factor	0.9	0.9
Nominal Case Thickness (inch)	0.65	0.97
Nominal Chamber Pressure (psi)	698	600
MEOP (psi)	799	720

Table 3.2.9-12

A plot of motor weight as a function of case material allowable is shown in Figure 3.2.9-11. The motor weight is not inversely proportioned to the allowable, since such items as the liner and nozzle are included. The broken line indicates the minimum weight obtainable, based on the case stability criterion of minimum wall thickness.

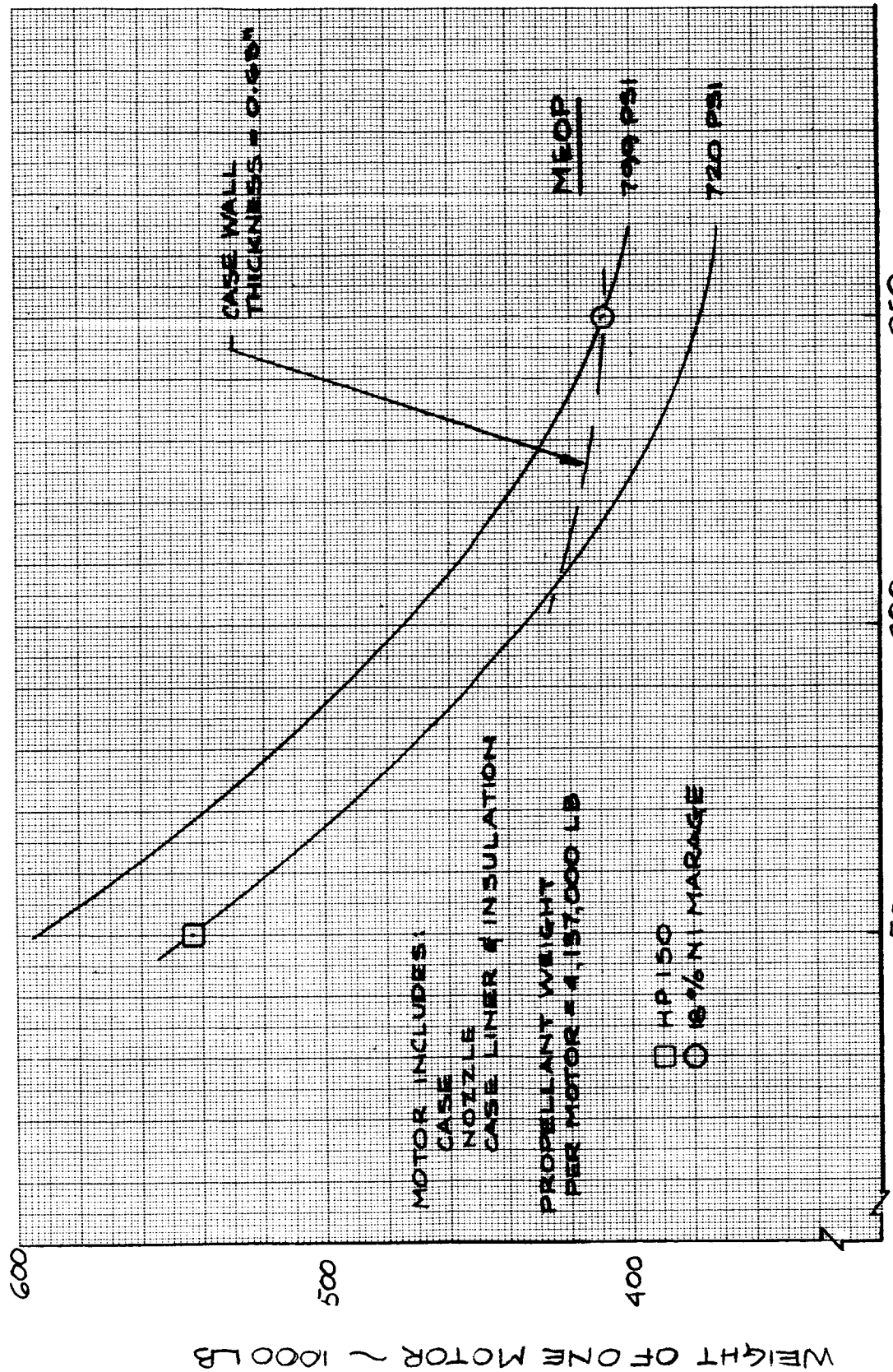

Figure 3.2.9-11 EFFECT OF CASE ALLOWABLE ON MOTOR WEIGHT

WEIGHT COMPARISON First-Stage Solid-Propellant Case Materials				
	Type of Steel			
	18 Ni (F_{tu} = 250,000 psi)		HP 150 (F_{tu} = 150,000 psi)	
	One Motor	Stage	One Motor	Stage
(Basic Motor)	409,680	2,458,090	543,920	3,263,520
Cylinder	246,900	1,481,400	359,920	2,154,780
Forward Head	7,700	46,200	11,350	68,100
Aft Head	6,710	40,260	9,490	56,940
Y Rings	13,900	83,400	20,200	121,200
Nozzle Boss	4,020	24,120	4,320	25,920
Handling Skirts	6,160	36,960	6,010	36,060
Nozzle, Gimbaled	93,670	562,000	100,170	601,000
Other	30,620	183,750	33,250	199,500
(Structural Provisions)		391,220		391,220
TVC System		21,900		21,900
(Equipment)		19,710		24,010
(Unused Propellant)		79,500		84,100
Total Inert Weight	409,680	2,970,420	543,920	3,784,750
Total Weight Change			+134,240	+814,510
Percent Change in Weight			+32.7	+27.4
Mass Fraction, λ' *	0.9099	0.8931	0.8838	0.8677

* W_{P1} (Six Motors) = 24,820,000

Table 3.2.9-13

A summary of the weight changes is shown in Table 3.2.9-13. The weight increase in utilizing HP 150 is less than might be anticipated because of the chamber pressure difference indicated above. The difference in nozzle weights is also due to the change in chamber pressure. The net stage-weight increase for the change from 18 Ni marage steel to HP 150 is 814,510 pounds or 27.4 percent of first-stage inert weight.

3.2.9.7 Preliminary Design Vehicle

The weights for the final vehicle resulting from the trade studies conducted and the details generated in various areas are shown in Tables 3.2.9-14 through 3.2.9-19. Vehicle weight statements are shown for the escape mission and for the orbital mission (Tables 3.2.9-14 and 3.2.9-15, respectively). Semidetailed weight statements are shown for the solid-propellant stage (Table 3.2.9-16), the LO_2/LH_2 second stage (Table 3.2.9-17), the orbital transfer stage (Table 3.2.9-18), and the LO_2/LH_2 escape stage (Table 3.2.9-19).

The orbital payload configuration is essentially the same as that shown in Figure 3.2.9-5, with the payload as shown in Table 3.2.9-14. The escape stage configuration is shown in Figure 3.2.3-16.

3.2.9.7.1 Weights Analysis

The criteria, ground rules, and analysis methods are similar to those in 3.2.9.4.1 except for the items described below, and the changes indicated in Tables 3.2.9-20 and -21. In addition, weights described in 3.2.9.4.1 as extrapolated from previous data have been supplemented by detail calculations and design by the cognizant technologies, and the current weights reflect these efforts.

First Stage —

- Case Liner — Liner weights are based on the total inner surface of the motor case being coated with a 0.1-inch-thick rubber-based liner with a density of 0.042 pound per cubic inch.
- Internal Insulation Bulkheads — Motors have phenolic-based insulation (ρ = 0.063 lb/in^3) for the forward and aft bulkheads. The insulation weight for the forward bulkhead is based on an average thickness of 0.5 inch. The aft bulkhead insulation is a function of chamber pressure and burn time and the average thickness is 3.7 inches.

LO_2/LH_2 Second Stage —

- Tankage — The LO_2/LH_2 tankage pressure shells are designed by pressure test requirements, rather than mission loads. This results in an increase of approximately 15 percent of tank weight over the vehicle requirements. The bulkheads have been designed as zonal sections, whose thickness is determined by the local curvature and pressure requirements. The non-propellant-carrying cylindrical segments are designed by the 20-degree angle of attack condition at maximum q. The tank structure is 2219-T87 aluminum waffle and the intertank, structure, etc., is aluminum semimonocoque with integrally milled stiffeners. The design limit ullage pressures are 42 psi for the LO_2 and 38 psi for the LH_2 tank, including venting tolerances.

VEHICLE WEIGHT STATEMENT

T65D Vehicle

	Payload (567-kilometer orbit)	1,070,000
Ws 3c	ORBIT TRANSFER STATE AT CUTOFF	20,400
Ws 3d	Stage Dry Weight	17,115
W7*	Unusable Propellants and Gases	765
W7.2,6	Δ V Reserve Propellant	2,400
W7.11	Maximum P.U. Residual	120
Wv 3c	Vehicle Weight at Transorbit Stage Cutoff	1,090,400
W8	Orbit Transfer Stage Propellant	74,600
Ws 2c	SECOND-STAGE WEIGHT AT CUTOFF	873,200
Ws 2d	Stage Dry Weight	596,450
W7*	Unusable Propellant and Gases	81,050
W7.2,6	Δ V Reserve Propellant	154,000
W7.11	Maximum P.U. Residual	41,700
Wv 2c	Vehicle Weight at Second-Stage Cutoff	2,038,200
W8	Second-Stage Propellant	8,064,000
Wv 2i	Vehicle Weight at Second-Stage Ignition	10,102,200
W9	Second-Stage Weight Loss During Sep./Start	44,900
Ws 1c	FIRST-STAGE WEIGHT AT BURNOUT	3,093,870
Ws 1d	Stage Dry Weight	3,000,870
W7	Unused Propellant and Slivers	93,000
Wv 1c	Vehicle Weight At First-Stage Burnout	13,240,970
W8	First-Stage Propellant	24,820,960
Wv 1L	Vehicle Weight at Liftoff	38,061,930

*W7, less 7.2, 7.6, and 7.11

Table 3.2.9-14

VEHICLE WEIGHT STATEMENT

Escape Payload Vehicle

	Payload (Escape)	466,000
Ws 3c	ESCAPE-STAGE AT CUTOFF	69,000
Ws 3d	Stage Dry Weight	46,290
W7*	Unusable Propellants and Gases	4,110
W7.2,6	Δ V Reserve Propellant	15,000
W7.11	Maximum P.U. Residual	3,600
Wv 3c	Vehicle Weight at Escape-Stage Cutoff	535,000
W8	Escape-Stage Propellant	630,000
Ws 2c	SECOND-STAGE WEIGHT AT CUTOFF	873,200
Ws 2d	Stage Dry Weight	596,450
W7*	Unusable Propellant and Gases	81,050
W7.2,6	Δ V Reserve Propellant	154,000
W7.11	Maximum P.U. Residual	41,700
Wv 2c	Vehicle Weight at Second-Stage Cutoff	2,038,200
W8	Second-Stage Propellant	8,064,000
Wv 2i	Vehicle Weight at Second-Stage Ignition	10,102,200
W9	Second-Stage Weight Loss During Sep./Start	44,900
Ws 1c	FIRST-STAGE WEIGHT AT BURNOUT	3,093,870
Ws 1d	Stage Dry Weight	3,000,870
W7	Unused Propellant and Slivers	93,000
Wv 1c	Vehicle Weight at First-Stage Burnout	13,240,970
W8	First-Stage Propellant	24,820,960
Wv 1L	Vehicle Weight at Liftoff	38,061,930

*W7, less 7.2, 7.6, and 7.11

Table 3.2.9-15

SEMIDETAILED WEIGHT STATEMENT
SOLID PROPELLANT FIRST STAGE

T65D Vehicle

W3	STRUCTURE			2,380,930
	3.4	Solid Propellant Container		1,892,490
		3.4.1	Cylinder	1,488,700
		3.4.4	Forward Bulkhead	46,200
		3.4.5	Y-Rings	83,400
		3.4.6	Nozzle Boss	24,120
		3.4.8	Container Wall Liner	39,500
		3.4.9	Forward Bulkhead Insulation	14,600
		3.4.15	Aft Bulkhead	40,260
		3.4.16	Aft Bulkhead Insulation	81,550
		3.4.18	Cylinder Extensions	36,960
		3.4.26	Miscellaneous	37,200
	3.6	Structure Forward of Tanks		326,600
		3.6.1	Forward Interstage	145,000
		3.6.11	Cluster Structure	181,600
			3.6.11.1 Rings and Outer Ties	42,180
			3.6.11.2 Cross Beams	16,300
			3.6.11.3 Intercostals	4,100
			3.6.11.4 Motor Case Extensions	118,500
			3.6.11.5 Aft Ties	520
	3.8	Structure Aft of Propellant Containers		127,600
		3.8.11	Aft Support Structure	125,500
		3.8.12	Aft Aerodynamic Fairing	2,100
	3.14	Base Heat Protection		10,940
	3.26	Miscellaneous		23,300
W4	PROPULSION SYSTEM			587,570
	4.2	Nozzle (Gimbaled)		562,000
		4.10.1	Thrust-Vector-Control Hardware	14,470
			4.10.1.1 Support Structure	700
			4.10.1.2 Power Unit	7,770
			4.10.1.3 Actuators	6,000
	4.26	Miscellaneous		11,100

Table 3.2.9-16

SEMIDETAILED WEIGHT STATEMENT
SOLID PROPELLANT FIRST STAGE

T65D Vehicle

W6	EQUIPMENT AND INSTRUMENTATION		32,370
	6.1	Support Structure	500
	6.2	Environmental Control System	400
	6.5	Control System Electronics	
	6.7	Navigation and Tracking	
	6.8	Telemetering and Measuring	660
	6.11	Electrical System	3,160
	6.12	Range Safety	750
	6.17	Separation System	26,900
		6.17.1 Mounting Hardware	5,400
		6.17.2 Rocket Cases	21,000
		6.17.5 Explosive Devices	500
Ws 1d	DRY STAGE		3,000,870
W7	RESIDUAL PROPELLANTS AND SERVICE ITEMS		93,000
		7.9.13 Separation System Propellants	33,000
	7.11	Solid Propellant Slivers (Inert)	60,000
Ws 1c	STAGE WEIGHT AT CUTOFF		3,093,870
W8	PROPELLANT CONSUMPTION		24,820,960
	8.1	Solid Propellant	24,820,000
	8.4	TVC Drive Propellant	960
Ws 1g	STAGE WEIGHT AT GROUND IGNITION		27,914,830
Ws 1f	STAGE MASS FRACTION, λ'		0.8892

Table 3.2.9-16 (Cont.)

SEMIDETAILED WEIGHT STATEMENT
LO_2/LH_2 SECOND STAGE

T65D Vehicle

W3	STRUCTURE		465,150
	3.1	LH_2 Container	150,650
		3.1.1,2 Skin, including Stiffening	98,100
		3.1.4 Forward Bulkhead	16,810
		3.1.5 Aft Bulkhead	17,740
		3.1.10 Container Wall Insulation, Outer	4,400
		3.1.12 Forward Bulkhead Insulation, Outer	1,600
		3.1.14 Aft Bulkhead Insulation, Outer	1,600
		3.1.15 Antislosh Devices	6,000
		3.1.26 Miscellaneous	4,400
	3.2	LO_2 Container	88,000
		3.2.4 Forward Bulkhead	37,100
		3.2.5 Aft Bulkhead	44,900
		3.2.15 Antislosh Devices	3,500
		3.2.26 Miscellaneous	2,500
	3.6	Structure Forward of Tanks	22,000
	3.7	Structure Between Tanks	77,200
	3.8	Structure Aft of Tanks	37,000
	3.9	Thrust Structure	74,200
		3.9.1 Skin and Stiffening	40,400
		3.9.2 Longerons	3,840
		3.9.3 Beams	12,500
		3.9.26 Miscellaneous	17,400
	3.14	Base Heat Protection	4,000
	3.26	Miscellaneous	12,100
W4	PROPULSION SYSTEM AND ACCESSORIES		122,390
	4.1	Engines and Accessories	100,000
	4.7	Fuel System	12,175
		4.7.3 Fill and Drain System	400
		4.7.4 Distribution System	8,750
		4.7.7 Vent System	150
		4.7.8 Tank Pressurization System	1,400
		4.7.10 Antivortex Devices	125
		4.7.26 Miscellaneous	1,350

Table 3.2.9-17

SEMIDETAILED WEIGHT STATEMENT
LO_2/LH_2 SECOND STAGE

T65D Vehicle

	4.8	Oxidizer System	8,215
	4.8.3	Fill and Drain System	400
	4.8.4	Distribution System	5,850
	4.8.7	Vent System	150
	4.8.8	Tank Pressurization System	800
	4.8.10	Antivortex Devices	125
	4.8.26	Miscellaneous	890
	4.10	Control System Hardware (TVC)	2,000
W6		EQUIPMENT AND INSTRUMENTATION	8,910
	6.1	Support Structure	510
	6.2	Environmental Control System	250
	6.8	Telemetering and Measuring	790
	6.10	Propellant Utilization System	150
	6.11	Electrical System	3,200
	6.12	Range Safety	160
	6.17	Separation System	850
	6.17.1	Mounting Hardware	130
	6.17.2	Rocket Cases	420
	6.17.5	Explosive Devices	300
	6.18	Ullage System (Attachment Provisions)	3,000
Ws 2d		DRY STAGE	596,450
W7		RESIDUAL AND RESERVE PROPELLANTS	276,750
	7.1	LH_2 Pressurants	11,900
	7.2	LH_2 for ΔV Reserves	25,600
	7.3	LH_2 for Thrust Decay	2,100
	7.4	LH_2 Trapped	6,350
	7.4.3	In Lines	4,500
	7.4.6	In Engine	1,850
	7.5	LO_2 Pressurants	30,000
	7.6	LO_2 for ΔV Reserves	128,400

Table 3.2.9-17 (Cont.)

SEMIDETAILED WEIGHT STATEMENT
LO_2/LH_2 SECOND STAGE

T65D Vehicle

	7.7	LO_2 for Thrust Decay	10,400
	7.8	LO_2 Trapped	16,150
		7.8.3 In Lines	12,000
		7.8.6 In Engines	4,150
	7.9	Retrorocket Propellant	950
	7.11	Maximum Propellant Utilization Residual (LO_2)	41,700
	7.26	Miscellaneous	3,200
Ws 2c	STAGE WEIGHT AT CUTOFF		873,200
W8	PROPELLANT CONSUMPTION		8,064,000
	8.1	LH_2	1,357,950
	8.2	LO_2	6,706,050
Ws 2i	STAGE AT IGNITION		8,937,200
W9	WEIGHT LOSS PRIOR TO IGNITION		44,900
	9.1	Fuel for Start	1,300
	9.2	Oxidizer for Start	6,500
	9.3	Ullage System Propellants	29,600
	9.7	Ullage Rocket Cases	7,500
Ws 2s	STAGE AT SEPARATION		8,982,100
	STAGE MASS FRACTION, λ' *		0.9025

* $\lambda' = \frac{\text{Propellant Consumption}}{\text{Stage Weight at Ignition}}$

Table 3.2.9-17 (Cont.)

SEMIDETAILED WEIGHT STATEMENT
ORBIT TRANSFER STAGE

T65D Vehicle

W3	STRUCTURE		9,900
	3.1	Aerozine-50 Container	1,900
		3.1.4 Forward Bulkhead	840
		3.1.5 Aft Bulkhead	840
		3.1.7 Support Structure Brackets	220
	3.2	N_2O_4 Container	1,550
		3.1.4 Forward Bulkhead	690
		3.1.5 Aft Bulkhead	690
		3.1.7 Support Structure Brackets	170
	3.6	Structure Forward of Tanks	5,410
	3.9	Thrust Structure	350
	3.14	Base Heat Protection	350
	3.17	Tank Support Structure	140
	3.26	Miscellaneous	200
W4	PROPULSION SYSTEM AND ACCESSORIES		6,065
	4.1	Engines and Accessories (including TVC)	1,700
	4.7	Fuel System	3,945
		4.7.1 Fill and Drain	15
		4.7.4 Distribution System	60
		4.7.7 Vent System	20
		4.7.8 Tank Pressurization System (including N_2O_4)	3,840
		4.7.10 Antivortex Devices	10
	4.8	Oxidizer System	110
		4.8.3 Fill and Drain System	15
		4.8.4 Distribution System	65
		4.8.7 Vent System	20
		4.8.8 Tank Pressurization (included in 4.7.8)	
		4.8.10 Antivortex Devices	10
	4.26	Miscellaneous	310
W6	EQUIPMENT AND INSTRUMENTATION		1,150
	6.1	Support Structure	85

Table 3.2.9-18

SEMIDETAILED WEIGHT STATEMENT
ORBIT TRANSFER STAGE

T65D Vehicle

	6.2	Environmental Control	30
	6.4	Guidance System	600
	6.8	Telemetering and Measuring	120
	6.11	Electrical System	100
	6.17	Separation System	215
		6.17.1 Mounting Hardware	5
		6.17.2 Rocket Cases	10
		6.17.5 Explosive Device	200
Ws 3d	DRY STAGE		17,115
W7	RESIDUAL AND RESERVE PROPELLANTS		3,285
	7.1,5	Residual Propellants	600
	7.2	Aerozine-50 for ΔV Reserves	800
	7.4	Aerozine-50 Trapped	30
	7.6	N_2O_4 for ΔV Reserves	1,600
	7.8	N_2O_4 Trapped	45
	7.9	Retrorocket Propellant	20
	7.11	Maximum Propellant Utilization Residual (N_2O_4)	120
	7.26	Miscellaneous	70
Ws 3c	STAGE WEIGHT AT CUTOFF		20,400
W8	PROPELLANT CONSUMPTION		74,600
	8.1	Aerozine-50	24,870
	8.2	N_2O_4	49,730
Ws 3i	STAGE WEIGHT AT IGNITION		95,000
Ws 3f	STAGE MASS FRACTION, λ'		0.7853

Table 3.2.9-18 (Cont.)

SEMIDETAILED WEIGHT STATEMENT
LO_2/LH_2 ESCAPE STAGE

T65D Vehicle

W3	STRUCTURE		33,370
	3.1	LH_2 Container	8,640
		3.1.4 Forward Bulkhead	3,330
		3.1.5 Aft Bulkhead	3,810
		3.1.12 Forward Bulkhead Insulation, Outer	550
		3.1.14 Aft Bulkhead Insulation, Outer	550
		3.1.15 Antislosh Devices	200
		3.1.26 Miscellaneous	200
	3.2	LO_2 Container	3,170
		3.2.4 Forward Bulkhead	870
		3.2.5 Aft Bulkhead	2,050
		3.2.15 Antislosh Devices	150
		3.2.26 Miscellaneous	100
	3.6	Structure Forward of Tanks	5,050
	3.7	Structure Between Tanks	2,230
	3.8	Structure Aft of Tanks	11,170
	3.9	Thrust Structure	1,750
	3.14	Base Heat Protection	600
	3.26	Miscellaneous	760
W4	PROPULSION SYSTEM AND ACCESSORIES		11,160
	4.1	Engines and Accessories	9,300
	4.7	Fuel System	680
		4.7.3 Fill and Drain System	100
		4.7.4 Distribution System	320
		4.7.7 Vent System	50
		4.7.8 Tank Pressurization System	100
		4.7.10 Antivortex Devices	20
		4.7.26 Miscellaneous	90
	4.8	Oxidizer System	550
		4.8.3 Fill and Drain System	100
		4.8.4 Distribution System	210

Table 3.2.9-19

SEMIDETAILED WEIGHT STATEMENT
LO_2/LH_2 ESCAPE STAGE

T65D Vehicle

	4.8.7	Vent System	50
	4.8.8	Tank Pressurization System	100
	4.8.10	Antivortex Devices	20
	4.8.26	Miscellaneous	70
4.10	Control System Hardware (TVC)		630
W6	EQUIPMENT AND INSTRUMENTATION		1,760
6.1	Support Structure		60
6.2	Environmental Control System		50
6.4	Guidance System		600
6.8	Telemetering and Measuring		140
6.10	Propellant Utilization System		50
6.11	Electrical System		200
6.17	Separation System		250
	6.17.1	Mounting Hardware	10
	6.17.2	Rocket Cases	40
	6.17.5	Explosive Devices	200
6.18	Ullage System (Attachment Provisions)		410
Ws 3d	DRY STAGE		46,290
W7	RESIDUAL AND RESERVE PROPELLANTS		22,710
7.1	LH_2 Pressurants		980
7.2	LH_2 for ΔV Reserves		2,500
7.3	LH_2 for Thrust Decay		5
7.4	LH_2 Trapped		380
	7.4.3	In Lines	330
	7.4.6	In Engine	50
7.5	LO_2 Pressurants		1,470
7.6	LO_2 for ΔV Reserves		12,500
7.7	LO_2 for Thrust Decay		25
7.8	LO_2 Trapped		990
	7.8.3	In Lines	770
	7.8.6	In Engines	220

Table 3.2.9-19 (Cont.)

SEMIDETAILED WEIGHT STATEMENT
LO_2/LH_2 ESCAPE STAGE

T65D Vehicle

	7.9	Retrorocket Propellant	60
	7.11	Maximum Propellant Utilization Residual (LO_2)	3,600
	7.26	Miscellaneous	200
Ws 3c	STAGE WEIGHT AT CUTOFF		69,000
W8	PROPELLANT CONSUMPTION		630,000
	8.1	LH_2	106,170
	8.2	LO_2	523,830
Ws 3i	STAGE AT IGNITION		699,000
	STAGE MASS FRACTION, λ' *		0.9013

* $\lambda' = \frac{\text{Propellant Consumption}}{\text{Stage Weight at Ignition}}$

Table 3.2.9-19 (Cont.)

TANDEM VEHICLE SOLID PROPELLANT FIRST-STAGE WEIGHTS CRITERIA EVOLUTION

	Candidate Configuration T65A	Baseline T65C	Preliminary Design Vehicle T65D
No. of Motors/Diameter	6/260"	6/260"	6/260"
Total Thrust at Launch (10^6 lb)	53.1	54.9	56.3
Total Propellant Weight (10^6 lb)	24.9	24.82	24.82
Nominal Chamber Pressure (psi)	600	698	698
MEOP (psi)	720	804	804
Grain Cross-Sectional Loading, η_{cs}	0.718	0.693	0.693
Motor Volumetric Loading, η_v	0.709	0.684	0.684
Case Material	4330 steel	18% Ni Marage Steel	18% Ni Marage Steel
Retrorocket Capability	5 g's for 1 second plus 2 g's for 2 seconds	0.5 g for 3 seconds	1 g for 2 seconds
Slivers	extrapolated from task I	inert	inert

Table 3.2.9-20

TANDEM VEHICLE LO_2/LH_2 SECOND-STAGE WEIGHTS CRITERIA EVOLUTION

	Parametric Vehicle	Candidate Configuration T65A	Baseline T65C	Preliminary Design Vehicle T65D
Engines	5 M-1 at 1.5×10^6 lb. thrust	5 M-1 at 1.5×10^6 lb. thrust	5 M-1 at 1.5×10^6 lb. thrust	5 M-1 at 1.5×10^6 lb. thrust
Tank Configuration	nested tanks	nested tanks	separate tanks	separate tanks
Tank Material/Construction	2219-T87 aluminum/waffle	2219-T87 aluminum/waffle	2219-T87 aluminum/waffle	2219-T87 aluminum/waffle
Tank Material Allowable Yield Strength	55,000 (avg. at cryogenic temp)	55,000 (avg. at cryogenic temp)	function of temp at design condition	function of temp at design condition
Tank Sidewall Design Criterion	ground wind	0.4 psi overpressure	20° angle of attack at max q	proof test
Ullage Pressures, psi, (startburn/burnout)	LO_2 39/39 LH_2 36/36	45/29 43/39	45/29 43/39	43/27 38/35
Pressurization concept	Bleed	Bleed	Bleed	Bleed
Ullage gas mean temperature at burnout (°R)	LO_2 270 LH_2 160	270 160	270 160	270 180
Ullage Rocket Capability	0.1 g for 3 seconds	0.1 g for 3 seconds	0.1 g for 3 seconds	0.1 g for 4.5 seconds
Retrorocket Capability	1.0 g for 3 seconds	1.0 g for 3 seconds	1.0 g for 3 seconds	0.1 g for 3 seconds
Separation Plane	Engine gimbal plane	Engine gimbal plane	24 feet forward of engine gimbal plane	24 feet forward of engine gimbal plane

Table 3.2.9-21

- Insulation — No insulation is required on the LO_2 tank. The LH_2 tank insulation requirement is approximately 0.12 inch on the forward and aft bulkheads and 0.08 inch on the cylindrical sidewall.
- Propellant Loading/Utilization System — The open-loop, on-loaded fuel P.U. system requires no flow metering or control devices. It does, however, require a system to determine the tank loading at launch. The weight includes provision for level sensors and temperature probes, a stillwell, and the necessary wiring and support structure.
- Propellant Utilization Residual — The propellant required by the propellant utilization concept is:

  Maximum residual (2σ) = 41,700 pounds

  On-loaded fuel = 16,750 pounds

  The propellant required by performance for the nominal mission is 8,064,000 pounds. The propellant loaded at the loading mixture ratio is:

  8,064,000 pounds required propellant consumption

  \- 16,750 LH_2 on-load

  8,047,250 pounds

  \+ 41,700 Maximum residual

  8,088,950 pounds Total LO_2/LH_2 for nominal mission at loading mixture ratio

  Note that this system ensures the burning of 16,750 pounds of propellant in addition to the 8,047,250 pounds, and the 16,750 pounds burned may be either all LH_2 or a combination of LO_2/LH_2 out of the 41,700 pounds on-loaded. The maximum residual may be either all LO_2, all LH_2, or a combination at any mixture ratio.

Orbital Transfer Stage — The orbital transfer stage consists of a pair of N_2O_4/Aerozine-50 pressure-fed engines, 74,000 pounds of propellant, associated tankage, and hardware. The guidance package for the entire vehicle is contained in the transtage area. Included is 48 inches of cylindrical interstage to which the propulsion units are fixed. The weights criteria and ground rules are unchanged from Table 3.2.9-10.

Escape Stage — The escape stage is LO_2/LH_2 third stage powered by three J-2 engines. Analysis methods are generally the same as those for the second stage. Criteria and ground rules are listed in Table 3.2.9-22.

LO_2/LH_2 ESCAPE-STAGE WEIGHTS CRITERIA

Engines	3 J-2
Propellant Weight (including 15,000-pound ΔV Reserve)	645,000 pounds
Tankage	0.8 b/a ellipsoids
Tank Material	2219-T87 aluminum
Tank Construction	Zonal Sections
LO_2 Tank Diameter (feet)	13
LH_2 Tank Diameter (feet)	40
Limit Ullage Pressure (psia)	LO_2: 35 LH_2: 35
Pressure Design Requirement	Proof Test
Pressurization Concept	Bleed
Mean Gas Temperature at Burnout	GH_2: 160°R GO_2: 270°R
Ullage Rocket Capability	0.1 g for 4.5 seconds
Retrorocket Capability	0.1 g for 3 seconds
Reserve Velocity Capability	3.5 percent of (ΔV_{escape} - $\Delta V_{225\text{-km orbit}}$)

Table 3.2.9-22

BLANK

3.2.10 Environment and Control

3.2.10.1 Environmental Requirements

3.2.10.1.1 First-Stage Solid Motor

Solar Radiation — The vehicle will be assembled in a sheltered "launch building" providing adequate solar shielding during assembly.

Humidity — Motor cavity relative humidity will be controlled to below 60 percent at 60°F and 45 percent at 80°F.

Temperature — Temperature decay rates from the time of propellant curing to launch time using natural or forced cooling (or both) were established using a mathematical model that assumed a circular port of equal cross-sectional area as the star-port area.

Propellant cure temperature was assumed to be 140°F. The analysis starts after propellant has cured. The motor is cooled only on the exterior with 15 fps, 80°F ambient air for 1 month. At this time, the cavity wall temperature is 96.6°F and the outer-case propellant is at 80.49°F.

The motors are fitted with their respective hardware during the next month. The first motor is held until all six are fitted, assuming a production rate of six motors per month. The motors are then moved to the launch building where they will remain for 4 months for vehicle assembly and launch operations.

Considering the 4 months on the launch pad, two modes of motor cooling were analyzed. In the first mode, forced air was used to cool the cavity, and natural convection cooled the motor exterior. In the second mode, only the motor exterior was cooled, again by natural convection. The resulting temperature differences in the motor cavity are shown below for the first and last motor produced for that stage.

Cavity cooled	Cavity not cooled
Exterior natural convection	Exterior natural convection
Δ Temperature = 0.002°F	Δ Temperature = 0.601°F

Figures 3.2.10-1 and -2 show the temperature profiles for the first and last motors of the production run being cooled in the above modes. Cavity cooling was assumed in the motor variance study.

A temperature difference of 0.601°F between motors will result in an initial thrust difference of 0.06 percent; therefore, it is concluded that no cavity cooling during assembly on the launch pad is required on a motor variance basis. Temperature profiles influencing motor web time thrust were beyond the scope of this study.

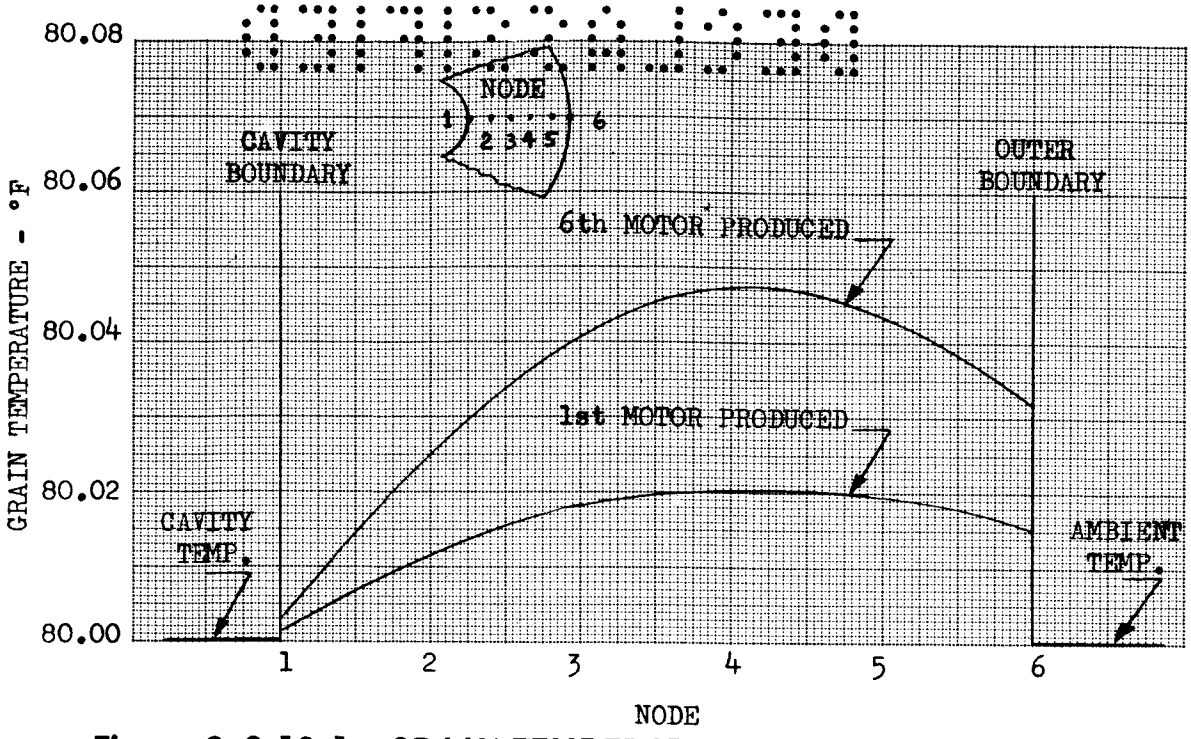

Figure 3.2.10-1 GRAIN TEMPERATURE PROFILE AT LAUNCH
Cavity Cooled During Assembly

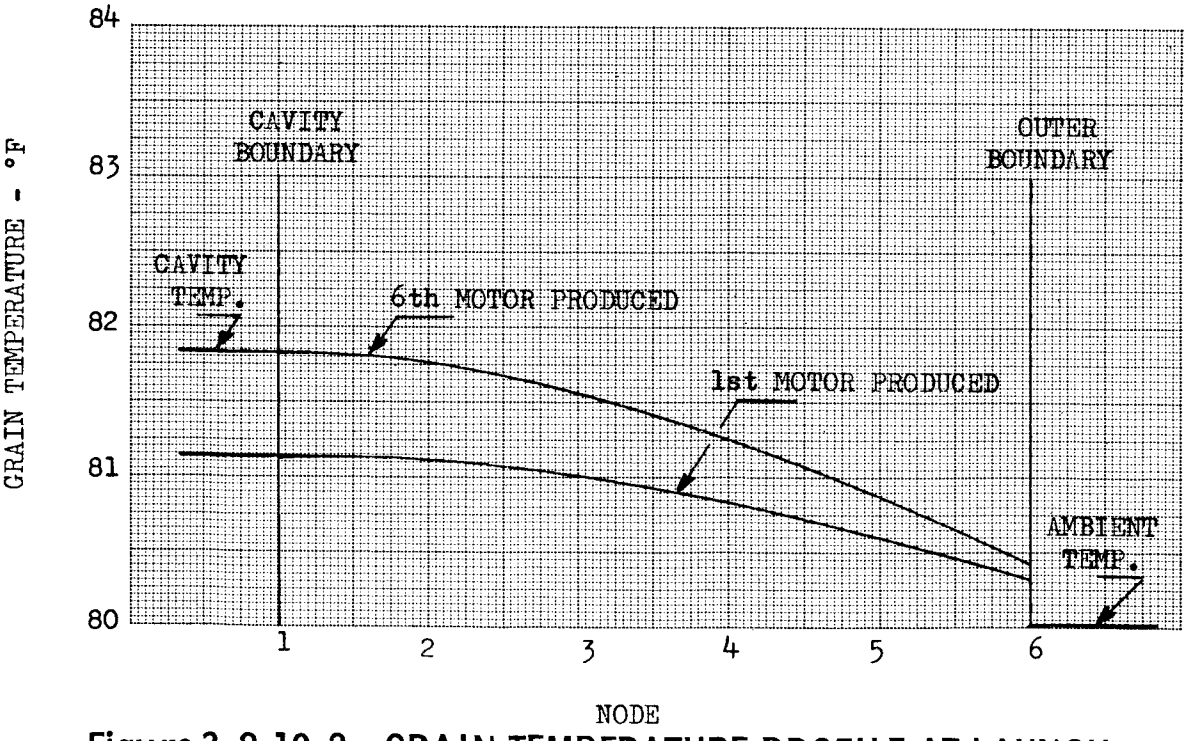

Figure 3.2.10-2 GRAIN TEMPERATURE PROFILE AT LAUNCH
Cavity Not Cooled During Assembly

3.2.10.1.2 Upper Stages

Detailed examination of the environment control requirements was beyond the scope of this study. However, certain operational hazards can be identified with liquid hydrogen that will impose insulation or conditioning requirements on specific areas of the vehicle. Hydrogen tankage and fill lines must either be insulated sufficiently to prevent condensation of liquid air or oxygen, or exposed only to a noncondensable atmosphere.

Conditioning requirements for LO_2/LH_2 engines are now evolving in the Saturn S-IV and S-II programs. Insufficient data are now available to define the M-1 engine requirements. However, several conditioning methods appear feasible:

- A warm engine installation, with propellant prevalves located sufficiently far upstream to prevent filled LO_2 or LH_2 line exposure to the atmosphere. Such an installation would require an in-flight chilldown cycle of several seconds late in the first-stage operating period. However, it would require no conditioning on the launch pad.
- A chilled system, with provisions for propellant recirculation around the turbopump. Effectively, this system will require no chilldown in flight, but would require extensive insulation or helium purging on the pad. Where feasible, this approach is considered the more desirable, since the chilldown can be monitored as another countdown function and any malfunction corrected.

The second-stage engine compartment, located over the open first-stage motor cluster, is difficult to insulate or purge efficiently. For this reason, it is tentatively proposed to use the warm-system approach and an in-flight chilldown for that stage.

The second-stage intertank cavity should be continuously purged with low pressure nitrogen or helium and a pressure relief provided to prevent overpressurization of the compartment. The lower head of the hydrogen tank is sufficiently insulated to prevent liquefaction of air (see 3.2.10.5.2).

No environment control is required for the transtage propulsion systems.

The escape-stage engine compartment should be sealed, vented, and purged with helium. The J-2 engines should be chilled on the pad, and a propellant recirculation system should be provided. The compartment should be vented during flight at a rate sufficient to prevent compartment pressurization during flight and slow enough to prevent ambient air entry.

The payload hydrogen tankage will require insulation or other means to prevent liquid oxygen or air from freezing on the tankage surface.

3.2.10.1.3 Atmospheric Contamination

The large volume of combustion gases expelled from the T65 vehicle during first-stage burning provide a potential source of atmospheric contamination. The gases are highly toxic, as indicated by the composition for a typical solid propellant in Table 3.2.10-1. The quantity of gas generated, in terms of time and altitude, is shown in Table 3.2.10-2. The volume of gas shown was calculated at 77°F and would, in practice, be several times greater because of its high temperature. A large vortexing gas cloud will rise through the atmosphere because of low gas density. Although some heat will be lost to the surrounding atmosphere by radiation, this loss will tend to be compensated by condensation within the rising cloud. Thus, the gas cloud will expand nearly adiabatically as it rises. The cloud would rise until its density equaled that of the surrounding atmosphere. This should occur at an altitude of slightly over 10 kilometers —near the top of the troposphere.

The extent of the atmospheric pollution problem will depend largely on the environmental conditions at any given time. With the planned testing of 260-inch-diameter development motors, additional data on atmospheric contamination will be accessible and should be gathered. The contamination requires further study in terms of corrosion protection necessary for ground equipment, cloud dissipation, and the weather conditions required to avoid precipitation scavenging of hydrogen chloride.

COMBUSTION PRODUCTS FOR A TYPICAL SOLID NOVA PROPELLANT
Each pound of propellant when burned yields 0.335 pounds of Al_2O_3 with a particle size of approximately 3 to 5 microns.
Each pound of propellant burned yields 0.665 pounds of gas having the following composition:
CO 36.72 wt %
CO_2 4.77
HCl 31.47
N_2 12.26
H_2O 11.57
H_2 3.48
The gas has an average molecular weight of 30.08 (air = 28.97).
The density at 77°F, 1 atm. = 0.0794 lb/ft^3 (air = 0.0765).
Temperature of gas when exhausted = 2359°C.

Table 3.2.10-1

EXHAUST GAS GENERATED BY SOLID FIRST STAGE
Vehicle T65C

Time (seconds)	Altitude (feet)	Propellant burned (pounds)	Volume of gas exhausted* (cu. ft)
0-10	ground level	2,355,000	19,721,000
10-12	750-1100	471,000	3,944,000
12-14	1100-1500	471,000	3,944,000
14-16	1500-2000	471,000	3,944,000
16-18	2000-2600	471,000	3,944,000
18-20	2600-3200	471,000	3,944,000
20-25	3200-5200	1,177,000	9,856,000
25-30	5200-7700	1,177,000	9,856,000
30-35	7700-10700	1,177,000	9,856,000
35-40	10700-14400	1,177,000	9,856,000
40-50	14400-23700	2,356,000	19,729,000
50-60	23700-35700	2,356,000	19,729,000
60-70	35700-50600	2,356,000	19,729,000
70-80	50600-68800	2,356,000	19,729,000
80-90	68800-95500	2,356,000	19,729,000
90-100	95500-128100	2,356,000	19,729,000
100-105.4	128100-146100	1,271,000	10,650,000

* at 77°F, 1 atmosphere

Table 3.2.10-2

3.2.10.2 Base Protection

3.2.10.2.1 Introduction

Heating to the base region of most multinozzle rocket vehicles is of sufficiently high magnitude to cause structural failure unless adequate thermal protection is provided for the load-carrying structure. Numerous model tests of specific configurations and some full-scale flight tests have been conducted to determine the distributions and levels of heating in the base area. Theoretical methods for

predicting this heating have not proven successful, primarily due to the complexity of the three-dimensional flow fields involved. Thus, even though the causes for base heating are well known, an empirical approach based on past test data appears to be the best method for estimating base heating when conducting preliminary design studies.

A discussion of various parameters affecting the base heating of a vehicle using an aluminized solid propellant is given in Reference 1. This discussion applies to the first stage of the T65C vehicle where base heating is caused by both radiation from exhaust gases of the solid propellant and by convection as the exhaust gases recirculate through the base. The second stage differs from the first stage in that liquid propellants consisting of liquid oxygen and hydrogen are used for propulsion, and radiation from the M-1 rocket-engine exhaust plume resulting from these propellants may be neglected.

3.2.10.2.2 Determination of the Base Heating Rates

3.2.10.2.2.1 Radiation from the Exhaust Plumes to the Base Region

Radiation heating of the base region can be a significant portion of the total heat input if the exhaust gases are strong radiators. Examination of the exhaust products of the second-stage LO_2/LH_2 rocket engine shows that these products are very weak radiators. The effective emissivity of the plume of these products is so low that, for preliminary design studies, radiation to the base area of the second stage can be neglected. The plume of the first-stage aluminized solid propellant rocket contains alumina particles which are strong radiators. The emissivity of a large cloud of alumina approaches one and produces a high radiation flux when combined with the high temperatures of the particles. Thus, consideration must be given to radiant heating of the first-stage base area.

The radiation heat flux from the plume to a point in the base is calculated from

$$\dot{q} = \epsilon \sigma \ T_p^4 F_{12} A_1 \qquad (Btu/ft^2 sec)$$

where $\dot{q}$ = Radiation heat flux ($Btu/ft^2 sec$)

σ = Stephan-Boltzman Constant (4.8×10^{-13} $Btu/ft^2 sec\ °R^4$)

ϵ = Emissivity

T_p = Plume temperature (°R)

$F_{12}A_1$ = View factor

In general, the temperature of the alumina particles varies along the plume length, but sufficient measurements are not available to establish the temperature distribution. For preliminary design purposes, a few of the available measured radiation heating rates are combined with a suitable view factor and

the equivalent plume temperature is calculated. This temperature is then scaled to the rocket under consideration by use of the combustion temperature.

The view factor geometrically relates the relative positions of the radiating and receiving surfaces. The plume radiating surface is assumed conical. This assumption is supported by Minuteman experience. The receiving surface can be taken as a small area of interest in the base region. A computer program (Reference 2) was used to calculate the view factors for this type of geometric system and a radiation heating rate distribution over the base region was obtained.

The resulting radiation heating rates and distributions to the base heat shield and exterior of nozzles are shown in Figures 3.2.10-3 through 3.2.10-6. These data show that (1) the radiant heat rate to a particular point is constant, and (2) radiation is the sole form of base heating up to an altitude of 27,000 feet.

3.2.10.2.2.2 Convective Heating of the Base Region Due to Recirculated Exhaust Gases

Determination of Base Flow Regimes — As the vehicle rises, the drop in ambient pressure causes the exhaust plumes to expand. Their intersection causes a shock wave, which forces a portion of the boundary layers of the plumes to flow back toward the base. The amount of reversed flow is affected by the ambient pressure until the flow chokes (i.e., sonic speed reached at a minimum area). At this time, the reverse flow becomes constant and is independent of the ambient pressure.

The method of Geothert (see Reference 3) was used to determine the flow regimes. The second stage operates at an altitude where there is always "choked" reversed flow; thus, no change occurs in the heating rate with altitude. The first-stage base flow consists of periods of ambient flow over the base, the onset of reversed plume gas flow, and the fully "choked" reversed flow. Since Goethert's results were for a four-nozzle configuration, a correction was made for the six-nozzle first stage in determining the altitudes that bound the various flow regimes. The results are:

- Ambient flow over the base up to the onset of reversed flow at 27,000 feet.
- "Choked" flow occurs at 52,000 feet and continues until stage burnout.

Convective Heating Rates — First-stage convective heating rates in the fully reversed plume flow regime were estimated by the four methods used in Reference 1. When the base parameters of the T65C vehicle were used in these methods (corrections being made for the six-engine configuration), the resulting convection heating rates to the center of the base ranged from 100 to 600 Btu/ft^2sec. This large variation is in direct contrast to very small variation in results obtained on the 500K vehicle (Reference 1). The failure of the four methods to predict a similar heating rate is an indication that the base

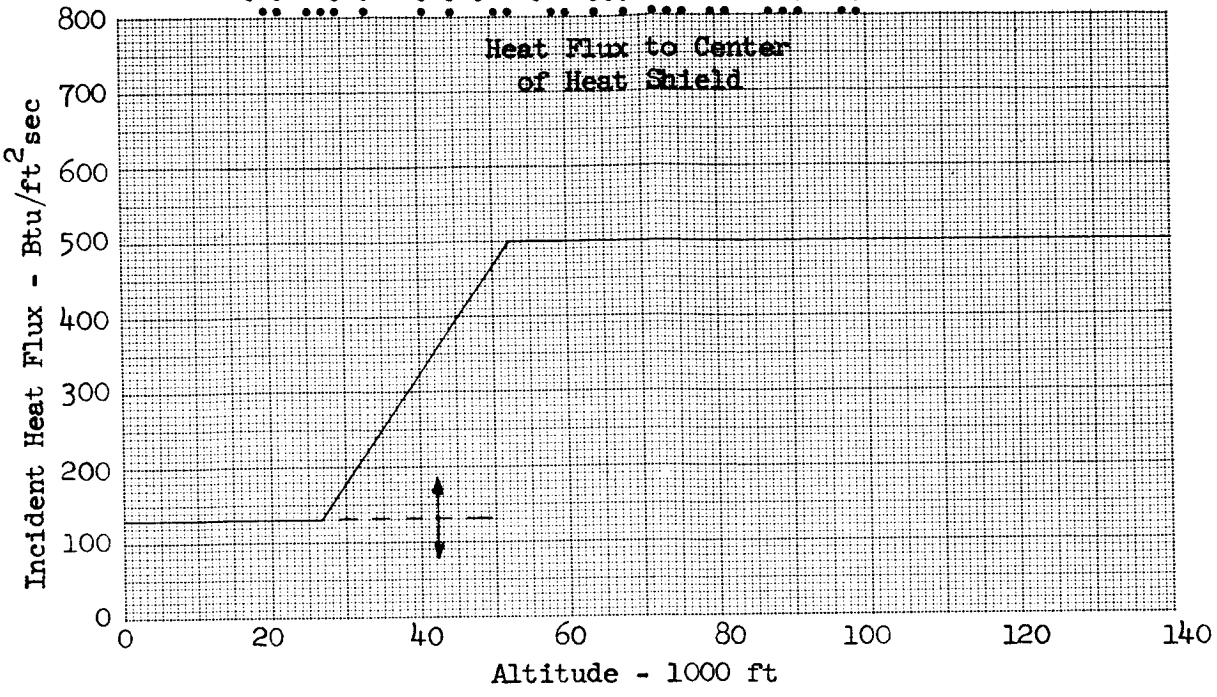

Figure 3.2.10-3 HEAT FLUX ESTIMATE FOR T65C FIRST-STAGE HEAT SHIELD

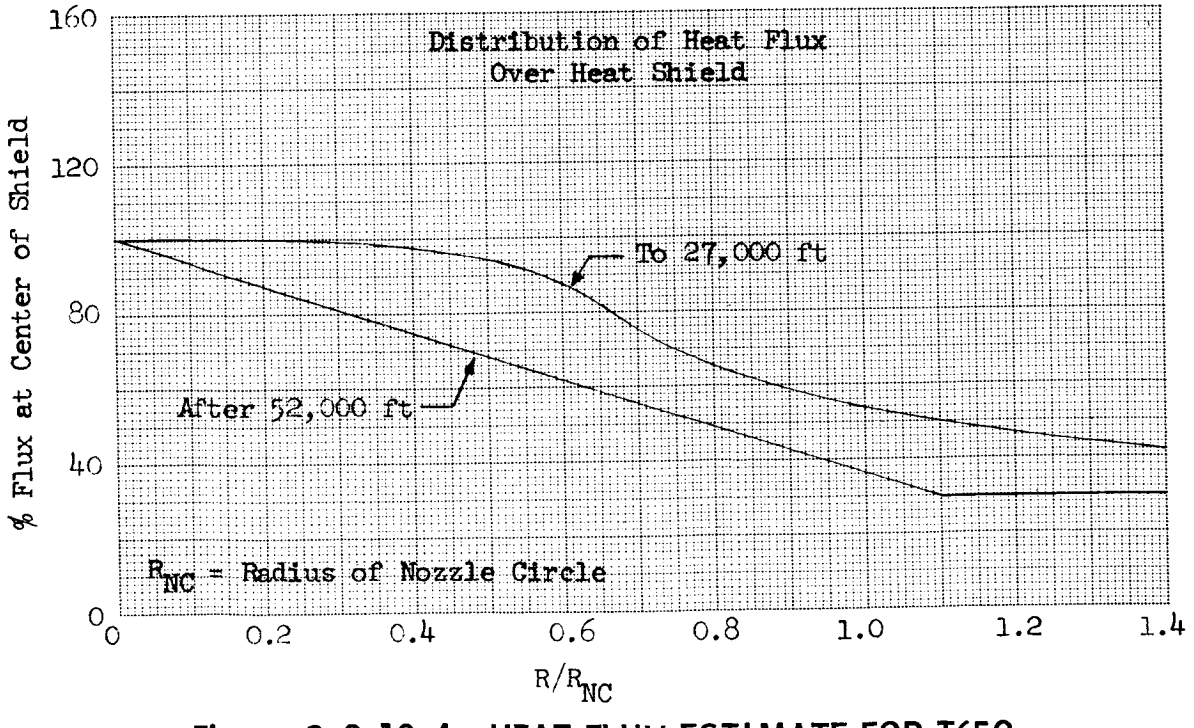

Figure 3.2.10-4 HEAT FLUX ESTIMATE FOR T65C FIRST-STAGE HEAT SHIELD

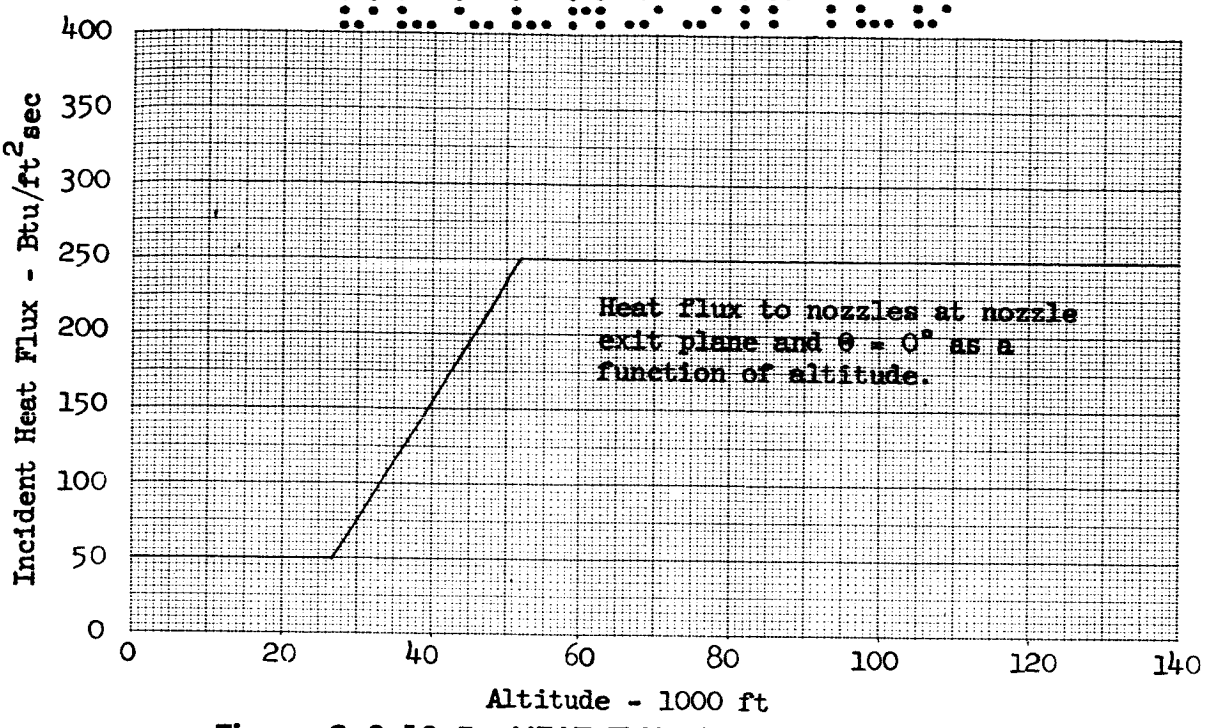

Figure 3.2.10-5 HEAT FLUX ESTIMATE FOR T65C
Exterior of First-Stage Nozzles

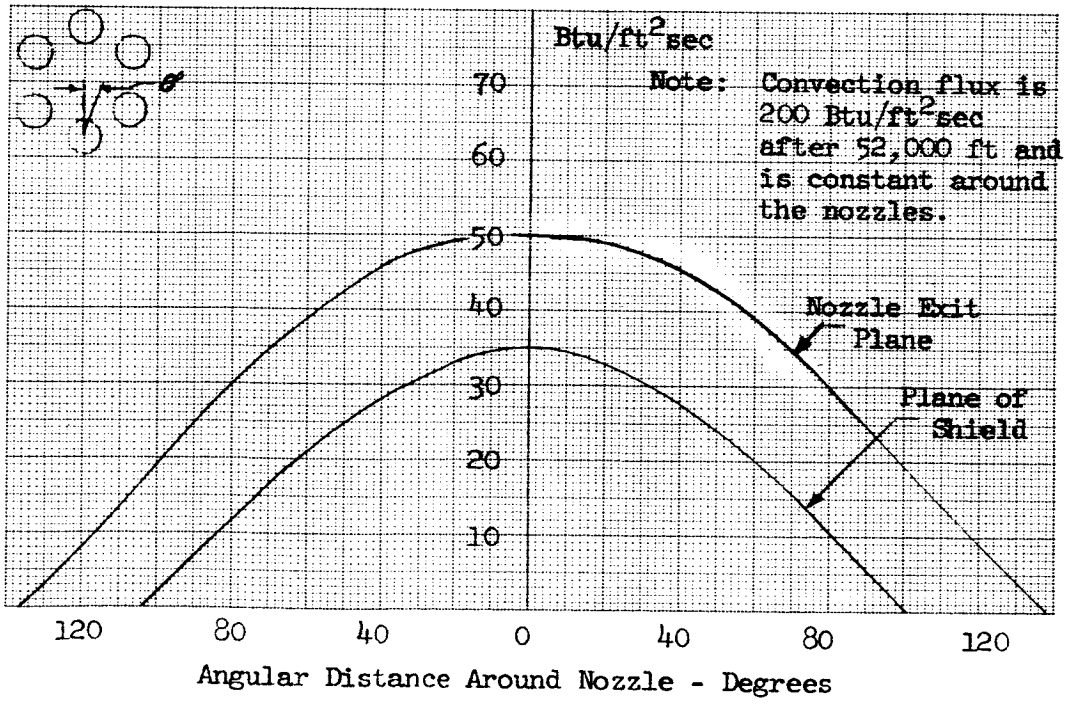

Figure 3.2.10-6 RADIATION HEAT FLUX TO NOZZLES

configuration of this vehicle presents problems beyond present prediction technology. Early model base heat testing of the base configuration is necessary to establish the convection heating rates.

For preliminary design purposes, a maximum convective heating rate to the base center of 370 Btu/ft^{2}sec* was assumed. The heating rate is based on a wall temperature of 520°R. This produces a total heating rate to the base center of 500 Btu/ft^{2}sec when combined with the radiation heating. This value is considerably higher than that measured on any operational vehicle and higher than the estimated rate for the Reference 1 vehicle. It is believed, though, to be realistic for this base configuration.

The maximum convective flux of 370 Btu/ft^{2}sec is for the choked-flow condition, which, as shown previously, occurs at 52,000 feet and continues until burnout. The heating magnitudes and distributions with base position are shown in Figures 3.2.10-3 through -6 as a function of altitude. These data are for the first stage.

The second-stage convection heating rate was determined from S-II base heating tests (see Reference 4). The tested configuration was quite close to the T65C vehicle second stage and the results were used directly. The heating rate will be constant over the burn time of the second stage. The heating distribution and rates are shown in Figure 3.2.10-7.

3.2.10.2.3 Base Thermal Protection

First Stage — Microballooned phenolic nylon (density = 30 lb/ft^3) was used to provide thermal protection of the first-stage base heat shield and nozzle skirts. This is a char forming plastic material having good ablation characteristics and fairly good insulation properties. The maximum load-carrying structural temperature was held to 200°F by providing sufficient ablation material to act as both an ablator and an insulator.

Other materials, such as NASA-designated M-31, were considered. Studies have shown, however, that microballooned phenolic nylon is an efficient material for providing thermal protection in the heating environment described in the preceding sections. The M-31 material is used on the base heat shield of the S-IC stage of the Saturn V vehicle. Very little data relative to its properties are available. Thus it is not known how this material would perform in the more severe thermal environment encountered by the base heat shield of the first stage of this vehicle.

---

* This value was chosen because it gives a total heating rate that agrees with extrapolated full-scale Polaris and Minuteman data.

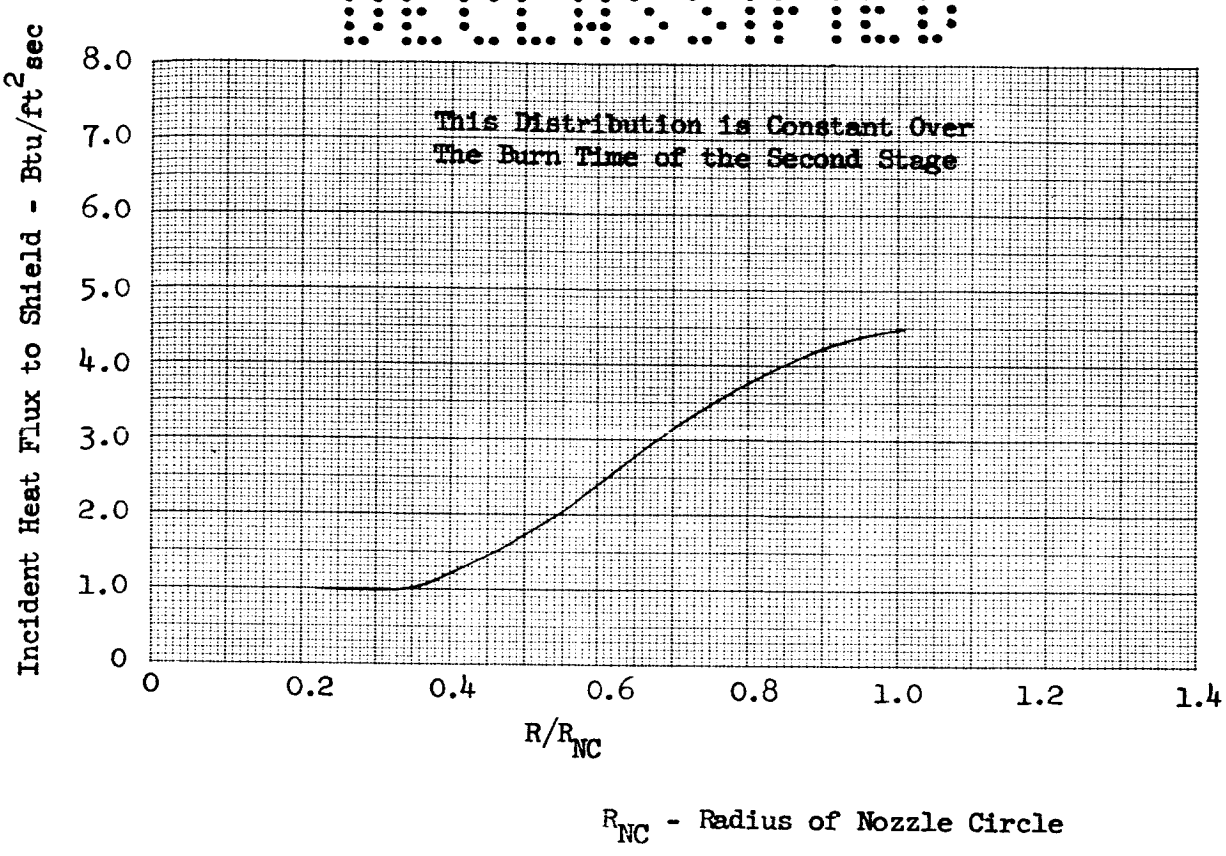

Figure 3.2.10-7 HEAT FLUX ESTIMATE FOR T65C SECOND-STAGE HEAT SHIELD

The thermal protection weights were determined by an IBM 7090 digital computer program. This program accounts for transient (1) char layer growth, (2) char surface temperature, and (3) mass loss rate, by solving a series of simultaneous equations. Transient heat conduction in the virgin plastic is accounted for by a system of finite difference equations. This results in temperature distributions throughout the ablation material.

The heating presented in 3.2.10.2.2 is primarily dissipated by (1) reradiation from the hot char surface temperature, (2) reflection of the radiant heat input, and (3) blockage of the convective heating by the injection of decomposition gases into the boundary layer. This results in a relatively small quantity of heat actually creating ablation and being conducted into the virgin plastic.

The resulting ablation material requirements are 0.58 inch at the heat shield outer edge and 0.78 inch at the center. The average ablation thickness on the interior of the nozzle skirts is 0.50 inch.

Second Stage — Maximum heating of the second-stage base area occurs at the outer edge of the heat shield (see Figure 3.2.10-7). This is due to the five-engine arrangement in which one of the engines is located in the center of the base.

The convective heating rate is rather low — a maximum of 4.5 Btu/ft^{2}sec. The long burn time, however, of the second stage (459 seconds) creates a substantial thermal protection requirement to maintain a maximum load-carrying structural temperature of 200°F.

The ablation requirements, using microballooned phenolic nylon, are 0.75 inch at the heat shield outer edge and 0.40 inch next to the interior engine.

3.2.10.3 External Heating

Heating of the boost vehicle while on the launch pad and during flight was examined to determine interstage temperatures and insulation requirements for the second-stage liquid hydrogen tank.

3.2.10.3.1 Heating While on the Launch Pad

Modes of heat transfer to the external tank wall while on the ground are radiation (solar) and convection. Solar radiation is considered of secondary importance and thus was neglected in this study. This is due to the availability of coatings having high emissivities and low absorptivities with respect to solar radiation.

Convective heating to the external hydrogen tank wall was investigated for free convection (no wind) and forced convection (definite wind). The primary ground conditions affecting convective heat transfer are air temperature, density, and wind velocity.

The heat transfer coefficient due to turbulence-free convection (no wind) to a vertical surface is given by:

$$h = 0.19 (T_{aw} - T_w)^{1/3}$$ (See Reference 5)

where h = Heat transfer coefficient (Btu/ft^{2}hr-°R)

T_{aw} = Adiabatic wall temperature (°R)

T_w = Wall temperature (°R)

The heat transfer coefficient due to forced convection created by the flow of air normal to a vertical surface is determined by:

$$N_{NU} = B \left(N_{RE}\right)^n$$ (See Reference 6)

where N_{NU} = Nusselt number, hD/k

N_{RE} = Reynolds number $DV\rho/\mu$

B = Reynolds factor

n = Reynolds number exponent

D = Diameter (feet)

V = Wind velocity (fps)

ρ = Air density (lb/ft^3)

μ = Viscosity of air (lb/ft-hr)

K = Thermal conductivity (Btu/ft-hr-°F)

Therefore, $h = \frac{BK}{D}\left(\frac{DV\rho}{\mu}\right)^n$

A 20-mph wind was selected as a reasonable design condition. Evaluating air properties at an average boundary layer temperature and taking B = 0.02 and n = 0.8 give the following heat transfer coefficient for the 70-foot-diameter tank.

$$h_v = 20 \text{ mph} = 2.52 \text{ Btu/ft}^2\text{hr °R}$$

3.2.10.3.2 Heating During Boost

Aerodynamic heating during boost was based on the thermal environment encountered in flying the trajectory given in Figure 3.2.10-8. Heat transfer coefficients to the sidewall of the tank were computed from the equation

$$h = 0.144\, K\, N_{PR}\, N_{RE}\, \frac{S}{X\,(\log_{10} N_{RE})\,2.45}$$

where K and N_{RE} are as defined in 3.2.10.3.1

S = Rubesin correction factor

X = Distance (feet)

N_{pr} = Prandtl number

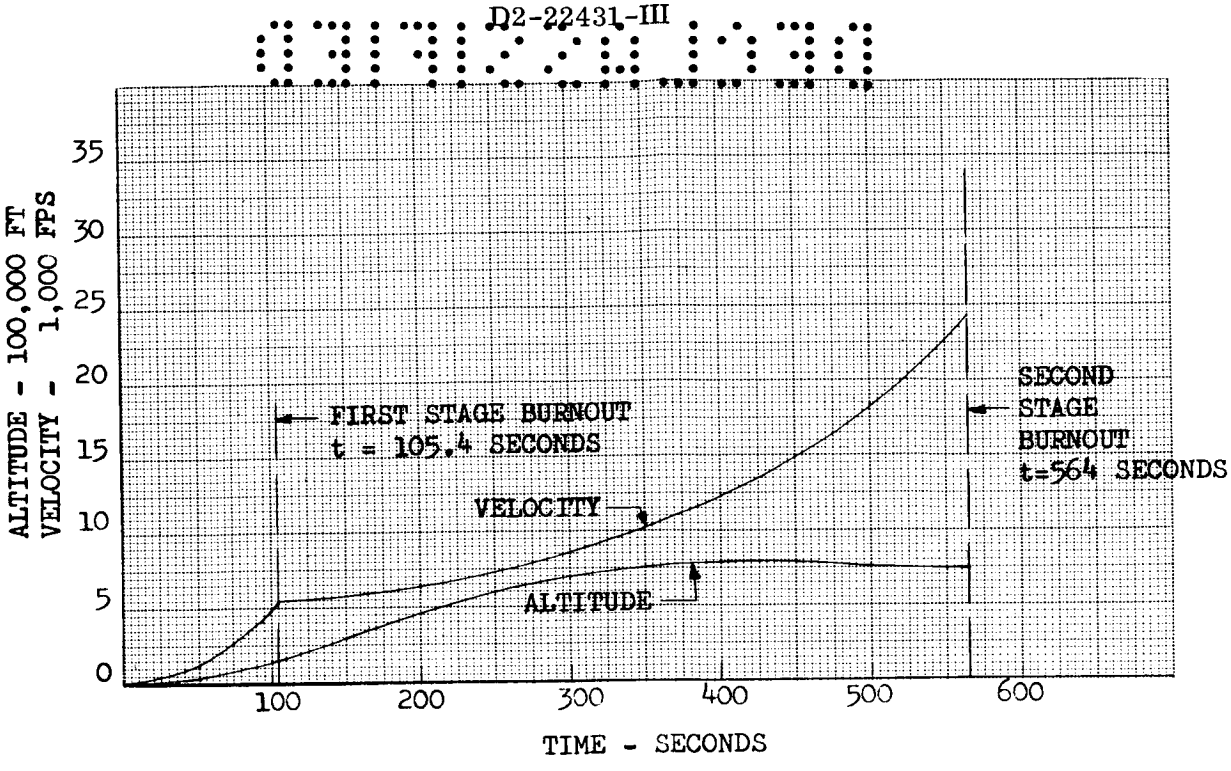

Figure 3.2.10-8 BOOST TRAJECTORY

The resulting heat transfer coefficients are given in Figure 3.2.10-9 for a wall temperature of 40°R and for an equilibrium wall temperature. These values are for turbulent flat-plate flow 180 feet from the nose.

Values of adiabatic wall temperature for the boost trajectory are presented in Figure 3.2.10-10.

3.2.10.4 Interstage

Temperatures occurring during boost flight are shown in Figure 3.2.10-11 for the interstage between the first and second stage, the intertank section of the second stage, and the interstage between the second stage and the payload.

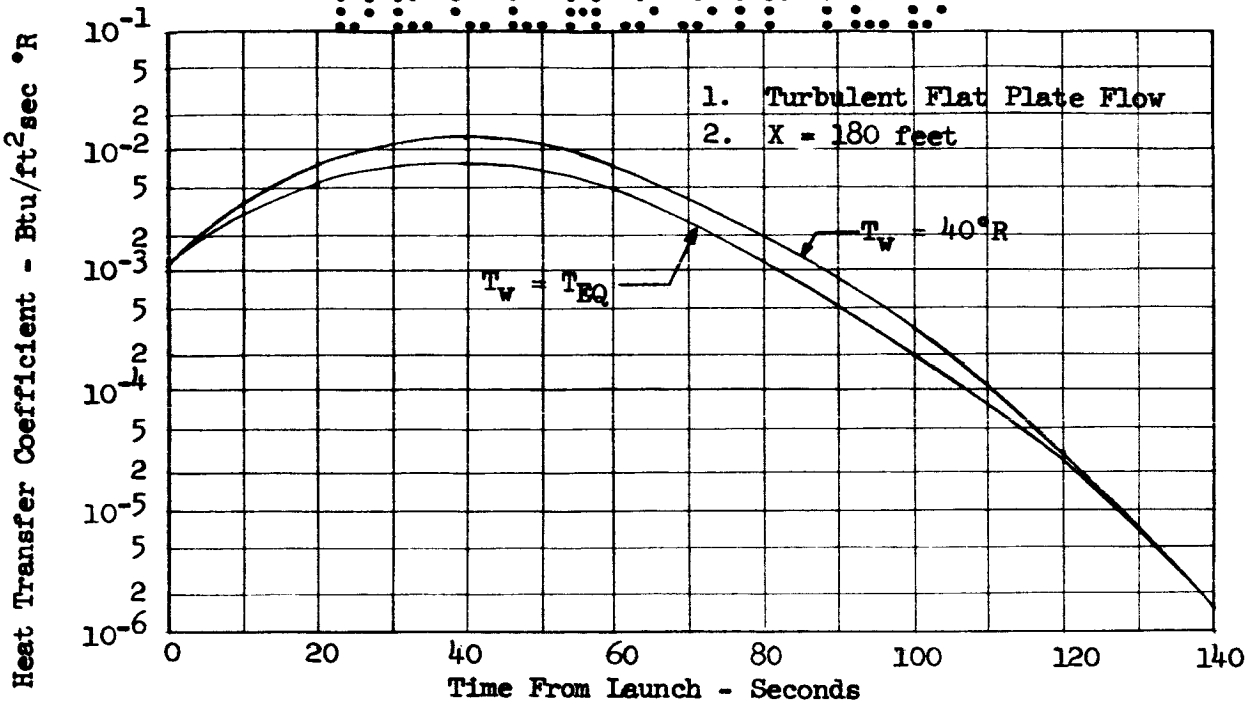

Figure 3.2.10-9 AERODYNAMIC HEAT TRANSFER COEFFICIENTS

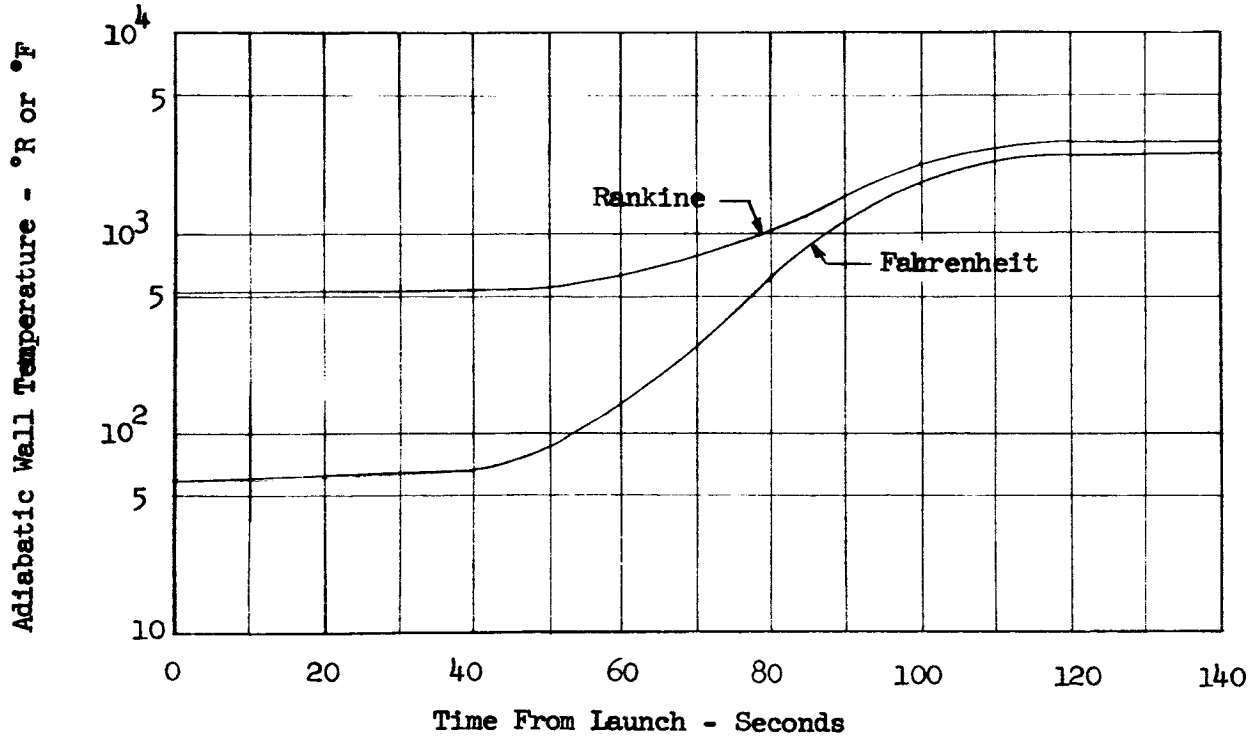

Figure 3.2.10-10 ADIABATIC WALL TEMPERATURE

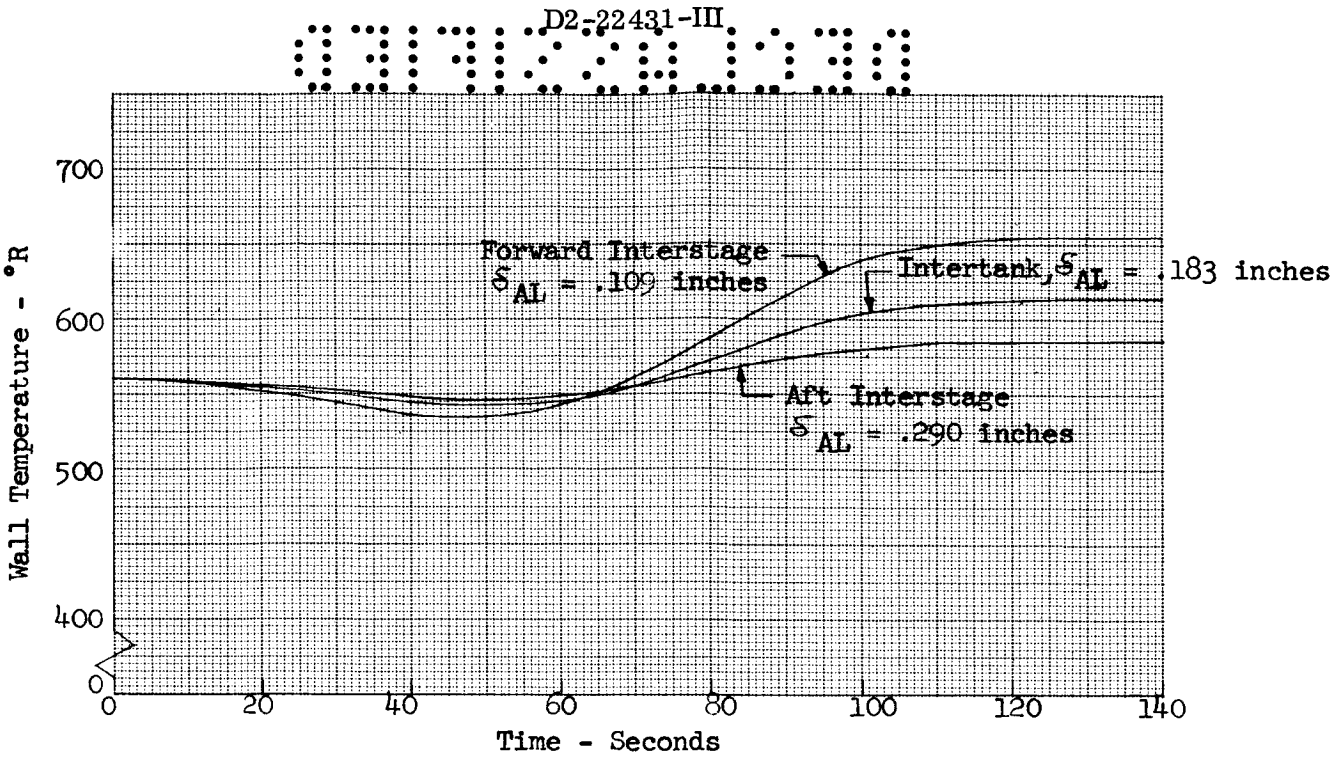

Figure 3.2.10-11 INTERSTAGE TEMPERATURE

These data are based on a transient analysis that accounts for the heat storage of the interstage walls and reradiation to space. Aerodynamic heat transfer coefficients shown in Figure 3.2.10-9 for $T_W = T_{eq}$ with appropriate corrections made for differences in distance from the nose and adiabatic wall temperatures given in Figure 3.2.10-10 were utilized in the analysis.

The variations in temperatures are due to differences in aluminum skin thicknesses. These differences, dictated by structural requirements for supporting loads encountered during boost, create substantial variations in the heat storage capability of the wall. This results in the temperature variations shown.

These data show that no insulation is required on the interstage or intertank section of the second stage.

3.2.10.5 Cryogenic Insulation

3.2.10.5.1 Introduction

Heat absorbed by an uninsulated second-stage liquid-hydrogen tank during first-stage flight produces excessive hydrogen boiloff. Thus, insulation is required on

the liquid hydrogen tank to minimize boiloff losses occurring during boost, and prevent liquefaction of air.

The latter requirement is necessary to reduce hazardous conditions around the launch pad.

Insulation requirements were optimized for flight conditions, since the design objective is to have no flight penalties attributable to ground environment. Heating on the ground was investigated to determine minimum insulation thicknesses necessary to prevent liquefaction of air and to determine refueling requirements resulting from boiloff while on the launch pad.

Cork was used for insulation based on 1) several studies showing that cork is a good insulator for producing minimum total weight of boost vehicles utilizing cryogenic propellants, and 2) tests conducted with cork applied to the exterior of small tanks filled with liquid hydrogen.

These tests demonstrate that cork can be applied externally to a liquid hydrogen tank without failure of the bondline, material, or sealing film. A thin mylar film is bonded to the cork exterior to prevent cryopumping. All studies are based on cork being applied to the outside of the tank.

3.2.10.5.2 Insulation Requirements to Prevent Liquefaction of Air

The outer temperature of the insulation must be equal to or greater than the liquefaction temperature of air — conservatively assumed as 170°R. This necessitates using sufficient insulation on the liquid hydrogen tank walls and bulkheads to provide the desired temperature profile through the insulation material. The critical design condition determining minimum thicknesses is created by the steady-state heating that occurs while the vehicle is on the launch pad.

3.2.10.5.2.1 Sidewalls

Steady-state heat flow through the insulation on the sidewalls is given by:

$$h(T_{aw} - T_w) = \frac{K_c}{l_c} (T_w - T_{prop})$$

where h = Heat transfer coefficient (Btu/ft^2-hr-°R)

$= 0.19 (T_{aw} - T_w)^{1/3}$ (See 3.2.10.3.1.)

T_{aw} = Adiabatic wall temperature (°R)

T_w = Cork outer surface temperature (°R)

T_{prop} = Propellant temperature, LH_2 (°R)

K_c = Conductivity of cork (Btu/ft-hr-°R)

l_c = Cork thickness (feet)

Assuming an air temperature of 100°F, a T_w of 170°R (conservative estimate of the liquefaction temperature of air), and a liquid hydrogen temperature of 43°R gives a minimum cork thickness of 0.06 inch.

3.2.10.5.2.2 Forward Bulkhead

The minimum insulation thickness required to prevent liquefaction of air on the forward bulkhead of the liquid hydrogen tank was determined by the following heat balances:

$$\text{Total heat input} = A_w h_1 (T_{w_1} - T_g)$$

$$A_w h_1 (T_{w_1} - T_g) = A_h h_2 (T_g - T_{w_2})$$

$$A_h h_2 (T_g - T_{w_2}) = A_h \frac{K_c}{l_c} (T_{w_2} - T_{prop})$$

where T_{w_1} = Intertank wall temperature (°R)

T_{w_2} = Cork outer-surface temperature (°R)

T_g = Mean compartment gas temperature (°R)

T_{prop} = Temperature of LH_2 propellant — 37°R

h = Free convection heat transfer coefficient for vertical planes (turbulent region) — $0.30 (\Delta T)^{1/4}$ (Btu/ft^2-hr-°R). (See Reference 7)

h_2 = Free convection heat transfer coefficient for spheres (turbulent region) — $0.25 (\Delta T)^{1/4}$ (Btu/ft^2-hr-°R). (See Reference 7)

A_w = Surface area of forward interstage — 6118 sq. ft.

A_h = Surface area of upper bulkhead of LH_2 tank — 6210 sq. ft.

K_c = Thermal conductivity of cork — 0.0103 (Btu/ft-hr-°R)

l_c = Cork thickness (feet)

The mean compartment gas temperature, T_g, is determined by using the equation

$$A_w h (T_w - T_g) = A_h h_2 (T_g - T_a)$$

Assuming a wall temperature of 560°R and applying the heat transfer coefficients explained in the nomenclature give a mean T_g of 378°R.

The minimum cork thickness is then given by the expression

$$l_c = \frac{K_c\,(T_a - T_{prop})}{h_2\,(T_g - T_a)} = 0.11 \text{ inch}$$

3.2.10.5.2.3 Aft Bulkhead

The heat balance equations to determine the minimum insulation requirement to prevent liquefaction of air are:

$$\text{Total heat input} = A_w h_1\,(T_{w_1} - T_g)$$

$$A_w h_1\,(T_{w_1} - T_g) = A_o h_2\,(T_g - T_{w_3}) + A_h h_2\,(T_g - T_{w_2})$$

$$A_h h_2\,(T_g - T_{w_2}) = A_h \frac{K_c}{l_c}\,(T_{w_2} - T_{prop})$$

where T_{w_1}, T_{w_2}, T_g, T_{prop}, h_1, h_2, K_c, and l_c are values defined in 3.2.10.5.2.2.

A_w = Surface area of intertank — 12,111 sq. ft.

A_o = Surface area of forward bulkhead of LO_2 tank — 6210 sq. ft.

A_h = Surface area of lower bulkhead of LH_2 tank — 6690 sq. ft.

T_{w_3} = Wall temperature of LO_2 tank — 143°R

Assuming T_{w_1} = 560°R, the mean compartment gas temperature, T_g, is determined from

$$A_w h_1\,(T_{w_1} - T_g) = A_o h_2\,(T_g - T_{w_3}) + A_1 h_2\,(T_g - T_{h_2})$$

$$\left(\frac{0.30\,A_w}{0.25\,(A_o + A_h)}\right)^{4/5} = \left(\frac{T_g - T_{w_3}}{T_{w_1} - T_g}\right)$$

$$T_g = 374°R$$

The minimum cork thickness is

$$l_c = \frac{K_c\left(T_{w_2} - T_{prop}\right)}{0.25\,(T_g - T_{w_2})}$$

$$= 0.00954 \text{ foot}$$

$$= 0.12 \text{ inch}$$

3.2.10.5.3 Insulation Requirements During Flight

Insulation thickness on the liquid hydrogen tank sidewalls and bulkheads was optimized for a system in which the hydrogen is warmed during flight until the fuel temperature raises to the level that boiloff commences (vapor pressure of the hydrogen equals the internal tank pressure). Any further heat input creates boiloff, which is vented overboard. The following items were considered for various cork thicknesses in the optimization process:

- Insulation weight.
- Attachment weight — 0.104 lb/ft^2 of adhesive and mylar.
- Boiled-off fuel that must be vented overboard.
- Increased tank weight to handle volume of boiloff.
- Increased tank weight to handle volume change due to density decrease in the fuel during first-stage flight.

3.2.10.5.3.1 Sidewalls

Insulation thickness for the sidewall was determined by the optimization procedure shown in Figure 3.2.10-12. A transient analysis using an IBM 7090 digital computer was performed to determine heat flow into the hydrogen during boost flight. These results for various cork thicknesses are presented in Figure 3.2.10-13. The aerodynamic heating is based on data in Figures 3.2.10-9 and 3.2.10-10.

The insulation thickness is considered constant over the entire tank sidewall, since variation in aerodynamic heating along the tank is negligible.

3.2.10.5.3.2 Bulkheads

Analyses were conducted using the minimum insulation thicknesses dictated by requirements shown in 3.2.10.5.2 for preventing liquefaction of air. These results showed that heat flow through the bulkhead and insulation during boost flight is insignificant. Thus, no additional insulation is required on the bulkheads.

3.2.10.5.4 Boiloff

Boiloff rates while the vehicle is on the launch pad were determined as a function of insulation thickness. Data for boiloff are given in Figure 3.2.10-14 for forced convection due to a 20-mph wind velocity. The heat transfer coefficients used are based on equations in 3.2.10.3.1.

The design gages of cork for the bulkheads and tank walls are shown. The sidewall thickness results from optimization to minimize total launch weight. The bulkhead gages are dictated by requirements to prevent liquefaction of air.

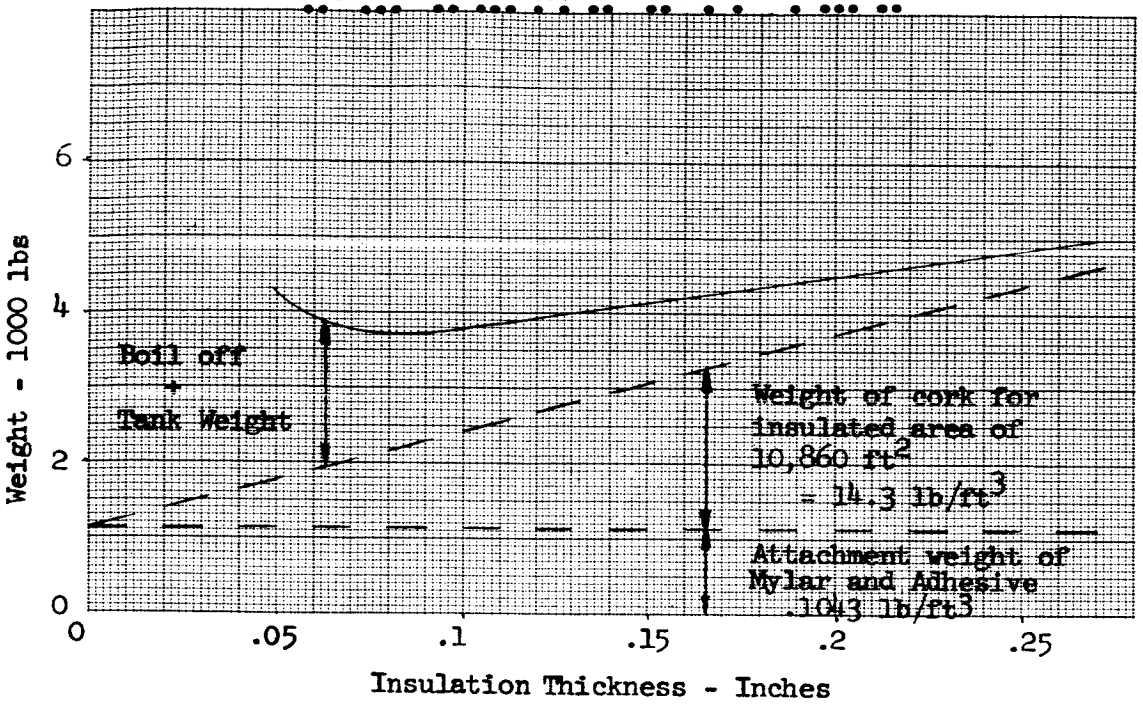

Figure 3.2.10-12 INSULATION OPTIMIZATION STUDY — BOILING SYSTEM

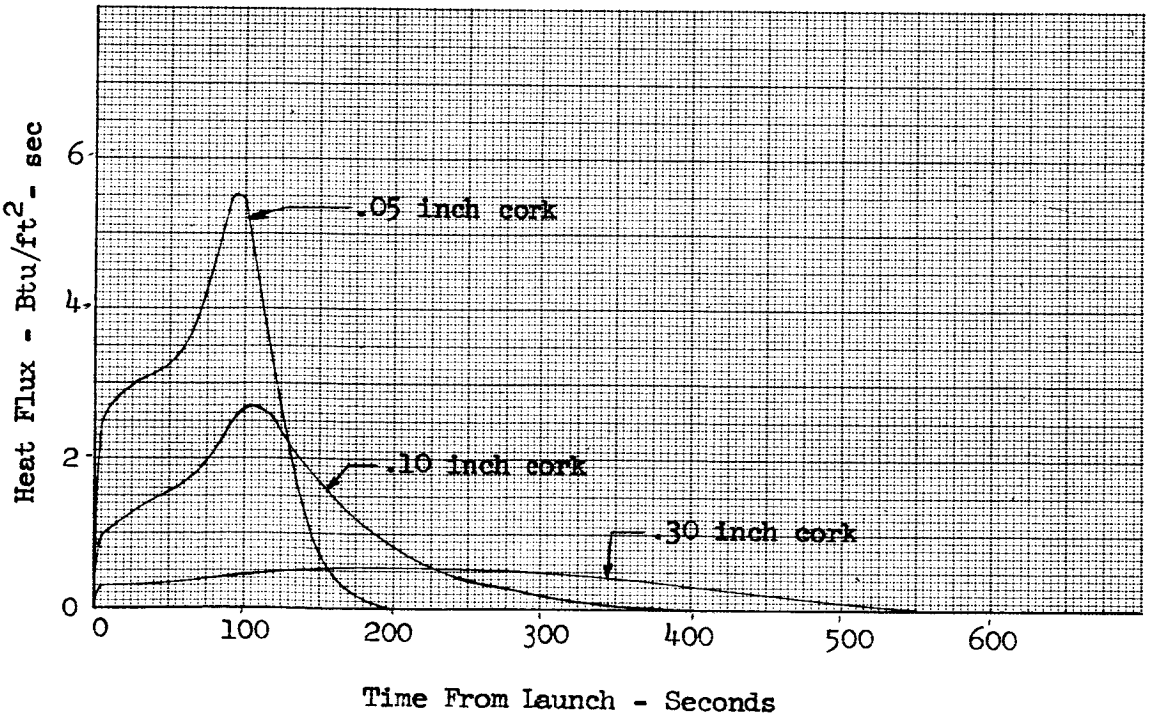

Figure 3.2.10-13 AERODYNAMIC HEATING RATE INTO LIQUID HYDROGEN

Use of these cork thicknesses results in 35,400 pounds of liquid hydrogen boiling off per hour in a 20-mph wind.

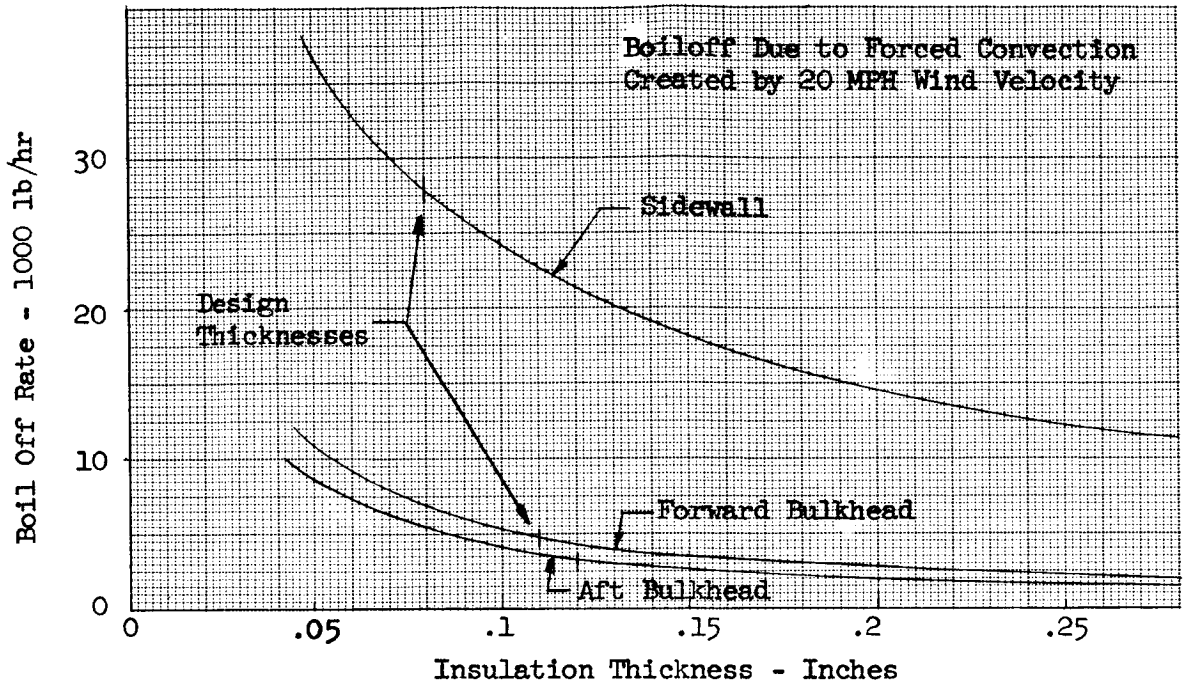

Figure 3.2.10-14 BOILOFF RATE DUE TO GROUND CONVECTIVE HEATING

REFERENCES

1. "Study of Large Launch Vehicles Using Solid First Stage," Volume IV, Report SSD-TDR-62-144, Section 6.5 (Confidential).

2. "Radiant Heat Transfer to a Plane From a General Axisymmetric Cone-Cylinder Combination," Boeing Document AS 1383.

3. Goethert, B.H., "Base Flow Characteristics of Missiles with Cluster-Rocket Exhausts," IAS Paper 60-89, July 1960.

4. Memorandum M-AERO-A-55-62, Marshall Space Flight Center, July 24, 1962.

5. McAdams, William H., Hot Transmission, Page 173.

6. McAdams, William H., Hot Transmission, Page 200.

7. Giedt, Warren H., Principles of Heat Transfer, Page 218.

3.2.11 Design Configuration

3.2.11.1 Introduction

Preliminary design drawings describing the final study vehicle structure and system concepts are presented in this section. The drawings and accompanying text summarize the results of the detail analyses conducted on the current technology vehicle. Advanced technology vehicle data is presented in Section 4.0.

3.2.11.2 Summary

The general arrangement of the final design vehicle in Figure 3.2.11-1 shows the overall vehicle and the relative size and the location of major components and subsystems.

Briefly, the first stage uses six 260-inch-diameter motors arranged in a circular pattern. All motor nozzles are gimbaled for vehicle attitude control. The motors are linked together at the base skirts and tied or assembled at their upper ends to a cross-beam cluster structure.

The 70-foot-diameter second stage consists of two independent tanks to contain the liquid oxygen and liquid hydrogen propellants. A cylindrical fairing connects the two tanks. The second stage is supported by a transition section interstage that matches the peripheral shape of the first-stage motor cluster structure. Five M-1 engines are mounted on a conical thrust structure. The engines are arranged in a cruciform pattern. The four outer engines are canted inward at the base to provide maximum clearance during single-plane separation of the first stage. After separation, the engines are programmed to gimbal as required.

A transtage propulsion system is located between the second stage and the payload. The system is composed of two independent storable-propellant propulsion units located 180 degrees apart. These engines are also canted inward for maximum clearance during second-stage separation. Each propulsion system is mounted on a relatively short length of interstage structure that remains attached to the payload until the time of transtage jettison.

Separation control rockets, retro and ullage, are mounted externally on the interstage structures. All rockets are housed in aerodynamic fairings except the first-stage retrorockets, which are in the aerodynamic shadow of the second stage. Nozzle closures are assumed on first-stage retrorockets.

Command destruct and telemetry antennas are shown on the first-to-second-stage interstage and on the second-stage-to-payload interstage. Transtage antenna requirements have not been defined.

Preliminary design drawings of the final vehicle are presented and described in the following section. Refer to the appropriate sections of the report for design analyses and detail system descriptions.

3.2.11.3 Design Conclusions

First Stage — In general, the first stage structural design of the T65 vehicle is an extension of the concept established for the 500K vehicle of the previous study increment (Reference 1). However, certain configuration differences have introduced changes in the governing design factors, as noted below.

The elimination of the fixed-cant requirement on the nozzles of the T65 vehicle permitted simplification of the base structure. In contrast, the use of six motors instead of four caused design problems in the carryover of the cross-beam cluster structure. Due to the short study time period, design consistency with the 500K vehicle was adhered to as closely as possible to take advantage of previously established design data. The resulting structure is more complicated than the 500K structure and more difficult to fabricate in some areas.

Second Stage — On the basis of a structural tankage trade study (see 3.2.8.3) and other considerations, the liquid oxygen is contained in a tank that is approximately 35-percent oversize. Additional and more rigorous studies may show vehicle improvements if (1) the tank is not off-loaded (e.g., use smaller diameter tank with conical support structure), (2) dual-plane separation is employed, or (3) the separation plane is moved forward of illustrated position. The separation plane can be moved only if the smaller oxygen tank is supported by a conical-shaped structure that extends further forward on the 70-foot-diameter shell.

Structural and manufacturing analyses have substantiated all structural concepts illustrated in the section; however, design simplification improvements could have been made had not time and certain design assumptions imposed restraints that limited the scope of the investigation and incorporation of design improvements.

3.2.11.4 First-Stage Design Features

Figure 3.2.11-2 illustrates the major design features of the first-stage cluster of six 260-inch-diameter solid motors. The motors are arranged in a circular cluster and were spaced to (1) minimize "hammer head" effect, (2) provide nozzle gimbal envelope clearance with structure, and (3) allow adequate space and clearance for vehicle support and leveling packs provided in the launch platform. The structural analysis of each of the structures is presented in 3.2.8.6.4.

3.2.11.4.1 Motor Base Support Skirt

Each motor base support skirt embodies three support pads, equally spaced about the motor axis. A hole is provided in the lower face of each pad to accommodate an indixing pin atop each support jack (see Section 3.1.9).

A welded aluminum structure of the "inverted A-frame" type carries the static loads from each pad into the support skirt. The support skirt is constructed of reinforced aluminum honeycomb and is flared to provide gimbaling clearance for the nozzle. Steel frames are provided at the top and bottom of the skirt to react the tangential loads introduced by the vertical support legs. Cutouts are made in the skirt for the legs, and splice fittings are used at the cutout points to maintain structural continuity. An aerodynamic fairing is provided over the outboard support legs.

The vehicle standing loads are transmitted through the support frames and skirts into the lower skirt extensions. These cylindrical aluminum structures are of the stiffened skin type and are reinforced with tapered longerons opposite the support leg termination points; splice fittings again provide structural continuity at the leg-longeron joints.

3.2.11.4.2 Clustering Structure

The first-stage clustering tie (Figure 3.2.11-3) is accomplished with an integral cross-beam structure at the forward end of the cluster and interlateral linkage members at the lower end. Previous parametric study (Reference 1) has shown this concept to be lighter and more efficient than other types.

The cross beam is an assembly of built-up aluminum box sections supplemented by six skirt extensions of reinforced aluminum skin and stringer construction. The latter components increase the bending stiffness of the cluster structure and provide a geometrical transition from the circular motor skirts to the cross beam. Bending continuity is effected between the skirt extensions and cross beam with stringer butt joint fittings and overlapping attachments to the beam members.

The clustering tie is completed with laterally positioned aluminum box section links located at the support-skirt/skirt-extension interface at the lower end of the cluster.

3.2.11.4.3 External Insulation

Base heat protection is provided by a centrally located honeycomb shield supported from the inboard base structure by aluminum cross beams. The outer face of the shield and all surfaces, including the motor nozzle, within the confines of the support skirts are protected with a phenolic nylon-type thermal insulation (see 3.2.8.6.4 and 3.2.10.2).

3.2.11.4.4 Motor Description

The solid rocket motor cases are fabricated of welded sections of 18-percent nickel alloy steel and mar-aged to 250,000 psi ultimate tensile strength (see 3.4.1.3.3). A bolted closure joint is used to attach the nozzle assembly to the

case. The propellant grain is monolithic with a seven-point star perforation. (See Figure 3.2.11-2 for motor case thicknesses and joint design features.) A monocoque stub skirt is provided at each end of the motor for mechanical attachment of cluster and base skirt structure.

3.2.11.4.5 Thrust-Vector-Control System

Thrust vector control during first-stage flight is provided by omniaxis gimbaling of the solid rocket nozzles. Dual hydraulic actuators deriving power from a solid propellant gas generator furnish the required control force to each nozzle. Actuation force requirements are reduced to a minimum through the use of full-length aerodynamic fairings at the outer periphery of the cluster (see Sections 3.1.3 and 3.1.4).

3.2.11.5 Second-Stage Design Features

3.2.11.5.1 Tankage

The tankage arrangement is shown in Figure 3.2.11-4. The propellants are contained in separate aluminum tanks, with the oxygen located aft. The lower heads of each tank are 0.80 to 1.0 ellipsoids and the upper heads of each tank are 0.70 to 1.0 ellipsoids. All heads are aluminum, mill tapered for minimum weight. Thickened land sections are provided at all weld joints. Y rings are used at the junction of the head and the cylindrical portion of the tankage. Short cylindrical aluminum waffle stub skirts are welded to the Y rings and provide the means to mechanically attach to adjacent structure. Waffle construction was employed here in preference to skin-stringer-frame construction to minimize weight and to eliminate a somewhat difficult design problem relating to stringer termination and frame requirements near the tank head and sidewall junction. A dual-purpose interstage field splice and transportation support ring are provided in the lower skirt of the oxygen tank. The cylindrical portion of the hydrogen tank is the only area of either tank requiring stiffening. The hydrogen sidewalls are of milled skin-stringer-frame construction. The skin and stringer thicknesses are varied locally to properly match the Y rings. The entire LH_2 tank is insulated with mylar-covered cork.

3.2.11.5.2 Intratank and Skirt Extensions

Conventional aluminum built-up skin-stringer-frame construction is used in these areas. Other methods of construction were not evaluated. These structures are mechanically attached to the waffle stub skirts previously mentioned. The oxygen tank skirt extends down to the point of attachment of the conical thrust structure and interstage structure.

The upper skirt of the hydrogen tank extends up to attach to the payload and to support the transtage propulsion systems. Two short cylindrical, monocoque sections are provided in this stringer-frame-stiffened structure to facilitate,

simplify, and reliably effect a linear-shaped charge separation of (1) second stage tankage, and (2) transtage propulsion and supporting structure.

3.2.11.5.3 Slosh and Antivortex Suppression

Stiffened aluminum cones, perforated with small holes, were assumed in this design. In-house studies and coordination with the Martin Company have indicated this design may be acceptable; however, insufficient data is available to define the detail requirements. Antivortex provisions include a number of radial baffles located between propellant outlets. The baffles are covered by a circular plate that also serves to prevent geysering during propellant loading.

3.2.11.5.4 Thrust Structure

The five M-1 engine thrust structure is an aluminum cone frustum (Figure 3.2.11-5). Construction is conventional skin-stringer-frame. Each end of the frustum terminates with a relatively heavy frame to react kick-loads. The four outer engines are mounted at the periphery of the cone. The center engine is mounted on a cruciform beam network that extends to the cone side walls. The beams are built up with web stiffening. Upper and lower longerons complete the assembly. Tapered longerons are used locally at each engine mount location to help distribute the thrust loads into the cone skin and beam webs.

Cutouts are provided in the cone for engine propellant feed lines. Design details of the base heat shields were not completely resolved; however, for weight estimation purposes, the shield was assumed to be mounted directly on the cone at the engine mount location. (See 3.2.8.6 for structural analysis and trade studies on the thrust structure and 3.2.10.2.3 for phenolic nylon insulation requirements.)

3.2.11.5.5 Interstage Structure

The interstage (Figure 3.2.11-6) is an aluminum skin-stringer-frame structure. The interstage provides the load path between the first and second stage in a smooth transition from the hexagonal shape of the first stage to the circular shape of the second stage. A mechanical attachment joint is provided at the lower and upper ends for assembly to the cluster structure cross beam and the second stage. The interstage remains attached to the first stage at separation. The separation plane is located in the structure immediately forward of the interstage.

Access doors are provided for servicing equipment inside the structure. The six first-stage retrorockets are mounted near the lower edge of the interstage (Figure 3.2.11-1). The structural analysis of the interstage is presented in 3.2.8.6.4.

3.2.11.5.6 Second-Stage Subsystems

The inboard profile of the second stage is shown in Figure 3.2.11-7. (Refer to 3.2.3.4 for detail description and design features of subsystems.) Second-stage propulsion is provided by a cluster of five M-1 engines. The cluster arrangement consists of one engine at the vehicle centerline, axially aligned and stationary. The four outer engines are mounted on a 520-inch-diameter circle (90 degrees on centerlines). These outer engines are canted inward 7.5 degrees during first-stage operation. Immediately after separation the engines are free to gimbal as required.

The propellants are contained in two independent tanks. The liquid oxygen tank is located below the hydrogen tank. The tanks are prepressurized with ground-supplied helium prior to flight. Gaseous hydrogen and gaseous oxygen are used for tank pressurization throughout second-stage flight. Heat exchangers located on the center engine supply the pressurants.

The propellant feed lines from each tank are 19.5 inches in diameter. Each line consists of rigid ducting, flexible bellows, gimbal joints, a prevalve, and a pressure-volume compensating duct. The liquid-hydrogen lines are routed through tunnels in the liquid oxygen tank to each engine. The oxygen lines extend from the bottom of the oxygen tank to each engine.

Tanking and draining of the tanks is accomplished through a single line per tank. The hydrogen line is 20 inches in diameter and the oxygen line is 24 inches in diameter. A special telescoping or equivalent-type section of ducting appears necessary when lines are routed through the engine thrust structure to the periphery of the vehicle in the interstage area. Without such a device, line routing, stage separation, and umbilical concepts will be adversely affected.

Each tank is vented using two large vent valves and one small vent or relief valve for the flight mode. Vent line diameters are 20 inches for hydrogen and 9 inches for oxygen. The small flight vent in each tank is 2 inches in diameter. The gaseous hydrogen will be ducted away by a connection to the umbilical before flight. Gaseous oxygen is vented into the atmosphere on the vehicle side opposite the umbilicals.

Ullage and retrorockets and the transtage propulsion systems have been described in other sections. For detail characteristics of these components refer to the related text.

3.2.11.6 Transtage

The transtage of the T65C vehicle consists of two propulsion packages placed between the top of the second-stage hydrogen tank and the bottom of the 567-kilometer-orbit payload, along the upper skirt of the hydrogen tank. This arrangement permits utilization of the space between the upper dome of the hydrogen

tank and payload without the necessity of lengthening the second-stage payload interstage. The arrangement of the transtage propulsion units is shown in Section 3.2.3, Figure 3.2.3-14. The two propulsion systems are pressure-fed storable engines each having 50,000 pounds thrust and are described in detail in 3.2.3.5. The transtage propulsion system has 77,000 pounds of N_2H_4-UDMH (50-50)/N_2O_4 propellant and has a stage mass fraction of 0.81. Performance of the transtage is discussed in 3.2.2.4.

3.2.11.7 Direct Escape Payload

A third stage, used for a direct escape mission with the first and second stages of the T65C vehicle, utilizes LO_2/LH_2 propellant and is powered by three J-2 engines. The third stage attaches to the forward skirt of the second-stage hydrogen tank where a stiffened cone forms a transition from the 70-foot-diameter second stage to the 40-foot-diameter third stage as shown in Figure 3.2.3-19. A 40-foot-diameter 0.8 ellipsoidal hydrogen tank is attached to the top of the interstage cone by a short skirt. The oxidizer tank is a 26-foot-diameter 0.8 ellipsoid mounted under the hydrogen tank and supported by a J-2 engine thrust cone. Performance of the escape stage is discussed in 3.2.2.6. The escape stage propulsion system is presented in 3.2.3.6.

REFERENCES

1. SSD-TDR-62-144, "Study of Large Launch Vehicles Using Solid First-Stages," Volume 4, Contract NAS8-2438, December 1962 (Confidential).

BLANK

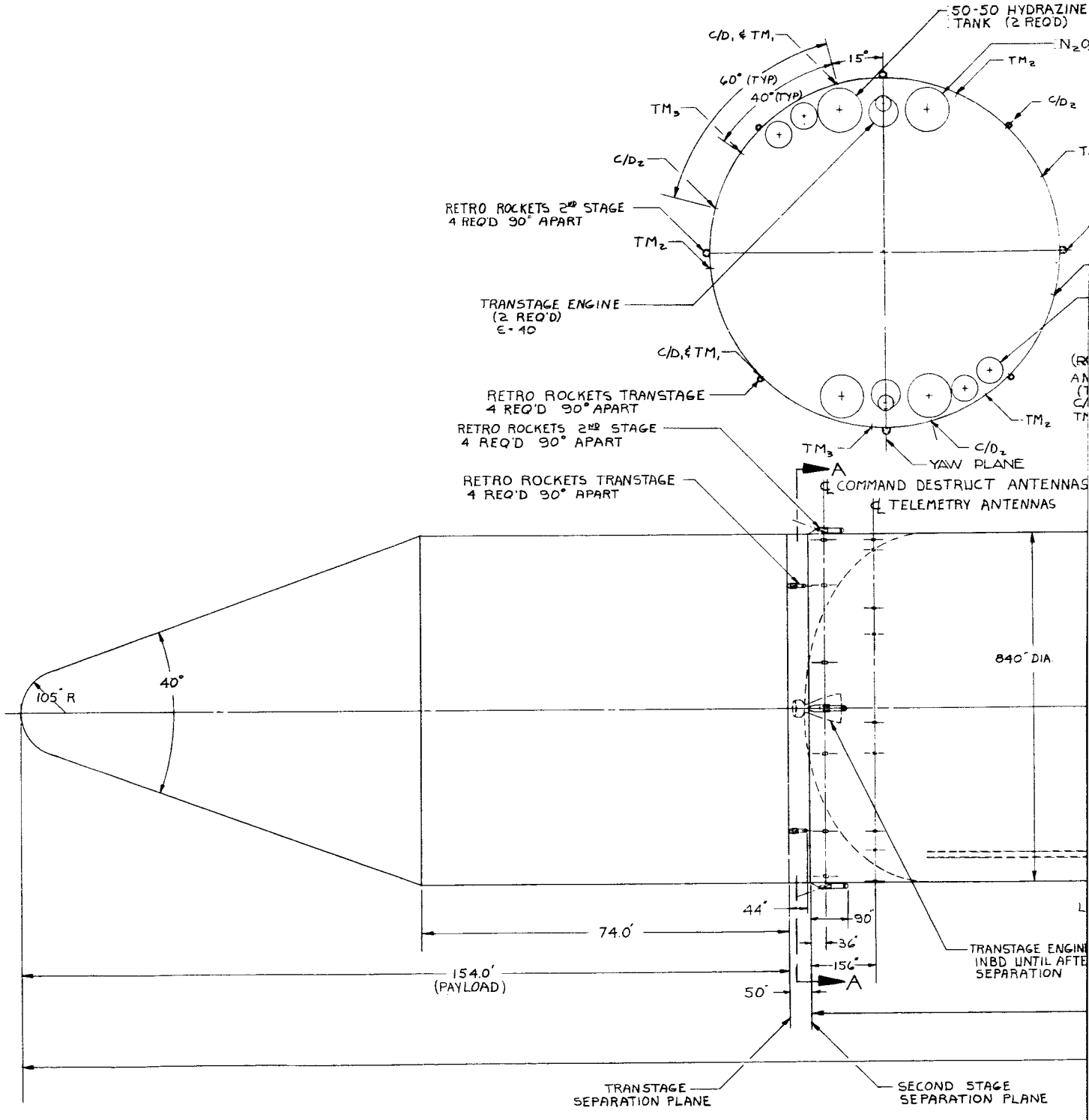

PAYLOAD TO 567 KM
1,070,000#

TRANSTAGE
W_p = 74,600#
F = 100,000#
X = .7853

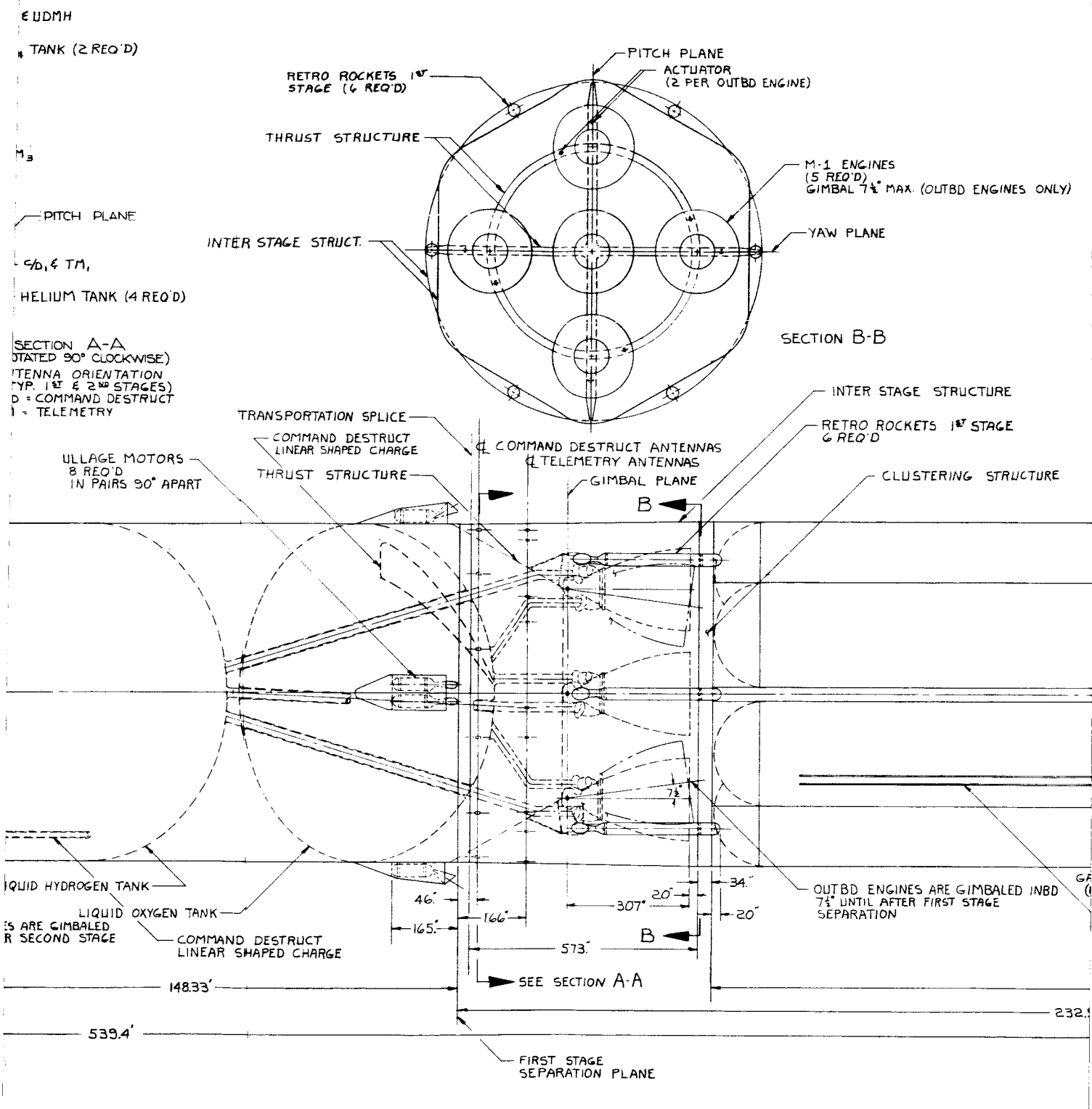

SECOND STAGE
W_p = 8,064,000*
λ' = .9025

FIRST
W_p = 24,
F = 58,
λ' = .88

Figure 3.2.11-1 VEHICLE T65D GENERAL ARRANGEMENT

2

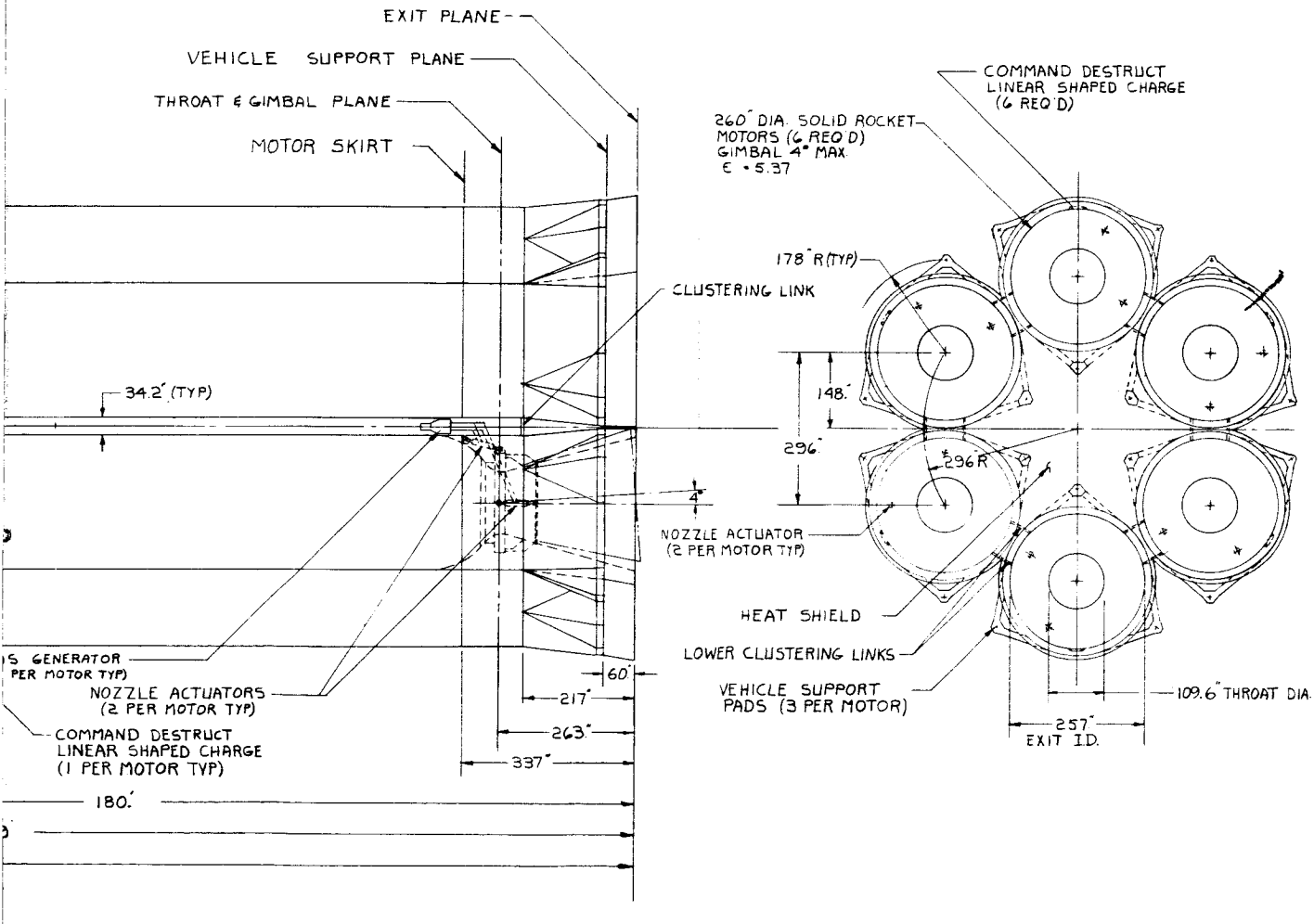

STAGE
320,960"
300,000"
92

VEHICLE LAUNCH WT. = 38,061,790"

3

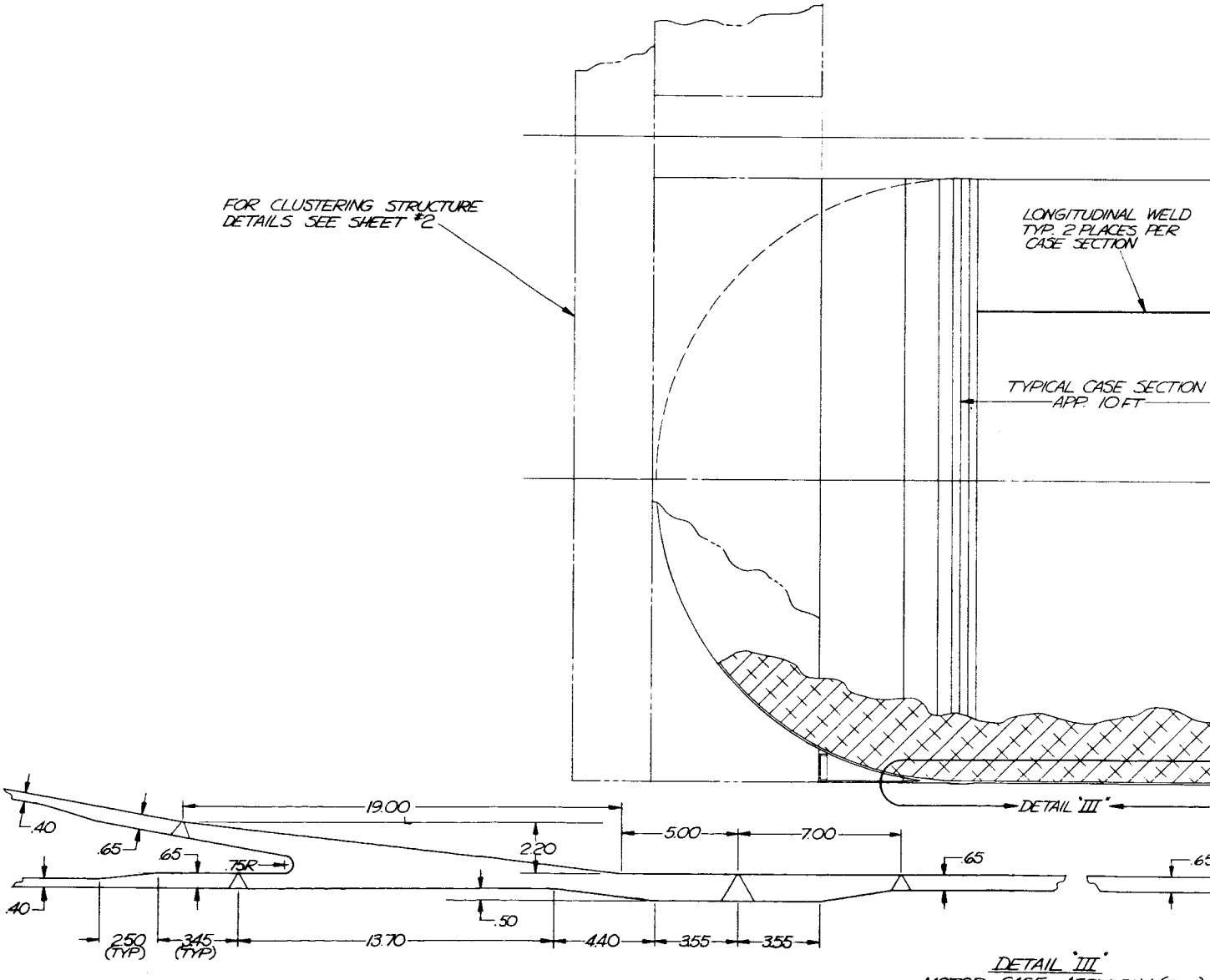

DETAIL "III"
MOTOR CASE ASSEMBLY (TYP)

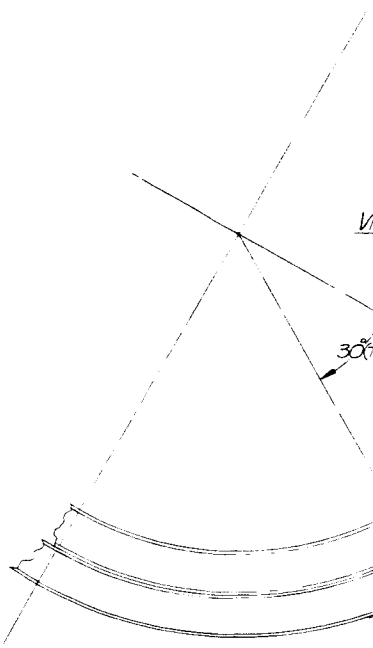

SEE FIG. 3.2.11-1 FOR COMMAND DESTRUCT SYSTEM DETAIL

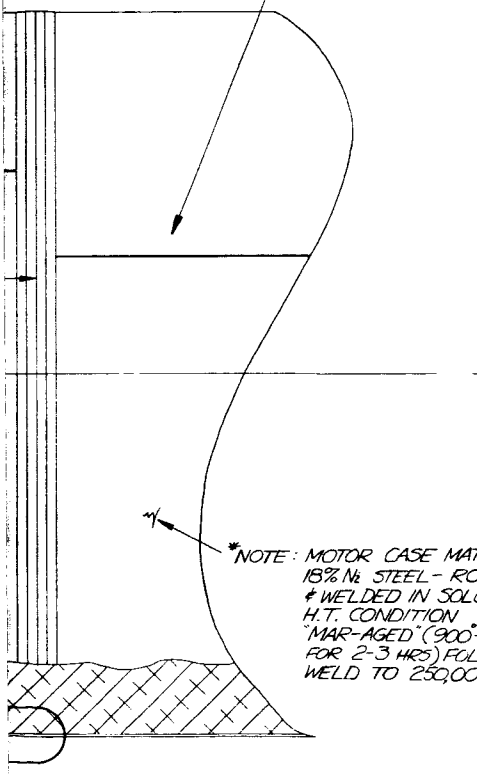

*NOTE: MOTOR CASE MATERIAL, 18% Ni STEEL - ROLLED & WELDED IN SOLUTION H.T. CONDITION "MAR-AGED" (900°-950°F FOR 2-3 HRS) FOLLOWING WELD TO 250,000 PSI U.T.S.

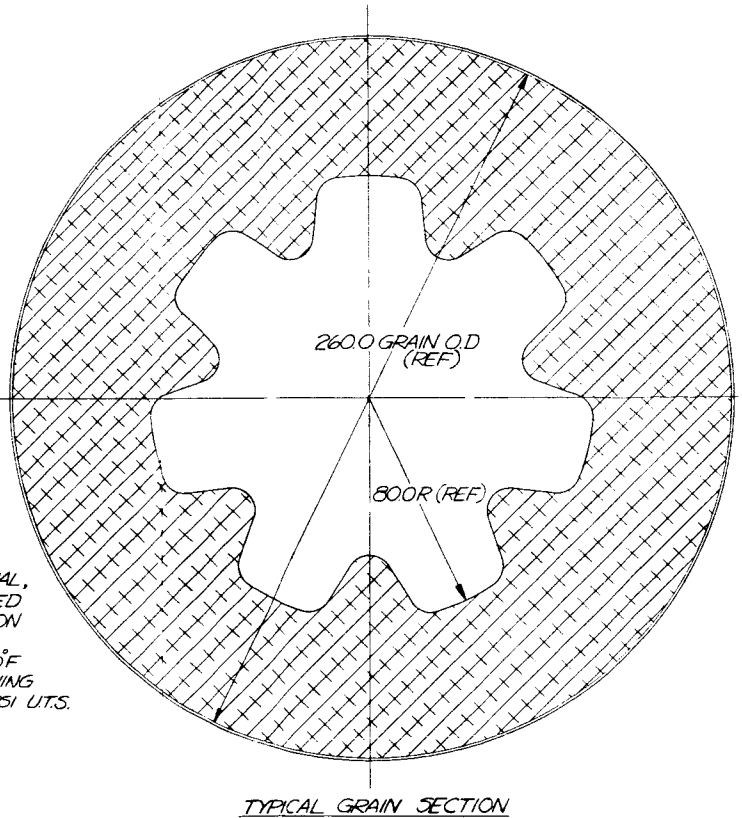

TYPICAL GRAIN SECTION

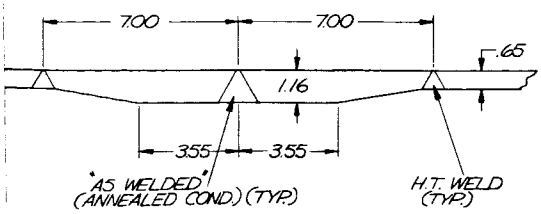

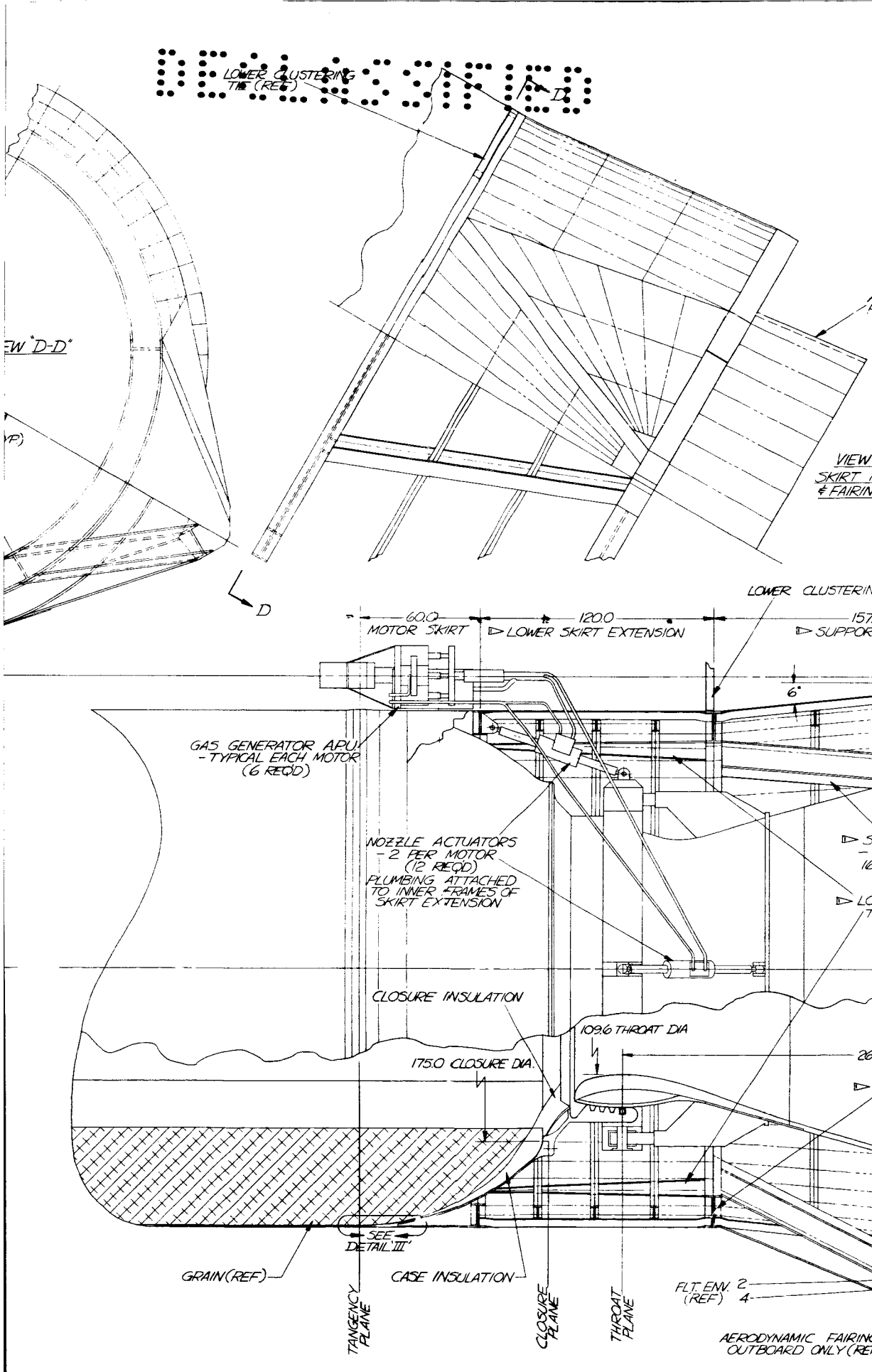

Figure 3.2.11-2 FIRST-STAGE STRUCTURE Configuration T65D (Sheet 1)

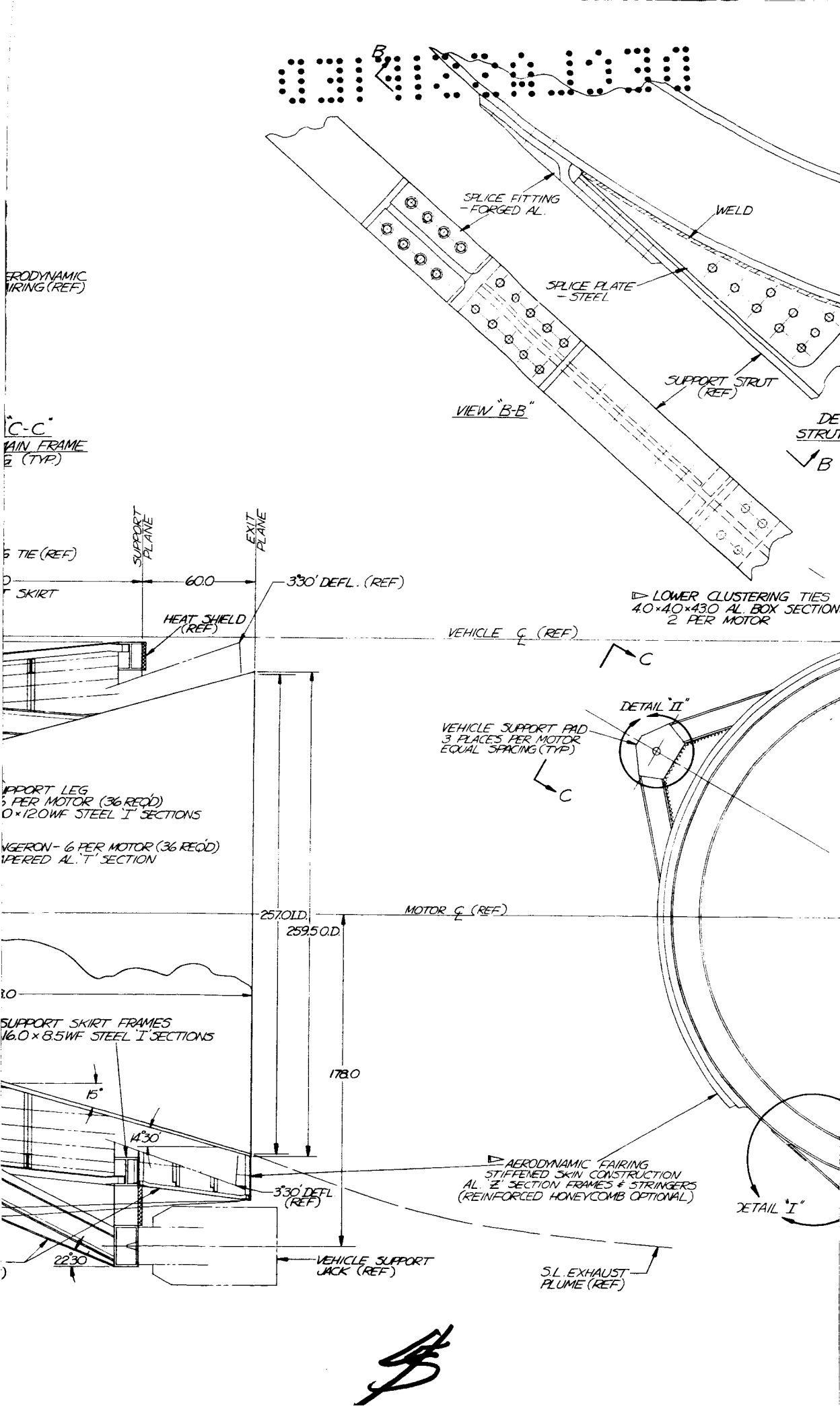
B
SPLICE FITTING - FORGED AL.
WELD
SPLICE PLATE - STEEL
SUPPORT STRUT (REF)
VIEW "B-B"
AERODYNAMIC FAIRING
C-C
MAIN FRAME
(TYP.)
TIE (REF)
SKIRT
SUPPORT PLANE
EXIT PLANE
60.0
3°30' DEFL. (REF)
HEAT SHIELD (REF)
LOWER CLUSTERING TIES
4.0×4.0×43.0 AL. BOX SECTION
2 PER MOTOR
VEHICLE ℄ (REF)
C
DETAIL "II"
VEHICLE SUPPORT PAD
3 PLACES PER MOTOR
EQUAL SPACING (TYP)
C
SUPPORT LEG
PER MOTOR (36 REQ'D)
×12.0 WF STEEL 'I' SECTIONS
GERON - 6 PER MOTOR (36 REQ'D)
APERED AL. 'T' SECTION
257.0 I.D.
259.5 O.D.
MOTOR ℄ (REF)
SUPPORT SKIRT FRAMES
16.0 × 8.5 WF STEEL 'I' SECTIONS
178.0
15°
14°30'
3°30' DEFL. (REF)
22°30'
VEHICLE SUPPORT JACK (REF)
AERODYNAMIC FAIRING
STIFFENED SKIN CONSTRUCTION
AL. 'Z' SECTION FRAMES & STRINGERS
(REINFORCED HONEYCOMB OPTIONAL)
DETAIL "I"
S.L. EXHAUST PLUME (REF)

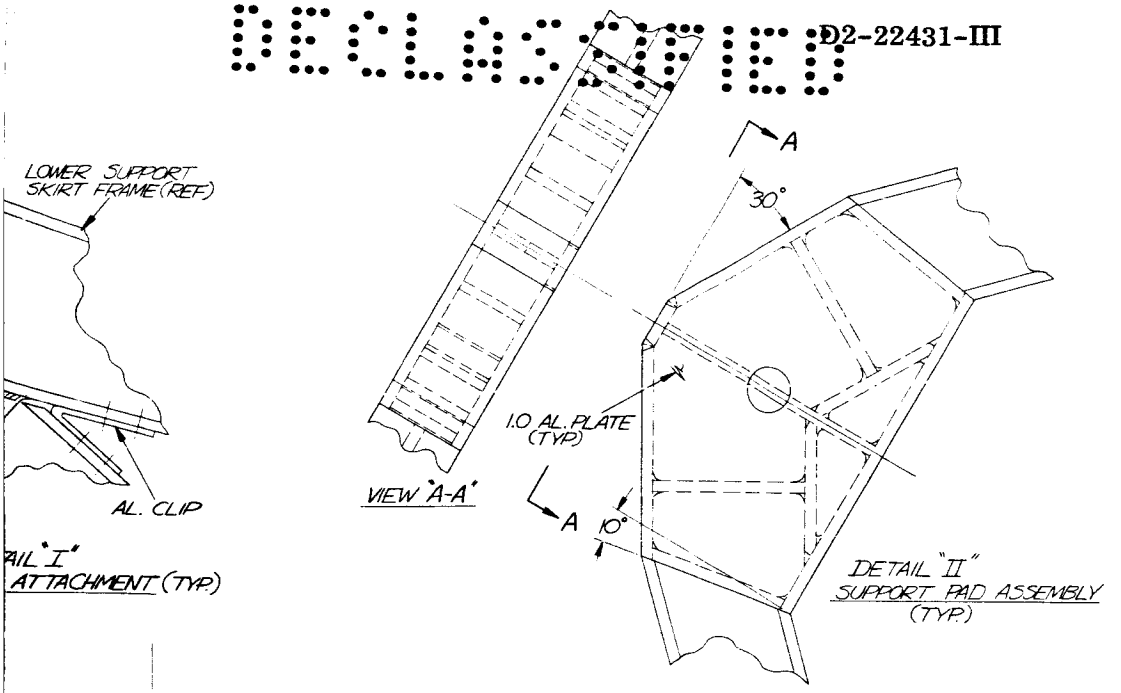

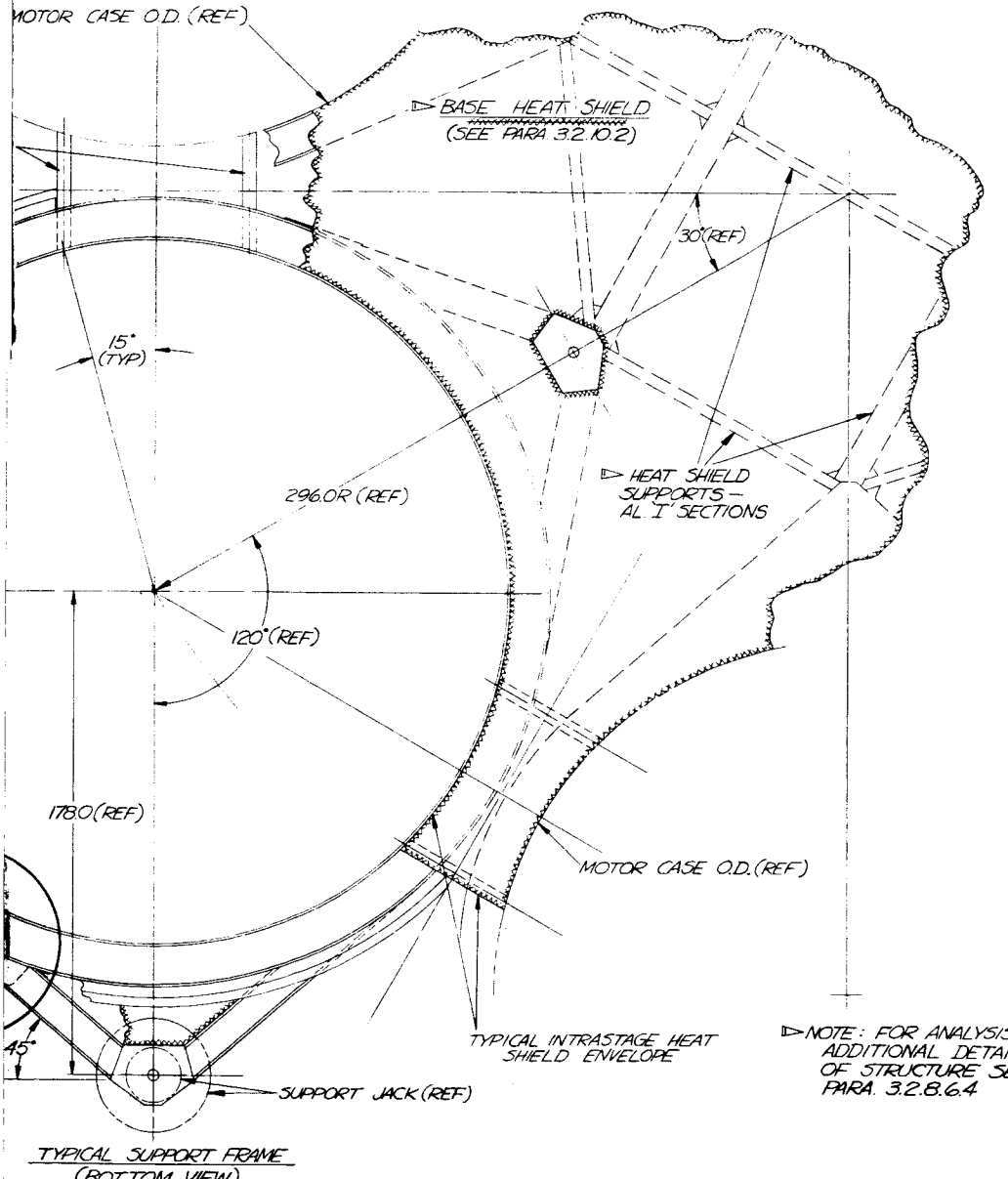

TYPICAL SUPPORT FRAME (BOTTOM VIEW)

5

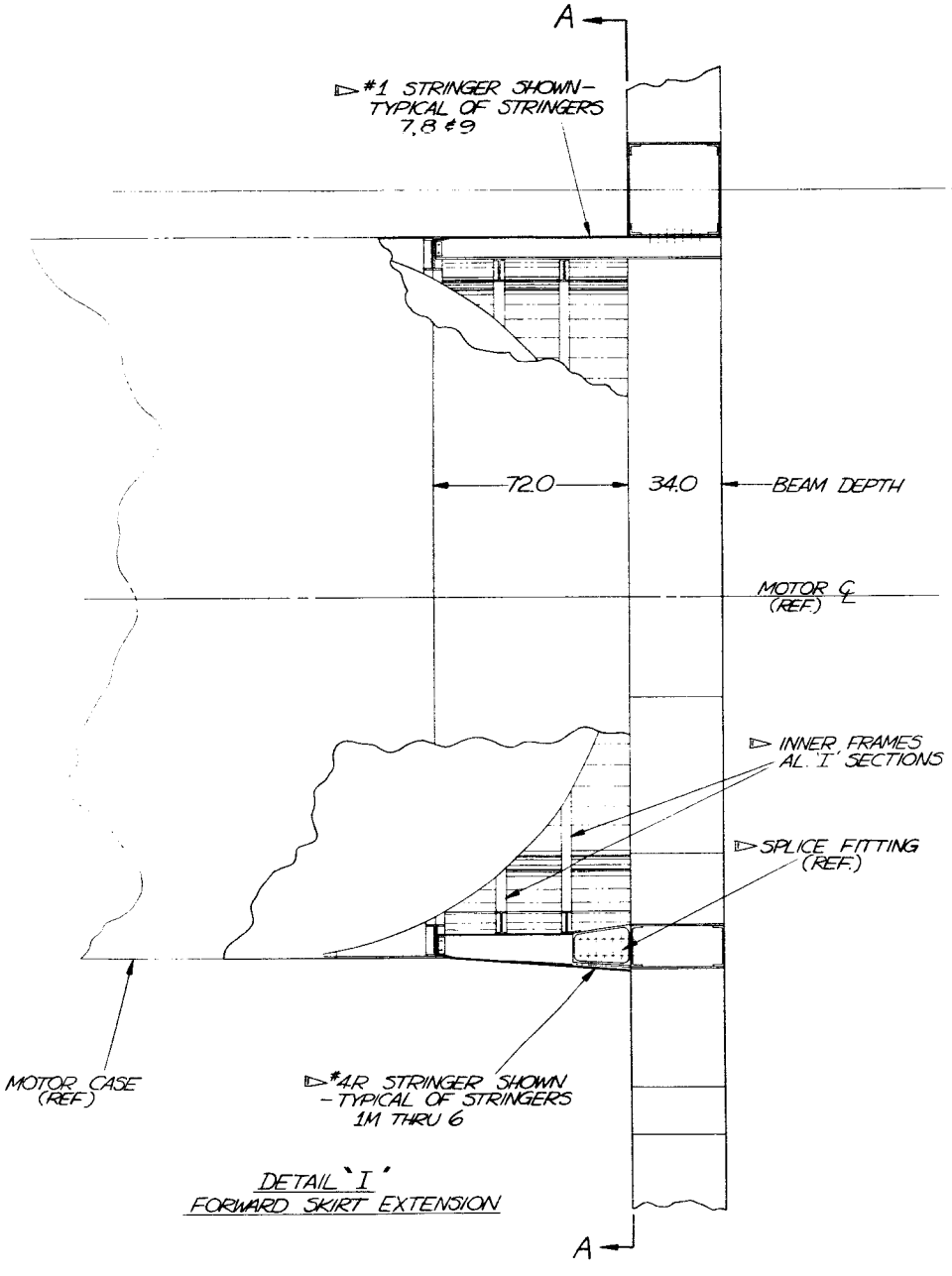

DETAIL 'I'
FORWARD SKIRT EXTENSION

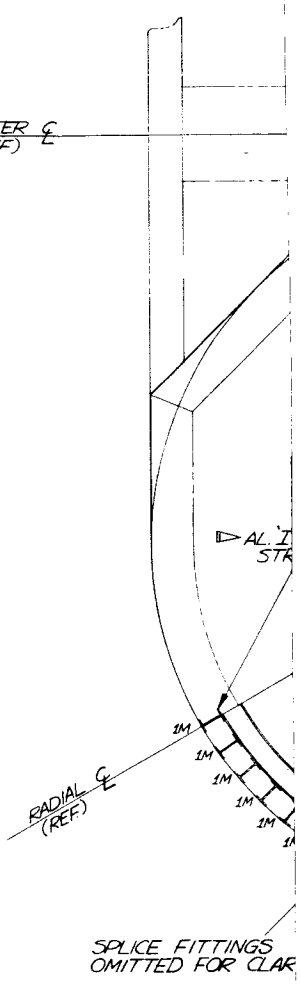

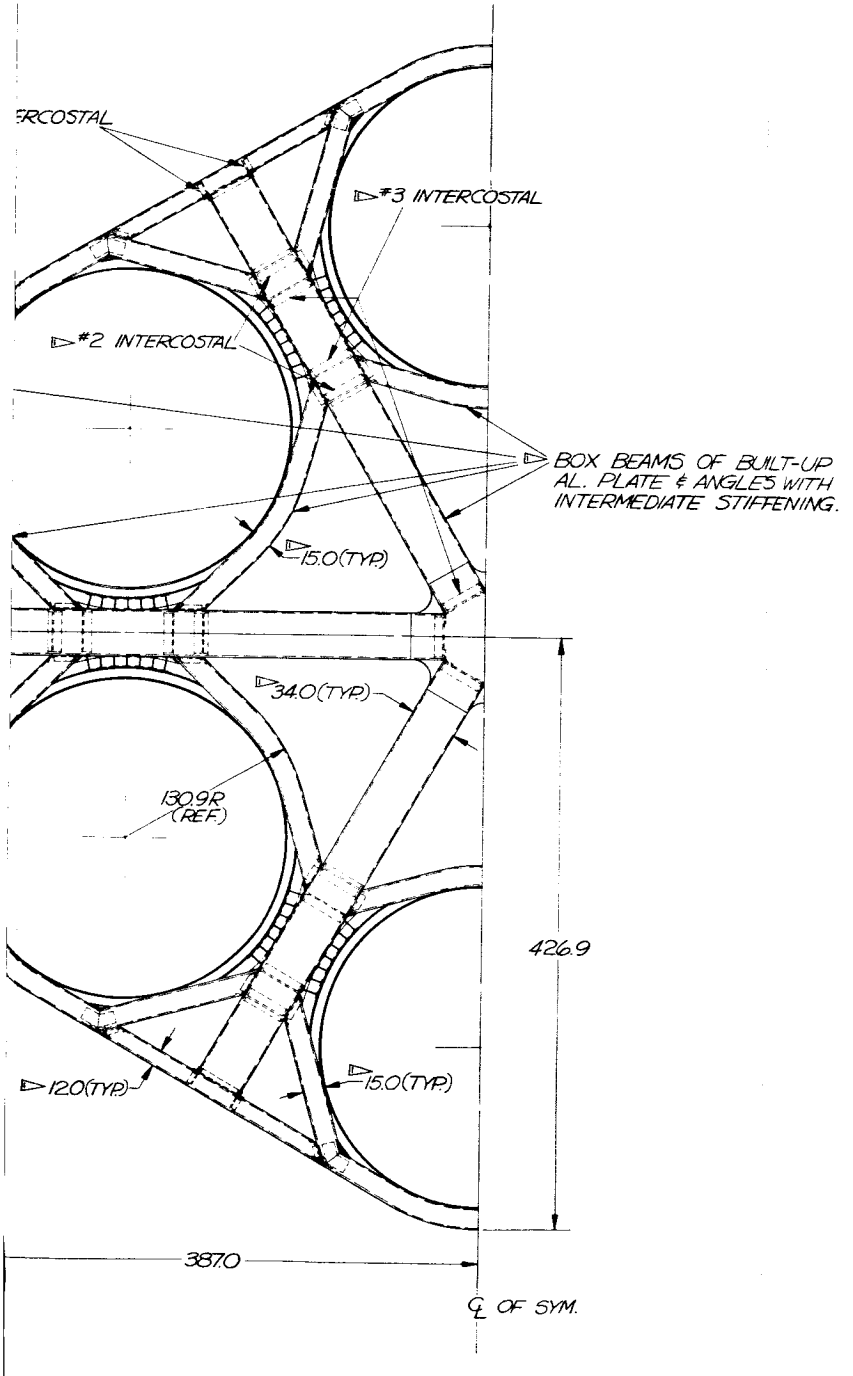

NOTE: FOR ANALYSIS & ADDITIONAL DETAILS OF STRUCTURE SEE PARA. 3.2.8.6.4

3

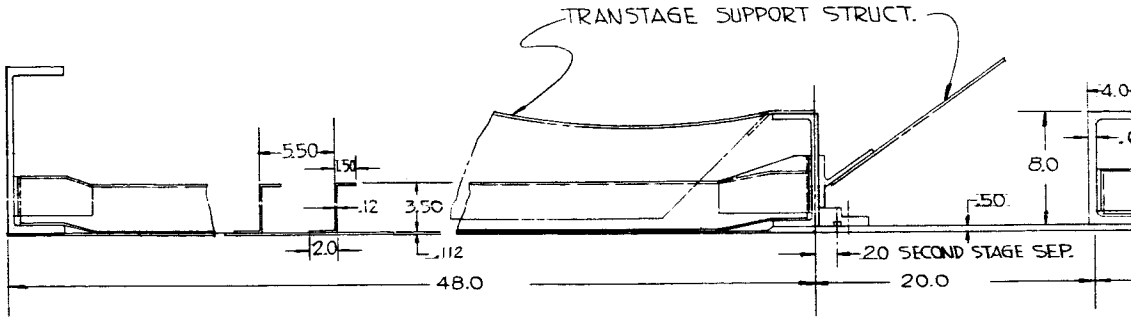

VIEW C
STAGE II TO PAYLOAD SKIRT

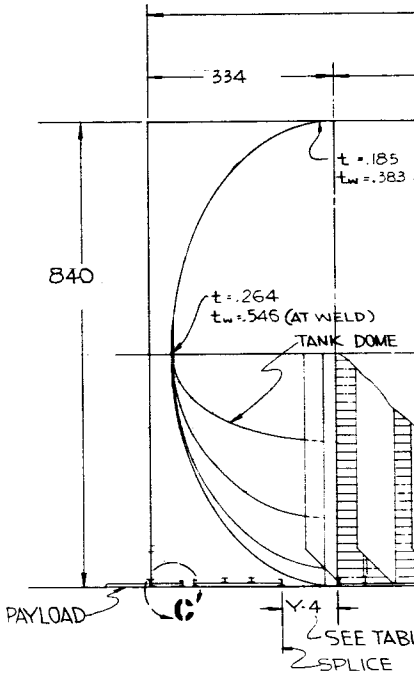

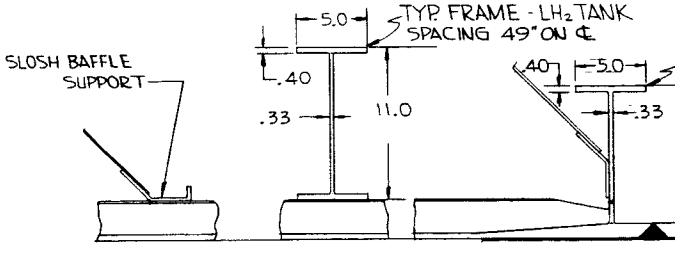

VIEW B

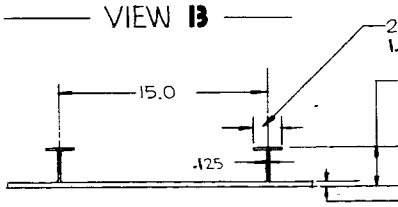

TYP. LH_2 TANK PANEL - EXTRUDED & MILL
MATERIAL - 2219-T87 ALUMINUM

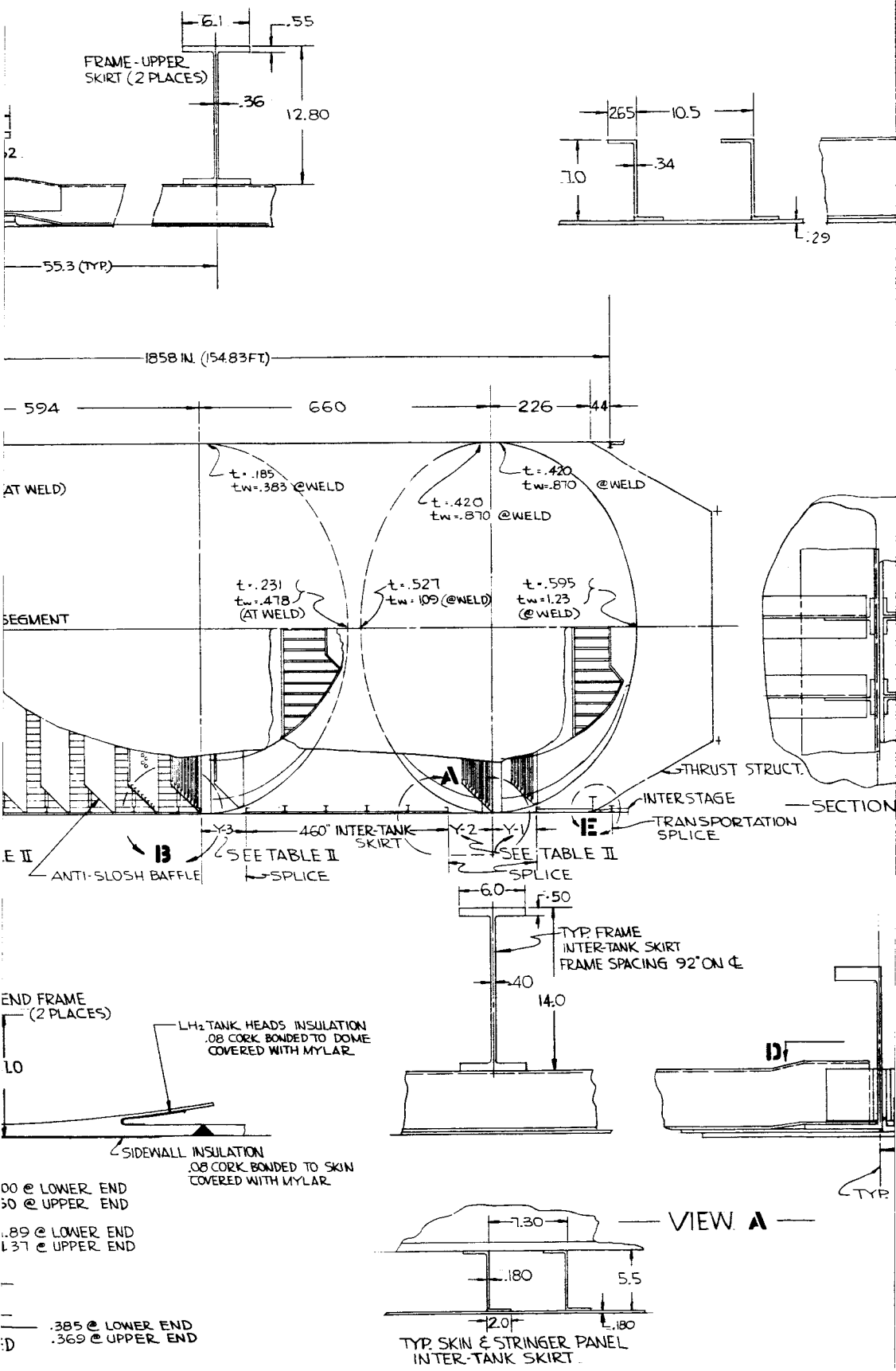

Figure 3.2.11-4 SECOND-STAGE STRUCTURAL DETAILS
Configuration T65D

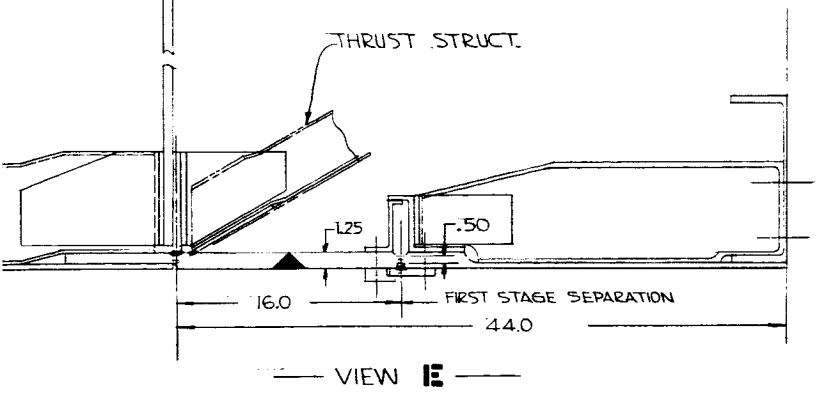

VIEW E

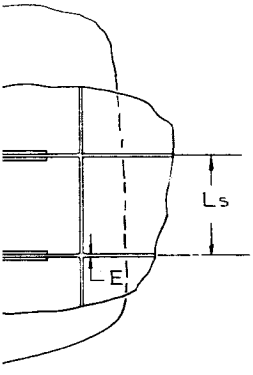

D

NOTE.
2219-T87 MATERIAL USED FOR ALL WELDED STRUCT.
7075-T6 MATERIAL USED FOR ALL UNWELDED STRUCT.

TABLE II 'Y' PANEL

PANEL	D	E	F	Ls
Y-1	.22	.22	3.75	5.3
Y-2	.22	.22	3.68	7.3
Y-3	.20	.20	3.46	7.3
Y-4	.15	.15	3.00	5.5

TABLE 'I'
'Y' RING DIMENSIONS

	A	B	C
UPPER LH_2 HEAD	.375	.375	.383
LOWER LH_2 HEAD	1.00	1.00	.383
UPPER LOX HEAD	1.25	1.25	.870
LOWER LOX HEAD	1.25	1.68	1.52

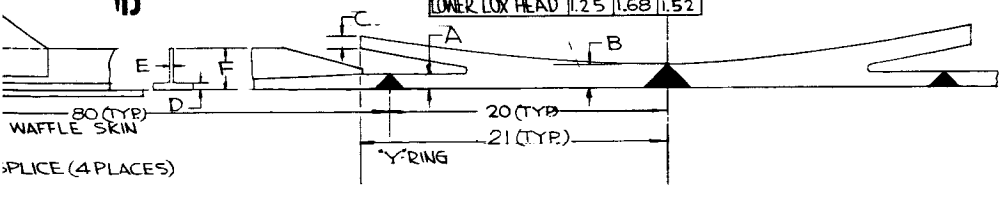

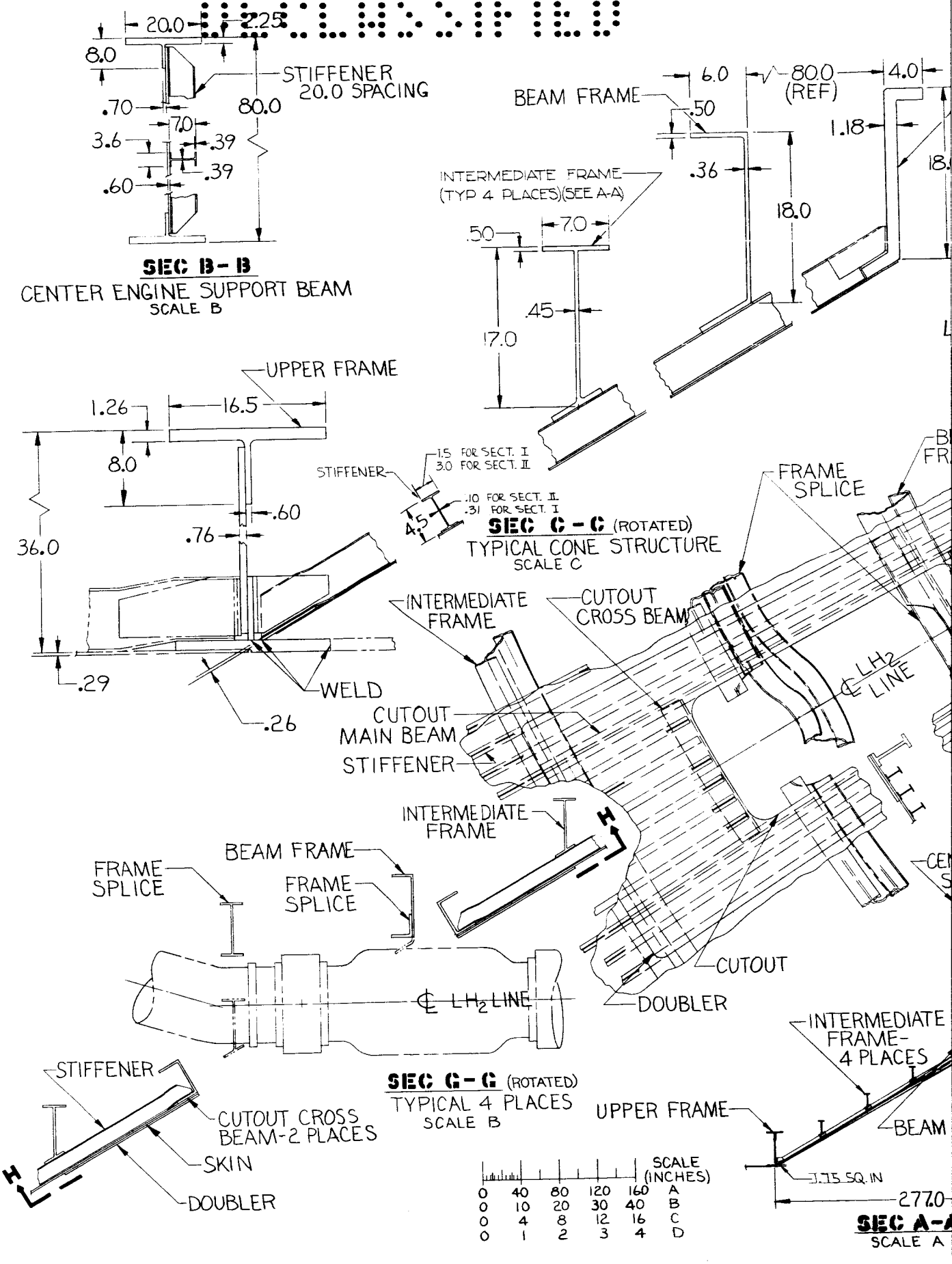

Figure

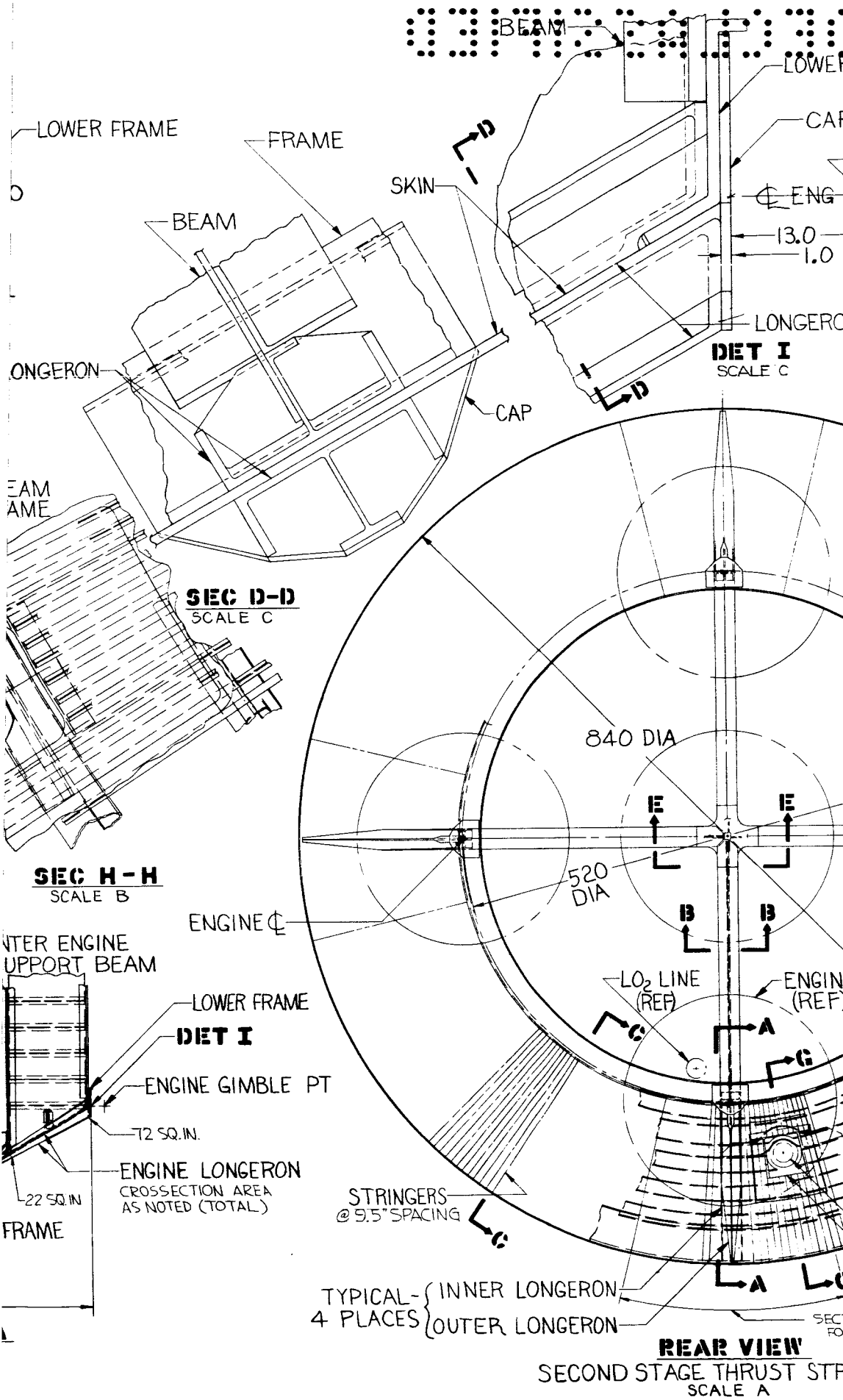

3.2.11-5 SECOND-STAGE THRUST STRUCTURE
Configuration T65D

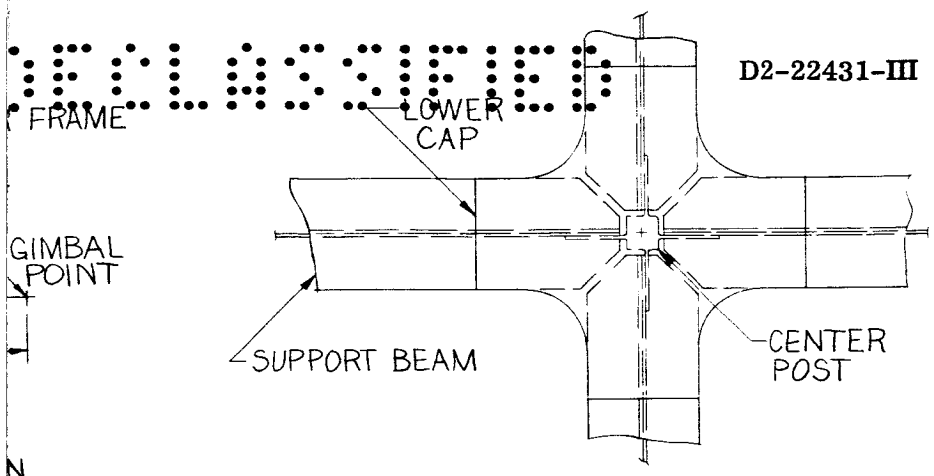

SEC F-F
SCALE B

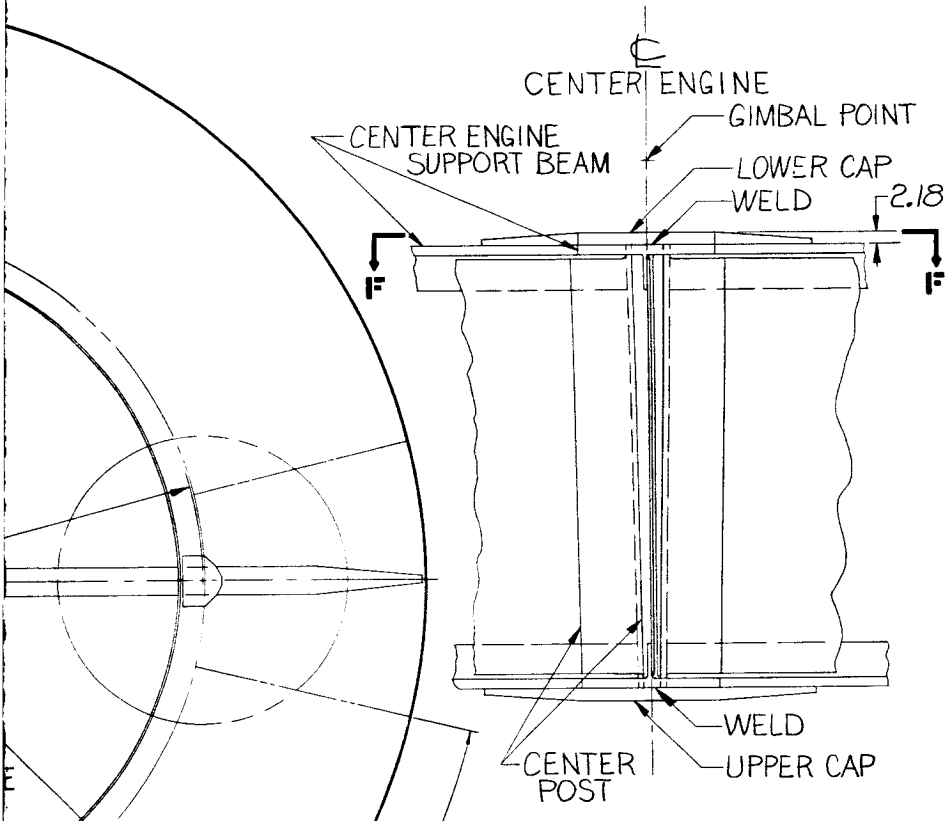

SEC E-E
SCALE B

NOTE: 2219-T87 MATERIAL USED FOR ALL WELDED STRUCTURE. 7075-T6 MATERIAL USED FOR ALL UNWELDED STRUCTURE.

SECTION II (4 PLACES)
.15 SKIN CONSTANT

LH_2 LINE (REF)

CUTOUT

TION I (TYP 4 PLACES)
R SKIN THICKNESS SEE PARA. 3.2.8

UCTURE

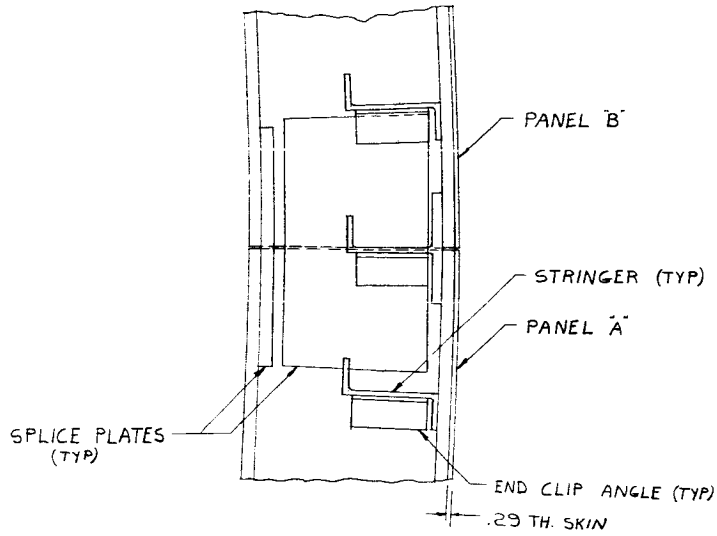

SECTION C-C

SPLICE PLA

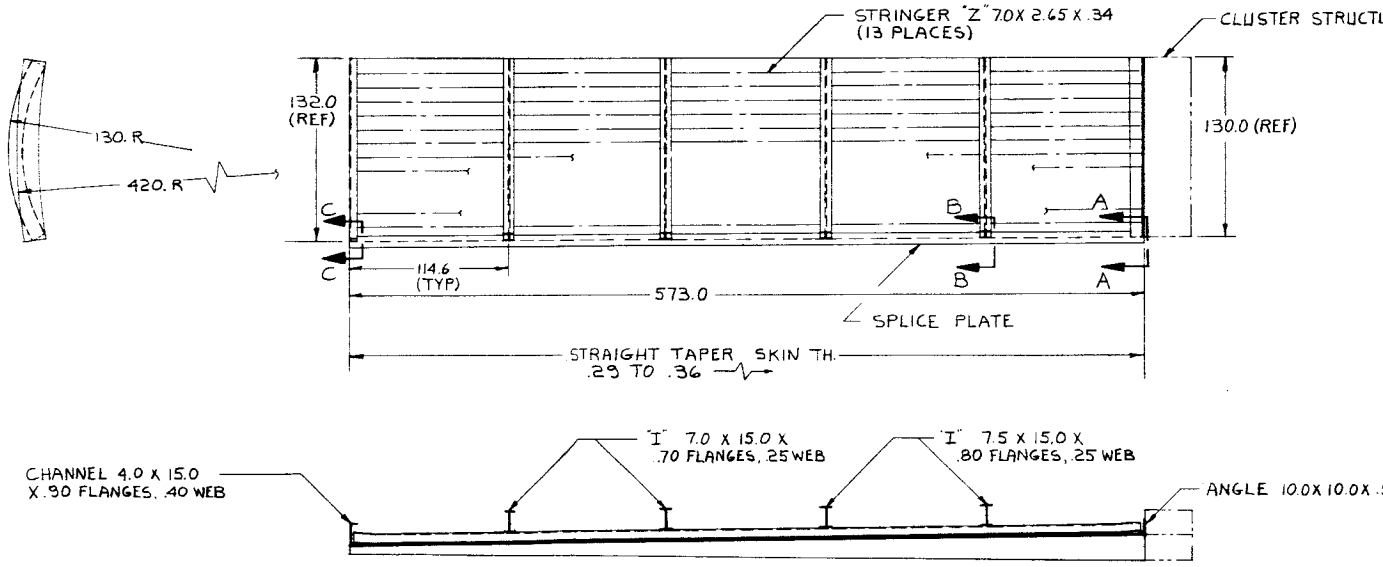

PANEL "B"
(6 REQ'D)

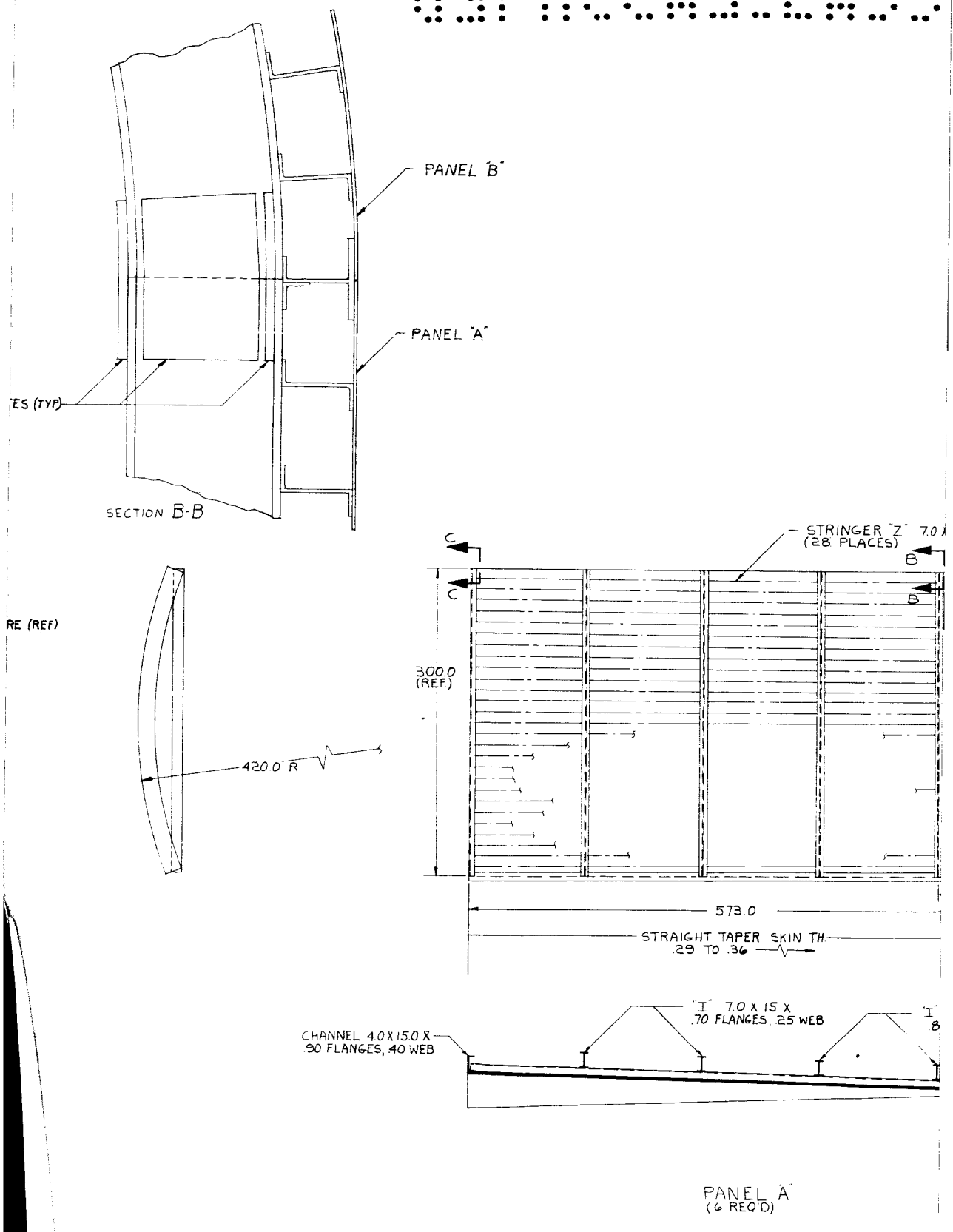

Figure 3.2.11-6 INTERST
Configuratio

2

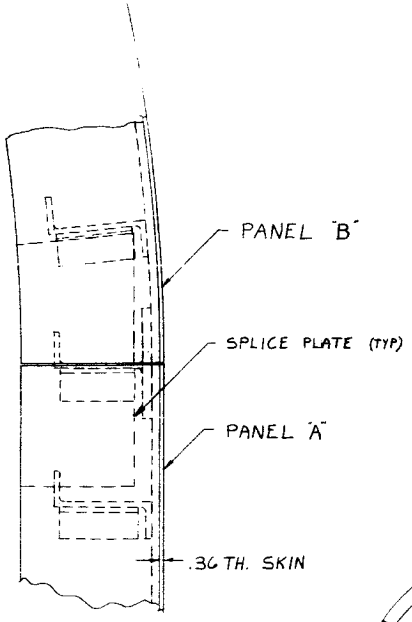

SECTION A-A

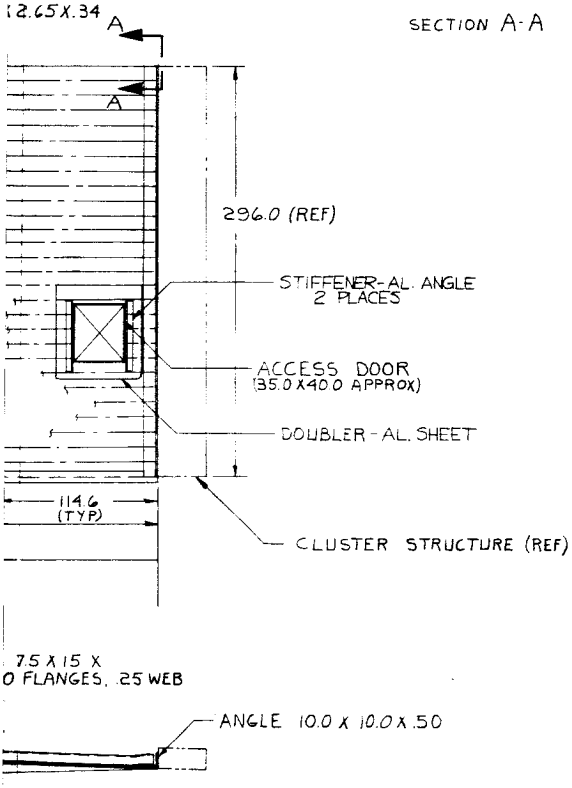

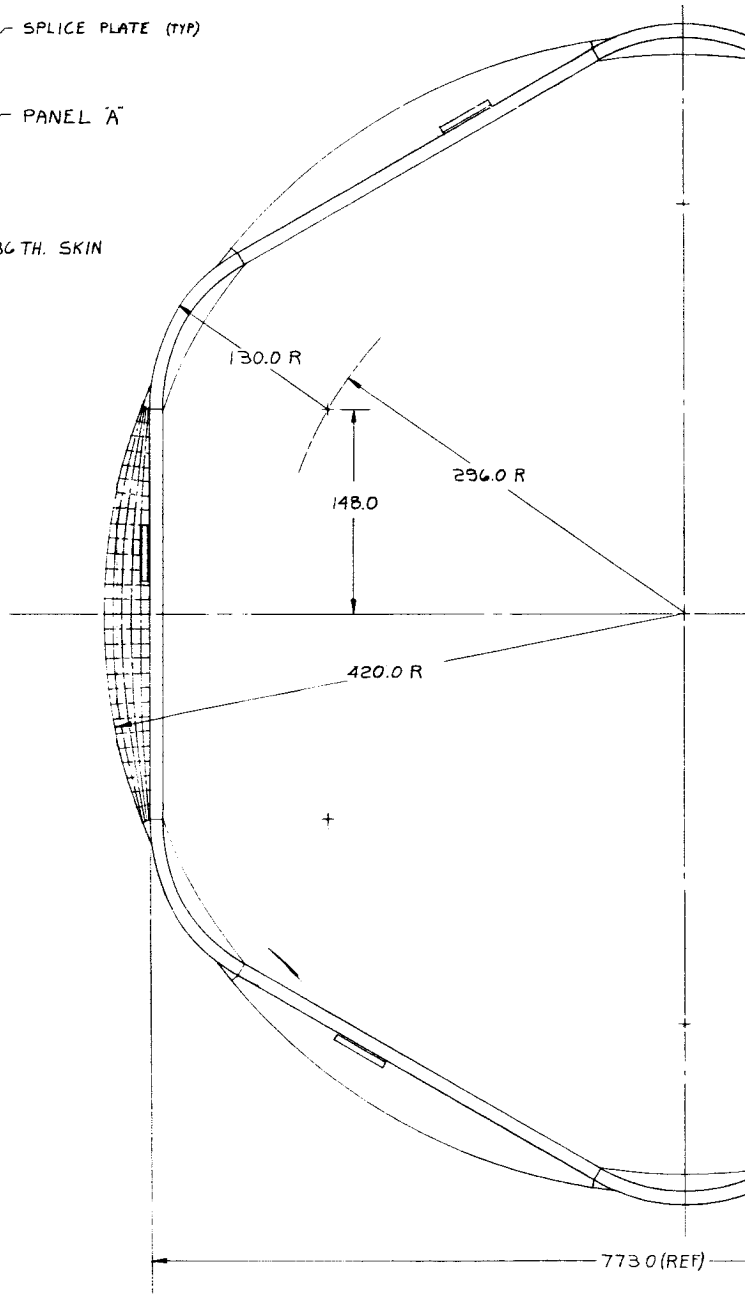

BOTTOM VIE

'AGE STRUCTURE
n T65D

3

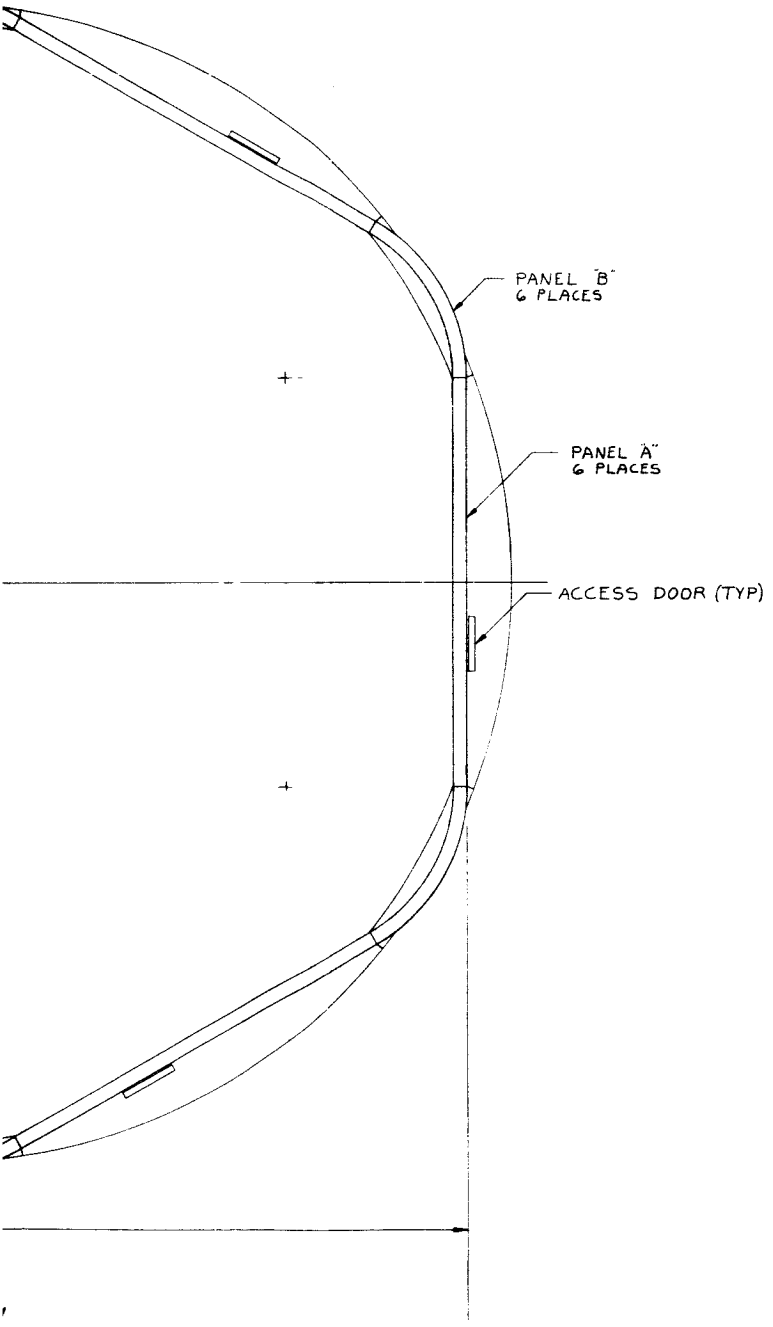
PANEL "B"
6 PLACES
PANEL "A"
6 PLACES
ACCESS DOOR (TYP)

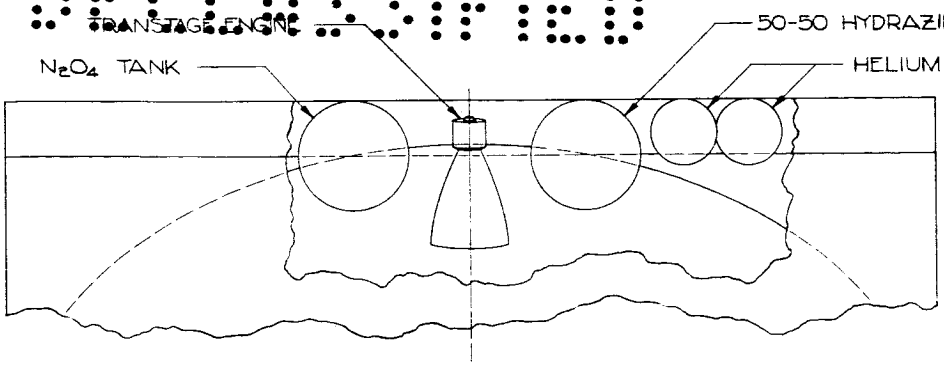

SECTION A-A
(ROTATED 90° CLOCKWISE)

℄ TELEME

℄ COMM
ANTEN

SECOND S
(4 REQ'D;
90° INT

SECOND
MOTOR

A

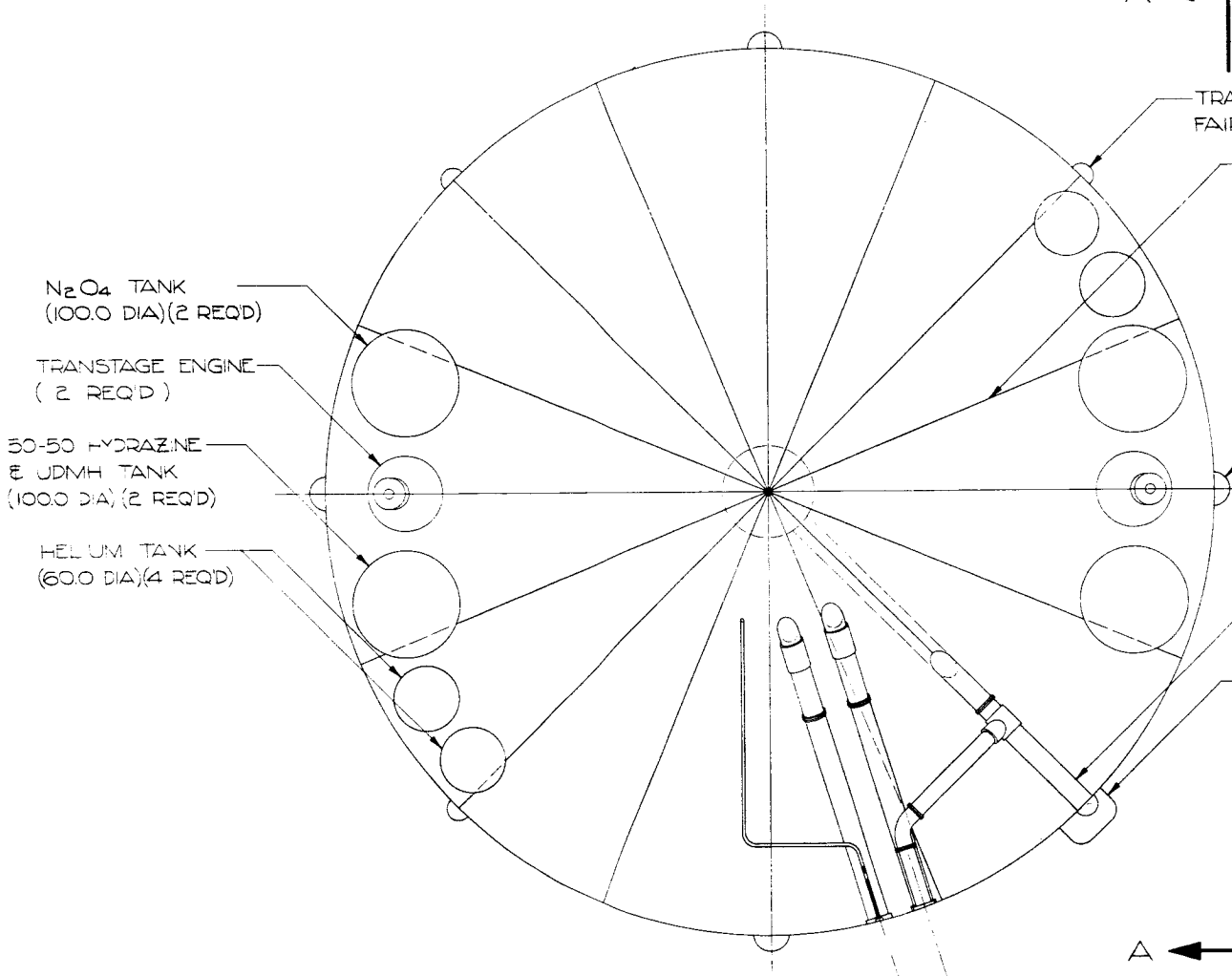

A

℄ LH_2 IN-FLIGHT VENT LINE (2.0 I.D.) ℄
LH_2 VENT LINE (20.0 I.D.)

℄ LH_2 PRE-PRESSURIZATION LINE (15.0 I.D.) ℄
LH_2 VENT LINE (20.0 I.D.)

PLAN VIEW

TRANSTAGE RETRO
MOTOR FAIRING

TRANSTAGE RETRO MOTO
(4 REQ'D; PLACED AT
90° INTERVALS)

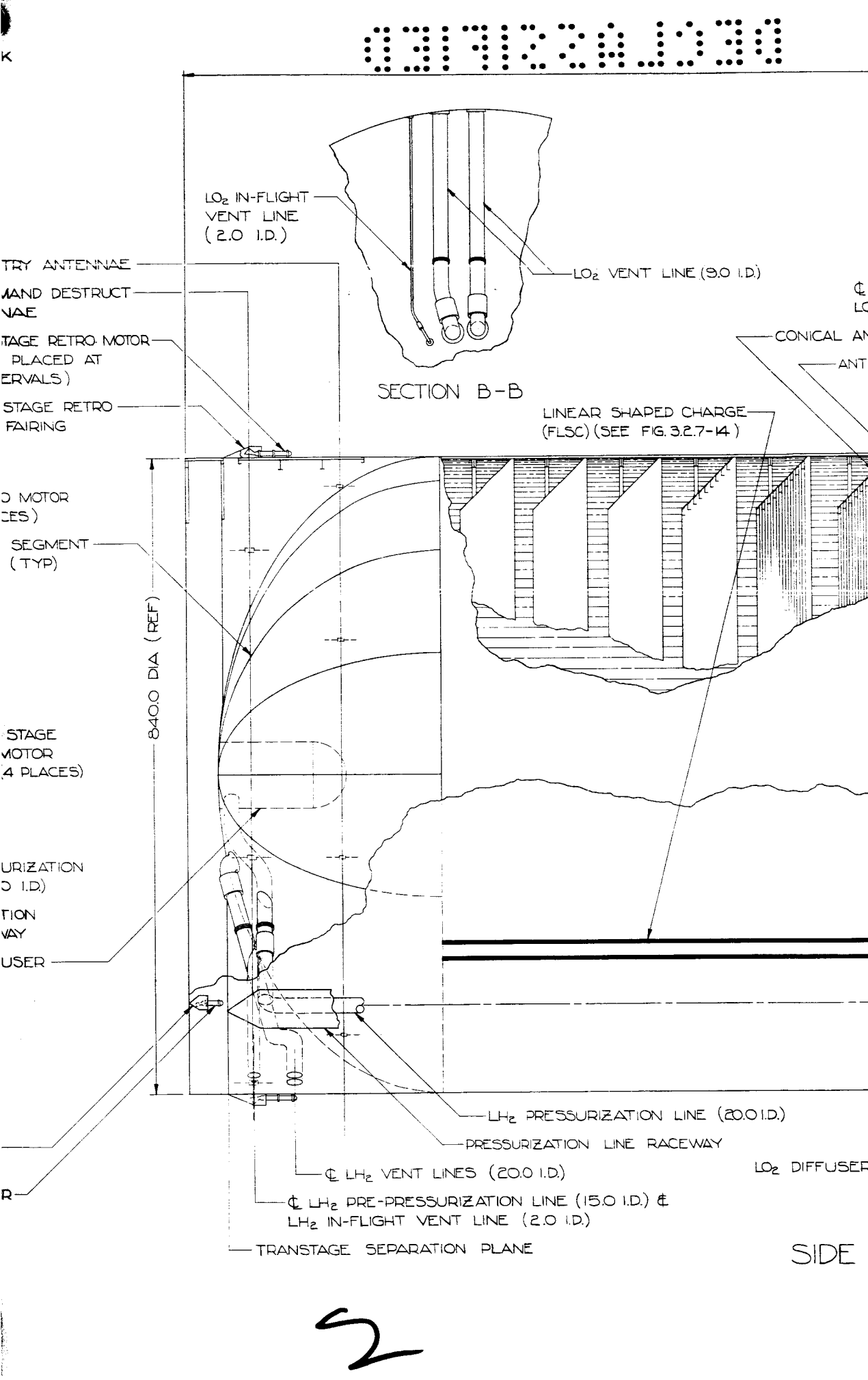
LO_2 IN-FLIGHT VENT LINE (2.0 I.D.)
LO_2 VENT LINE (9.0 I.D.)
SECTION B-B
LINEAR SHAPED CHARGE (FLSC) (SEE FIG. 3.2.7-14)
840.0 DIA (REF)
LH_2 PRESSURIZATION LINE (20.0 I.D.)
PRESSURIZATION LINE RACEWAY
℄ LH_2 VENT LINES (20.0 I.D.)
LO_2 DIFFUSER
℄ LH_2 PRE-PRESSURIZATION LINE (15.0 I.D.) ℄
LH_2 IN-FLIGHT VENT LINE (2.0 I.D.)
TRANSTAGE SEPARATION PLANE
SIDE

2

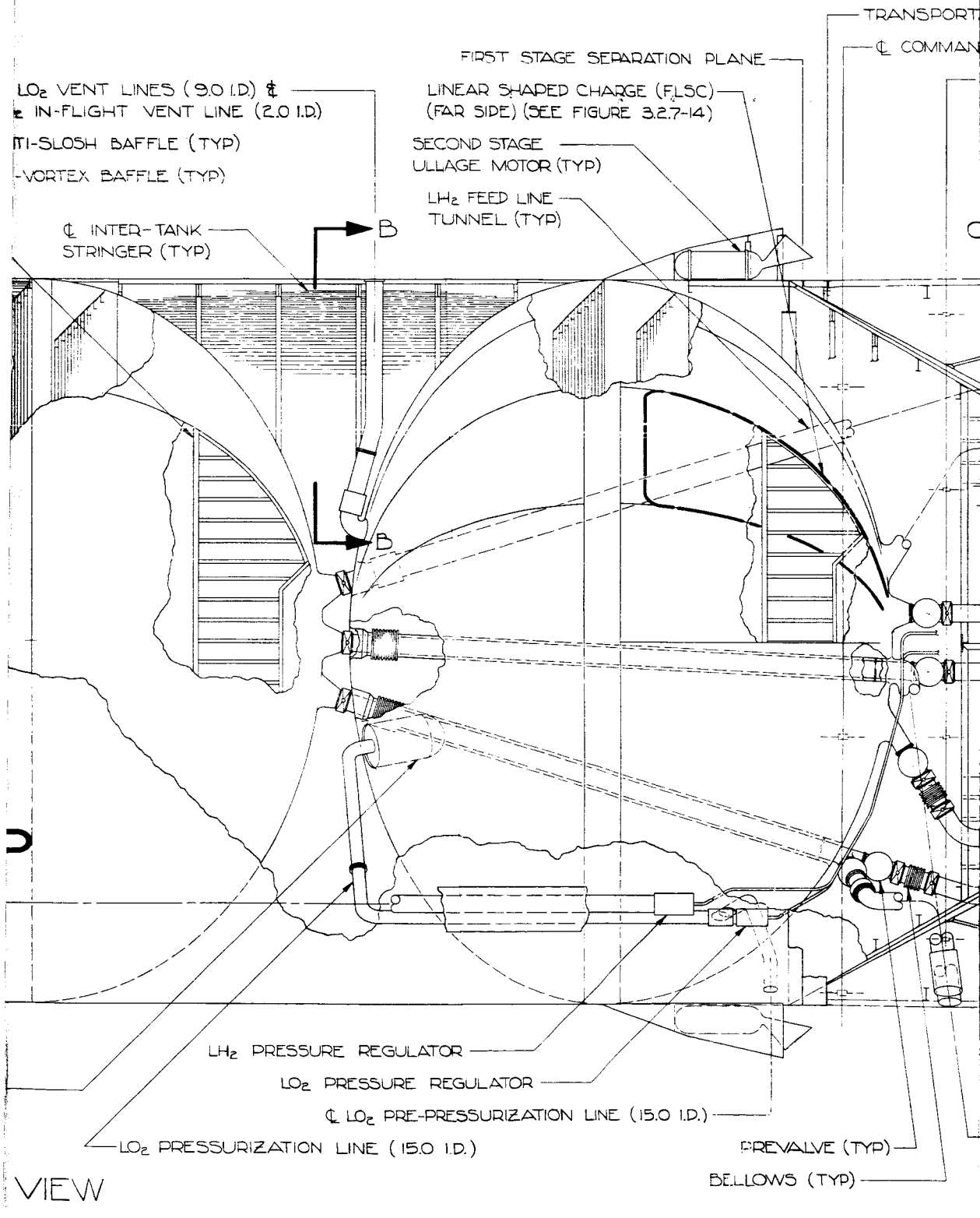

Figure 3.2.11-7 INBOARD PROFILE — SECOND STAGE Configuration T65D

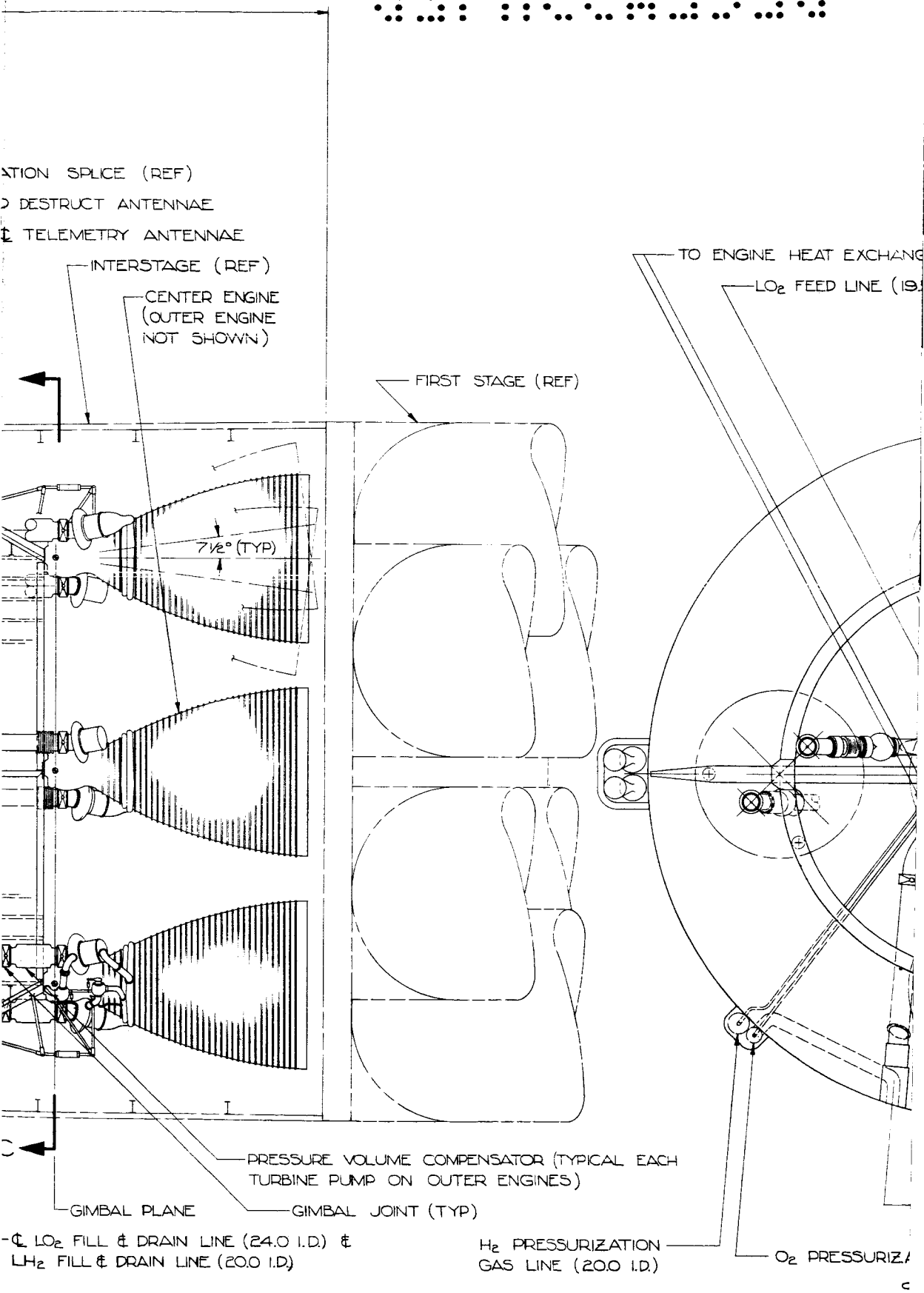

4

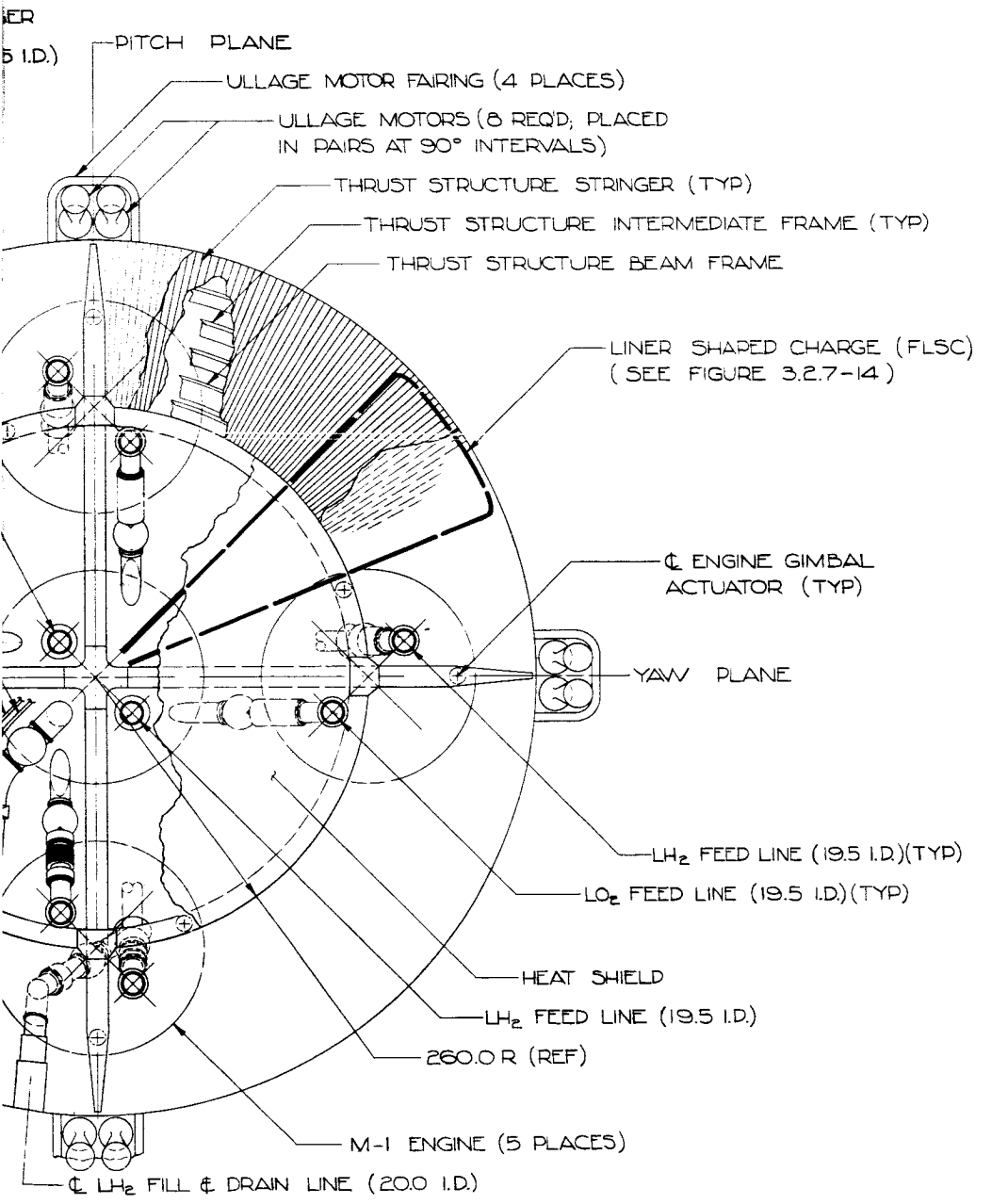

ECTION C-C

3.2.12 Payload Growth Potential

3.2.12.1 Introduction

Vehicle payload growth can be shown in a variety of ways, such as by increasing the number of M-1 engines in the second stage and restaging the vehicle, or increasing first-stage burnout velocity with a large increase in first-stage size thereby permitting the use of a lower thrust-to-weight ratio in the second stage. Generally, such payload increases are obtained at a considerable compromise in vehicle design, reliability, or performance efficiency.

Payload growth potential of the T65D vehicle was determined within the following constraints. The number and diameter of first-stage solid motors were held constant. The number of second-stage engines and second-stage and payload diameter were held constant. A maximum dynamic pressure of 950 psf was maintained. A 20-percent increase in M-1 engine thrust was assumed consistent with a vehicle growth development program. The approach by which payload growth is shown is generally conservative in retaining the basic vehicle design together with good performance efficiency.

3.2.12.2 Summary

Vehicle T65D has a payload growth capability to 1,460,000 pounds into a 225-kilometer orbit or an increase in payload of 25.3 percent over the preliminary design vehicle. The growth vehicle has a launch weight of 42,500,000 pounds, giving a launch-to-payload-weight ratio of 29.1 as compared with 32.7 for the T65D vehicle. Second-stage growth is limited by second-stage thrust-to-weight ratio. First-stage growth is limited by maximum dynamic pressure and second-stage growth.

3.2.12.3 Vehicle Description

The payload growth version of vehicle T65D has an overall length of 611 feet or an increase of 76 feet over the preliminary design vehicle. This increase in length is distributed as follows. The first stage was increased by 37 feet, the second stage hydrogen tank increase was 14 feet, and the payload became 28 feet longer. The increase in payload length assumes a 567-kilometer orbital payload of 1,341,000 pounds, using a transtage similar to that of the T65D vehicle. This vehicle has an estimated first-mode bending frequency of 1.15 cycles per second. The first stage was penalized to allow for an increase in motor case thickness to handle increased buckling loads. Motor operating chamber pressure was limited to 800 psia.

3.2.12.4 Performance Analysis

Performance has been determined for a growth configuration of the baseline vehicle. Five uprated M-1 engines are used in the second stage. Each engine

produces a vacuum thrust of 1.8 million pounds with a vacuum specific impulse of 426.5 seconds. The first-stage solid motors have a nominal sea level specific impulse of 238 seconds.

The effect of increasing first stage propellant loading was examined. At a constant chamber pressure, an increase in solid-propellant loading causes increases in thrust, launch weight, and payload. Two considerations limit the propellant that can be used in the first stage. These are the maximum dynamic pressure limit of 950 psf and the minimum permissible second-stage thrust-to-weight ratio.

For large solid-propellant loadings, maximum payload tends to occur at burnout velocities which give excessively high maximum dynamic pressure (q_{max}). To reduce q_{max} to 950 psf at a specified first-stage propellant weight, the burnout velocity must be reduced by adding additional second-stage weight. However, since second-stage thrust is fixed, this additional weight leads to an unacceptably low second-stage thrust-to-weight ratio. These considerations place an upper limit on solid-propellant weight of about 27,000,000 pounds when upper-stage thrust is limited to five uprated M-1 engines. A second-stage thrust-to-weight ratio of 0.74 is about the minimum acceptable value. Using first- and second-stage mass fractions of 0.8896 and 0.9235 gives a growth vehicle launch weight of 42,500,000 pounds. First-stage motors produce a total thrust of 61,200,000 pounds. This vehicle has a payload capability of 1,460,000 pounds into a 225-kilometer orbit.

3.2.12.5 Propulsion System Growth

The potential for increasing the impulse delivered by the first and second stages was briefly examined. The following paragraphs present the results of an analytical study of first-stage motor growth, and an estimate of the characteristics of an M-1 engine uprated to 1.8 million pounds vacuum thrust.

3.2.12.5.1 First-Stage Motor Growth

Higher delivered impulse is most economically achieved in a production solid-propellant motor by increasing propellant weight and motor case cylindrical length while maintaining grain configuration and design pressure. This confines major modifications to the nozzle. An eventual limit is imposed on this growth by propellant erosive-burning effects at low port-to-throat-area ratio. While this degrades the stage performance only slightly, it does cause early burnout of the aft portion of the propellant grain, and longer tailoff time. A port-to-throat-area ratio of 1.3 was arbitrarily selected as the lower limit in this study.

If other factors such as motor processing facilities or vehicle body bending frequency limit motor length, the alternative path to increased impulse is through higher chamber pressure. In this case, a slight modification of the

propellant would be required to maintain web burn time. A more severe operating environment is imposed on the nozzle, and heavier case wall thicknesses would be necessary. The shape of the thrust-time trace of the motor would remain essentially constant unless the grain configuration were altered. These considerations generally apply to the case of a constant first-stage velocity increment.

Assignment of a lower velocity increment to the first stage of a heavier vehicle at the same maximum dynamic pressure would require higher thrust and shorter burn time of the first stage. This requirement could be met by increasing the propellant burning rate and maintaining the same grain configuration. Either the nozzle throat area or the operating pressure would have to be increased. Moderately higher propellant burning rates than the 0.5 inches/second used in the T65 motor are currently available.

A higher first-stage velocity increment imparted to a heavier vehicle at the same maximum dynamic pressure would require both higher thrust and longer burn time of the first stage. This, in turn, would require both propellant reformulation and higher pressure or larger throat area of the constant-section motor.

The use of higher performance propellant as a means of achieving higher first-stage performance was not considered in this study. While several approaches are now being investigated in ARPA-sponsored programs, all involve materials requiring substantially different processing techniques and leave unanswered the serious question of operational safety. The slight theoretical growth remaining for hydrocarbon-aluminum-ammonium perchlorate systems in general requires higher solids loading than propellant of the performance assumed. This in turn means more difficult processing.

First-stage motor growth data, calculated for motors of constant propellant type and grain configuration, are shown in Figure 3.2.12-1. Sea-level thrust, motor-case length-to-diameter ratio, and port-to-throat-area ratio are plotted as functions of propellant weight for several values of nominal maximum head-end pressure. Corresponding maximum expected operating pressures (MEOP) are 630, 840, and 1050 psia, respectively. The difference between P_{Fnmax} and MEOP (1.051 P_{Fnmax}) reflects the combined effects of expected motor-to-motor variations and the operating ambient temperature range of 80 ± 20°F.

The T65 motor design points are shown. Maximum available expansion ratio was assumed at each chamber pressure, using the same nozzle exit area as the T65 motor.

These data indicate the flexibility of the basic motor design and a growth potential at 800 psia up to about 5.4 million pounds of propellant at an assumed minimum port-to-throat-area ratio of 1.3. This is an increase of about 15 percent in propellant weight and thrust. Propellant erosive burning was considered in the computation of these data.

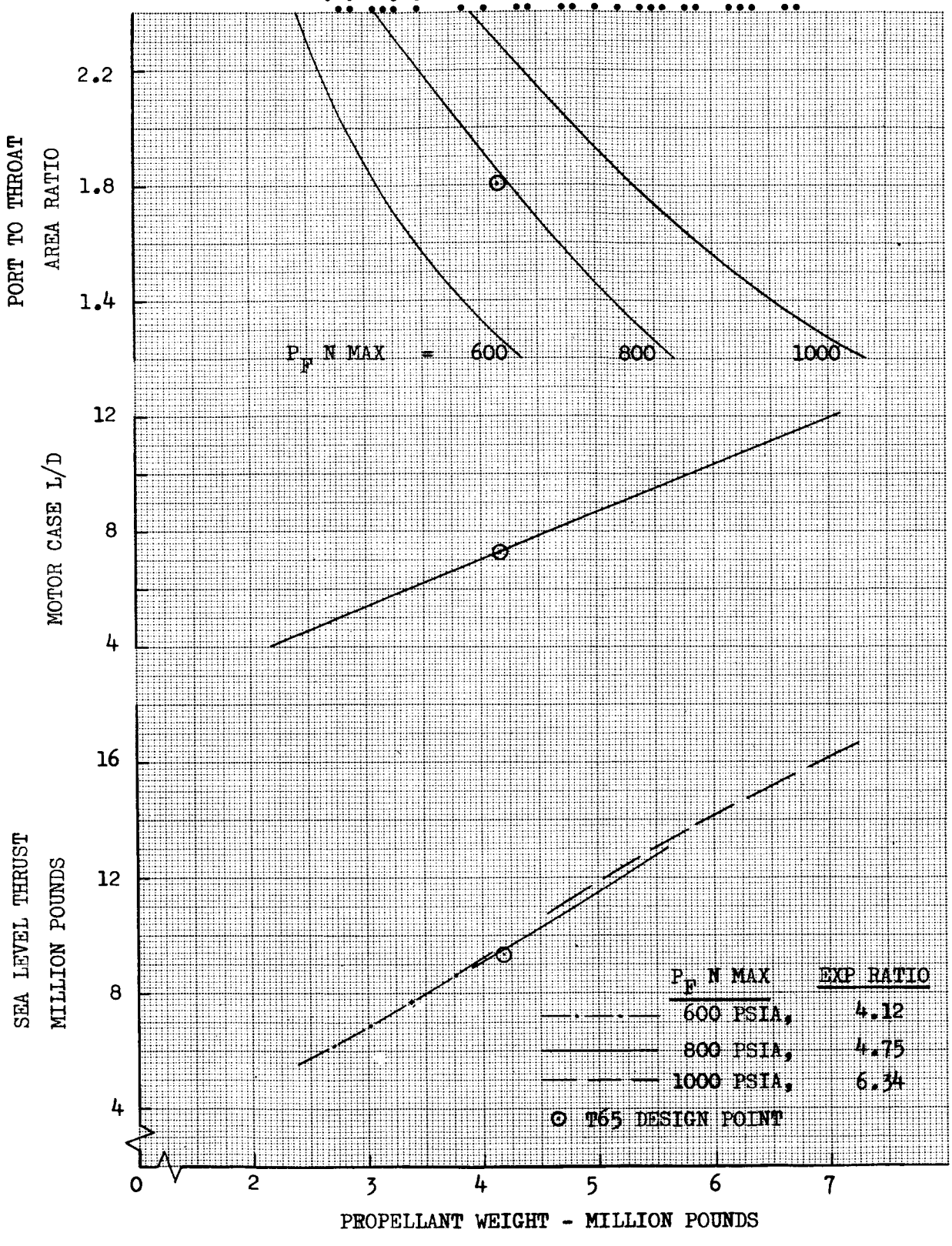

Figure 3.2.12-1 FIRST-STAGE MOTOR GROWTH DATA

Structural dynamic effects of the increased motor length are discussed in 3.2.12.6.

3.2.12.5.2 M-1 Engine Thrust Increase

Performance and weight data were estimated for an M-1 engine uprated from 1.5 to 1.8 million pounds vacuum thrust. This increase was assumed to be achieved by operating the engine at higher mass flow rate and chamber pressure.

Higher turbopump power-out will be required. At the same suction specific speed, both oxidizer and fuel must operate at about 5-percent higher rpm. It is assumed that the pump volumetric capacity is adequate.

Weight of the uprated engine was estimated. Turbopump weight was assumed to be proportional to pump horsepower to the 0.8 power. New thrust chamber weight was calculated from an empirical relationship developed by Rocketdyne. An additional allowance was made for increases in the weight of the injector and miscellaneous items such as plumbing, gas generator, and engine controls.

A slight reduction in engine specific impulse is expected because of the proportionately higher turbopump gas-generator flow requirement and the reduced dissociation in the nozzle at the higher chamber pressure. Overall dimensions of the engine were assumed to remain unchanged.

Principal characteristics of the uprated engine are as follows:

Thrust (vac., lbs.)	Chamber Pressure, (psia)	Dry Wt. (lbs.)	Nozzle Expansion Ratio	Engine I_{sp} (sec.)
1.8×10^6	1200	23,600	40	426.5

3.2.12.6 Structural Limits

In most structures a structural limit cannot be defined exactly because as more strength is required more structure can be added. Therefore, the structural limit can be defined only by the decision that the extra weight is not justified by either performance or cost. This discussion will, therefore, be limited to defining the areas where additional structure will be required if growth is desired.

The vehicle diameter is fixed; therefore, growth will occur by increasing vehicle length. The increase in vehicle length will produce larger bending moments, which will require an increase in gages of all bending material — particularly the hydrogen tank and transtage transition section. Increased axial loads will also result from the larger weight and thrust. This increases interstage and clustering structure weight. Fluid head pressures and, therefore, skin gages will increase in the second stage due to the greater fluid depth.

Motor-case skin gage increases will be required to carry the greater launch weight.

The first-mode frequency will approach 1 cps at a vehicle fineness ratio of approximately 9.